VULNERABILITY OF RESIDENTIAL INFRASTRUCTURE IN HURRICANE PRONE REGIONS

By

SYLVIA TERESA LABOY-RODRÍGUEZ

A DISSERTATION PRESENTED TO THE GRADUATE SCHOOL
OF THE UNIVERSITY OF FLORIDA IN PARTIAL FULFILLMENT
OF THE REQUIREMENTS FOR THE DEGREE OF
DOCTOR OF PHILOSOPHY

UNIVERSITY OF FLORIDA

2013

To my parents for all their support and inspiration

ACKNOWLEDGMENTS

I want to express my gratitude to my advisor, Dr. Kurt Gurley for his encouragement, advice, guidance, valuable time and support which helped to improve the outcome of this study. In addition, I would like to thank Dr. Masters for his advice, support, and participation in this study. My sincerest gratitude to Dr. Cook and Dr. Shanker for being part of my committee members.

I am eternally grateful to my parents, Blanca M. Rodriguez and Raul Laboy for being my inspiration and support, and for encouraging me with their patience and counseling to attain one of my greatest achievements. Finally, I would like to thank my family and dear friends (extended family) for supporting me and adding color and happiness to my life.

This research was supported by the Florida Building Commission (Chapter 2) and the Southeast Region Research Initiative (SERRI), which is managed by Oak Ridge National Laboratory for the U.S. Department of Homeland Security (Chapters 3 and 4). Any opinions, findings, and conclusions or recommendations expressed in this document are those of the authors and do not necessarily reflect the views of the sponsors.

TABLE OF CONTENTS

page

LIST OF TABLES

LIST OF FIGURES

LIST OF ABBREVIATIONS

ANSI	American National Standards Institute
AS	Australian Standard
ASCE	American Society of Civil Engineers
BS	British Standard
C & C	Components and Claddings
C_{DIR}	Directional Factor
C_P	Pressure Coefficients
COV	Coefficient of Variation
FEMA	Federal Emergency Management Agency
FL	Florida
GC_P	Combined Gust Factor and External Pressure Coefficient
K_D	Wind Directionality Factor
M	Meters
M_D	Wind Directional Multiplier
MPH	Miles per hour
MRI	Mean Recurrence Interval
MWFRS	Main Wind Force Resisting System
NI	Not Included
NIST	National Institute of Standard and Technology
NOAA	National Oceanic and Atmospheric Administration
NZS	New Zealand Standard
ORNL	Oak Ridge National Laboratory
PDF	Probability Density Function
PSF	Pound per square foot

RTD	Roof Tile Debris
SC	South Carolina
S_D	Direction Factor
SERRI	Southeast Region Research Initiative
UD	Directional Wind Speed
UK	United Kingdom
UO	Basic Wind Speed
WBD	Windborne Debris

Abstract of Dissertation Presented to the Graduate School
of the University of Florida in Partial Fulfillment of the
Requirements for the Degree of Doctor of Philosophy

VULNERABILITY OF RESIDENTIAL INFRASTRUCTURE IN HURRICANE PRONE REGIONS

By

Sylvia Teresa Laboy-Rodríguez

August 2013

Chair: Kurt Gurley
Major: Civil Engineering

Post-hurricane assessments have documented wind damage in residential and commercial buildings with over than 375 billion dollars in damage and over 20,685 fatalities (Blake et al. 2011). Protecting the building envelope from windstorm events is an important factor to avoid failures where identifying the weakest link can improve the building performance. This dissertation addresses two aspects of building envelope vulnerability.

The first aspect investigated the vulnerability of roof tile systems and metal shutters to roof tile debris using a three phase approach. The first two phases evaluated the tile fragment size and quantified the puncture vulnerability of common metal panel shutter systems as a function of tile fragment impact speed. The third phase provided context for interpretation of the experimental results through the use of a tile trajectory model. The results provide evidence that window shutters provide significant protection against windborne debris, however, are vulnerable to tile fragment puncture in design level tropical cyclones.

The second aspect evaluated the efficacy of K_d in ASCE 7 on components and cladding (C&C) for hurricane prone regions. The first part of the study reviewed the

development of the wind directionality concept. The second part of the study uses Monte Carlo simulation concepts and wind tunnel pressure data to simulate experiments that physically interpret the directionality factor concept. This methodology is first developed using individual taps and then extended to area averages. These numerical experiments are conducted with three approaches. The first two approaches ignore the climatology specific to hurricane landfalls, and adopt the ASCE 7 assumption that wind damage is due to a single gust coming from a single direction. The third approach adopts a scenario analysis whereby the duration of high winds and the variation of wind direction during the passage of a hurricane were directly incorporated into the Monte Carlo directionality assessment framework. The outcomes of this scenario analysis support the conclusion that the C & C K_d in ASCE 7 is not conservative and is inappropriate for hurricane prone structures. A K_d value no smaller than 0.95 can be justified where a value of 1.0 is defensible.

CHAPTER 1
INTRODUCTION

Damage to the building envelope is a major contributor to the overall losses to low-rise buildings from hurricanes. This chapter provides an overview of the importance of quantifying the vulnerability of the building envelope during hurricanes. The problem statement, scope, and approach of this study are then presented.

1.1 Background

Since 1965 more than 375 billion dollars in damage and over 20,685 fatalities have resulted from hurricanes in the United States (Blake et al. 2011). Almost half of the costliest hurricanes have occurred during the last ten hurricane seasons (Blake et al. 2011). These losses are expected to continue increasing in proportion to the coastal population.

Post-hurricane assessments have documented wind damage in residential and commercial buildings. Figure 1-1 shows common observed damage related to roof covering, wall coverings, windows, and nonstructural elements, impact damage caused by windborne debris (e.g., trees, roof tiles, shingles, among others), and failures of roof, truss systems. Common contributors to damage include: (1) internal pressurization caused by an opening (e.g., breakage of a window), (2) poor construction (e.g., connections failure) or (3) poor performance of older buildings (FEMA 488, 549). These assessments provide an overview of how vulnerable low-rise residential buildings are to damage, leading to the question of whether appropriate wind loads and factors have been used for design.

A  B  C 

Figure 1-1. Hurricane Charley components and claddings damage. A) Roof covering loss in Captiva Island (Photo courtesy of FEMA 488). B) Poor performance of cladding due to breaching of roof between Charlotte Harbor and De Soto County (Photo courtesy of FEMA 488). C) Tile debris damage in Punta Gorda, FL (Photo courtesy of Laboy et al. 2012).

Protecting the building envelope from windstorm events is an important factor to avoid progressive failures in buildings (Minor 2005). This dissertation addresses two aspects of building envelope vulnerability. The first is the susceptibility of window protection systems to windborne debris. The second is the appropriateness of the load-reducing directionality factor in ASCE 7 for components and cladding on buildings in hurricane prone regions.

1.2 Problem Statement

The building envelope is the first line of defense against wind and water intrusion. Previous hurricane seasons have demonstrated that the building envelope can suffer significant damage. Openings may be highly vulnerable, and must be designed to withstand wind pressure and protected from debris impact to avoid internal pressurization and allow rain water ingress.

Protecting windows from debris impact is commonly addressed through the use of a rigid covering that is installed prior to hurricane land fall. Metal panel shutters are a

popular window protection system, and the subject of this study. Among the many sources of debris available in a hurricane wind field, roof covering from neighboring houses is the most widely observed debris. In neighborhoods where clay or concrete roof tile systems are prevalent, whole tiles and fragments have been observed to produce widespread damage (Meloy et al. 2007). This can include damage to the window protection systems and the windows being protected. Whether damage to window protection systems from roof tiles is a likely event or a rare outlier is an open question.

Roof tile debris can be generated by the failure of tiles due to uplift wind loads or by the impact of windborne debris on a tile roof. FEMA 488 states that C&C, such as windows and doors can help in protecting the envelope of breaching. However, post Hurricane Charley assessments raised the question of whether common metal panel window shutters are able to provide significant protection against a prevalent form of windborne debris in tile roof neighborhoods.

With regard to design wind loads, ASCE 7 allows a reduction in the applied wind load based on the assumption that the extreme wind event may not approach the building from the worst aerodynamic direction (thus the pressure coefficients would be perhaps too conservative). However, the premise that component and cladding damage is a product of a single peak gust from a given direction is suspect in the case of a hurricane wind event, characterized by a sustained period of strong winds whose approach direct changes during the storm duration. The FEMA Region IV Capabilities Gap 2010-M-014 highlighted the concern of whether the design load reduction wind

directionality factor (K_d) for C&C used in ASCE 7 is appropriate for hurricane prone regions.

1.3 Research Scope and Approach

The primary objective of this research is to study the vulnerability of C&C on low-rise residential buildings located in hurricane prone regions. The study investigates: (1) the vulnerability of roof tile systems and metal hurricane shutters to roof tile debris and (2) the appropriateness of the current implementation of the load reducing directionality factor K_d in ASCE 7. The studies involved in the investigation are:

1. Roof tile frangibility and puncture of metal shutters: This study quantifies the likelihood of puncture of metal shutters based on hurricane intensity. Two experimental phases address the performance of tile roof systems and metal shutters under RTD impact. A numerical modeling phase addresses the RTD during flight, and provides some context for interpretation of the experimental results in terms of hurricane wind conditions.

2. Revisiting the wind directionality factor in ASCE 7: The purpose of this study is to evaluate the efficacy of K_d in ASCE 7 on (C&C) for hurricane prone low-rise residential structures. The first part of the study (Chapter 3) reviewed the development of the K_d factor in ASCE 7 and the incorporation of directionality effects in standards around the world. The second part of the study (Chapter 4) calculated the wind directionality for C&C on low rise buildings using point pressure coefficients instead of spatial area averaged pressure coefficients following the scenarios analysis. The third part of the study (Chapter 5) focuses on the development of a directionality factor for C&C loads on hurricane prone structures following a deterministic, probabilistic, and scenario analysis.

1.4 Dissertation Organization

This dissertation consists of six chapters. Chapter 1 discusses the background, problem statement and research scope and approach. Chapter 2 presents the literature review, methodology and results that quantified the probability of puncture of metal shutters for specific hurricane intensity. A literature review of the initial development of the K_d concept, as well as a comparison of how wind directionality is addressed in fifteen building standards from around the world is presented in Chapter 3. Chapter 4

presents a preliminary study of the directionality factor that lead to the newly proposed work in Chapter 5. The research regarding the evaluation of the directionality factor using area averaged is provided in Chapter 5. The conclusions of the dissertation are presented in Chapter 6.

CHAPTER 2
ROOF TILE FRANGIBILITY AND PUNCTURE OF METAL WINDOW SHUTTERS

This chapter presents a study that evaluates the vulnerability of roof tile systems and metal hurricane shutters to roof tile debris (RTD). Two experimental phases addressed the performance of tile roof systems and metal shutters under RTD impact. A numerical modeling phase addressed the RTD during flight, and provides some context for interpretation of the experimental results in terms of hurricane wind conditions. A manuscript describing the methods and findings was accepted for publication in October 2012 in the Journal of Wind and Structures (Appendix A). This chapter offers more detail than appears in the journal article.

This study provides supporting evidence that common metal panel window shutters are capable and likely to provide significant protection against a prevalent form of windborne debris (WBD) in tile roof neighborhoods. Puncture of these shutters from roof tile fragments is possible with a likelihood that increases with wind speed. These findings correlate strongly with observations made after Hurricane Charley. The study also emphasizes the importance of designing tile roof systems to resist extreme wind events, as the probability of puncture is proportional to the quantity of tile debris.

2.1 Background

Windborne debris is a large contributor to building envelope damage during windstorm events. This problem can be defined in terms of the WBD load (types and sources of debris, trajectory and speed, and probability of impact) and the vulnerability of building components to the WBD load (the capacity of components to withstand debris impact). The existing literature addresses the former problem in numerous studies of WBD trajectories via numerical modeling and experiments. The subject of

component capacity has largely focused on glass damage and the development of impact standards for protective devices. The current study addresses both aspects of the problem within the context of roof tile fragments impacting metal hurricane shutters.

2.1.1 Observed Windborne Debris

The 2004 Atlantic hurricane season demonstrated that roof tile WBD caused severe damage to the building envelope. Figure 2-1 shows two examples of such damage in Punta Gorda, FL after Hurricane Charley. The center and right pictures in Figure 2-1 illustrate the specific problem to be addressed in this study, where it can be observed that roof tile debris has penetrated a metal window shutter and shattered the glass being protected. Tile debris was identified to be the primary source of WBD in Punta Gorda since all homes were required to have concrete or clay tile roofs (Meloy et al. 2007). Tile roof systems are vulnerable to breakage from uplift or WBD. Post hurricane assessment also revealed deficiencies in the installation process (FEMA 2004).

Figure 2-1. Tile debris damage after hurricane charley, Punta Gorda, FL 2004 (Photos courtesy of Laboy et al. 2012).

2.1.2 Debris Damage Studies

Many studies (e.g., Beason 1974, Minor 1994 and 2005) have been conducted to quantify the vulnerability of fenestration in high winds and windborne debris. UF investigators have contributed to this body of work with studies to quantify damage due to roof covering impacting the building envelope. Masters et al. (2010) conducted an experimental investigation to quantify the momentum threshold required to damage residential window glazing due to the impact of asphalt roof shingles and wooden dowels. It was concluded that if commonly used asphalt shingles become airborne, they are almost certain to achieve momentum sufficient to break unprotected double strength annealed glass in mild category 2 hurricane conditions. Figure 2-2 summarizes these findings. Each icon in these plots shows the experimentally evaluated percentage of glass specimens (out of 20) that were damaged from an impact at a given debris type, momentum, and flight condition (from Masters et al. 2010). The tested specimens were common residential unprotected double strength annealed glass. The study confirms that the use of window protection to mitigate damage from windborne debris is appropriate.

Fernandez et al. (2010) continued the physical testing of the building envelope by measuring the performance of metal shutters under impact from concrete roof tiles and 2 x 4 lumber. Steel and aluminum shutters with different thicknesses were subjected to impact tests using a whole concrete roof tile (9 lb) and 2 x 4 lumber (9 lb) at a speed of 15.25 m/s. Permanent (plastic) and total (plastic and elastic) shutter deformations were recorded. Figure 2-3 shows an example of the results. The wide bars show deformation from tile impact, and the thin bars show deformation of that same product from lumber impact, all other conditions equal. The red bar indicates the distance between the

window and shutter for normal installation, thus any deformation beyond the red line indicates that the shutter failed to protect the window. The results indicate that there is a significant difference in the shutter deformation when impacted by the roof tiles and 2 x 4 lumber of identical weight and speed.

Shutter puncture was not observed in these tests, but known to occur from field observations. The current study (Laboy et al., 2012) is an extension of the work by Fernandez et al. (2010), focusing on impact of tile fragments on shutters (rather than whole tiles). The distribution of tile fragment sizes generated by a roof tile impacting a tile roof system, and the impact speed threshold for puncture of various metal shutter products (aluminum, steel, several gages) are quantified experimentally.

Following the experimental evaluation of the vulnerability of metal window shutters to puncture from roof tile fragments, this study also evaluates the likelihood of the occurrence of the conditions that produced puncture. For example, for two roof tile fragment sizes what is the flight distance, and wind speed (hurricane intensity) necessary to produce the experimentally observed punctures? To address this issue, a 2D windborne debris flight trajectory model was developed and used to provide some context for interpretation of the experimental results in terms of hurricane wind conditions. A review of flight trajectory models is presented next, followed by the presentation of the methodology and results of Laboy et al. (2012).

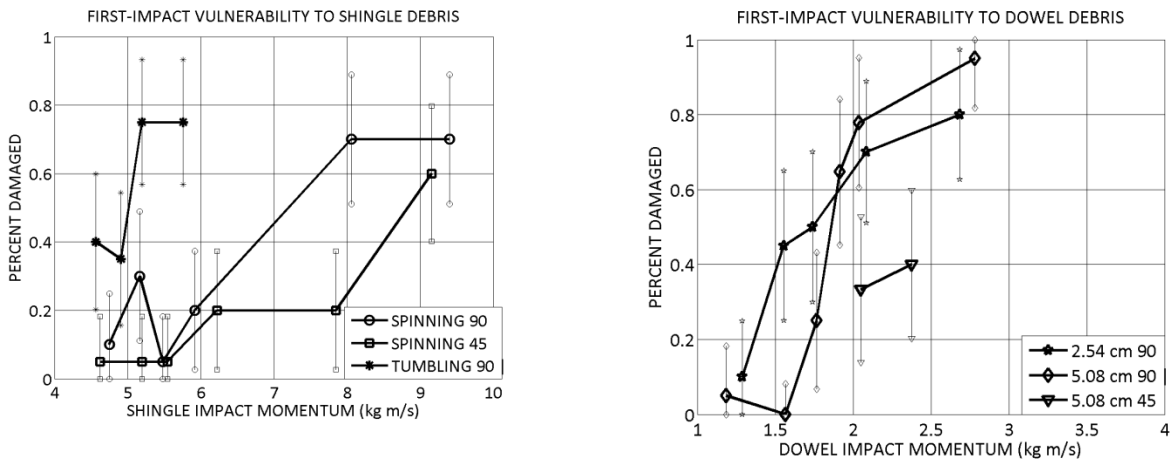

Figure 2-2. Vulnerability results for shingle and dowel impact. Probability of glass damage from impact as a function of debris momentum (Photos courtesy of Masters et al. 20010).

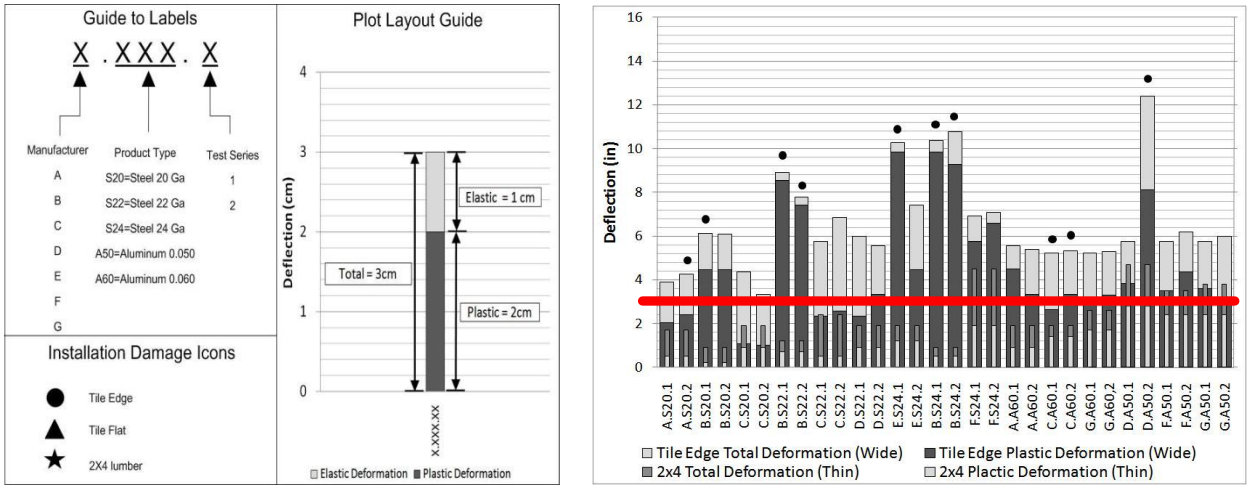

Figure 2-3. Metal shutter deformation from tile and 2x4 lumber impact. Red line is 3 inch shutter setback from glass (Photos courtesy of Fernandez et al. 2010).

2.1.3 Debris Models

During the past few decades researchers have developed numerical and experimental methods to predict the trajectory of WBD in two dimensional (2D) motions. Tachikawa (1983, 1988) conducted experiments to measure the trajectory of debris in a wind tunnel and compared the results with the numerical solutions by applying the two

dimensional equations of motion for square and rectangular flat plates in uniform flow. Wills, et al. (2002) modeled and validated a flight initiation condition. Wang (2003) conducted wind tunnel tests to investigate flight initiation speed and behavior for sheet debris. Holmes and Mullins (2001) presented an analysis that estimates the distance and travel time of debris. Holmes (2004) studied the trajectories of spheres in severe storm weather considering the effect of turbulence in the wind velocities. Lin, et al. (2006) conducted wind tunnel and full scale experiments to investigate the trajectory, and velocity of plate type debris. Holmes, et.al (2006) developed a numerical model of a square plate and presented a comparison of the results with the experimental data obtained from Tachikawa. Baker (2007) presented equations of motion for sheet and compact objects, and presented a comparison of the numerical solutions with experimental results of Tachikawa (1983) and Wills, et al. (2002). Visscher and Kopp (2007) studied the flight mechanics for a plate initially mounted on a roof of a 1:20 scale model to determine the motion type and the trajectory. Following this study, Kordi, et al. (2010) conducted experiments to analyze the flight of sheathing panels subjected to different wind directions. Kordi and Kopp (2009a) performed an analysis of windborne plates based on the quasi-steady model and compared the numerical solution with the experimental results from Tachikawa (1983) and Lin, et al. (2006). A dynamic analysis on the 2D equations for sheet debris by comparing aerodynamic coefficients of two models was conducted by Scarabino and Giacopinelli (2010) conducted. Richards, et al. (2008) presented a 3D model of the trajectory of windborne debris.

2.1.3.1 Tachikawa (1983, 1988)

Research that combines numerical simulation with wind tunnel was developed by Tachikawa (1983, 1988). In the 1980's he conducted experiments to measure the

trajectory of debris in a wind tunnel and compared the results with the numerical solutions by applying the two dimensional equations. The equations of motion for a two dimensional plates were presented in the study as:

$$m\ddot{x} = \frac{1}{2}\rho A\{(v-\dot{x})^2 + \dot{y}^2\}(C_D\, cos\beta - C_L sin\beta) \quad (2\text{-}1)$$

$$m\ddot{y} = mg - \frac{1}{2}\rho A\{(v-\dot{x})^2 + \dot{y}^2\}(C_D\, sin\beta + C_L cos\beta) \quad (2\text{-}2)$$

$$I\ddot{\theta} = \frac{1}{2}\rho Al\{(v-\dot{x})^2 + \dot{y}^2\}C_M \quad (2\text{-}3)$$

where $\beta = tan^{-1}\left\{\frac{\dot{y}}{(v-\dot{x})}\right\}$, ρ is the density of air, A is the area of the plate, l is the chord length, v is the wind velocity, g is the acceleration of gravity, m is the mass, I is the moment of inertia, and C_D , C_L, and C_M are the aerodynamic drag, lift, and moment coefficients , respectively.

Then, dimensionless variables $X = \left(\frac{g}{v^2}\right)x$, $Y = \left(\frac{g}{v^2}\right)y$, and $T = \left(\frac{g}{v}\right)t$ were applied in order to express the equations of motion in a dimensionless form.

$$\ddot{x} = K\{(1-\dot{x})^2 + \dot{y}^2\}(C_D\, cos\beta - C_L sin\beta) \quad (2\text{-}4)$$

$$\ddot{y} = 1 - K\{(1-\dot{x})^2 + \dot{y}^2\}(C_D\, sin\beta + C_L cos\beta) \quad (2\text{-}5)$$

$$\ddot{\theta} = \frac{K}{L_n I_n}\{(1-\dot{x})^2 + \dot{y}^2\}C_M \quad (2\text{-}6)$$

where the ratio of wind force due to gravity force $K = \frac{\rho v^2 A}{2mg}$, dimensionless chord length $L_n = \frac{gl}{v^2}$, and $I_n = \frac{I}{ml^2}$. Finally, the aerodynamic coefficients of auto-rotating (C_D , C_L, and $C_{M)}$ were measured experimentally from a wind tunnel test.

2.1.3.2 Holmes and Mullins (2001)

Based on previous work on flight initiation and trajectory of missiles, Holmes and Mullins (2001) addressed the mechanics of flying debris in severe wind storms. In the study they presented the airborne criteria in which debris after becoming airborne will continue to accelerate until: (1) its flight speed approaches the wind speed, or (2) it impacts the ground or an object, i.e., a building. Also, equations to determine the accelerating force, and the distance travelled (S) were defined.

2.1.3.3 Wills et al. (2002)

Wills et.al (2002) presented the debris flight initiation criteria. The model established a flight initiation condition for loose and better restrained debris which remained attach until: (1) wind loading exceeds the product of the weight and a friction coefficient, or (2) when lift force exceeds its weight, or (3) when the drag on it exceeds the friction force. Also, the speed at flight initiation for the three major debris classifications, e.g., particles, sheets, and rods objects, were presented in the study. In addition, the study introduced a damage function based on debris speed to predict the damage to the structure when impacted by debris.

2.1.3.4 Wang (2003)

Wang (2003) conducted wind tunnel tests to investigate the flight initiation speed and behavior for sheet debris subjected to different restrained forces. The experiment considered two types of restrained forces (1) loose objects when the restrained force is less than the weight of the object, and (2) fixed objects when the restrained force is greater than the weight of the object. The results were compared with Wills et.al (2002) and similar data was found.

2.1.3.5 Holmes (2004)

Holmes (2004) studied the flight characteristics of spheres. In the study equations to determine the horizontal and vertical acceleration of the sphere were defined as:

$$\frac{d^2x}{dt^2} = \frac{\rho_a C_D (U - u_m)\sqrt{[(U - u_m)^2 + {v_m}^2]}}{2\rho_m l} \quad (2\text{-}7)$$

$$\frac{d^2z}{dt^2} = \frac{\rho_a C_D (-v_m)\sqrt{[(U - u_m)^2 + {v_m}^2]}}{2\rho_m l} - g \quad (2\text{-}8)$$

Moreover, the effect of turbulence was incorporated into the calculations by using a method based on an inverse fast Fourier transform. For the spectral density of the horizontal component the von Karman was assumed and for the vertical component the Bush and Panofsky as defined in equations 2.9 and 2.10, respectively.

$$\frac{n.S_u(n)}{{\sigma_u}^2} = \frac{4(nl_u/\bar{U})}{[1 + 70.8(nl_u/\bar{U})^2]^{5/6}} \quad (2\text{-}9)$$

$$\frac{n.S_w(n)}{{\sigma_w}^2} = \frac{2.15(nz/\bar{U})}{[1 + 11.16(nz/\bar{U})^{5/3}]} \quad (2\text{-}10)$$

2.1.3.6 Lin et al. (2006)

Lin et.al (2006) conducted wind tunnel simulation and full scale tests for three types of debris: (1) cubes and spheres, (2) plates, and (3) rods to evaluate their mode of motion, trajectory, and velocity. The wind tunnel test was carried out at Texas Tech University where a digital video camera was used to record the flight time and coordinates. Horizontal and vertical displacements were calculated as follows:

$$x = 0.0105{x_c}^3 - 0.0415{x_c}^2 + 1.0474x_c - 0.1158 \quad (2\text{-}11)$$

$$z = z_c + 0.0004{x_c}^3 - 0.0012{x_c}^2 + 0.0238x_c - 0.0029 \quad (2\text{-}12)$$

where; x_c is the camera's x-coordinate, and z_c is the camera's z-coordinate. Horizontal and vertical velocities were obtained from the displacements.

2.1.3.7 Holmes (2006)

As a subset, the authors developed a numerical model of a square plate and compared the results with the experimental data obtained from Tachikawa. Horizontal, vertical, and angular acceleration of the plate were defined as:

$$\frac{d^2x}{dt^2} = \frac{\rho_a(C_D cos\beta - C_L sin\beta)[(U-u_m)^2 + {v_m}^2]}{2\rho_m h} \quad (2\text{-}13)$$

$$\frac{d^2z}{dt^2} = \frac{\rho_a(C_D sin\beta + C_L cos\beta)[(U-u_m)^2 + {v_m}^2]}{2\rho_m h} - g \quad (2\text{-}14)$$

$$\frac{d^2\theta}{dt^2} = \frac{\rho_a C_M Al[(U-u_m)^2 + {v_m}^2]}{2I} \quad (2\text{-}15)$$

2.1.3.8 Baker (2007)

Baker (2007) presented mathematical solutions of the general equations of motion for plates and compact objects in a dimension and dimensionless form. By applying Newton's second law in the horizontal, vertical, and rotational direction the general equations in the dimension form were defined as:

$$M\frac{d^2x}{dt^2} = \left(\frac{A\rho}{2}\right)(C_D\, cos\alpha - (C_L + C_{LA})sin\alpha)((U_w-u)^2 + (V_w-v)^2\ ) \quad (2\text{-}16)$$

$$M\frac{d^2y}{dt^2} = \left(\frac{A\rho}{2}\right)(C_D\, sin\alpha + (C_L + C_{LA})cos\,\alpha)((U_w-u)^2 + (V_w-v)^2\ ) - mg \quad (2\text{-}17)$$

$$I\frac{d^2\theta}{dt^2} = \left(\frac{(C_M + C_{MA})Al\rho}{2}\right)((U_w-u)^2) + (V_w-v)^2 \quad (2\text{-}18)$$

where; $sin\alpha = \frac{V_w - v}{\sqrt{((U_w-u)^2+(V_w-v)^2)}}$, m is the mass, I is the mass moment of inertia, U_w and V_w are the wind velocities in the horizontal and vertical direction, u and v are the debris velocities in the x and y directions, θ is the angular rotation, ρ is the density of air, l is

the reference length, C_D, C_L, and C_M are the quasi steady coefficients, and C_{LA} and C_{MA} are the lift force and pitching coefficients due to autorotation of the debris and were defined as follows.

$$C_D = 0.75\left(1 + 0.65sin\left(2\beta - \frac{\pi}{2}\right)\right) \quad (2\text{-}19)$$

$$C_L = 1.2sin(2\beta) \quad (2\text{-}20)$$

$$C_M = 0.2cos(\beta)\left(C_D sin(\beta) + C_L cos(\beta)\right) \quad (2\text{-}21)$$

$$C_{LA} = k_{LA}\frac{\omega}{\omega_m} \quad (2\text{-}22)$$

$$C_{MA} = k_{MA}\left(1 - \frac{\omega}{\omega_m}\right)\left(\frac{\omega}{\omega_m}\right) \quad (2\text{-}23)$$

where; $\omega_m = 0.64$, $k_{LA} = 0.4$, $k_{MA} = 0.12$, ω is the angular velocity, and β is the direction of the wind relative to the axis of the object as presented equation 2.24.

$$\beta = \theta + cos^{-1}\left(\left(\frac{\bar{U} + U' - \bar{u}}{\sqrt{(\bar{U} + U' - \bar{u})^2 + (V' - \bar{v})^2}}\right)\right) \quad (2\text{-}24)$$

2.1.3.9 Richards et al. (2008)

Richards, et al. (2008) presented the first known instance of a 3D model to predict the trajectory of windborne debris. A 6–DOF model was proposed based on wind tunnel experiments where damping and hysteresis effects were considered. Trajectories were found to be consistence with results obtained for a model scale.

2.2 Methodology and Results

A detail overview of the methodology and results of the three phases and findings can be found in Appendix A which contains the manuscript in the form that it will be appear in the in the Journal of Wind and Structures. Two experimental phases (conducted by another graduate student) addressed the performance of tile roof

systems and metal shutters under RTD impact. A numerical modeling phase (conducted by Laboy) addresses the RTD during flight, and provides some context for interpretation of the experimental results in terms of hurricane wind conditions. Phase 1 experimentally quantified the statistical distribution of tile fragment sizes (ratio of tile fragment weight to full tile weight) produced when a tile roof system is impacted by a tile. This provided guidance regarding appropriate fragment sizes to use for phase 2. Phase 2 experimentally quantified the probability of metal shutter puncture when impacted by a tile fragment. Phase 3 numerically evaluated the velocity of a tile fragment impacting the roof and windows of a house through the use of a trajectory model and coefficients adopted from the literature (Tachikawa 1983,1988, Holmes 2004, Holmes, et al. 2006, Baker 2007, Lin, et al. 2007, Kordi and Kopp 2009b]. The outcomes of the three phases were combined to provide an assessment of the risk of tile fragments puncturing shutters as a function of wind conditions.

2.3 Chapter Summary

Chapter 2 presented the vulnerability of roof tile systems and metal hurricane shutters to roof tile debris (RTD). The methodologies available to predict the 2D motion of windborne debris were also introduced in order to address their shortcomings and limitations within the framework of the proposed research. The literature review assisted in identifying the approach that should be selected for this study. A detail explanation of the methodology used to address the aspects of the problem within the context of roof tile fragments impacting metal hurricane shutters were also presented (Appendix A). The results of all three phases were combined to provide the probability of metal shutter puncture in reference to the Saffir-Simpson Hurricane Wind Intensity rating scale. The

findings correlate strongly with observations made by some of the authors after Hurricane Charley.

CHAPTER 3
REVISITING THE WIND DIRECTIONALITY FACTOR IN ASCE 7: BACKGROUND AND LITERATURE REVIEW

The directionality factor (K_d) used in the ASCE 7 wind load provisions for components and cladding is a load reduction factor intended to take into account the less than 100% probability that the design event wind direction aligns with the worst case building aerodynamics. There is concern that in hurricane prone regions the current value of K_d underestimates the real vulnerability of the building system due to building envelope components that are susceptible to damage from multiple wind directions, and hurricane events with high wind speeds that include a significant direction swath. In the case of, for example, roof corners, the likelihood of the worst aerodynamics aligning with the direction of strongest winds for at least one roof corner is significantly increased, and thus so is the probability of damage to at least a portion of the roof. Similarly, windows are typically located on all elevations and collectively very likely to experience the worst wind direction, particularly given the multiple approach directions of high winds during a hurricane.

A three part study evaluates the efficacy of the current incarnation of the K_d factor for hurricane prone regions. This chapter presents part one of the study, consisting of a review of the initial development of the K_d concept, as well as a comparison of how wind directionality is addressed in fifteen building standards from around the world. Parts 2 and 3 of the study (Chapters 4 and 5) analyze existing wind tunnel datasets, coupling the directional load data with historical hurricane winds. A directionality factor for hurricane prone regions will then be developed using the current

state of knowledge of extreme winds, which has progressed since K_d was first developed.

The proposed definition of K_d explicitly incorporates the random nature of the pressure coefficients, the unknown orientation of a building with respect to approach wind direction, and the influence of extreme wind duration and direction change associated with a hurricane passage.

This hurricane duration and direction change issue is currently not considered in the ASCE 7 wind load provisions. In fact it can be argued that this important aspect of loading is explicitly excluded by applying the current K_d value of 0.85 for components and cladding, which was derived based upon the concepts of: 1) a single design gust approaching from one direction, and 2) components and cladding damage treated as a first-passage problem rather than a low cycle fatigue phenomenon. Neither of these concepts has been shown to be valid for hurricane wind events, and do not correlate well with observed hurricane wind induced residential component and cladding damage.

3.1 Introduction

Chapters 3, 4 and 5 address the FEMA Region IV Capabilities Gap 2010-M-014: Research into the adjustment of the K_d factor in ASCE 7. The following excerpt from the Capabilities Gap Statement provides the motivation for the current study:

"The current value of K_d used in ASCE 7 is designed to take into account the probability that the wind directions associated the strongest winds aligns with the worst aerodynamic coefficient. This assumption is reasonable for a single component such as a single garage door that is located on one side of a building. In the case of a roof corner, where there are usually four separate corners the likelihood of the worst aerodynamics aligning with the wind directions associated the strongest winds is

significantly increased, and consequently ,so is the probability of failure of the roof (if failure is defined as the loss of a roof panel on any corner). Similarly, windows are usually located on all 4 walls and the likelihood of at least one wall experiencing the worst wind direction, worst coefficient combination is higher than for a component located on one wall.

A proposal to eliminate K_d for components and cladding was put forward for consideration in the last cycle of ASCE 7 but was defeated because there was no data to support the proposal. Current modelers and researchers who support the development of codes and standards feel that the current value of K_d used in the standards and codes underestimates what might result in building damage and failure. Without performing these studies, K_d for components and cladding will continue to be a constant value of 0.85 likely leading to underestimates of the true design loads for many components."

The above problem statement implies that the current K_d value of 0.85 in ASCE 7 is not conservative. However, this position was not assumed in the current study. This study is developed and conducted with no pre-disposition as to the appropriateness of the current K_d value of 0.85 in ASCE 7. The goal is to provide evidence that either defends or suggests modifications to the current K_d value. This is a controversial and important topic, as ASCE 7 is referenced by many widely used codes and standards documents (e.g., Florida Building Code, International Building Code).

The wind directionality factor (K_d) has been included in the load combination equations since the early 1980's in the ASCE 7, previously ANSI A58.1. The 1.3 wind factor used between 1982 until 1995 included a wind directionality factor of 0.85

(i.e.,Ellingwood et al. 1980 and Ellingwood 1981). In 1998, the ASCE 7 task committee on wind loads separated the wind directionality effect from the load combinations and presented it as an independent factor. At this time the load factor was also changed from 1.3 to 1.6 in order to balance both sides of the equation. The wind directionality factor inherent in the load combination was of 0.85 and the load factor needed for balance was therefore 1.53. However, the load factor of 1.6 was implemented for simplification purposes (i.e., rounding effects). The value of 1.6 lends additional safety that represents an effective K_d of ~ 0.89.

Currently, the directionality factor is used in the velocity pressure calculation as defined in Eq.3-1. (ASCE 7-10 Eq. 27.3-1)

$$q_z = 0.00256 K_z K_{zt} \boldsymbol{K_d} V^2 \qquad (3\text{-}1)$$

where: q_z is the velocity pressure (psf), K_z is the pressure exposure coefficient based on height z above ground level and exposure type, K_{zt} is the topographic factor, V is the basic wind speed (mph) that is specific to the region. K_d is the directionality factor that ranges from 0.85 to 0.95, dependent on the structural type as shown Table 3-1 (ASCE 7-10 Table 26.6-1). The K_d being considered in this study is indicated in bold in Table 3.1.

Figure 3-1 illustrates a wind speed and direction time history measured at 33 ft (10 m) near a residential neighborhood in Vero Beach, FL during Hurricane Jeanne (2004). As can be seen, the strongest winds were sustained over a 5 hour period with a direction swath of 135 degrees. A potentially design level wind load may not occur from a single direction as implied by the current K_d implementation. This chapter presents a literature review of the initial development of the K_d concept, as well as a comparison of

how wind directionality is addressed in fifteen building codes. Chapters 4 and 5 present details of the proposed methodology and findings.

Table 3-1. Directionality Factor (ASCE 7-10 Table 26.6-1)

Structural Type	Directionality Factor, k_d
Buildings - Main Wind Force Resisting System - ***Components and Cladding***	 0.85 ***0.85***
Arched Roofs	0.85
Chimneys, tanks, and similar structures - Square - Hexagonal - Round	 0.90 0.95 0.95
Solid freestanding walls and solid freestanding and attached signs	0.85
Open signs and lattice framework	0.85
Trussed Towers - Triangular, square, rectangular - All other cross sections	 0.85 0.95

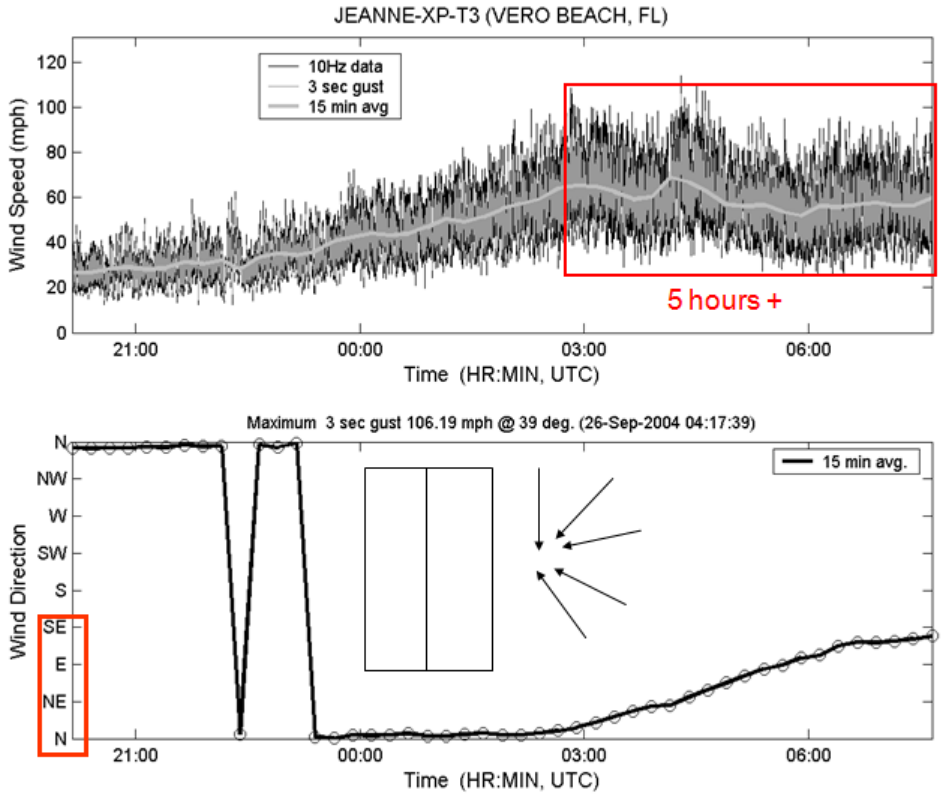

Figure 3-1. Hurricane Jeanne (2004) wind speed and direction time history.

3.2 Background

During the past 40 years, wind directionality effects on structures have been considered in the assignment of design wind loading. A brief summary of critical works is presented next, followed by a more detailed presentation of these studies.

Davenport (1969) noted that wind may approach from any direction, leading to different responses. The importance of including wind directional effects in the prediction of design loads was highlighted by Vickery (1974). A methodology that derives a wind reduction factor from a Rayleigh distribution was developed by Davenport (1977). Following Davenport, Holmes (1981) estimated wind reduction factors for seven response variations and four mean recurrence intervals. The author

concluded that the values obtained are higher than the range of 0.75 to 0.85 suggested for application in standards. Afterward, Holmes (1986, and 1990) presented a methodology following an Extreme Values Type I distribution to obtain reduction factors for wind direction; however, reduction factors were not reported. Simiu and Filliben (1981) determined reduction factors for non-hurricane regions and eight cardinal directions leading to the conclusion that it is not appropriate to multiply loads by a reduction factor of 0.80 to account for wind directionality effect. The development of a directional factor using Fisher Tippet Type I distribution to fit the directional extreme values assuming that the wind comes from an independent direction was introduced by Cook (1983). Cook and Miller (1999) presented a correction to the directionality methodology presented by Cook (1983), wherein the directional factors were adjusted to account for exposure. The effect of wind direction for cases where the structural orientation is known and unknown based on Davenport's approach with a minor difference was studied Wen (1983). Huang and Rosowsky (2000) analyzed the effects of wind direction on low-rise structures in hurricane prone regions to estimate wind speed and load directionality factors. Vega (2008) proposed a reliability-based approach to account for wind directionality effects on low-rise buildings located in non-hurricane regions. The study performs a probabilistic analysis to provide estimates of wind load and wind directionality factors using full scale pressure data. Vega (2008) recommends eliminating the wind directionality factor from codes/standards until appropriate calibrations between the wind directionality factors and load coefficients are performed. Recently, Isymov et al. (2013) studied the effects of wind directionality for 3 tall buildings located in extra-tropical and tropical climates. The study applied four different methods

and used two different locations in order to capture any differences with respect to the wind directionality effect. Based on the results the authors recommended a K_d factor of 0.90 for hurricane prone regions.

3.2.1 Davenport (1977)

Davenport observed that the implementation of directional influence in codes and standards can be difficult since buildings are usually built without knowing the orientation of the worst wind. An approach was presented by considering dependencies related to wind speed distributions and ignoring direction in the structural response. A response relationship was defined as in Eq.3-2:

$$R = \frac{1}{2}\rho V^2 C(\theta) \qquad (3\text{-}2)$$

where: ρ is the air density, V is the wind speed, and $C(\theta)$ is the variation of the aerodynamic coefficient as a function of direction Θ. Three directional variations were evaluated:

Case A. $C(\theta) = 1$

Case B. $C(\theta) = cos^2\theta$ $\quad -\frac{\pi}{2} < \theta < \frac{\pi}{2}$, θ = 0 elsewhere

Case C. $C(\theta) = \delta(\theta)$ C = 1 when θ = 0, C =0 elsewhere

Case A represents the scenario that the worst response arises regardless of the wind direction and is used as a frame of reference. Case B represents the scenarios between the lower (conservative case A) and upper limit (Case C). Case C represents the responses that are dependent on direction. A Rayleigh distribution was used to derive response boundaries and crossing rates for the three directional variations. A Type I extreme value distribution for annual responses was presented for each case. Davenport concluded from the annual extreme distributions that the factor that varies

the most due to the direction effect is the mode. Case A was used to normalize in order to calculate the wind direction factors (ϕ): Case A = 1.0, Case B = 0.72, Case C = 0.56.

3.2.2 Holmes (1981, 1986, and 1990)

In Holmes (1981), wind reduction factors for seven response variations and four mean recurrence intervals were calculated. Holmes concluded that the values obtained are higher than the range of 0.75 to 0.85 suggested for application. Holmes (1986, 1990) presented a methodology following an Extreme Values Type I distribution to obtain reduction factors for wind direction; however, reduction factors were not reported. Holmes stated in 1986 that a reduction factor of 0.9 on wind speeds and 0.81 on pressure forces is recommended for the Australia non-cyclonic wind speeds. Holmes (1990), cited that a reduction factor of 0.95 on wind speed was implemented in the Australian Standard (AS 1170) based on a committee decision following the approaches presented by Davenport (1977), and Holmes (1981).

3.2.3 Simiu and Filliben (1981)

This study presented an approach to estimate the design wind loads for a given mean recurrence interval considering directional effects for cladding panels and rigid structures located in non-hurricane regions. Random variables were defined to represent the maximum annual wind effect (e.g., pressure, force, etc). The best cumulative probability distribution that fits the data generated from the random variable for a consecutive amount of years was found. The study presented an application where four ratios were obtained for different locations for a 20 and 50 years period. The authors concluded that it is not appropriate to multiply loads by a reduction factor of 0.80 to account for wind directionality effects. The authors stated an intention to extend the approach to hurricane prone regions.

3.2.4 Cook (1983) and Cook and Miller (1999)

Cook (1983) presented the development of three factors to quantify the variation of dynamic pressure. These factors are: statistical (C_T), directional (C_θ), and seasonal (C_s). Only the directional factor is presented herein. The approach first introduced $c_\theta\{\theta\}$as the ratio of the 50 years return period dynamic pressure for a specific direction ($q_{50}\{\theta\}$) to the basic dynamic pressure. The approach used a Fisher Tippet Type I distribution to fit the directional extreme values and assumes that the wind comes from an independent direction. The directional factor for a standard risk of 0.02 was defined as in Eq.3-3

$$C_\theta\{\theta\} = kc_\theta\{\theta\} \quad (3\text{-}3)$$

where *k* is the scaling parameter found to have a consistent value of 1.24 in the United Kingdom (U.K.) region. Table 3-2 presents a summary of the proposed values of directional factor for U.K. that were computed for the standard overall risk of 0.02.

Cook and Miller (1999) presented a correction to the directionality methodology presented by Cook (1983), wherein the directional factors were adjusted for exposure. Also, a new equivalent factor on wind speed (k_v) was defined as in Eq.3-4:

$$k_v = \frac{wind\ speed\ with\ 0.02\ annual\ risk\ overall, equally\ distributed\ by\ sector}{wind\ speed\ with\ 0.02\ annual\ risk\ in\ 30^\circ\ wide\ sector} \quad (3\text{-}4)$$

The directional factors were normalized in the direction of the strongest wind (Θ = 240º) for unity. The authors concluded that no design safety was affected by using the previous approach.

Table 3-2. Directional Factors (C_θ) for United Kingdom (from Cook 1983)

Direction (deg.)	Directional Factor (C_θ)
0	0.66
30	0.57
60	0.59
90	0.59
120	0.58
150	0.69
180	0.80
210	0.95
240	1.10
270	1.07
300	0.91
330	0.74

3.2.5 Wen (1983)

This study presented the effect of wind direction on structural reliability based on Davenport's approach with a minor difference for cases where the structural orientation is known and unknown. The wind direction effect was analyzed assuming that the structural orientation is unknown, where outcrossing rates and the probability of annual maximum response were derived. Reductions factors were obtained to measure the sensitiveness of the response to wind effects following two different response functions. The study also investigated the effect of wind direction when the structure orientation is known, but reduction factors were not reported. It was found that for cases in which the orientation of the structure is unknown the failure rate is relative to the "effective direction window width" leading to reductions in the response with respect to worst direction case. In contrast, for cases that the orientation is known sensitivity to the orientation is found.

3.2.6 Ho (1992)

This study presents the variability of wind loads on low buildings due to the effects of surroundings. Aerodynamic data was measured for four identical flat-roofed

buildings randomly located for cases where surroundings (a radius of ~ 1,100 ft) and isolation effects are considered. A Monte Carlo approach was used to account for the variations of wind loads attributable to building shape, length, width, height, roof slope, immediate surroundings and exposure. A reduction of the aerodynamic data to account for the wind directionality effects was calculated for the variations considered in the study (i.e., various sizes, surroundings, upstream exposure) following Davenport approach. A mean value of 0.75 was obtained which justify the value of 0.8 used in most codes and standards. Also, the variability of parameters, such as reference dynamic pressure, exposure factors, and peak coefficients were statistically analyzed. The results proved that using isolated buildings wind loads are close to the worst case and by considering the surroundings effects wind loads are reduced.

3.2.7 Huang and Rosowsky (2000)

This study evaluated the effects of wind direction in low-rise structures in hurricane prone regions. Florida (FL) and South Carolina (SC) were chosen as case studies to evaluate the directionality effects. All terrains were assumed to be located in open terrain. The study simulated 15,000 and 31,500 hurricane events for SC and FL, respectively, in which the maximum wind from each direction and the average wind speeds were saved. The wind speed or load directionality factor was defined as the ratio of the N year mean recurrence interval (MRI) wind speed or wind load in each direction divided by the non-directional N-year MRI. The values were normalized by the non-directional MRI in order to make them applicable for regions that have the equivalent wind climate and are located a similar distance from the coast. The directionality factors obtained range from 0.43 to 0.98 for 16 cardinal directions and four MRI for the areas of Charleston, Columbia, Miami, Orlando, and Panama City. The

authors concluded that the factors increase as the wind approaches from the water and as the MRI increases. Exposure adjustments were defined.

3.2.8 Vega (2008)

This methodology used the probability distributions of wind speeds with respect to wind direction and followed the independent storm method for the extreme value analysis. Wind speed exposure corrections and a process that separates extreme wind speeds from records with smaller duration via atmospheric pressure were also presented. The study presented a probabilistic analysis to provide estimates of wind load and wind directionality factors. The wind directionality factors were defined by building zone for a given MRI using full scaled pressure data.

A prefabricated metal building mounted in a turntable (30ft W x 45ft L x 13 ft H) with 204 pressure taps was used as a full scale model to measure the point pressure coefficients as defines Eq.3-5. The experimental setup consisted of 693 runs of 15 minutes.

$$C_{p,T}(t) = \frac{p(t) - p_o(t)}{\frac{1}{2}\rho_{air} * [V_{o,T}(t)]^2} \quad (3\text{-}5)$$

where, p (t) is the induced surface pressure, p_o (t) is the ambient static atmospheric pressure, V_o is the wind speed at reference height. The aerodynamic data was divided in 16 sectors for every 22.5 degrees where the maximum loading coefficients were retained. This data was used to decouple the pressures measured at the building surfaces by calculating a pseudo pressure coefficient (Eq.3-6) for 15th, 37th, 50th, 63th, 80th , and 95th percentiles which are then used for the extreme analysis for a 1 hour period.

$$\widetilde{C_{p,T}} = C_{p,T}(t) * \frac{1}{{G_T}^2} \quad (3\text{-}6)$$

where G is the ratio of the peak to mean wind speed over in time T. However, for the analysis area average pressure coefficients are used for the calculations involved in the process. For the directional analysis the author uses a combination of the sector by sector and one directional approach. The one directional approach uses annual maxima data and a pseudo pressure coefficient that has been attributed to a specific sector for an assigned building orientation as

$$\widehat{X_{T,\iota}}(\theta) = \frac{1}{2} * \rho_{air} * \max\left[\widetilde{C_{p,T}}(\theta) * \left[\widehat{V_{T,\iota}}(\theta)\right]^2\right] \quad (3\text{-}7)$$

where C_p is taken from wind tunnel or full scale data for each direction and V corresponds to the annual maxima for each direction extracted from meteorological data from over 20 years.

Vegas stated two limitations related with this method: (1) variations of the peak or pseudo steady loading coefficients for a given sector are not considered and (2) it assumes that the extreme wind speed occurs at the same time that the maximum loading coefficient. On the other hand, the sector by sector approach performs extreme analysis for each direction independently.

Since the author decoupled the pressure coefficients (Eq.3-6) the two variables used (V_{peak} and C_{p_pseudo}) for the load effects calculations were assumed to be independent and the joint probability was used. A Monte Carlo simulation was used to recreate the Fisher Tippet Type I distributions for the appropriate M-highest (5^{th} highest was used) for each year since non-deterministic approach is assumed due to the fact

the highest speed of a particular year might not coincide with the peak load coefficient.

The Monte Carlo process consists of 50,000 trials for the 5th highest as follows:

- Step 1: the parameters mode (U) and dispersion (1/α) are determined to obtain the product of Uα.
- Step 2: a matrix n x n (based on the method of independent storms) that contains years of probabilities is generated.
- Step 3: the reduced variate y_v is obtained [$P = \exp(-\exp(-y)]$ and sort in ascending order.
- Step 4: the M-highest values of y_v are selected (5-highest was used)
- Step 5: a trial of probabilities of five is generated using uniform random generator in order to solve for the variate y_v following [$P = \exp(-\exp(-y)]$
- Step 6: using the results obtained in step 1, 3, and 5 a non-dimensional peak wind load can be obtained as $\hat{x} = \left[1 + \frac{y_c}{\alpha_c U_c}\right] * \left[1 + \frac{y_v}{\alpha_v U_v}\right]^2$
- Step 7: out of the five generated peak wind loads for a year (trial)the maximum value from the extreme analysis from step 9 is save
- Step 8: steps 1 through 7 are repeated N times (50,000 simulations were used)
- Step 9: the N maximum non-dimensional peak wind loads are sorted in ascending order.
- Step 10: the values in the Gumbel plot are used to extract peak wind loads

A pseudo MRI was set for the directional extreme value analysis following the pseudo MRI concept used in wind engineering. Two assumptions were considered for the wind directionality factor: (1) the parameters (mode and dispersion) of the three highest directions were assumed to eliminate the effects of other directions with smaller wind speeds and (2) a random orientation of the building (β) determines the reductions related to a specific building component or zone. Five building orientations (β =0, 195, 240, 270, and 285 with respect to north) were considered in defining the angle of attack as shown in Fig. 3-2. The building zones were defined based on similarities in the wind flow regimes. The wind directionality factor of a building zone or component for non-hurricane regions (Eq.3-8 to 3-11) is obtained for each design wind direction considered (j= West 270°, West-Northwest 292.5°, and Northwest 315°) where a randomly drawn single set of FT1 parameters (mode and dispersion) is picked for a random angle of

attack. This process was repeated 1000 times (N) where the maximum wind direction is retained.

$$K_{d,i}(MRI, BldgZone) = \frac{max<|\widetilde{C_{p,T}}(\theta) * [V_{T,\widetilde{pseudo}-MRI}(\theta)]^2|}{|max_\theta[\widetilde{C_{p,T}}(\theta)] * max_\theta[\widetilde{V^2}_{T,MRI}(\theta)]} \quad (3\text{-}8)$$

$$K_{d,i}(MRI, BldgZone) = \frac{max_j<|X_{T,Pseudo-MRI,J,i}\{\theta_v=\widetilde{J_{1,\ldots,}J_{16}}, \alpha_{c,i}[rand(\beta_i)]\}}{\frac{1}{2}|max_\theta[\widetilde{C_{p,T}}(\theta)] * max_\theta[\widetilde{V^2}_{T,MRI}(\theta)]} \quad (3\text{-}9)$$

$$\overline{K_d}(MRI, BldgZone) = \frac{\sum_{i=1}^{N} K_{d,i}}{N} \quad (3\text{-}10)$$

$$\sigma_{K_d}(MRI, BldgZone) = \sqrt{\frac{1}{N}\sum_{i=1}^{N}(K_{d,i} - \overline{K}_d)^2} \quad (3\text{-}11)$$

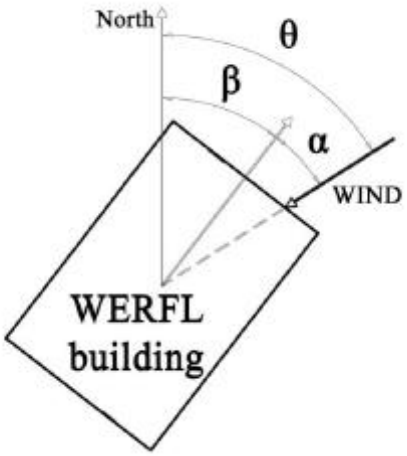

Figure 3-2. Wind direction (Θ), building orientation (β) and angle of attack (α) definitions (Photo courtesy of Vega 2008).

The results were presented for four MRI and different building zones having a range of 0.45 to 0.84 for claddings and 0.70-1.07 for external forces. Coefficients of variation and probabilities of exceedance of the wind directionality factors were determined. Based on results it was found that the wind directionality factor is not sensitive to the MRI. Vega recommended eliminating the wind directionality factor from

codes/standards until appropriate calibrations between the wind directionality factors and load coefficients are performed.

3.2.9 Isyumov et al. (2013)

Recently, the effects of wind directionality were study for 3 tall buildings located in extra-tropical and tropical climates. In order to experience the variations between extra-tropical and tropical climates the study considered two locations one in the gulf coast and one in the mid-west. The study used wind tunnel data and predicted the extreme values following four different methods: (1) worst case, (2) sector by sector, (3) upcrossing, and (4) a time domain analysis. The worst case method ignores any dependencies between the aerodynamic data and wind direction. The sector by sector considers the dependencies of the aerodynamic data and the wind direction, but does not consider the difference of wind events with respect to the sector. The upcrossing event was first introduced by Davenport (1977) which uses all the wind speed and direction data rather than relying on extreme values. The fourth method is the time domain analysis which considers the variation of the wind speed and direction through the storm duration. The wind directionality factor (K_d) was determined with respect to the building acceleration and moment for each method as

$$K_d = \frac{Prediction\ obtained\ for\ a\ particular\ method}{Correponding\ to\ the\ worst\ case\ (method\ 1)} \quad (3\text{-}12)$$

The study determined that the current $K_d = 0.85$ can be conservative for the acceleration, however, might be around average for the moment response. Also, it was found that for tropical winds the current K_d value might not be conservative. Based on the results presented in the study the authors recommended to use a $K_d = 0.90$ for hurricane prone regions.

3.3 Wind Directionality Factors in Building Codes and Standards

Fifteen building codes/standards from around the world (Figure 3-3) were reviewed to verify whether an independent factor that captures the wind directionality is incorporated within the wind load provision (Table 3-3). Of all the codes/standards reviewed, eight have implemented an independent wind directionality factor. However, others may have a reduction factor in the load combinations.

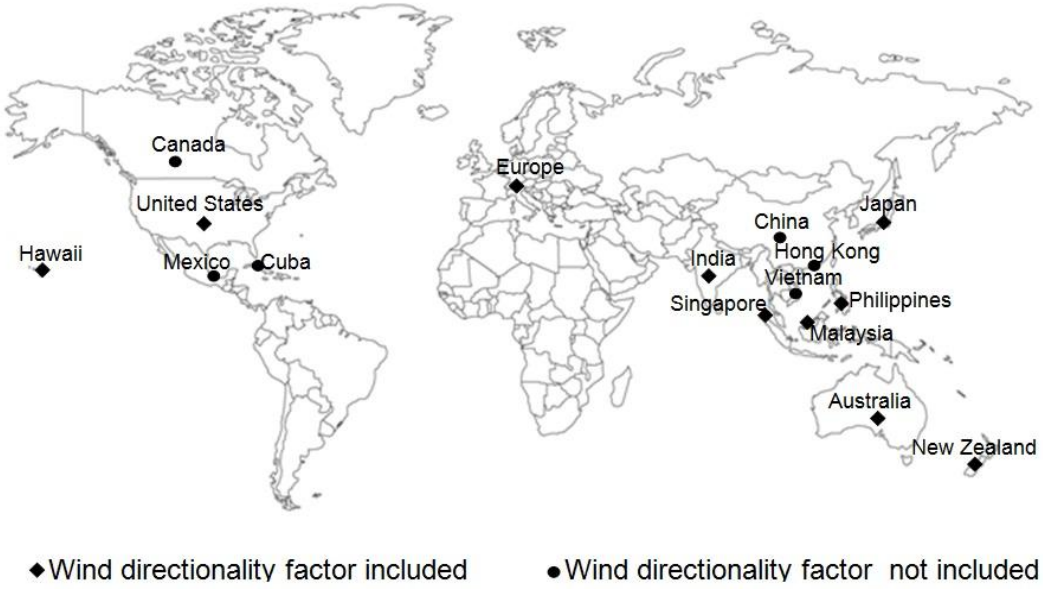

Figure 3-3. Building codes/standards reviewed (Map courtesy of http://www.theodora.com/maps).

3.3.1. ASCE 7

Ravidra et al. (1978) proposed to implement a reduction factor based on Davenport's (1977) work and other criteria. Ellingwood (1979, 1980, and 1981) suggested a reduction factor of 0.85 to account for wind directionality effects in the A58 standard. The wind directionality factor has been included in the load combination equations since the early 1980's in ASCE 7, previously ANSI A58.1. The 1.3 wind factor

used between 1982 until 1995 (Table 3-3) included a wind directionality factor of 0.85 (ASCE 7-98). As stated in the commentary of the ASCE 7-98, the factor is intended to capture the reduced probability that maximum winds approach from the worst direction. In 1998, the ASCE 7 task committee on wind loads separated the wind directionality effect from the load combinations and presented it as an independent factor to be used in the velocity pressure calculation. The K_d factors range from 0.85 to 0.95, dependent on the structural type for cases that the load combinations are used.

Table 3-3. ANSI A58.1 and ASCE 7 Load Combinations

Year	Load Combinations Strength Design *
1972	This method is not used shows the load combinations
1982	1.2D+**1.3W**+0.5L+0.5(L_r or S or R) 0.9D-(**1.3W** or 1.5E)
1988	1.2D+**1.3W**+0.5L+0.5(L_r or S or R) 0.9D-(**1.3W** or 1.5E)
1993	1.2D+**1.3W**+0.5L+0.5(L_r or S or R) 0.9D-**1.3W** or +1.5E)
1995	1.2D+**1.3W**+0.5L+0.5(L_r or S or R) 0.9D+(**1.3W** or 1.0E)
1998	1.2D+**1.6W**+0.5L+0.5(L_r or S or R) 0.9D+**1.6W**+1.6H
2002	1.2D + **1.6W** + L + 0.5(Lr or S or R) 0.9D + **1.6W** + 1.6H
2005	1.2D + **1.6W** + L + 0.5(Lr or S or R) 0.9D + **1.6W** + 1.6H
2010	1.2D + **1.0W** + L + 0.5(Lr or S or R) 0.9D + **1.0W**

3.3.2. Australian and New Zealand Standard (AS/NZS 1170.2)

In the 2002 ed., the wind directional multipliers (M_d) were introduced and obtained from probability distributions of gust wind speeds from meteorological data. AS/NZS 1170.2 followed the assumption that the probability of a certain load occurring

is restricted to two 45° directional sectors, but stated that this is not valid for circular structures. However, it is cited that any assumption should be based on a probability analysis, such as the one presented by Davenport (1977), Simiu and Filliben (1981), Holmes (1981), and Melbourne (1984). The M_d values range between 0.80 to 1.0 which are presented for nine cardinal directions and two regions of Australia and New Zealand. For all other regions, M_d should be taken as 0.95 or 1.0 depending on the structure type.

3.3.3. British Standard (BS 6399-2)

The BS 6399-2:1997 is the last instance of the British Standard (BS) before the implementation of the Eurocode and the subsequent changes to National Annexes. However, it is the design guideline which remains in force in Singapore. S_d is the direction factor implemented in 1995 ed. that works as an adjustment to reproduce wind speeds with the same risk of exceedance in any direction. The BS 6399-2 states that these factors have been adjusted for the UK region and were obtained based on the analysis of maximum wind speeds from each 30° wind direction sector. The standard provides the directional factors for wind direction of 30° increments ranging from 0.73 to 1.0 for cases that the orientation of the building is known. Otherwise, S_d should be taken as 1.0.

3.3.4. Eurocode 1: Actions on Structures -Wind Actions

The European Standard has been implemented in the following countries: Austria, Belgium, Cyprus, Czech Republic, Denmark, Estonia, Finland, France, Germany, Greece, Hungary, Iceland, Ireland, Italy, Latvia, Lithuania, Luxembourg, Malta, Netherlands, Norway, Poland, Portugal, Slovakia, Slovenia, Spain, Sweden, Switzerland and United Kingdom. A directional factor (c_{dir}) is presented and taken as 1.0

if further recommendations are not found in the country specific National Annexes. Of the National Annexes reviewed, Denmark's Annex is the only one that does not retains a unit value and presents a table for wind direction of 30° increments for a range of 0.80 to 1.0.

3.3.5. Honolulu

The city and county of Honolulu follows ASCE-7. However, site specific topographic effects and directional factors were estimated (Chock et al. 2005 and Chock and Yu 2013). The procedure to derive the wind directionality factor is composed of two steps. First, using the value of 0.85 from the ASCE 7 the hurricane wind outcrossing exceedance probability was determined. Second, the directionality factor K_d associated with the selected response function is determined to guarantee an exceedance probability that corresponds to the control site. Directional factors were developed for Main Wind Force Resisting System (MWFRS) and components and claddings (C&C) for topographic locations in the area of Oahu, Hawaii. For non-buildings structures the K_d factors from the ASCE 7 should be adopted. The K_d values range from 0.65 to 0.95. Some of the values presented in Chock et al. (2005) differ by a factor of 0.05 to 0.10 from the values implemented in the Honolulu Building Code.

3.3.6. India (IS 875, part 3)

The third revision of IS 875 part 3 (2003-2004) introduced a wind directional factor (K_d). This factor was taken as 0.9 except for circular/axisymmetric sections and cyclonic regions when a value of 1.0 should be used.

3.3.7. Japan (AIJ RLB 2006)

In the 2004 revision the wind directionality factor (K_D) was incorporated to represent the directional characteristic of the extreme wind that is dependent on the

geographical location. The commentary in AIJ RLB 2006 indicates that Monte Carlo simulation and statistical analysis of non-typhoon observation were performed to calculate the K_D. According to Tamura et al. (2003) the K_D factor was defined as the ratio of the average directional wind speed (U_D) to the 100 year recurrence basic wind speed (U_o), setting a lower limit of 0.85 due to tornado and downburst effects. Factors with a range between 0.85 to 1.0 for 142 cities and eight cardinal sectors were obtained.

3.3.8. Malaysian Standard

The MS 1553 is the wind provision in force. M_d is the wind direction multiplier that is implemented as 1.0.

3.3.9. National Structural Code of the Philippines

The wind loads procedure was adopted from ASCE 7-05. K_d are the same as in ASCE 7.

3.4 Chapter Summary

A review of development and application of wind directionality effects was presented. Researchers such as, Davenport (1977), Holmes (1981, 1986), Simiu and Filliben (1981), Wen (1983), Cook (1983), and among others, have developed methodologies based on probability analysis to incorporate wind directionality effect into the design process. Some building codes and standards around the world have included reduction factors.

Table 3-4. Wind Directionality Factor in Building Codes/Standards

Country/Region	Code	Wind Directionality Factor		Intended Use	
		Symbol	Values		
Australia & New Zealand	AN/NZS 1170	M_d	0.80-1.0	Wind site speed	$V_{sit,\beta} = V_R \boldsymbol{M_d} (M_{z,cat} M_s M_t)$
Canada	NBCC	NI	NI		NI
China	GB 50009-2001	NI	NI		NI
Cuba	NC 285	NI	NI		NI
Europe	Eurocode (BS EN 1991-1-4)	c_{dir}	1.0	Basic wind speed at 10m	$v_b = \boldsymbol{c_{dir}} c_{season} v_{b,0}$
Czech Rep	National Annex	c_{dir}	1.0		
Denmark	National Annex	c_{dir}	0.8-1.0		
Finland	National Annex	c_{dir}	1.0		
France	National Annex	c_{dir}	1.0		
Germany	National Annex	c_{dir}	1.0		
Romania	National Annex	c_{dir}	1.0		
Hong Kong	Code of Practice	NI	NI		NI
Honolulu	Honolulu Building Code/ Chock (2005)	K_d	0.65-0.95	Velocity pressure	$q_z = 0.00256 K_z K_{zt} \boldsymbol{K_d} V^2$
India	IS 875 (Part 3)	K_d	0.9 &1.0	Design wind pressure	$p_d = \boldsymbol{k_d} k_a k_c 0.6 (V_b k_1 k_2 k_3 k_4)^2$
Japan	AIJ RLB	K_D	0.85-1.0	Design wind speed	$U_H = U_0 \boldsymbol{K_D} E_H k_{rw}$
Malaysia	MS 1553	M_d	1.0	Wind site speed	$V_{sit} = V_S \boldsymbol{M_d} M_{z,cat} M_s M_h$
Mexico	Additional Standard	NI	NI		NI
Philippines	NSCP	K_d	0.85-0.95	Velocity pressure	$q_z = 0.00256 K_z K_{zt} \boldsymbol{K_d} V^2$
Singapore	BS 6399-2	S_d	0.73-1.0	Site wind speed	$V_s = V_b * S_a * \boldsymbol{S_d} * S_s * S_p$
Singapore	BS 6399-2	S_d	0.73-1.0	Site wind speed	$V_s = V_b * S_a * \boldsymbol{S_d} * S_s * S_p$
United States	ASCE 7	K_d	0.85-0.95	Velocity pressure	$q_z = 0.00256 K_z K_{zt} \boldsymbol{K_d} V^2$
Vietnam	TCVN 2737	NI	NI		NI

NI: Not included

CHAPTER 4
REVISITING THE WIND DIRECTIONALITY FACTOR IN ASCE 7: INTRODUCTION TO THE SCENARIO ANALYSIS

This chapter presents the second part of the study regarding the directionality factor (K_d). The methodology and results of this study were presented at the 2012 ATC/SEI Advances in Hurricane Engineering Conference (Miami, FL). The feedback from the wind tunnel modeling and ASCE 7 Wind Load Provisions development communities provided the motivation for the new research tasks proposed in Chapter 5.

In summary, the completed study in this chapter is the original incarnation of the probabilistic scenario analysis. Herein, the approach to be described was applied to individual taps, and K_d at each tap was averaged over the ASCE7 Cp zones. Existing wind tunnel datasets and ground level wind velocity model outputs from four recent hurricanes were coupled to develop a directionality factor methodology that explicitly includes the influence of duration and change of wind direction associated with hurricane wind fields.

Wind directionality factors were derived for the zones specified in ASCE 7, for components located on 1, 2, 3 and 4 sides of a building. The analysis indicated that a C&C K_d value no smaller than 0.95 can be justified, and a value of 1.0 is acceptable and slightly conservative. However, these conclusions are not final, as feedback from the community led to the revisions to the methodology, as presented in Chapter 5.

4.1 Methodology

This section presents the development of the directionality factor specifically for components and cladding on hurricane prone residential construction. The methodology considered specialized concerns that may not be properly accounted in the current ASCE 7 application of K_d, such as: design level events with wide severe wind swath,

wind duration effects, multi-directional vulnerability of C&C, and uncertainty of the pressure coefficients (C_p) which are addressed following a Monte Carlo simulation framework. The four components of the methodology are: (1) modeling C_p uncertainty by accessing and processing wind tunnel datasets of surface pressures on low rise buildings, (2) producing hurricane wind velocity time histories by accessing and processing wind velocity model outputs from historical hurricane, (3) conducting Monte Carlo analyses that utilize these datasets to define K_d for a specific structure, location and hurricane, and (4) expanding to multiple buildings, locations and hurricanes to provide a statistical basis for recommending a rational K_d consistent with the current ASCE 7 GC_p framework. The methodology is presented by its four components.

4.1.1 Wind Tunnel Data: Pressure Coefficient C_p as a Random Variable

Wind tunnel data consisting of external surface pressure coefficients (C_p time histories) on low rise buildings were accessed from the online NIST Aerodynamic Database. Five different buildings were accessed, varying in height, roof slope and plan dimensions. Data was provided for both open and suburban terrain experiments for each of the five buildings, resulting in a total of ten datasets. Table 4-1 presents the characteristic of the buildings used in this study. Figure 4-1 shows the 1:100 scale model of building m11 (right figure), and the red dots represent the locations of the pressure taps on this model (left figure). Pressure time history was provided at 36 increments of 5 degrees (180 degree swath). The tap layout allowed the remaining 180 degree swath to be determined via symmetry.

The pressure coefficient C_p is a random variable that relates the approach wind speed to the surface pressure. The occurrence of severe pressure is of most interest for design loads, and thus the observed peaks of the C_p time history (minimum $-C_p$ in

suction, maximum +C_p for positive pressure) were analyzed to define a peak C_p probability density function (PDF). The ASCE 7 concept is based on a simplified representation of the C_p random variable as a scalar value corresponding to a prescribed probability of exceedance from the peak C_p PDF.

Table 4-1. Buildings Characteristics (Source: NIST Aerodynamic Database)

Building Number	NIST Database Building Label	Exposure	Model Scale	Roof Slope	Eave Height (ft)	Plan Dimensions (ft x ft)
1	t21 t22	Open Suburban	1:100	½ :12 (2.39°)	16	50 x 100
2	ee1 ee2	Open Suburban	1:100	1:12 (4.76 °)	16	80 x 125
3	eg1 eg2	Open Suburban	1:100	1:12 (4.76 °)	32	80 x 125
4	m11 m12	Open Suburban	1:100	3:12 (14°)	16	80 x 125
5	m31 m32	Open Suburban	1:100	3:12 (14°)	32	80 x 125

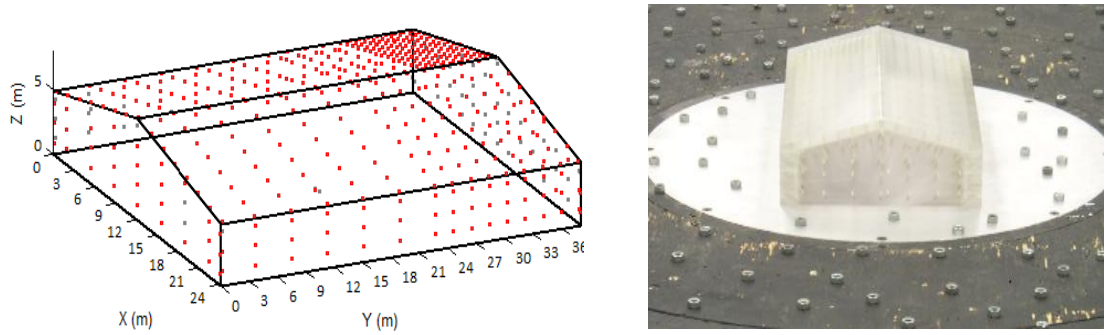

Figure 4-1. NIST low-rise building m11 (Table 4-1). Source: NIST Aerodynamic Database.

In this study the peak C_p PDF was separately modeled for each of several hundred taps and 72 approach wind directions (five degree increments) using the available NIST database time history data, and stored in a peak C_p PDF library (Figure

4-2). The peak C_p PDF modeling was conducted using a translation technique based on Sadek and Simiu (2002), developed by Peng et. al (2013). The scalar C_{p_peak} for each tap and each direction was identified as that corresponding to a 22% probability of exceedance based on the modeled peak C_p PDF (Figure 4-2, lower right). For each tap the largest magnitude C_{p_peak} among the 72 approach wind directions was retained as the $C_{p\_worstcase}$ (Figure 4-2, lower left). The $C_{p\_worstcase}$ thus conceptually emulates the worst case direction enveloping procedure used in the current ASCE 7 to define GC_p.

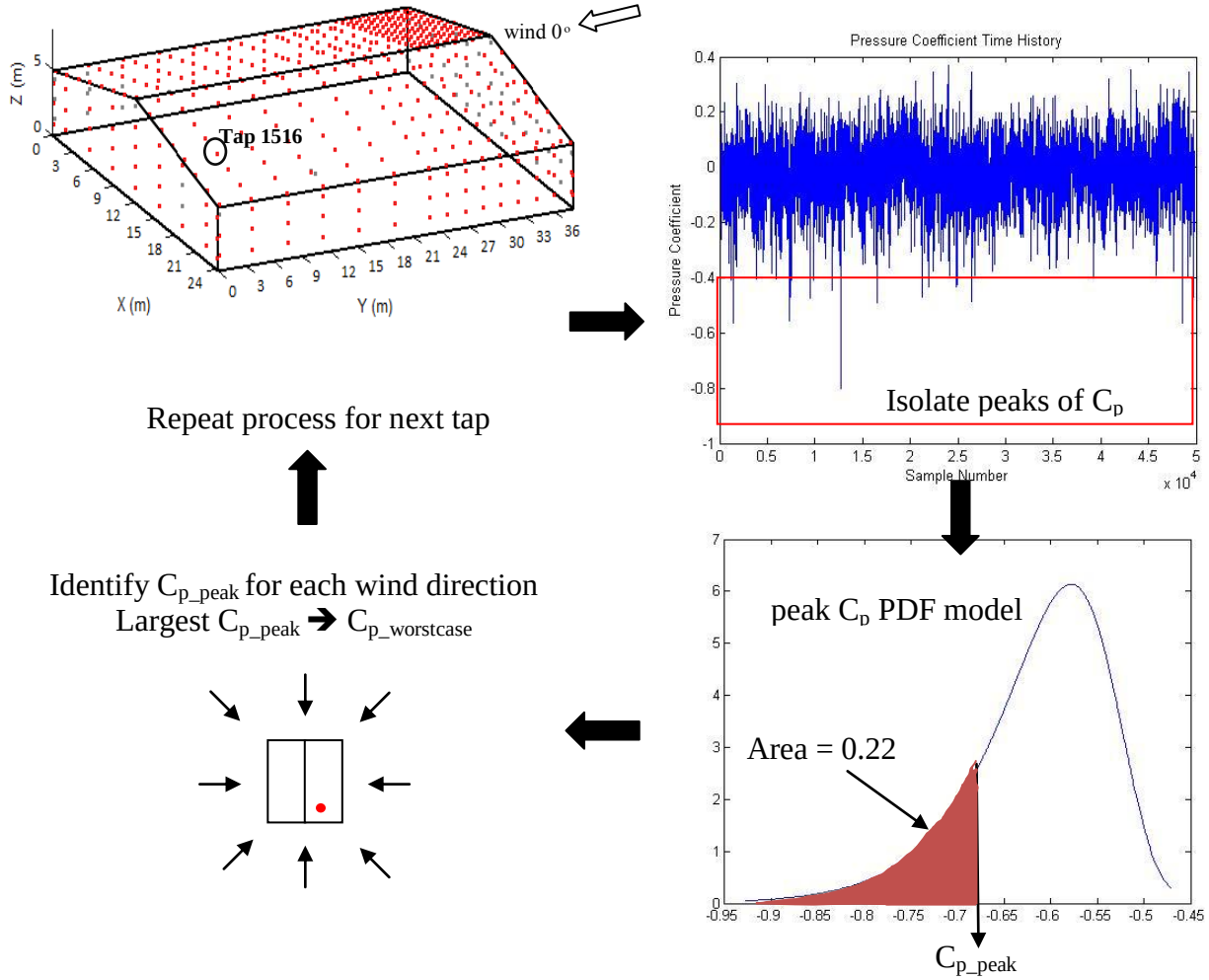

Figure 4-2. Analysis of building m11, tap 1516, 0°approach wind direction.

4.1.1.1 Application of Symmetry

The NIST database does not include a wind swath from 0 through 360 degrees. Symmetry was used to re-cast wind directions less than 180°by using the data available from 180°- 360°. The tap layout for the NIST buildings is well suited to a ridgeline symmetry approach. Let the direction parallel to the ridgeline be the y-axis and the direction spanning the short dimension the x-axis as shown in Figure 4-3. The origin is taken at the geometric center of the roof plan and the surface left of the ridgeline be

denoted W (windward), and the surface right of the ridgeline be denoted L (leeward). Ridgeline symmetry requires that a tap on W has a partner tap on L with the same y-axis value and equal and opposite x-axis value. For instance, if the wind direction is 100 degrees (0 degrees is aligned with y-axis), the C_p CDF for tap 4007 located in the W would be represented by the C_p CDF for tap 1516 at 260 degrees. Conversely, the C_p CDF for 1516 would be represented by the C_p CDF for 4007 as presented in Figure 4-4. That is, for any assigned wind direction (AWD) less than 180 degrees, the ridgeline symmetric tap serves as the C_p CDF using a surrogate wind direction (SWD).

The NIST buildings are almost entirely ridgeline symmetric with the exception of the more densely spaced tap collection on the upper windward section. In this densely spaced tap section, every other tap in every other row is ridgeline symmetric with the L tap losing access to those taps that are not symmetric in the dense section. Wall taps are likewise ridgeline symmetric. This concept creates a complete CDF library (0-360 degrees) for all the taps that have a partner tap. As each tap is analyzed for a given direction AWD (180 -360) the resultant C_p CDF and C_p 22% will be assigned to two libraries: 1) the given tap at the AWD, and 2) the surrogate tap at the SWD as illustrates Figure 4-4.

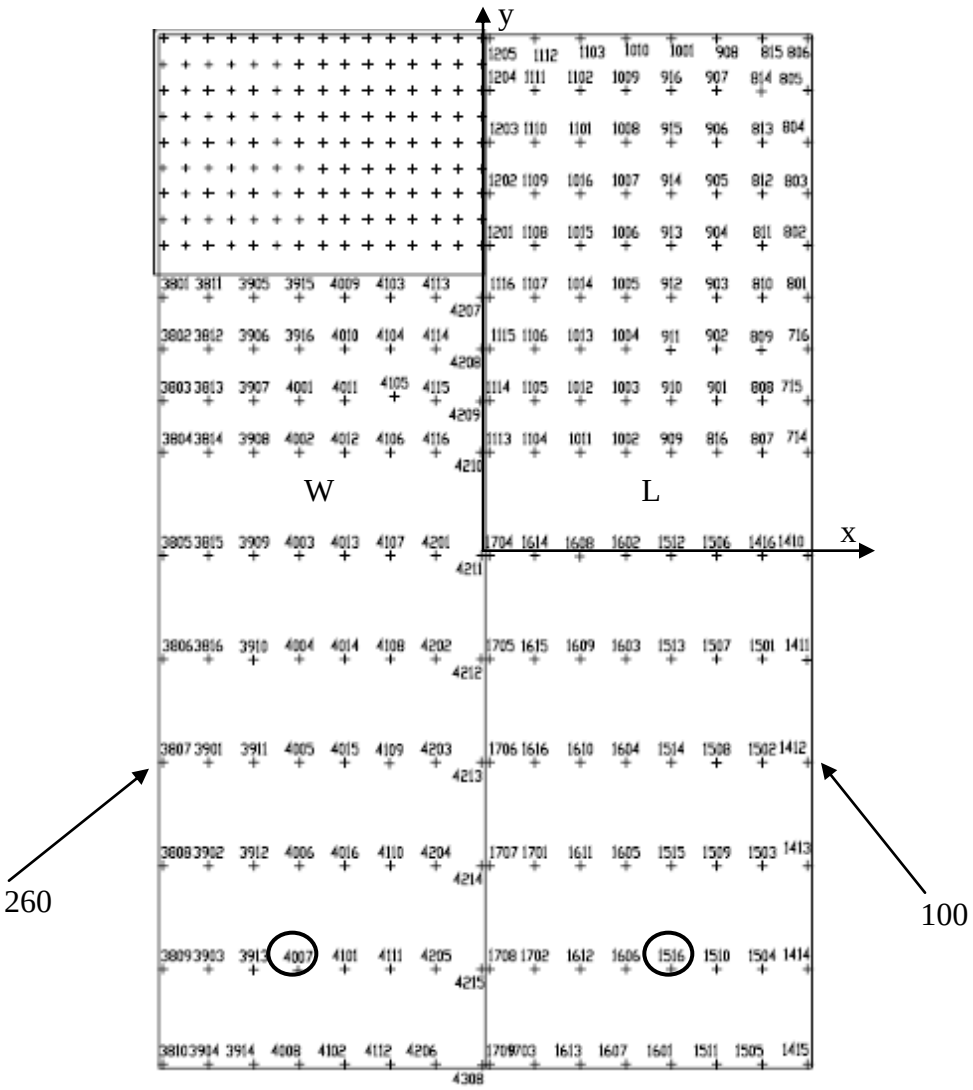

Figure 4-3. Example of Ridgeline Symmetry for a Given Wind From 100 Degrees. (Photo courtesy of NIST Database).

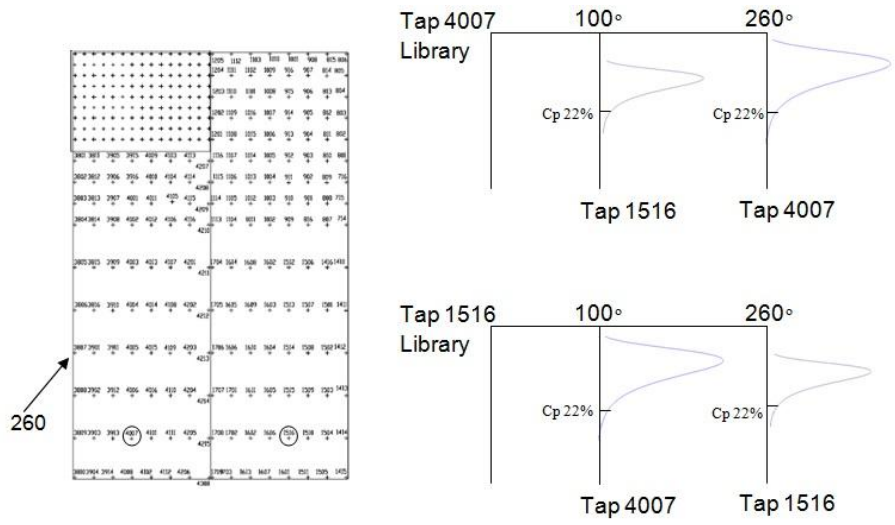

Figure 4-4. Assignments of CDF Cp and Cp 22 from each tap and are assigned to two library locations.

To validate the symmetry concept a contour plot of the percentage difference between the worst case Cp 22% among ridgeline symmetric taps was created in order to identify whether a zero residual (zero % difference) between ridgeline symmetric taps exist as illustrates Figure 4-5. The percentage difference does not quantify the difference between taps symmetric about the horizontal axis of symmetry, only about the vertical axis of symmetry. As can be seen, a minor variation can be noticed, however, it was identified that the variation is due to the peak Cp 22% of 12 taps that occurred for a wind of 180◦and 360◦where the symmetric concept is not applicable.

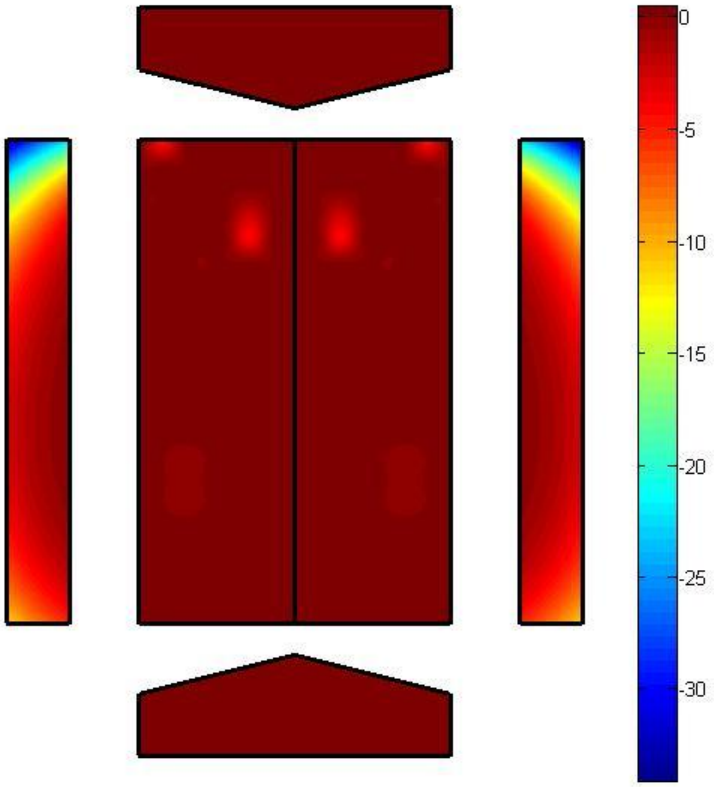

Figure 4-5. Percentage Difference Contour Plot.

4.1.2 Historical Hurricane Datasets: Hurricane Wind Speed and Direction Time Histories

Time histories of ground level wind speed and wind direction through the duration of four land-falling hurricanes were accessed from the NOAA Hurricane Research Division Atlantic Oceanographic and Meteorological Laboratories (HRD AOML) H*Wind Surface Wind Analysis tool. H*Wind provides a snapshot of the ground level wind speed and direction over a spatial grid of the impacted area in three hour increments. The snapshot provides the maximum 1 minute sustained wind speed in open terrain. For this study, the speed and direction time histories from H*Wind were resampled to 30 minute

increments using linear interpolation. Hurricanes Frances (2004), Ivan (2004), Katrina (2005) and Rita (2005) were used in this study.

4.1.3. Monte Carlo Simulation: Combining Peak C_p PDF Models and Historical Hurricanes

Using the H*Wind database, the time history of wind velocity was projected onto a low-rise building in the NIST database. For a given building orientation, geographic location and corresponding location specific hurricane wind velocity time history, the peak C_p PDF library provides the means to evaluate the probability that the resultant surface pressure exceeds the value obtained using the ASCE 7 approach of assuming a single gust from the worst case direction.

The methodology to develop the proposed K_d definition is explained in this section within the context of one NIST building at a single location impacted by one historical hurricane. Additional buildings, locations and hurricanes are then introduced to demonstrate the sensitivity of K_d to these variables and provide the statistical evidence to support the conclusions.

Consider the placement of a NIST low rise building in a coastal location impacted by a hurricane. The time history of wind speed and direction imparted by this historical hurricane at the location of the building was determined from the H*Wind Surface Wind Analysis tool in 30 minute increments.

Two surface pressure analyses were conducted for the building. The first is a representation of the concepts used in ASCE 7. The highest wind speed (V_{max}) during the hurricane at the building location was assumed to approach from a direction aligned with the worst case aerodynamic direction for each tap. The resultant worst case pressure $P_{\_worstcase}$ is defined in Eq. 4-1 as:

$$P_{worstcase}(i) = C_{p_{worstcase}}(i) \times V^2{}_{max} \quad (4\text{-}1)$$

where i references the individual taps on the building, $C_{p\_worstcase}$ was defined previously as the largest C_{p_peak} for a given tap among all approach directions, and C_{p_peak} was defined as the C_p corresponding to a 22 percent probability of exceedance based on the modeled peak C_p PDF (Figure 4-2).

The ASCE 7 approach considers the highest wind from the worst direction assumption to be overly conservative and motivates the use of a reduction factor. However, this approach does not consider that $C_{p\_worstcase}$ is a scalar simplification of the random variable C_p. A given random sample of a peak C_p has a defined probability of exceeding $C_{p\_worstcase}$, and therefore $P_{\_worstcase}$ (i) may be exceeded by a subset of sampled pressures as defined in Eq. 4-2:

$$P(i) = C_p(i) \times V^2 \quad (4\text{-}2)$$

where V is any of the wind speeds in the hurricane velocity time history, and C_p (i) is a random sample from the peak C_p PDF model associated with that tap and direction. Thus, $P_{\_worstcase}$(i) resulting from the first of the two surface pressure analyses was used as a benchmark to define a rational directionality factor for each tap, K_d(i), based on a probability of P(i) exceeding $P_{\_worstcase}$(i) at any time during the passage of a hurricane.

The second surface pressure analysis subjected the building to the time history of wind velocities during the passage of the hurricane, rather than just V_{max}. The peak C_p value for each tap was randomly sampled from the peaks C_p PDF model assigned for that tap and approach wind direction, rather than applying the simplified $C_{p\_worstcase}$. In this manner, a hurricane passage time history of peak pressure was generated for each tap on the building surface

$$P(i,k) = C_p(i,k) \times V(k)^2 \quad (4\text{-}3)$$

where i and k are the tap and 30 minute time increment, respectively, and $V^2(k)$ is the squared wind speed at time increment k. For every time increment, the C_p (i,k) values were resampled from the peak C_p PDF model assigned for the tap i and approach wind direction.

For each tap, the largest magnitude pressure through the duration of the hurricane was retained as shown in Eq.4-4

$$P_{i\_max} = \max\big(P(i,k)\big), over\ all\ k \quad (4\text{-}4)$$

P_{i_max} is thus a single random sample of the highest pressure value occurring at tap i as the hurricane passed, where the random components are the assigned C_p at each time increment k, and the orientation of the building which is fixed through the hurricane passage.

This analysis was repeated using a Monte Carlo framework, where each simulation assigned a new random building orientation (assuming a uniform distribution [0,2π]) and resampled C_p(i,k) values used in Eq. 4-3 from the peak C_p PDF library. The building was subjected to the same hurricane velocity time history, and the C_p(i,k) values were again resampled from the appropriate peak C_p PDF model. P(i,k) was reconstructed and the largest magnitude produced a new sample of P_{i_max} at each tap. This process was repeated 500 times, generating 500 samples of P_{i_max} at each tap as shows Fig. 4-6.

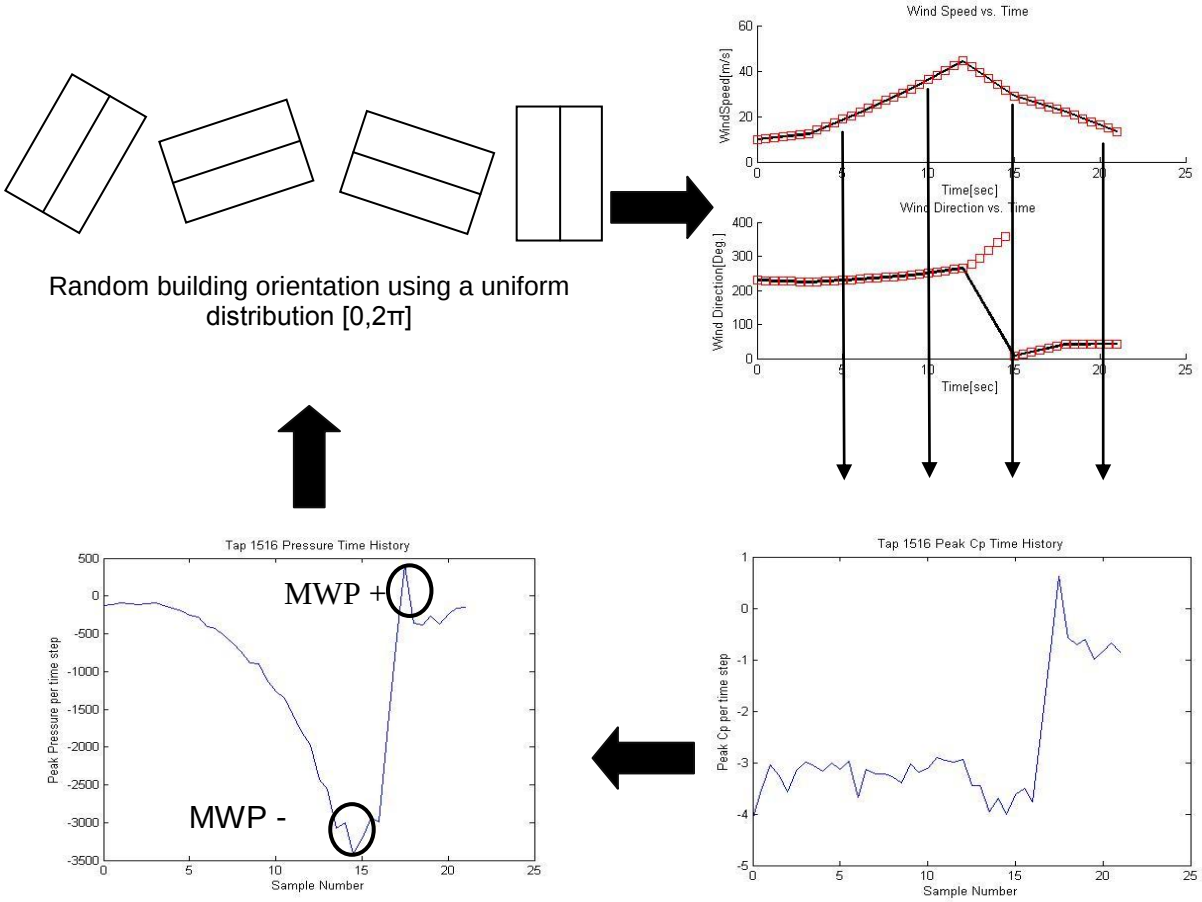

Random building orientation using a uniform distribution [0,2π]

For each tap, the largest magnitude pressure through the duration of the hurricane was retained

$P_{i\_max} = \max(P(i,k)), over\ all\ k$

A time history of peak pressure was generated for each tap on the building surface

$P(i,k) = C_p(i,k) \times V(k)^2$

Figure 4-6.Monte Carlo Analysis for Tap 1516.

We propose that a rational value for the design C_p is that value corresponding to a 5% probability of exceeding $P_{\_worstcase}$ during the passage of a hurricane. K_d is determined for each tap, K_d(i), by identifying the P_{i_max} corresponding to the 5% probability of exceedance ($P_{i\_max\_5\%}$) from the 500 sample sequence. The directionality

factor may be expressed within the context of the current ASCE 7 concept ($P_{\_worstcase}$) by applying the ratio as defined by Eq.4-5

$$K_d(i) = \frac{P_{i\_\max\ \_5\%}}{P_{worstcase}(i)} \tag{4-5}$$

The proposed K_d is thus the fraction of $P_{\_worstcase}$ that corresponds to a 5% probability of exceedance. The resultant K_d may be less than, equal to, or greater than one, may vary with location on the building, and may be different for positive and negative pressure.

Figures 4-7 through 4-10 present a sample outcome of the above proposed methodology to define K_d. Building m11 (building m1 in open terrain) is subjected to the hurricane Katrina wind velocity time histories at two locations, one on the strong side and one on the weak side (Figure 4-7). K_d was determined according to Eq. 4-5 at each tap on the building surface and presented in Figure 4-8 for both locations. The differences in K_d between the two locations is a result of the difference in the hurricane wind velocity time history at these two locations, and demonstrates that K_d is sensitive to building location. The rounded color contours at the corners of the walls is an affectation of having very few pressure taps on the model in these regions.

ASCE 7 provides building surface zones to assign pressure coefficients. The mean K_d value among all taps within a zone is a convenient presentation format for the analysis and is consistent with ASCE 7 wind load concepts. The data in Figure 4-8 was processed to present the mean K_d per zone, shown in Figures 4-9 and 4-10. The results demonstrate that a majority of the mean K_d values exceed 0.85. However, the conclusion that K_d = 0.85 is too low is tempered by two issues: 1) The sensitivity of the methodology outputs to a number of factors must be determined (addressed next), and

2) As a result of expert feedback, the methodology presented above was altered to consider area averaged pressure time histories (addressed in Chapter 5).

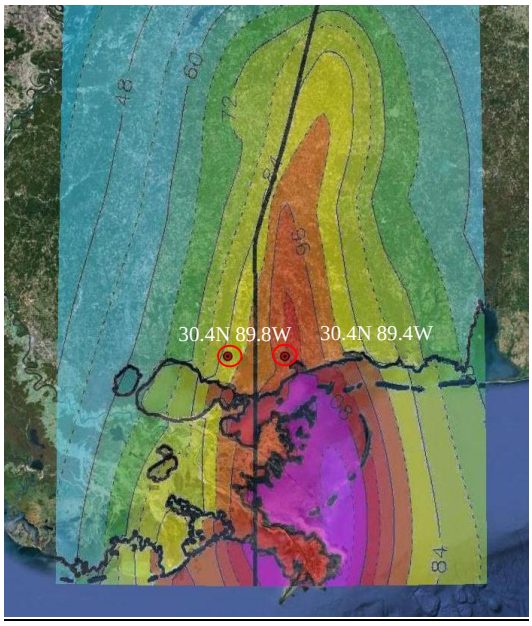

Figure 4-7. Hurricane Katrina peak wind speed swath (NOAA HRD AOML H*Wind) and two building locations highlighted (30.4N, 89.8W and 30.4N, 89.4W). Map courtesy Google Earth.

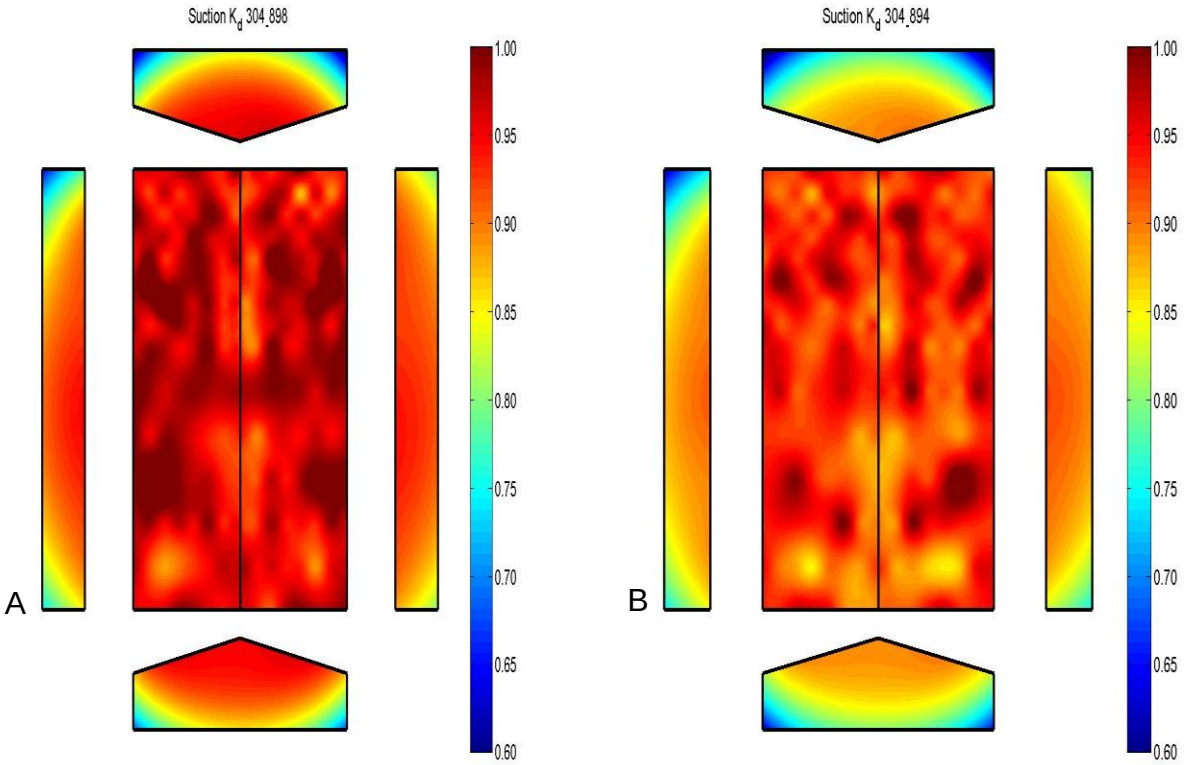

Figure 4-8. K_d contour for suction. A) 30.4N, 89.8W. B) 30.4N, 89.4W.

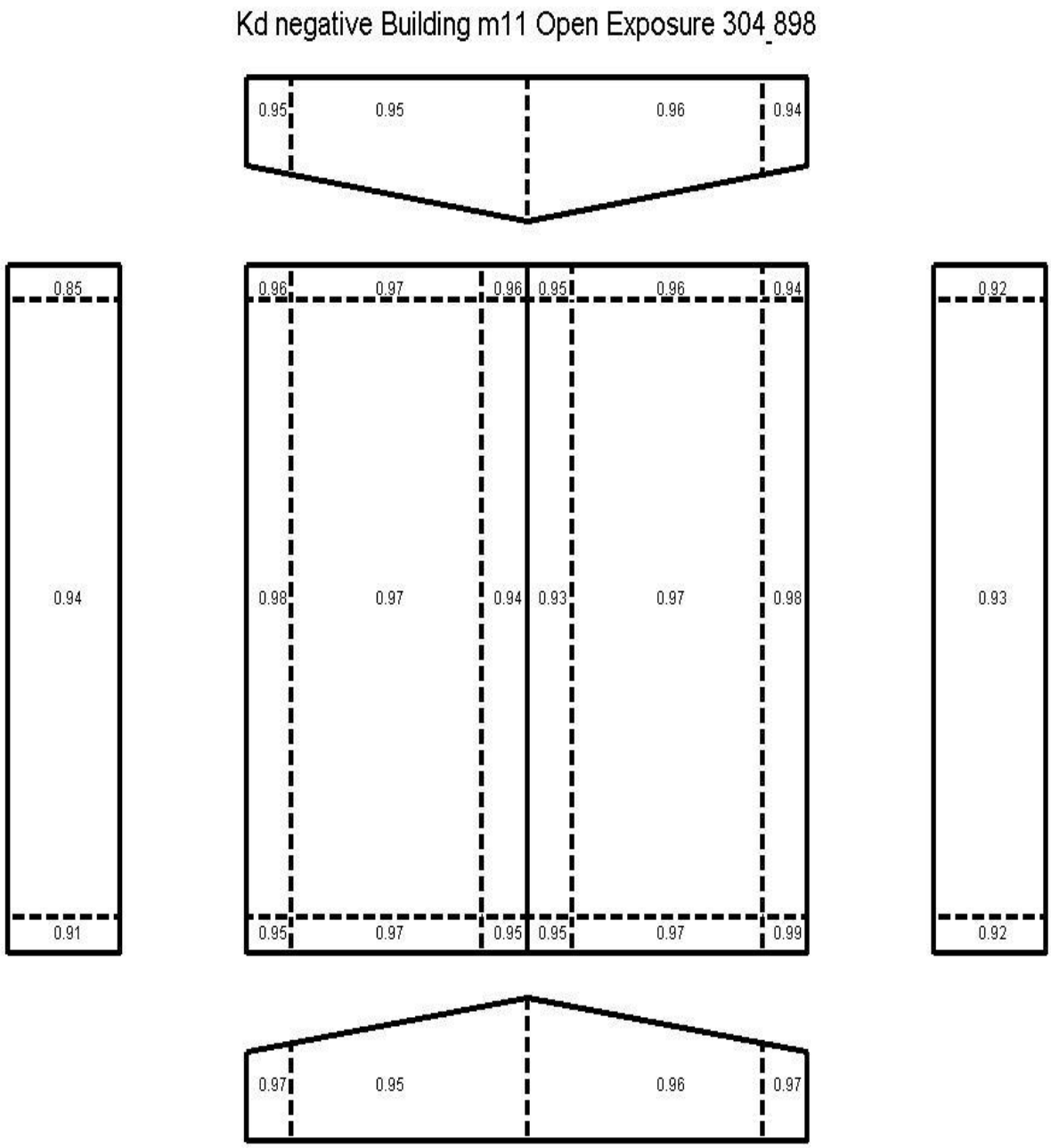

Figure 4-9. Mean K_d by zone in suction 30.4N, 89.8W.

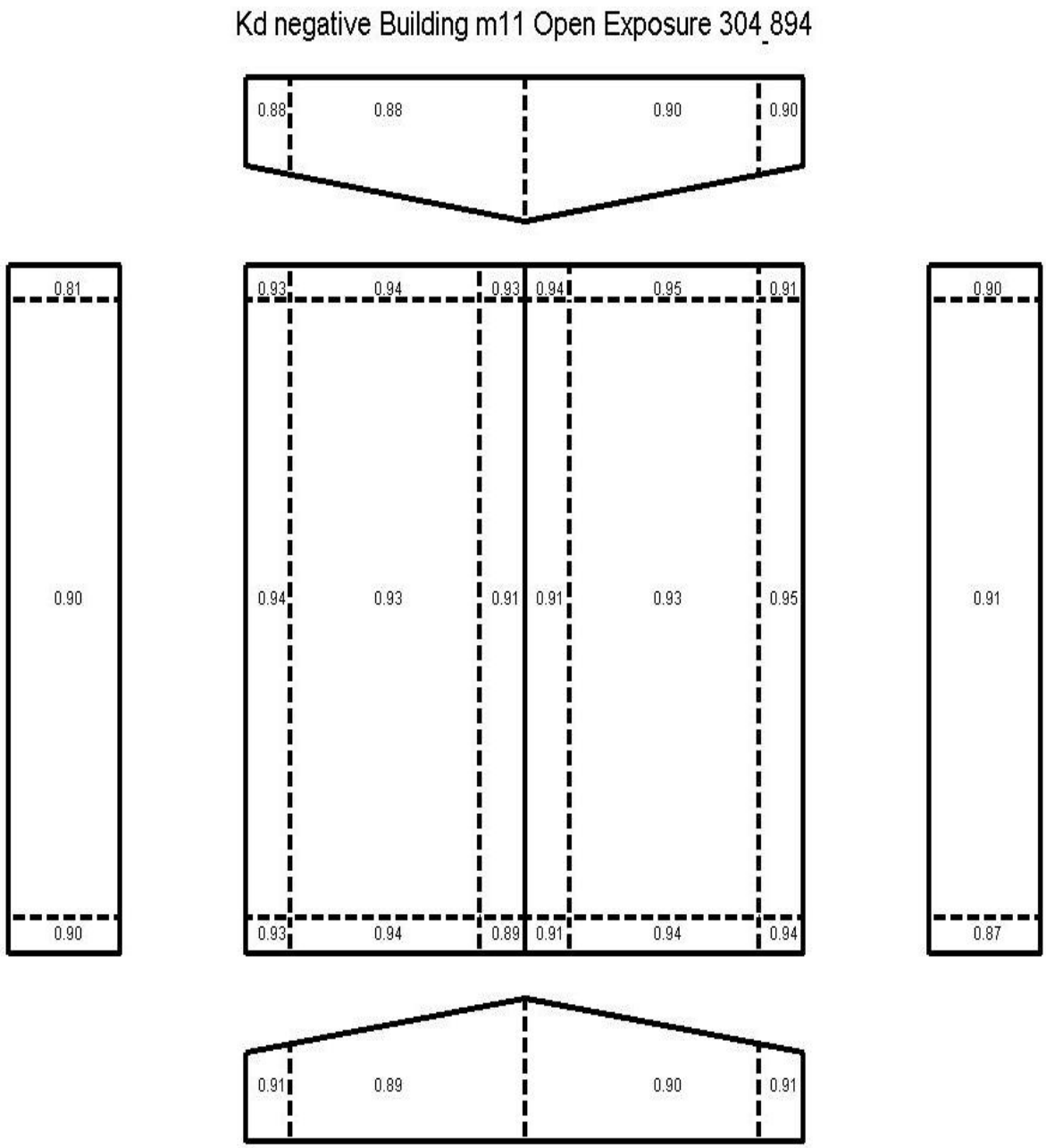

Figure 4-10. Mean K_d by zone in suction 30.4N, 89.4W.

4.1.4. Monte Carlo Results: Expansion to Multiple Buildings, Locations and Hurricanes

Any change in input variables that alters the wind velocity time history or peak C_p PDF library will potentially alter the resultant K_d (i) values. Moving the same building from one location to another in the same hurricane (e.g. Figure 4-11) will change the wind time history, as will using a different historical hurricane. Changing the building model or the exposure of the building (Table 4-1) will change the peak C_p PDF library, since the library is derived from the experimental data. It is therefore important that the influence of building type, terrain exposure, building location, and historical hurricane on the K_d results (e.g. Figures 4-9 & 4-10) be determined. The observation from the previous example (Figures 4-7 through 4-10) that K_d = 0.85 is too low may not be a consistent observation as building type, location, and historical hurricane change.

The previously outlined 500 simulation Monte Carlo K_d analysis methodology was repeated for 5 buildings, two exposures per building (open and suburban), four hurricanes, and multiple building locations per hurricane. The outcomes are then combined to provide a preliminary assessment of the current K_d factor for components and cladding in ASCE 7. The variables in this study include:

- Buildings and exposure (Table 4-1): t21, t22, ee1, ee2, eg1, eg2, m11, m31, m12, m32
- Hurricanes (Figure 4-11): Frances (2004), Ivan (2004), Katrina (2005), Rita (2005)
- Locations (Figure 4-11):
    - Frances: 38 locations
    - Ivan: 42 locations
    - Katrina: 42 locations
    - Rita: 58 locations

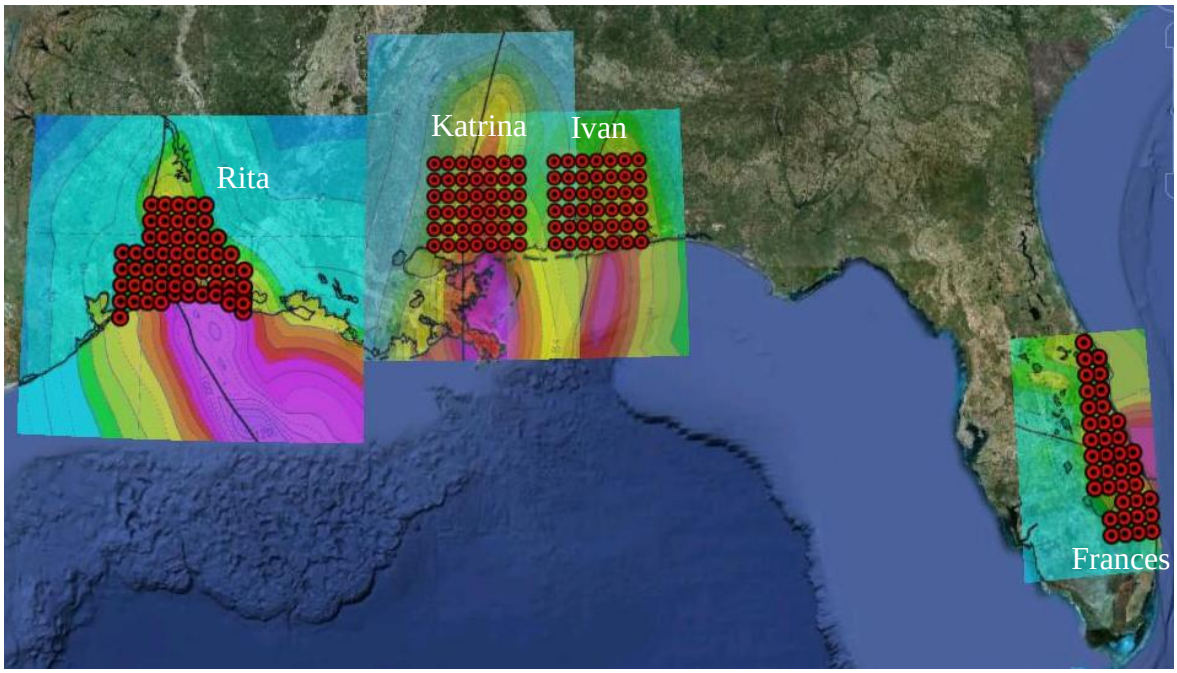

Figure 4-11. Historic hurricanes and building locations analyzed (Map courtesy Google Earth).

4.1.4.1. Analysis of all locations, all hurricanes

There are a total of 180 locations among the four hurricanes. Each of the models in Table 4-1 was analyzed at these 180 locations. For each building and location, results were gathered using the mean K_d per zone as in Figures 4-9 and 4-10. The mean and coefficient of variation (COV) were then calculated among the 180 locations. The percent of the mean K_d values among the 180 building locations that exceed 0.85 was also calculated.

Figures 4-12 and 4-13 present a view of the building surfaces with each zone labeled with a generic reference, where R refers to roof locations and W refers to wall locations. The ASCE 7 zone layout changes with roof slope. Figure 4-12 applies to buildings t21, t22, ee1, ee2, eg1 and eg2. Figure 4-13 applies to buildings m11, m12, m31, m32. Table 4-2 presents the mean and COV (as %) of the mean K_d values among

the 180 building locations for the roof zones shown in Figures 4-12 and 4-13. Table 4-2 presents the mean and COV (as %) of the mean K_d values among the 180 building locations for the wall zones shown in Figures 4-12 and 4-13. Table 4-3 presents the percent of the mean K_d values among the 180 building locations that exceed 0.85 for the roof zones. Table 4-4 presents the percent of the mean K_d values among the 180 building locations that exceed 0.85 for the wall zones.

The far right column in each of the Tables 4-2 through 4-6 contains the mean value across that row, and the bottom of the right column presents the overall mean. It can be observed that for the roof taps the overall mean K_d among all zones, locations and buildings is 0.97 with an overall (unweighted) mean COV of 5.17 (Table 4-2). For the wall taps the overall mean K_d among all zones, locations and buildings is 0.95 with an overall (unweighted) mean COV of 5.81 (Table 4-3). The overall mean of the percent of the K_d values that exceed 0.85 for roof zones is 98.2 (Table 4-3). The overall mean of the percent of the K_d values that exceed 0.85 for wall zones is 95.5 (Table 4-4).

These statistics support the conclusion that the components and cladding K_d value 0.85 in ASCE 7 is not conservative and is inappropriate for hurricane prone regions. A K_d value of 0.95 to 1.0 is recommended in place of the current 0.85.

This conclusion is contingent upon the acceptance of the proposed methodology to determine K_d (Eq. 4-5), the selection of a 5% probability of exceedance threshold in Eq. 4-5, and the use of individual taps to determine K_d. Chapter 5 will address these variability of K_d as a function of these three issues.

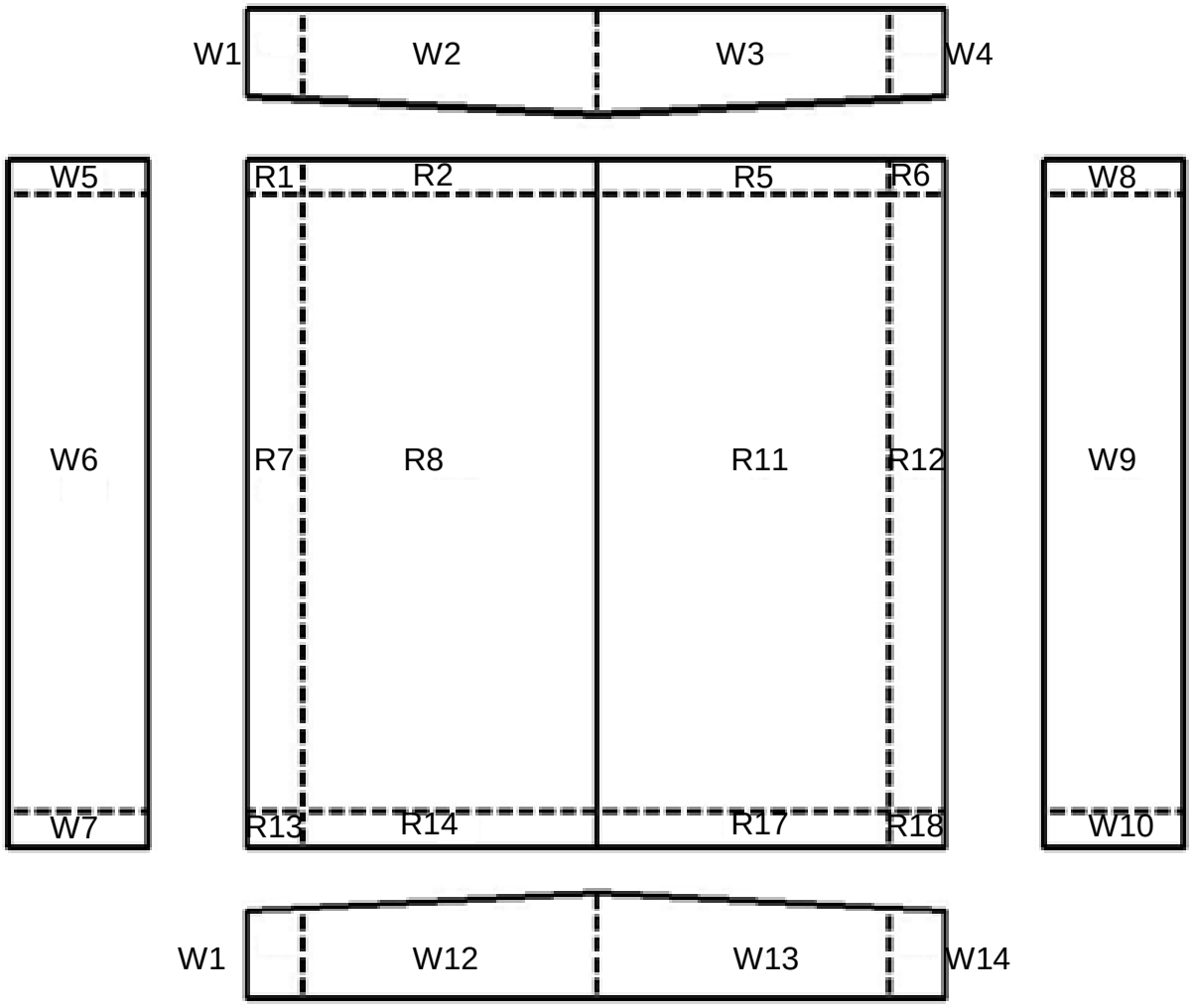

Figure 4-12. Generic wall and roof zone labeling for buildings t21, t22, ee1, ee2, eg1, eg2.

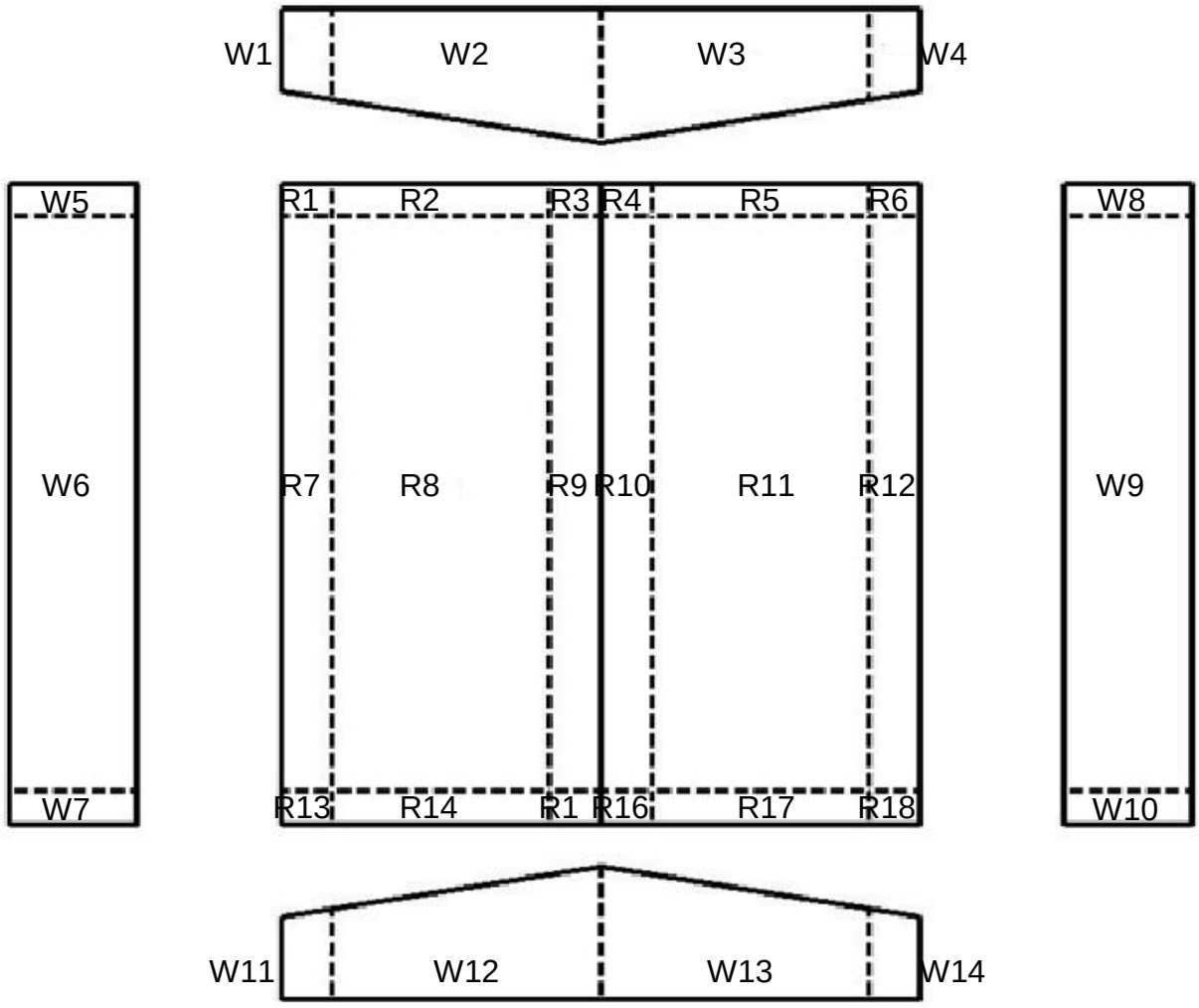

Figure 4-13. Generic wall and roof zone labeling for buildings m11, m12, m31, m32.

Table 4-2.K_d mean and % COV across 180 locations, roof, by zone. All buildings

		NIST DATABASE BUILDING LABEL (SEE TABLE 4)										
		t21	**t22**	**ee1**	**ee2**	**eg1**	**eg2**	**m11**	**m12**	**m31**	**m32**	**mean**
R1	K_d mean	0.93	0.95	0.96	0.96	0.94	1.00	0.95	0.96	0.96	0.97	0.96
	K_d COV	6.95	6.11	6.57	5.03	5.63	5.11	5.27	5.61	6.62	6.50	5.94
R2	K_d mean	0.96	0.98	0.98	1.00	0.95	0.99	0.97	0.98	0.94	0.98	0.97
	K_d COV	6.02	5.27	4.18	4.21	6.44	5.35	4.60	5.31	7.01	5.66	5.41
R3	K_d mean							0.96	0.97	0.94	0.95	0.96
	K_d COV							4.03	4.57	4.98	5.44	4.76
R4	K_d mean							0.96	0.97	0.94	0.95	0.96
	K_d COV							4.28	4.73	4.91	5.36	4.82
R5	K_d mean	0.97	0.98	0.99	1.00	0.95	0.99	0.97	0.98	0.94	0.98	0.98
	K_d COV	5.98	5.19	4.15	4.13	6.47	5.09	4.67	5.33	6.99	5.65	5.37
R6	K_d mean	0.93	0.96	0.97	0.96	0.94	1.00	0.94	0.96	0.94	0.96	0.96
	K_d COV	6.79	6.07	6.81	4.73	5.65	4.91	4.97	5.49	6.67	6.22	5.93
R7	K_d mean	0.97	0.99	0.97	0.97	0.95	0.98	0.98	0.95	0.97	0.99	0.97
	K_d COV	4.56	4.87	4.56	5.56	4.97	5.42	4.93	5.71	4.78	4.98	5.03
R8	K_d mean	0.97	1.00	0.97	1.00	0.95	0.98	0.97	0.96	0.95	0.98	0.97
	K_d COV	4.74	5.51	5.04	5.45	5.97	5.89	5.23	6.10	6.52	6.31	5.68
R9	K_d mean							0.94	0.96	0.96	0.97	0.96
	K_d COV							4.66	6.02	4.69	4.96	5.08
R10	K_d mean							0.94	0.96	0.96	0.97	0.96
	K_d COV							4.70	6.11	4.71	4.93	5.11
R11	K_d mean	0.97	1.00	0.97	1.00	0.95	0.98	0.97	0.98	0.95	0.98	0.98
	K_d COV	4.71	5.50	5.04	5.39	5.96	5.95	5.21	5.86	6.53	6.23	5.64
R12	K_d mean	0.97	.99	0.97	0.97	0.95	0.98	0.98	0.99	0.98	0.99	0.98
	K_d COV	4.58	4.91	4.46	5.47	4.87	5.48	4.99	5.78	4.71	4.99	5.02
R13	K_d mean	0.90	0.96	0.97	1.00	0.96	0.97	0.98	0.98	0.98	1.01	0.97
	K_d COV	6.25	5.50	5.00	5.05	4.22	5.01	4.30	5.58	4.09	4.85	4.99
R14	K_d mean	0.94	0.99	0.98	1.00	0.95	0.98	0.98	0.94	0.96	1.00	0.97
	K_d COV	6.66	5.62	4.12	4.86	4.32	4.81	4.74	6.69	3.96	4.73	5.05
R15	K_d mean							0.95	0.89	0.95	0.97	0.94
	K_d COV							4.16	5.47	4.03	4.88	4.64
R16	K_d mean							0.94	0.89	0.95	0.97	0.94
	K_d COV							4.34	5.50	3.81	4.64	4.57
R17	K_d mean	0.95	0.99	0.99	1.01	0.97	0.97	0.98	0.94	0.96	1.00	0.98
	K_d COV	6.61	5.53	4.04	4.28	4.45	4.89	4.72	6.48	4.05	4.79	4.98
R18	K_d mean	0.91	0.96	0.97	1.00	0.96	0.97	0.98	0.99	0.98	1.01	0.97
	K_d COV	6.36	5.90	4.98	4.98	4.06	5.20	4.20	5.47	4.26	4.92	5.03
								Overall mean of K_d mean				0.97
								Overall mean of K_d COV				5.17

Table 4-3.Percent K_d mean values > 0.85 among 180 locations, roof, by zone. All buildings

		NIST DATABASE BUILDING LABEL (SEE TABLE 4)										
		t21	t22	ee1	ee2	eg1	eg2	m11	m12	m31	m32	mean
R1	% > 0.85	90	98	99	100	97	100	100	100	92	96	97.2
R2	% > 0.85	95	100	100	100	92	100	100	100	91	100	97.8
R3	% > 0.85							100	100	99	99	99.5
R4	% > 0.85							100	100	99	99	99.5
R5	% > 0.85	96	100	100	100	92	100	100	100	91	100	97.9
R6	% > 0.85	88	98	99	100	97	100	100	100	93	97	97.2
R7	% > 0.85	99	100	100	100	99	99	100	100	99	100	99.6
R8	% > 0.85	99	100	99	100	96	99	99	99	94	99	98.4
R9	% > 0.85							100	97	99	100	99
R10	% > 0.85							100	97	99	100	99
R11	% > 0.85	99	100	99	100	96	99	99	100	94	100	98.6
R12	% > 0.85	99	100	100	100	99	99	100	100	99	100	99.6
R13	% > 0.85	83	100	100	100	100	100	100	100	100	100	98.3
R14	% > 0.85	92	100	100	100	100	100	100	93	100	100	98.5
R15	% > 0.85							100	79	100	100	94.8
R16	% > 0.85							100	79	100	100	94.8
R17	% > 0.85	94	100	100	100	100	100	100	94	100	100	98.8
R18	% > 0.85	84	100	100	100	100	100	100	100	100	100	98.4
											Overall mean	98.2

Table 4-4. K_d mean and % COV across 180 locations, walls, by zone. All buildings

		NIST DATABASE BUILDING LABEL (SEE TABLE 4)										
		t21	**t22**	**ee1**	**ee2**	**eg1**	**eg2**	**m11**	**m12**	**m31**	**m32**	**mean**
W1	K_d mean	0.94	0.97	0.93	0.93	0.96	0.94	0.93	0.95	0.95	0.97	0.95
	K_d COV	5.70	5.94	6.76	6.37	5.69	7.18	5.20	5.82	5.58	6.31	6.06
W2	K_d mean	0.96	0.95	0.97	0.93	0.94	0.98	0.94	0.95	0.95	0.96	0.95
	K_d COV	4.86	6.53	4.85	6.65	5.60	5.86	5.66	6.55	5.49	6.14	5.82
W3	K_d mean	0.96	0.95	0.97	0.93	0.94	0.98	0.94	0.96	0.95	0.96	0.95
	K_d COV	4.81	6.66	4.76	6.55	5.48	5.83	5.84	6.60	5.54	6.14	5.82
W4	K_d mean	0.95	0.97	0.93	0.93	0.96	0.95	0.93	0.95	0.94	0.97	0.95
	K_d COV	5.67	5.95	6.64	6.21	5.64	7.13	5.44	5.83	5.58	6.38	6.05
W5	K_d mean	0.95	0.98	0.89	0.93	0.93	0.92	0.85	0.90	0.93	0.95	0.92
	K_d COV	5.40	6.40	7.72	6.53	6.12	6.48	7.58	7.13	6.18	6.39	6.59
W6	K_d mean	0.96	0.98	0.95	0.97	0.95	0.94	0.94	0.95	0.95	0.95	0.95
	K_d COV	4.91	6.30	5.51	6.54	5.79	7.32	5.39	6.70	5.92	7.15	6.15
W7	K_d mean	0.95	0.96	0.89	0.99	0.93	0.96	0.93	0.93	0.91	0.95	0.94
	K_d COV	5.23	5.93	6.43	6.28	6.05	6.46	5.76	6.40	7.35	6.63	6.25
W8	K_d mean	0.96	0.97	0.93	0.91	0.93	0.95	0.94	0.94	0.94	0.92	0.94
	K_d COV	5.27	6.72	5.87	7.26	5.94	6.47	6.44	6.42	5.57	6.89	6.29
W9	K_d mean	0.97	0.96	0.93	1.00	0.88	0.98	0.91	0.96	0.85	0.91	0.94
	K_d COV	2.15	3.00	2.30	6.01	2.76	2.05	3.91	3.55	3.29	3.04	3.21
W10	K_d mean	0.96	0.96	0.90	0.99	0.93	0.97	0.93	0.94	0.91	0.93	0.94
	K_d COV	5.07	5.80	6.27	6.15	5.90	6.65	5.86	6.27	7.81	6.96	6.27
W11	K_d mean	0.96	0.98	0.91	0.96	0.94	0.97	0.95	0.94	0.94	0.97	0.95
	K_d COV	5.46	5.73	5.60	5.71	6.18	6.19	4.91	5.98	5.94	7.11	5.88
W12	K_d mean	0.96	1.00	0.98	0.97	0.95	0.98	0.94	0.96	0.94	0.96	0.96
	K_d COV	4.82	5.47	5.07	5.37	5.44	6.07	5.81	5.29	5.23	6.52	5.51
W13	K_d mean	0.96	1.00	0.98	0.97	0.95	0.98	0.94	0.96	0.94	0.96	0.96
	K_d COV	4.87	5.53	4.94	5.24	5.33	6.05	6.05	5.46	5.20	6.46	5.51
W14	K_d mean	0.96	0.98	0.91	0.96	0.94	0.97	0.95	0.94	0.94	0.97	0.95
	K_d COV	5.61	5.90	5.45	5.64	6.19	6.06	5.16	6.04	6.01	7.10	5.92
								Overall mean of K_d mean				0.95
								Overall mean of K_d COV				5.81

Table 4-5. Percent K_d mean values > 0.85 among 180 locations, walls, by zone. All buildings

		NIST DATABASE BUILDING LABEL (SEE TABLE 4)										
		t21	**t22**	**ee1**	**ee2**	**eg1**	**eg2**	**m11**	**m12**	**m31**	**m32**	**mean**
W1	% > 0.85	98	100	88	94	99	91	97	98	99	99	96.3
W2	% > 0.85	100	97	100	92	97	100	98	98	98	98	97.8
W3	% > 0.85	100	96	100	92	98	100	97	97	99	99	97.8
W4	% > 0.85	98	100	89	94	99	92	96	99	98	99	96.4
W5	% > 0.85	99	99	72	94	94	91	49	76	93	97	86.4
W6	% > 0.85	99	98	98	97	97	90	98	96	97	93	96.3
W7	% > 0.85	100	99	76	100	92	99	96	95	81	97	93.5
W8	% > 0.85	100	98	94	77	95	97	95	96	98	88	93.8
W9	% > 0.85	100	100	100	100	75	100	100	100	50	100	92.5
W10	% > 0.85	100	99	77	100	96	98	95	96	80	90	93.1
W11	% > 0.85	99	100	91	99	94	99	100	95	96	98	97.1
W12	% > 0.85	100	100	100	100	98	100	96	100	99	98	99.1
W13	% > 0.85	100	100	100	100	98	100	96	100	99	98	99.1
W14	% > 0.85	99	100	92	100	94	100	100	94	95	98	97.2
												95.5
											Overall mean	

4.1.4.2. Analysis stratified by hurricane

The previous section presented results combining all locations in each of the four hurricanes. The sensitivity of the results to a given hurricane was investigated by stratifying results by hurricane. The mean K_d and COV among locations for a given hurricane were calculated for each zone for each hurricane. The plots are provided for each building, exposure, and hurricane in results are condensed as the range of mean K_d and COV values observed among the zones in these plots as reported in Table 4-6. For example, the K_d mean range for building m11 for hurricane Frances was 0.89-1.01, and the COV range was 4.84-8.91. These are the highest and lowest observed values among the zones, calculated using only the Frances locations rather than all 180 locations. Observe in Table 4-6 that the low end of the range for any given building and storm rarely approaches 0.85.

Table 4-6. Ranges among ASCE-7 zones -- all locations per storm

BUILDING	NIST DATABASE BUILDING LABEL		HURRICANE			
			Frances	Ivan	Katrina	Rita
1	t21	COV range	5.01-7.89	4.21-6.52	4.06-6.04	4.13-6.60
		K_d mean range	0.93-0.99	0.89-0.96	0.90-0.97	0.89-0.96
	t22	COV range	5.42-7.57	4.47-6.20	4.19-5.98	4.45-6.13
		K_d mean range	0.99-1.03	0.94-0.99	0.95-1.00	0.94-0.99
2	ee1	COV range	4.58-8.87	3.70-7.35	3.65-6.58	3.57-7.23
		K_d mean range	0.92-1.01	0.88-0.98	0.89-0.98	0.88-0.98
	ee2	COV range	4.84-8.25	3.75-6.98	3.34-6.20	3.57-6.33
		K_d mean range	0.94-1.03	0.89-0.99	0.91-1.00	0.85-0.97
3	eg1	COV range	5.17-7.03	3.59-6.35	3.38-6.05	3.54-6.31
		K_d mean range	0.96-0.99	0.92-0.96	0.92-0.96	0.91-0.96
	eg2	COV range	5.53-7.98	4.47-7.10	4.08-6.57	4.28-6.82
		K_d mean range	0.96-1.03	0.91-0.99	0.93-1.00	0.91-0.99
4	m11	COV range	4.84-8.91	3.79-7.32	3.55-7.08	3.60-6.61
		K_d mean range	0.89-1.01	0.84-0.97	0.85-0.98	0.84-0.98
	m12	COV range	5.07-8.33	4.17-6.75	3.78-6.07	4.09-6.35
		K_d mean range	0.92-1.02	0.88-0.98	0.89-0.99	0.88-0.98
5	m31	COV range	4.57-9.12	3.35-7.74	3.41-6.67	3.31-6.93
		K_d mean range	0.94-1.01	0.90-0.98	0.91-0.98	0.90-0.98
	m32	COV range	5.38-8.02	4.21-6.96	3.80-6.50	4.02-6.80
		K_d mean range	0.96-1.04	0.91-1.00	0.92-1.01	0.91-1.00

4.2 Chapter Summary

Chapter 4 presented the vulnerability of low-rise buildings subjected to different wind swaths and directions during windstorm events. The study evaluated the efficacy of the K_d factor on components and cladding for hurricane prone low-rise residential structures. The first part of the study (Chapter 3) reviewed the development of the K_d factor and documented the incorporation of directionality effects in standards around the world. The second part of the study (Chapter 4) introduced the original incarnation of the probabilistic scenario analysis. The approach was applied to individual taps and evaluated whether the use of the worst case direction to define GCp is demonstrably conservative (necessitating a reduction factor $K_d < 1$) in the case of hurricane events, in which strong winds are often associated with a wide swath of wind directions. The methodology addressed hurricane specific concerns that may not be accounted in the current ASCE 7 application of K_d.

The third part of the study (Chapter 5) presents a revision to the methodology presented in Chapter 4. This new methodology focuses on the development of a directionality approach for components and cladding loads on buildings in hurricane prone regions using area averaged pressure time history instead of single taps. The methodology is composed of three main approaches. The first two follow the ASCE 7 assumption that wind damage is due to a single gust coming from a single direction. The third approach follows the stochastic scenario analysis introduced in Chapter 4. An additional important consideration introduced in Chapter 5 is the perspective of treating individual components as a system, where failure of the most vulnerable component indicates system failure. For example, all windows may be viewed as a fenestration system.

CHAPTER 5
REVISITING THE WIND DIRECTIONALITY FACTOR IN ASCE 7: REFINED SCENARIO ANALYSIS

The purpose of this study is to provide a more detail evaluation of the efficacy of K_d on components and cladding for hurricane prone low-rise residential structures by taking into consideration suggestions made by modelers and researches during the 2012 ATC/SEI Advances in Hurricane Engineering Conference (Miami, FL). The methodology presented herein is composed of three main approaches: (1) deterministic, (2) probabilistic, and (3) scenario analysis. The first two approaches ignore the effects of hurricane climatology and adopt the ASCE 7 assumption that wind damage is due to a single gust coming from a single direction. These two approaches provide a frame of reference to contrast results when the hurricane climate is explicitly considered. The third approach follows the scenario analysis presented in Chapter 4 where the duration and variation of wind during the passage of a hurricane was considered. Rather than performing the analysis on individual pressure taps as in the Chapter 4 analysis, area averaged pressure data is used to reflect the ASCE 7 area averaging procedures used to produce components and cladding pressure coefficients. Thus the analysis in this chapter is more consistent with ASCE7 derivation of pressure coefficients. A modification to the Monte Carlo analysis is made with respect to assigned building orientation. Finally, this chapter introduces the use of a system perspective, whereby the vulnerability of multiple similar components on the same building is treated in a weakest-link in the system format rather than as individual components. A detailed explanation of each approach follows.

5.1 Methodology

The three approaches considered are: (1) deterministic approach, (2) probabilistic approach, and (3) scenario analysis (modified version of Chapter 4).

The deterministic approach follows the assumption of the ASCE 7 that wind damage is based on a single gust coming from a single direction. This analysis uses the pressure coefficient corresponding to 22% percentile to define the loads from any direction. The historical hurricane wind velocity time history is not utilized. Monte Carlo analysis is not applied, as no random variables are sampled in the analysis.

The probabilistic approach introduces the probabilistic nature of pressure coefficients by using a random sampling from the CDF library instead of the 22% pressure coefficient. The historical hurricane wind velocity time history is not utilized. Monte Carlo analysis is applied as pressure coefficients are randomly sampled from the peak PDF library introduced in Chapter 4.

The scenario analysis accounts for the long duration and wind direction variations as a hurricane passes via the methodology in Chapter 4. This analysis considers multiple gusts and wind directions throughout the duration of the storm.

Each of these three approaches is applied to analyze K_d from both a component and system perspective. The component perspective evaluates each building component individually, per the current ASCE 7 approach. The system perspective considers, for example, all four roof corners as a single entity, where failure of one corner equates to failure of that system.

5.1.1 Deterministic Approach

This method identifies the wind directionality effect for each of the individual subdivided areas over the building surface. The building is subjected to a single gust

speed coming from each of 72 wind directions (from 5°to 360°in 5°increments). This analysis follows a five step procedure for each surface area: (1) Area Averaging: Perform an average of the pressure coefficient time histories of the individual taps contributing to predefined building surface areas, (2) Create a peak Cp CDF library consisting of each area averaged time history for each wind direction, (3) Identify the 22% percentile for each peak Cp CDF in the library, (4) Define $C_{p\_worstcase}$ for each surface area at that corresponding to the maximum $C_{p\_22\%}$ among all directions, (5) Determine the worst case pressure and the wind directionality factor. Treatment of components as individual entities and as a system will be explained during the detailed discussion of the five steps.

Step 1: Area Averaging of the external pressure coefficients time histories for each building surface area

This study uses wind tunnel data from the online NIST Aerodynamic Database. The characteristics of the building used in this study are presented in Table 5-1.

Table 5-1. Building Characteristics (Source: NIST Aerodynamic Database)

Building Number	NIST Database Building Label	Exposure	Model Scale	Roof Slope	Eave Height (ft)	Plan Dimensions (ft x ft)
1	m11 m12	Open Suburban	1:100	3:12 (14°)	16	80 x 125

The effect of the spatial area averaged of the external pressure coefficients is introduced to account for correlations between the individual taps (point taps) within an area. To calculate the area averaged pressure coefficient time history the tributary area (A_i) corresponding to each individual tap is identified. Then, a weighting factor (δ_i) for

each tap is defined (Eq. 5-1) as the ratio between the tributary area (A_i) over the total area (A_T) corresponding to a predefined zone (Fig. 5-1).

$$\delta_i = \frac{A_i}{A_T} \tag{5-1}$$

ASCE 7 provides guidance for C&C zones for the purpose of defining the appropriate pressure coefficients. These zones were used to define the building surface areas as a simple first-cut trial as this algorithm was developed. Figure 5-1 illustrates the zone definition for a gable roof less or greater than 7 degrees. Once the individual weighting factor for each tap has been determined, the pressure time history of a given tap is multiplied by its corresponding weighting factor. The weighted pressure time histories within the predefined zone are summed to determine the area averaged time history as defined in Eq. 5-2. This is performed for each of the 72 wind directions.

$$C_{p\_area\_average\_zone} = \sum_{i=1}^{n} C_{p1} \times \delta_1 + C_{p2} \times \delta_2 + \cdots + C_{pn} \times \delta_n \tag{5-2}$$

where $C_{p\#}$ is the pressure time history of a given tap, δ is the weighting factor corresponding to a given tap, i is the tap number, n is the total number of pressure taps in the predefined zone, and $C_{p\_area\_average\_zone}$ is the area averaged pressure time history.

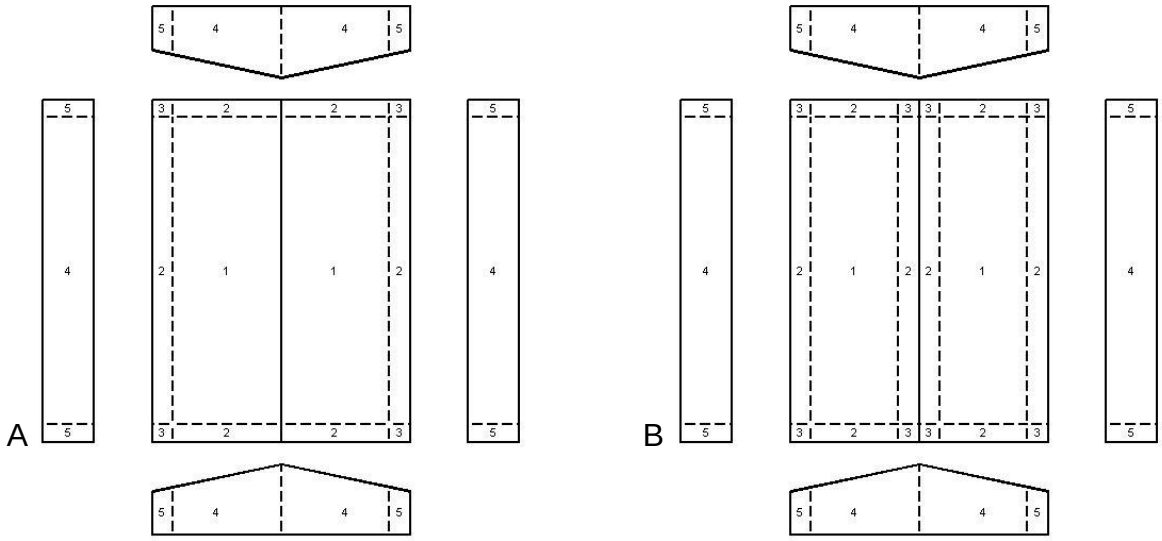

Figure 5-1. ASCE 7 Zones 1,2,3,4, and 5 of the building for Enclosed, Partially Enclosed Buildings. A) Zones for C &C With a Gable Roof $\theta \leq 7^{o}$. B) Zones for C & C With a Gable Roof $7^{o} < \theta \leq 27^{o}$.

The area averaging procedure is applied to squared areas 3ft x 3ft, 5ft x 5ft, and 7ft x 7ft. The individual taps time histories whose tributary area falls partially of fully within squared area are used to create the area averaged time history. The areas used in this study are relatively close to effective wind areas (less than $100ft^2$) presented in the ASCE 7 for external pressure coefficients which are representative of common sizes of C&C.

Step 2: Peak CDF library as a function of wind direction

A probability density function (PDF) model of the peak Cp values in each area averaged time history and direction is fitted (minimum -Cp in suction, maximum +Cp for positive pressure). The peak Cp PDF modeling is conducted using a translation

technique designed for use in modeling the peaks pressure coefficients in wind tunnel data (Peng et al., 2013).

An example of the area averaging is presented in Figure 5-2. The individual time histories measured at four adjacent taps (1, 2, 3, and 4), and their peak CDF models are shown in the top right figure. The center right figure presents the resultant area averaged pressure coefficient time history and its peak CDF model. The analyses in Chapter 4 utilized the individual tap time series, while the analysis in this chapter uses the area averaged time histories to reflect the ASCE 7 area averaging procedures used to produce components and cladding pressure coefficients.

Steps 3 and 4: Probability of exceedance of the peak C_p PDF and C_p worst case

The scalar C_{p_peak} for each area and each direction is identified as that corresponding to a 22% percentile based on the modeled peak C_p PDF (Figure 5-2, lower right). For each area the largest magnitude C_{p_peak} among the 72 approach wind directions is retained as the $C_{p\_worstcase}$ (Figure 5-2, lower right). The $C_{p\_worstcase}$ thus conceptually emulates the worst case direction enveloping procedure used in the current ASCE 7 to define GC_p.

Step 5: Worst case pressure and wind directionality factor

The resultant worst case pressure $P_{\_worstcase}$ is defined in Eq. 5-3 as:

$$P_{worstcase}(i) = C_{p_{worstcase}}(i) \times V^2{}_{Design} \quad (5\text{-}3)$$

where i indicates the specific building area, $C_{p\_worstcase}$ is the maximum C_{p_peak} among the 72 approach, and V_{design} is the design wind speed.

The wind directionality factor is intended to quantify a multiplier that bridges the assumption that the design wind speed will approach from the worst direction and the

reality that the design wind speed likely will not approach from the worst direction. The probability that the design wind speed occurs from any of the 72 directions is assumed to be equally likely. The pressure for each area and wind direction is quantified in Eq. 5-4 as

$$P(i,j) = C_{p_{22}\%}(i,j) \times {V_{design}}^2 \quad (5\text{-}4)$$

where i and j are the area and the wind direction, respectively, $C_{p\_22\%} = C_{p\_peak}$ for the area, and V_{design} is the design wind speed. The direction weighted pressure per area is then the sum of the pressure from individual directions, weighted by the probability of each direction

$$P_i = \sum_{j=1}^{72} P(i,j)/72 \quad (5\text{-}5)$$

The directionality factor K_d for each area is then defined as the ratio of the direction weighted pressure to the worst case pressure

$$K_d(i) = \frac{P_i}{P_{worstcase}(i)} \quad (5\text{-}6)$$

In this approach, each building area is considered separately, referred to as the component perspective. The next section makes an adjustment to the above methodology to address the perspective that multiple components on a building should be viewed as a single system. For example, the windows on the four building elevations can be viewed as a window system. The approach is to evaluate whether any of the windows of that system are subjected to the worst case pressure load under any given wind direction. If any window receives the worst case pressure, the window system is considered to receive the worst case pressure. The concern is not the likelihood of each window receiving the worst case pressure, but rather whether any window receives the worst case pressure.

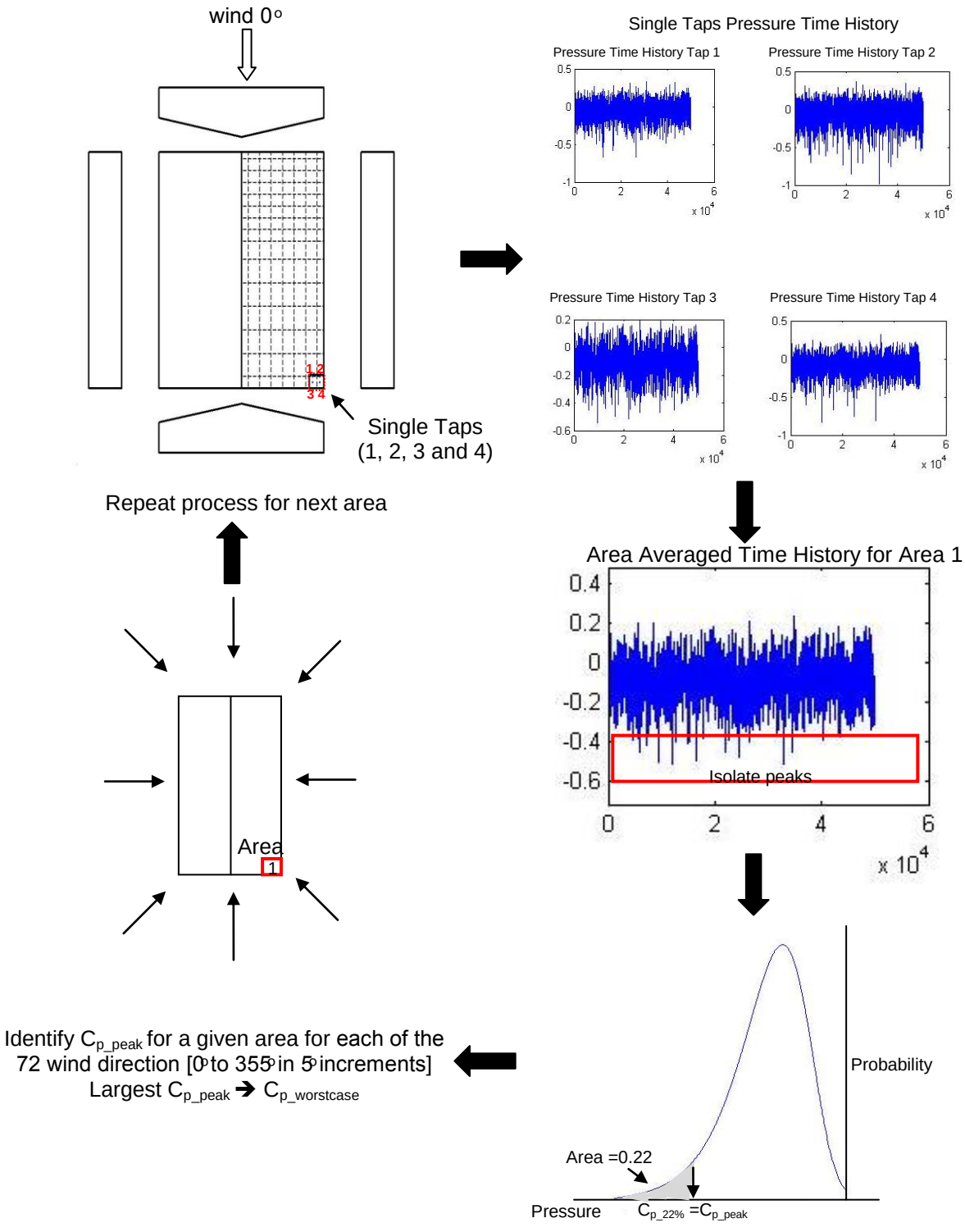

Figure 5-2. Analysis of averaged area 7 ft x7ft (area 1= single component) for 0° approach wind direction.

5.1.1.2. System perspective

To introduce the system perspective, roof corners are treated as part of a system to study the perspective of loading by identifying the weakest link of the chain (or the highest load among the components in the system). The perspective is whether any corner receives the worst case pressure load, rather than individually evaluating each corner as a separate component.

Step 5: Modification of the pressure definition

The system analysis follows the steps (1-4) in the previous section (5.1.1.1). However, step 5 is modified such that for any given wind direction, the pressure coefficient in Eq. 5-4 is selected as the maximum among the components in the system (each of four corners as shows Fig. 5-3). Eq. 5-4 is replaced with Eq. 5-7

$$P(i,j) = \left[max\left(C_{p1_{22}\%}, C_{p2_{22}\%}, C_{p3_{22}\%}, C_{p4_{22}\%}\right) \times V_{design}{}^{2}\right] \quad (5\text{-}7)$$

where the pressure coefficient is taken as the largest magnitude among all four corners ($C_{p1\_22\%}$, $C_{p2\_22\%}$, $C_{p3\_22\%}$, $C_{p4\_22\%}$).

The K_d factor is obtained for the system using Equations. 5-5, 5-6 and 5-7. Results are presented in Figure 5-4 for building 1 (Table 5-1) located in open exposure (left column) and suburban exposure (right column). Each figure contains the minimum, mean, and maximum K_d value among all areas (3ft x 3ft, 5ft x 5ft, and 7ft x 7ft) on the walls and roof of the building. The vertical and horizontal axes represent the K_d value and the squared areas. Figure 5-4 presents the results for the component (Eq.5-4) and for the system (Eq. 5-7) perspective. The results illustrates that the K_d range is reduced (i.e., lower spread) as the area averaged increases and as the exposure changes (from open to suburban).

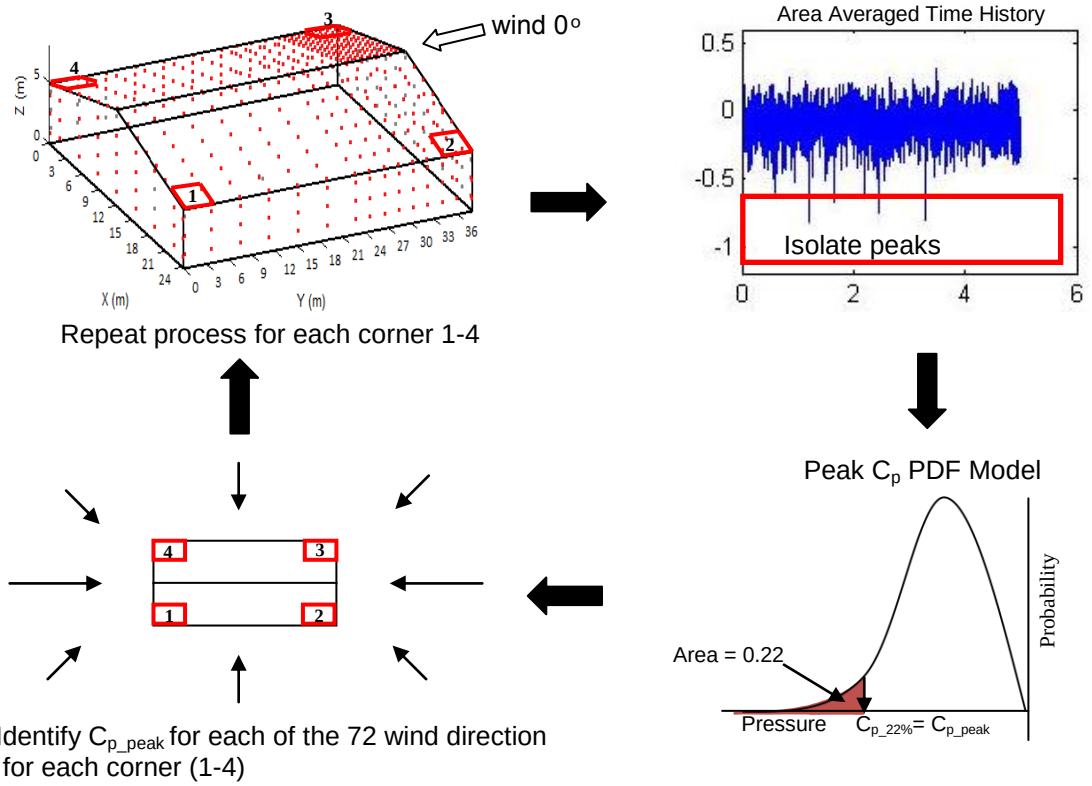

$C_{p\_22\%}$ of the system ➔ max [$C_{p1\_22\%}$, $C_{p2\_22\%}$, $C_{p3\_22\%}$, $C_{p4\_22\%}$]

Figure 5-3. Analysis of a Roof Corner System For 0°Approach Wind Direction.

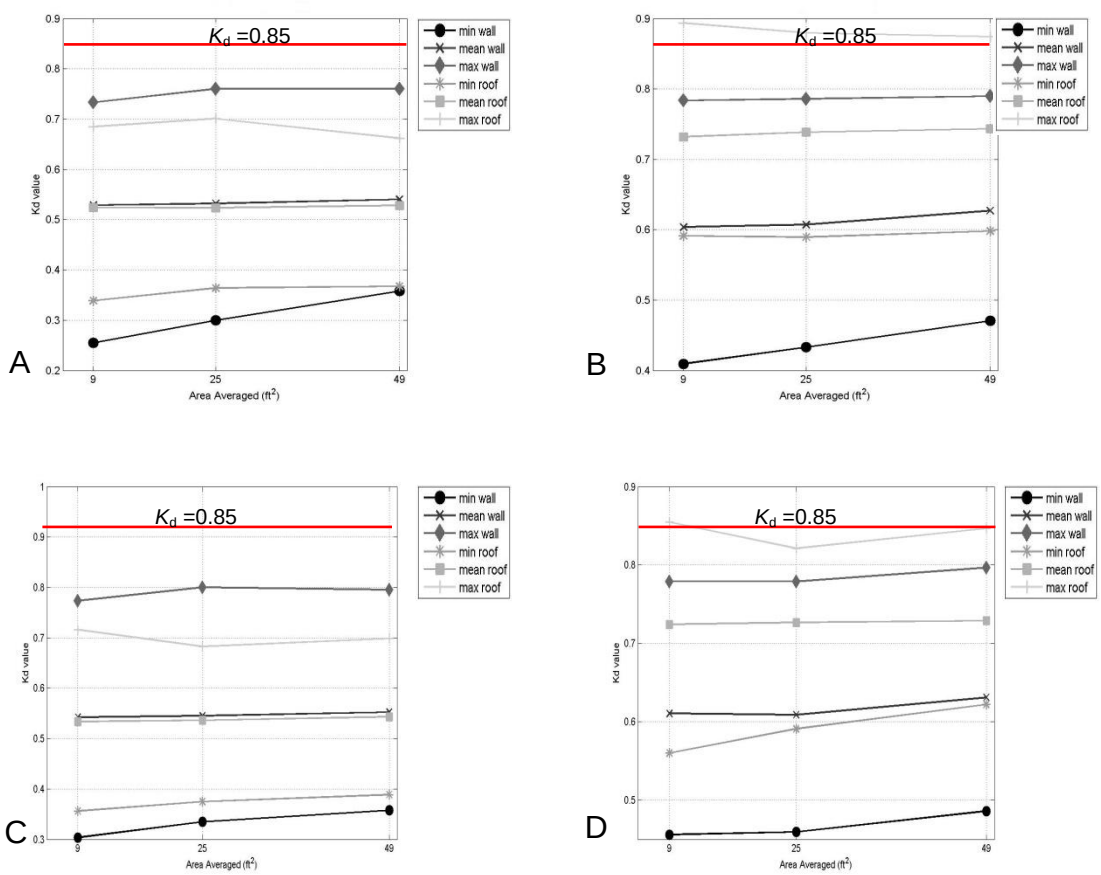

Figure 5-4. Minimum, mean, and maximum K_d factor for wall and roof following deterministic approach for squared areas 3ft x 3ft, 5ft x 5ft, and 7ft x 7ft. A) Component perspective in open exposure. B) System perspective in open exposure. C) Component perspective in suburban exposure. D) System perspective in suburban exposure.

5.1.2. Probabilistic Approach

The previously discussed deterministic approach calculates pressure from the product of velocity squared and a C_{p_peak} value representing the 22% percentile from the CDF library for a given direction. This treatment of the C_p as a fixed (deterministic) value is a simplification of the probabilistic nature of the pressure coefficient. The probabilistic approach directly incorporates the random nature of C_p by randomly sampling C_{p_peak}

values from the CDF library rather than using the 22% percentile. This is conducted using a Monte Carlo framework, where each simulation draws a random C_p value from the peak CDF library for each squared area and wind direction (Fig.5-5). This process is repeated 1000 times, generating 1000 samples of the K_d factor for each squared area. This process alters step 5 (equations 5-4 and 5-6 for the component and equation 5-7 for the system analyses) as follows.

Component perspective

Steps 1-4 of the component perspective remain the same, and step 5 is modified. The pressure (load) still assigns an equal probability of occurring from any of the 72 wind directions, however, the $C_{p\_22\%}$ is now replaced by a draw from the peak CDF library for an area per wind direction. Eq. 5-4 is re-defined as

$$P(i,j) = C_{p_{random}}(i,j) \times V_{design}{}^2 \tag{5-8}$$

where i and j are the area and the wind direction, respectively, C_{p_random} is the random C_p value drawn, and V_{design} is the design wind speed. This calculation is repeated 1000 times for each building area per wind direction, generating 1000 samples of the K_d factor per area. The final K_d factor per area is obtained by identifying a threshold as the 5% percentile ($K_{d\_5\%}$) from the 1000 K_d samples sequence. Equation 5-6 is replaced by

$$K_d(i,jj) = \frac{P(i)}{P_{worstcase}(i)} \tag{5-9}$$

$$K_{d\_final} = K_{d_5\%}[K_d]_{1000x1} \tag{5-10}$$

where i and jj are the area and the simulation. The sensitivity of the threshold used to identify the final K_d is also investigated by calculating the K_d corresponding to different percentiles in Eq. 5-10 (i.e., 5%, 10%, 20%, 22%, among others).

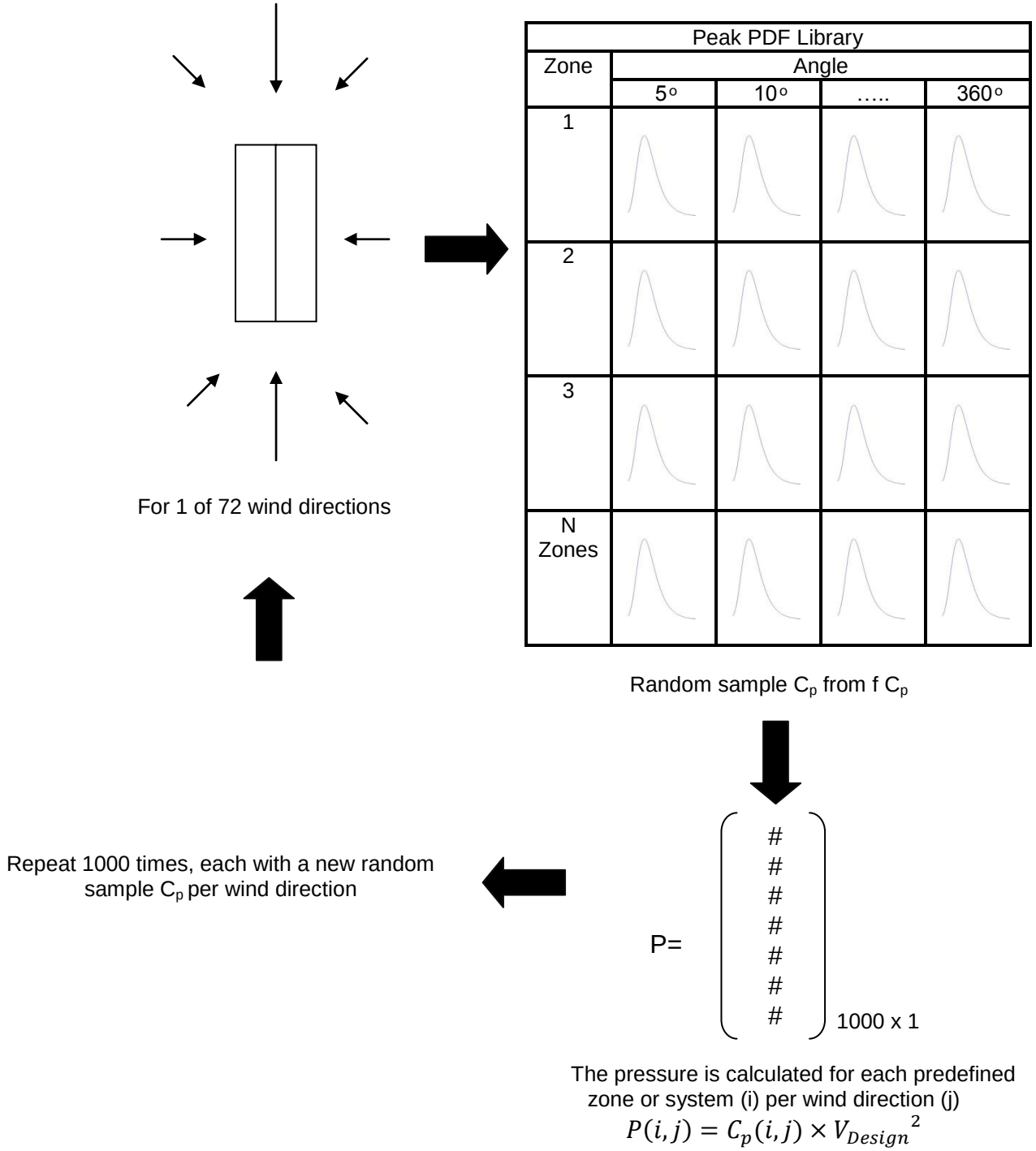

Figure 5-5. Monte Carlo analysis for an assigned design wind speed per wind direction.

System Perspective

To apply the system perspective, the assignment of the pressure coefficient is substituted by a draw from the maximum among the four symmetric corners in the system per wind direction. Eq. 5-8 is re-defined as

$$P(i,j) = C_{p_{random}}(i,j) \times V_{design}{}^{2} \quad (5\text{-}11)$$

$$C_{p_{random}}(i,j) = max[C_{p_{random_1}}, C_{p_{random_2}}, C_{p_{random_3}}, C_{p_{random_4}}] \quad (5\text{-}12)$$

where i and j are the area and the wind direction, respectively, C_{p_random} is the maximum random C_p value among all four symmetric corners per wind direction, and V_{design} is the design wind speed. This calculation is repeated 1000 times for each building area, generating 1000 samples of the K_d factor per area. The final K_d factor per area can be obtained by identifying the K_d factor corresponding to 5% probability of exceedance from the 1000 samples sequence (Eqns. 5-9 and 5-10). This 5% probability of exceedance applied in Eq. 5-10 is somewhat arbitrary, and represents a small permissible probability of exceeding the worst case pressure (the ASCE 7 concept). Figure 5-6 presents the threshold definition used in the analysis and how this value can change depending on the desired tolerance for a specific risk level. For example, if this 5% probability is relaxed to say 20%, it should result in a lower K_d value. Conversely, if this 5% limit is tightened to 1%, the resultant K_d should increase. Results are thus presented using this probability threshold as an independent variable.

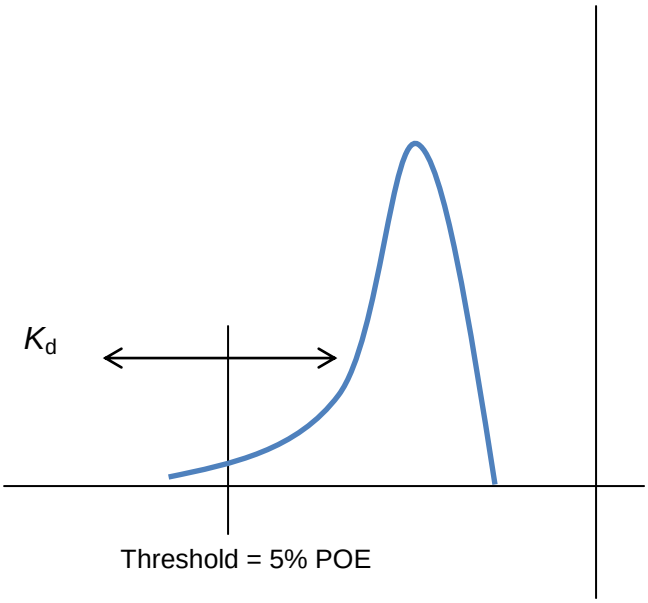

Figure 5-6. Threshold definition.

5.1.2.1 Results interpretation

Figures 5-7 and 5-8 present the K_d factor obtained for building 1 using two exposures for the component perspective (left column) and system perspective (right column). Within each plot the K_d values are represented as the minimum, mean, and maximum among all areas in the building. The top, middle, and bottom rows in each figure are the results for the area averaged 3 ft x 3ft, 5ft x 5ft, and 7ft x 7ft. The horizontal axis is the complement of the probability of exceedance associated with Equation 5-10, or the probability of non-exceedance. Thus 95% on the x-axis in Figures 5-7 and 5-8 corresponds to the 5% specified in Eq. 5-10. The results illustrate that the range (spread) of the K_d value is reduced as the area increases and as the exposure changes from open to suburban. It is observed that K_d increases as the probability of non-exceedance (horizontal axis) increases. As expected, moving from the component to the system perspective (from left column to right) shows an increase in the K_d values.

The deterministic and probabilistic analyses of the wind directionality factor thus far presented do not consider the nature of the climatology associated with the hurricane hazard. The design wind speed is assumed to occur once, from a random direction, and without regard to the wind behavior preceding and following the occurrence of this peak wind. For this reason, the relative behavior of K_d as a function of the control variables (exposure, area size, component vs. system perspective, and permissible probability of non-exceedance) is of interest in Figures 5-7 and 5-8, but the comparison of K_d values vs. the ASCE 7 value of 0.85 is not considered valuable.

The next section presents the scenario analysis, whereby the single gust wind speed is replaced with a time history of wind speed and direction through the duration of a land falling hurricane from the historical record. The probabilistic nature of the relationship between wind speed, direction and load is maintained by adapting the probabilistic approach within the scenario analysis. It is proposed that this scenario analysis is a better representation of the true vulnerability of the building to hurricane wind loading, and therefore a more appropriate approach for determining the directionality factor.

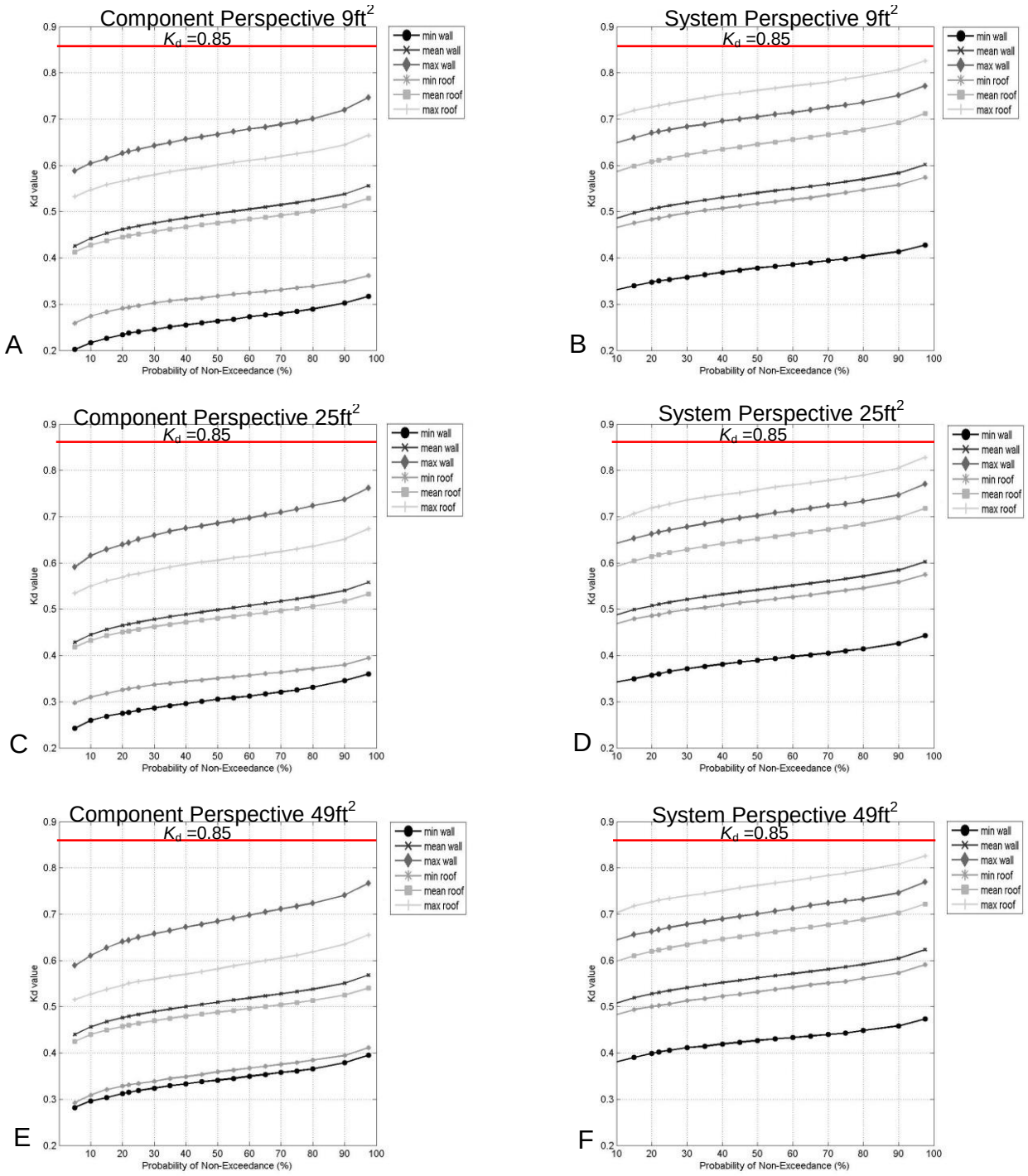

Figure 5-7. Minimum, mean, and maximum K_d factor for wall and roof following probabilistic approach for different probability of non-exceedance in open exposure. A) 9 ft^2 component perspective. B) 9 ft^2 system perspective. C) 25 ft^2 component perspective. D) 25 ft^2 system perspective. E) 49 ft^2 system perspective. F) 49 ft^2 system perspective.

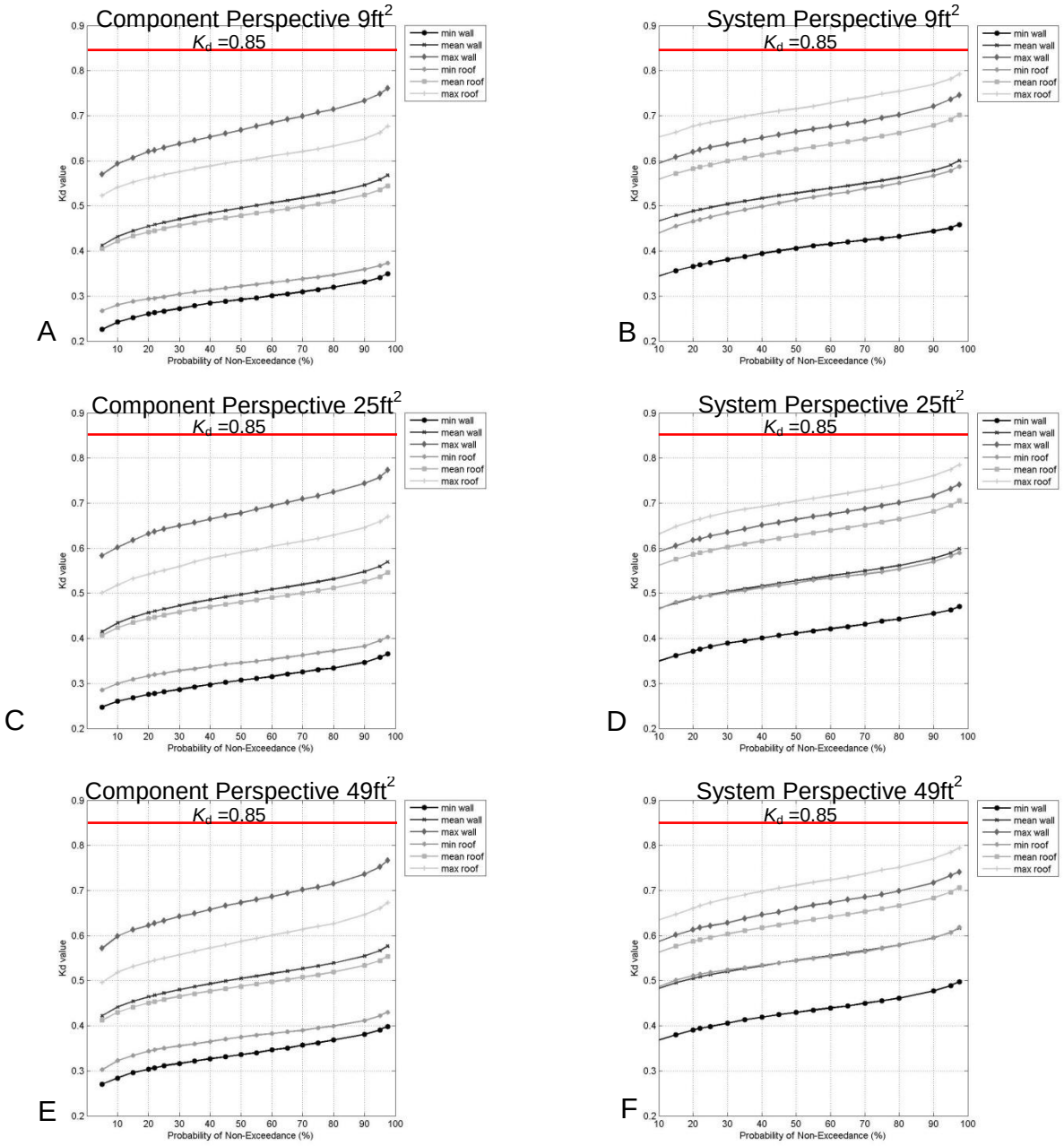

Figure 5-8. Minimum, mean, and maximum K_d factor for wall and roof following probabilistic approach for different probability of non-exceedance in suburban exposure. A) 9 ft^2 component perspective. B) 9 ft^2 system perspective. C) 25 ft^2 component perspective. D) 25 ft^2 system perspective. E) 49 ft^2 system perspective. F) 49 ft^2 system perspective.

5.1.3. Scenario Analysis

This section presents the development of a directionality factor methodology specifically for components and cladding on hurricane prone residential construction, where clearly the duration and associated changing direction of the high wind event presents a significantly different wind hazard than the presumed one gust, one direction concept.

The methodology explained in section 4.2 is adapted to this analysis, with several modifications. For clarity, the methodology is presented full at the cost of some repetition of the material in Chapter 4.

Steps 1-4: Area averaged pressure time, peak CDF library, and worst case C_p

The procedure explained section 5.1.1.1 (steps 1-4) is also applied for the scenario analysis. The wind tunnel data consisting of external surface pressure coefficients (C_p time histories) on low rise buildings is accessed from the online NIST Aerodynamic Database. The characteristics of the building used in this study are presented in Table 5-1. For details of the process refer to section 5.1.1.1 (Steps 1-4).

Step 5: Historical hurricane datasets: hurricane wind speed and direction time histories

Time histories of ground level wind speed and wind direction through the duration of four land-falling hurricanes are also accessed from the NOAA Hurricane Research For this study, the speed and direction time histories from H*Wind in three hour increments are resampled at 30 minute increments using linear interpolation. Hurricanes Frances (2004), Ivan (2004), Katrina (2005) and Rita (2005) are used.

Step 6: Monte Carlo simulation: combining peak C_p PDF models and historical hurricanes

Using the H*Wind database, the time history of wind velocity was projected onto the building. For a given building, terrain exposure and hurricane wind velocity time history, the peak Cp PDF library provides the means to evaluate the probability that the resultant surface pressure exceeds the value obtained using the ASCE 7 approach of assuming worst case direction applied to a fixed Cp_worstcase value.

The methodology used for the K_d definition is explained in this section within the context of one NIST building at two locations impacted by one historical hurricane. Additional building locations, exposures and hurricanes are then introduced to demonstrate the sensitivity of K_d to these variables and provide the statistical evidence to support the conclusions.

Consider the placement of a NIST low rise building in a coastal location impacted by a hurricane. The time history of wind speed and direction imparted by this historical hurricane at the location of the building was determined from the H*Wind Surface Wind Analysis tool in 30 minute increments.

Two surface pressure analyses were conducted for the building. The first pressure is a representation of the concepts used in ASCE 7. The highest wind speed during the hurricane at the building location (V_{max}) was assumed to approach from a direction aligned with the worst case aerodynamic direction for each area. The resultant worst case pressure $P_{\_worstcase}$ is defined in Equation 5-13 as:

$$P_{worstcase}(i) = C_{p_{worstcase}}(i) \times V^2{}_{max} \quad (5\text{-}13)$$

where i indicates a particular location (area) on the building, $C_{p\_worstcase}$ was defined previously as the largest C_{p_peak} among all approach directions, and C_{p_peak} was defined as the C_p corresponding to a 22% percentile based on the modeled peak C_p PDF (Fig. 5-2, lower right).

The second surface pressure analysis subjected the building to a series of wind velocities during the passage of the hurricane, rather than just V_{max}. The peak C_p value for each area was randomly sampled from the peaks C_p PDF model assigned for that area and approach wind direction. A time history of peak pressure was generated for each area on the building surface (Equation 5-14)

$$P(i,k) = C_p(i,k) \times V(k)^2 \quad (5\text{-}14)$$

where i and k are the area and 30 minute time increment, respectively, and $V^2(k)$ is the squared wind speed at time increment k. For every time increment, the C_p (i,k) values were resampled from the peak C_p PDF model assigned for the area (i) and approach wind direction.

For each area, the largest magnitude pressure through the duration of the hurricane was retained as shown in Equation 5-15

$$P_{i\_max} = \max\big(P(i,k)\big), over\ all\ k \quad (5\text{-}15)$$

P_{i_max} is thus a single random sample of the highest occurring pressure value at area (i) as the hurricane passed, where the random components are the assigned C_p at each time increment k, and the orientation of the building which is fixed through the hurricane passage and simulation.

This analysis is repeated using a Monte Carlo framework, where for each simulation the building is given the same orientation and subjected to the same

hurricane velocity time history. The $C_p(i,k)$ values are again resampled from the appropriate peak C_p PDF model. P(i,k) is reconstructed and the largest magnitude produced a new sample of P_{i_max} at each area. This process is repeated 500 times for each of 72 building orientations, generating 500 samples of P_{i_max} at each area as shown in Figure 5-9. The assignment of the building orientation to each of 72 directions is a departure from the method in Chapter 4, where the building orientation was randomly assigned.

The K_d is determined for each area and building orientation by identifying the P_{i_max} corresponding to the 5% probability of exceedance ($P_{max5\%}$) of the 500 maximum wind pressure samples for an area and fixed building orientation as

$$K_d(i,g) = \frac{P_{max5\%}[MWP]_{1000x1}}{P_{worstcase}(i)} \quad (5\text{-}16)$$

where i and g are the area and building orientation, respectively. This process is repeated for the each of the 72 building orientations. An equal probability of the building being oriented with respect to any of the 72 wind directions is assumed. Then, the K_d factor for each predefined zone can be obtained as:

$$K_d(i) = \sum_{g=1}^{72} \left(\frac{1}{72}\right) \times K_d(i,g) \quad (5\text{-}17)$$

The sensitivity of the K_d factor to the probability of exceedance used to identify the maximum wind pressure and the worst case pressure coefficient is also investigated.

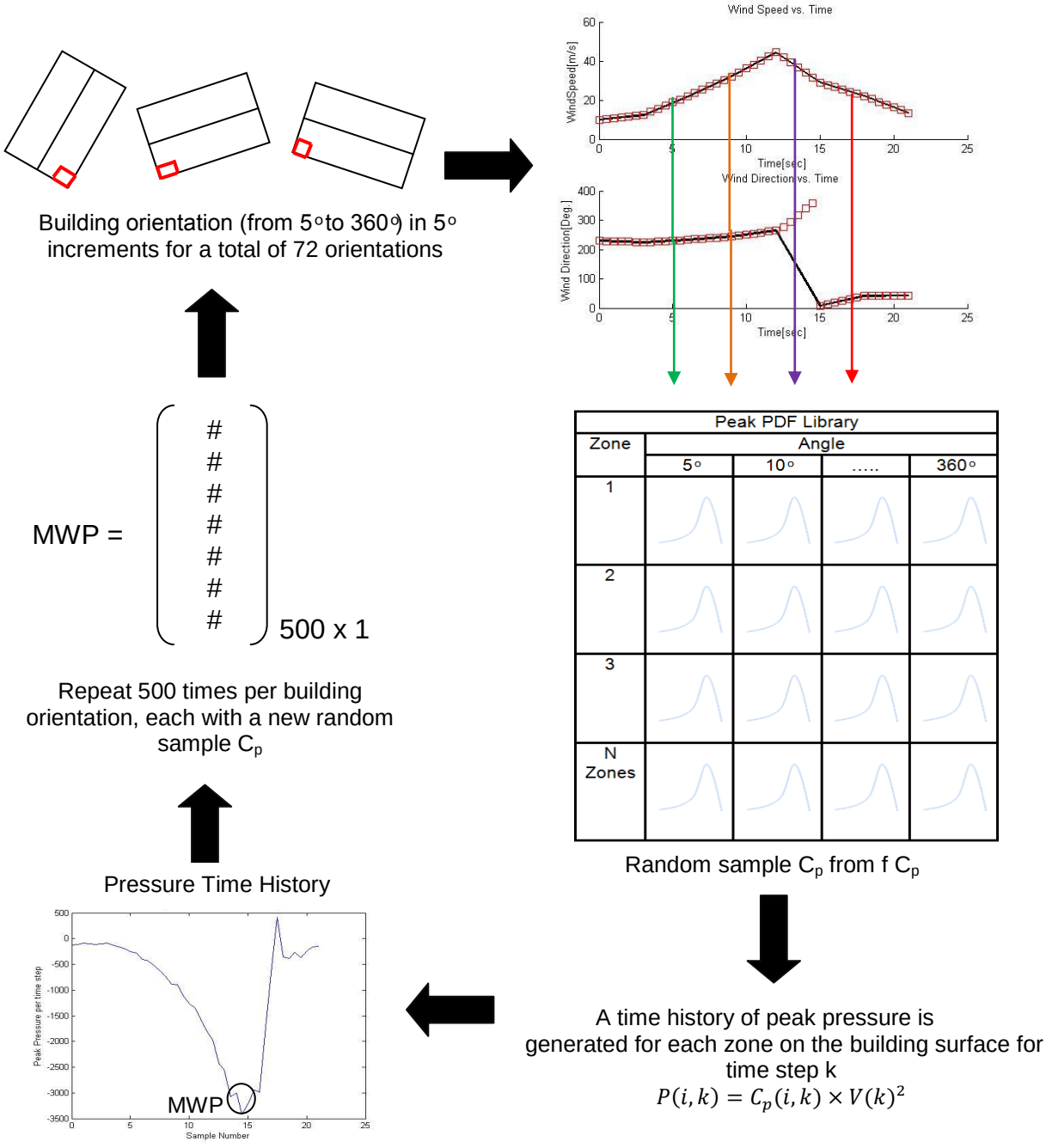

Figure 5-9. Monte Carlo analysis for each building surface area.

This process is performed using both the component and system perspectives for squared areas (3ft x 3ft, 5ft x 5ft, and 7ft x 7ft) and single taps. The results using area averaged (i.e., 3ft x 3ft) are then compared with the single taps in order to identify similarities or differences.

Figures 5-10 through 5-12 present a sample outcome for the squared area 7ft x 7ft of the above described methodology to define K_d. Building m11 (building m11 in open terrain) is subjected to hurricane Frances wind velocity time histories at two locations, one on the strong sided and one on the weak side (Figure 5-10). K_d was determined according to Equation 5-17 at each area on the building surface and presented in Figures 5-11 (weak side location, Figure 5-11) and 5-12 (strong side location, Figure 5-11) in a contour format. Each figure illustrates the K_d value for the component (left) and system (right) perspective as the probability of exceedance used in Eq. 5-10 varies from 95% (top row) to 2.5% (bottom column). The contours illustrate that the K_d increases as the probability of exceedance (percentile) specified in Eq. 5-10 decreases (representing a lower risk level). K_d values greater than 0.85 are noticed for the components perspective, but are more likely to occur when using the system perspective.

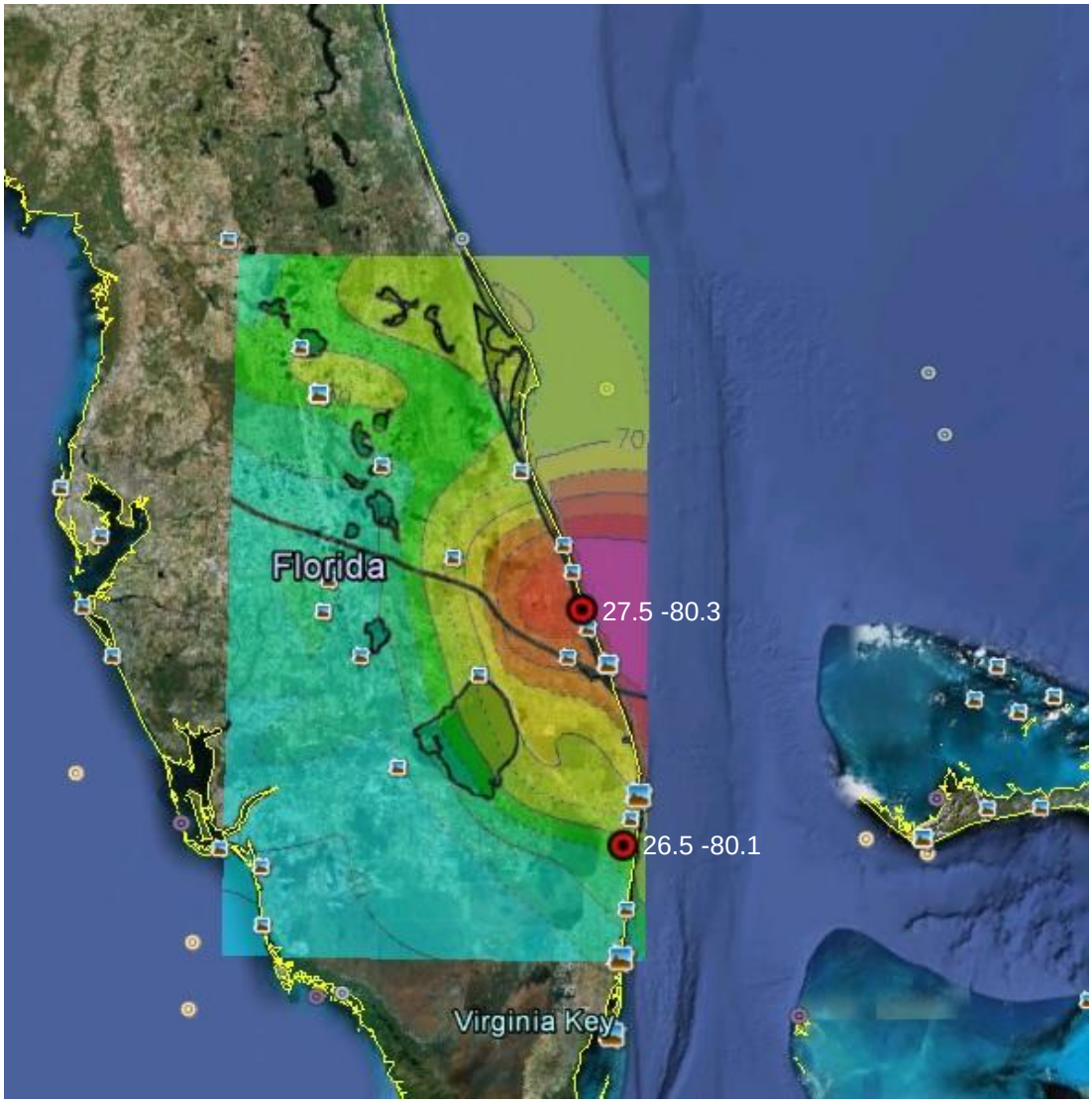

Figure 5-10. Hurricane Frances peak wind speed swath (NOAA HRD AOML H*Wind) and two building locations (26.5N,80.1W and 27.5N, 80.3W). Map courtesy Google Earth.

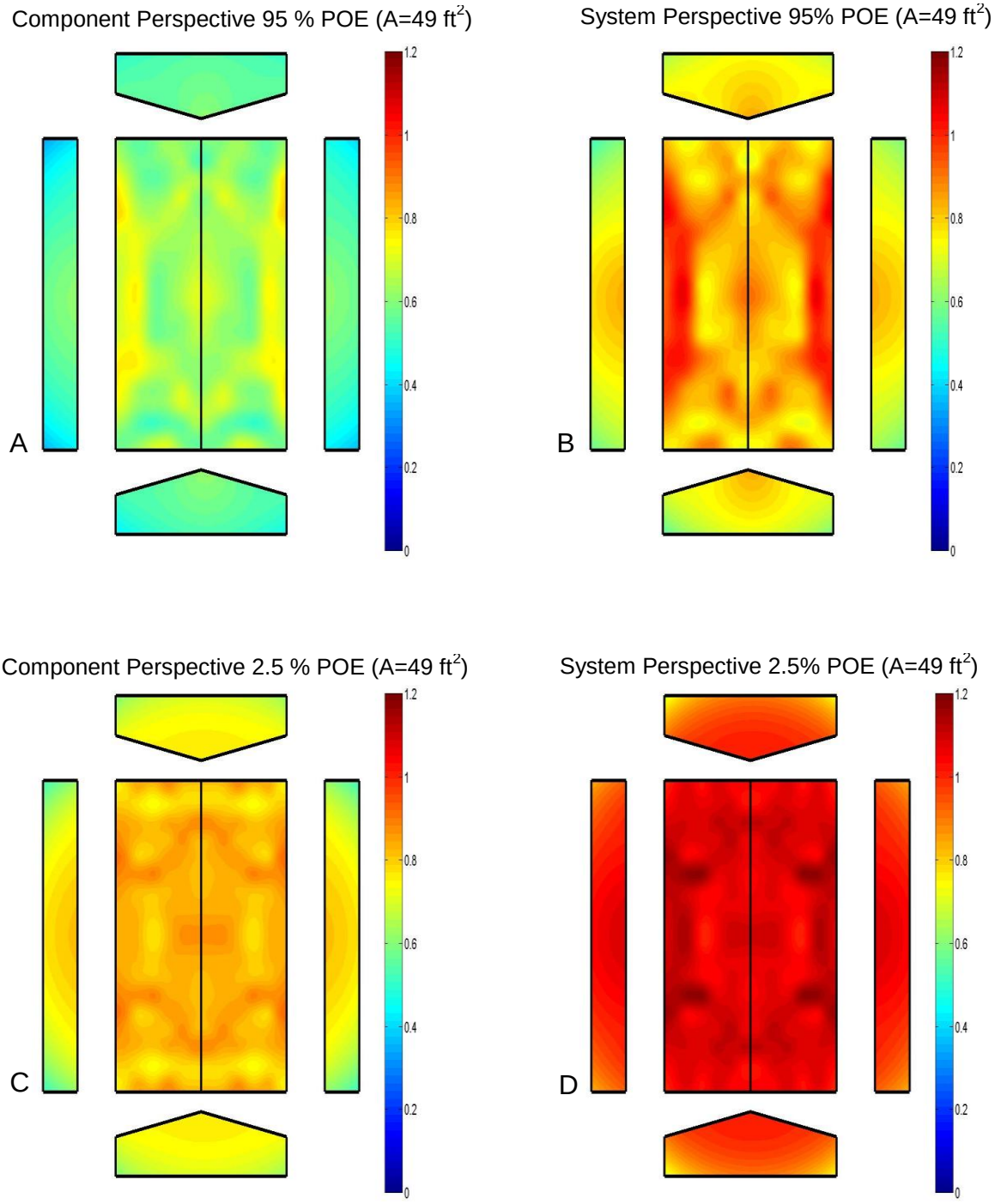

Figure 5-11. K_d contour for suction for area 7ft x7ft (26.5N, 80.1W). A) Component perspective for a 95% POE. B) System perspective for a 95% POE. C) Component perspective for a 2.5 POE. D) System perspective for a 2.5% POE.

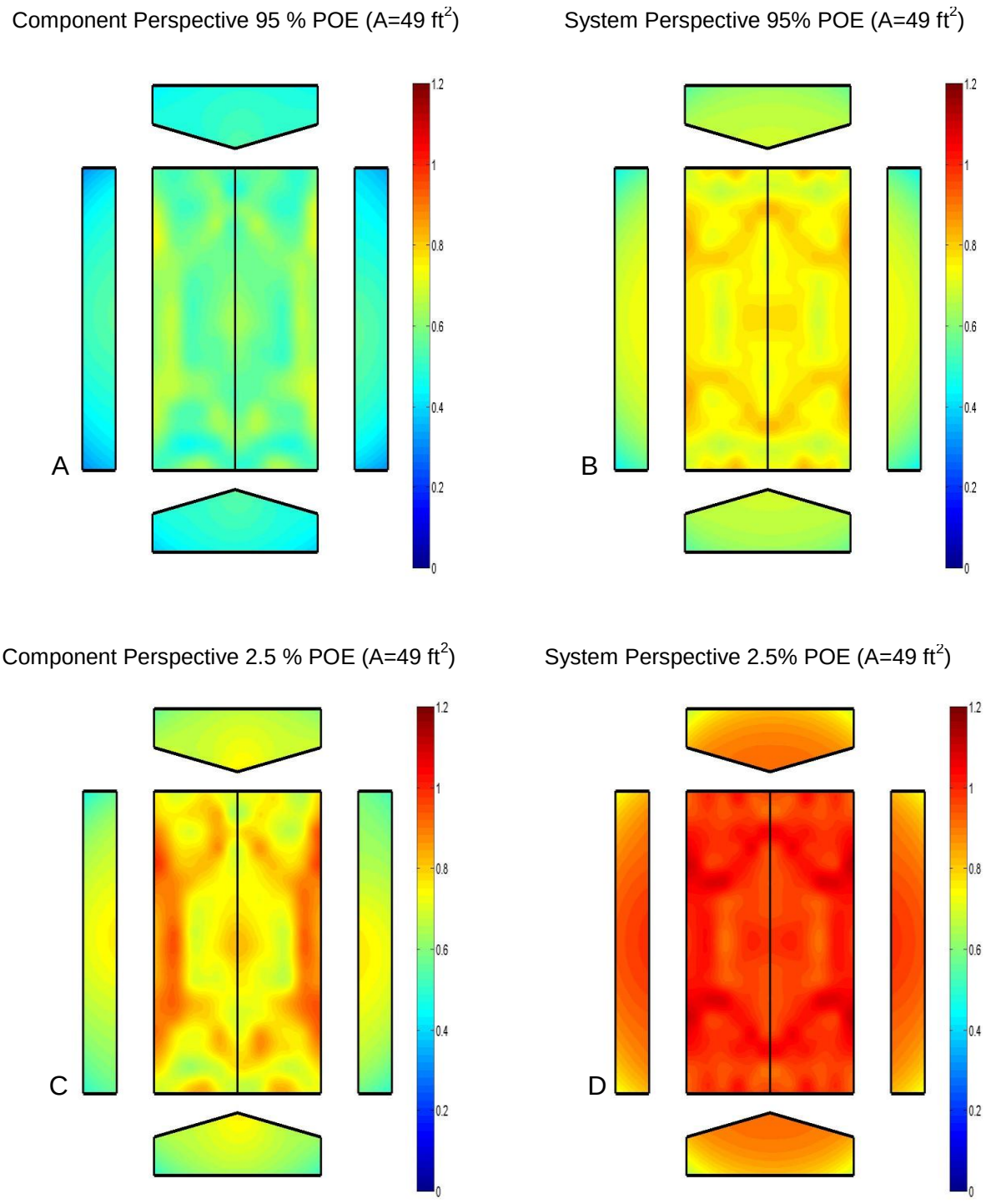

Figure 5-12. K_d contour for suction area 7ft x7ft (27.5N, 80.3W). A) Component perspective for a 95% POE. B) System perspective for a 95% POE. C) Component perspective for a 2.5 POE. D) System perspective for a 2.5% POE.

5.1.3.1. Monte Carlo Results: Expansion to Multiple Locations, Exposures, and Hurricanes

Any change in input variables that alters the wind velocity time history or peak C_p PDF library will potentially alter the resultant K_d(i) values. Building m11 (Table 5-1) is placed in multiple locations for multiple hurricanes in order to consider the variations in the wind time history. The variations in exposure (i.e., open and suburban) are also considered to evaluate the sensitivity of the peak C_p PDF library. The previously outlined 500 simulation Monte Carlo K_d analysis methodology is repeated for 1 building, two exposures per building (open and suburban), four hurricanes, and forty-three locations among the four hurricanes (Figure 5-13). The outcomes are then combined to provide an assessment of the current K_d factor for components and cladding in ASCE 7. The variables in this study include:

- Building and exposure (see Table 5-1): m11, and m12
- Hurricanes (Figure 5-13 and Table 5-2): Frances (2004), Ivan (2004), Katrina (2005), Rita (2005)
- Locations (Figure 5-12):
    1. Frances: 13 locations
    2. Ivan: 3 locations
    3. Katrina: 3 locations
    4. Rita: 24 locations

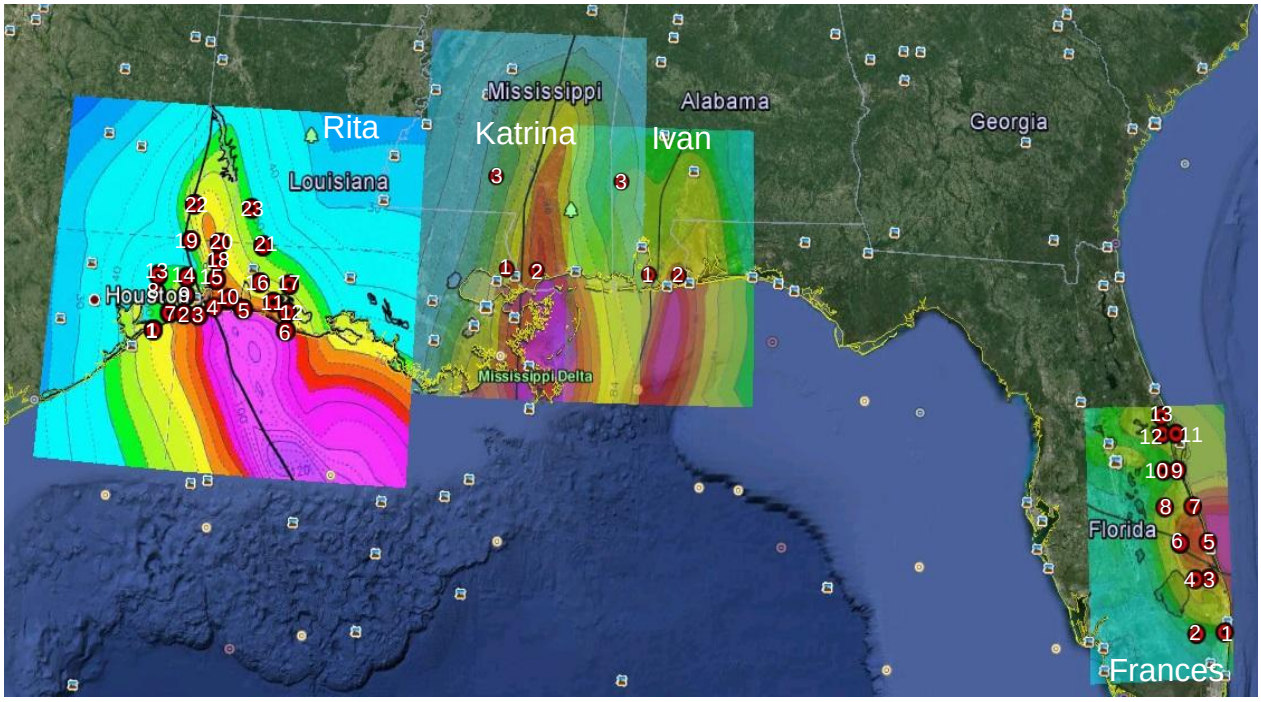

Figure 5-13. Historic hurricanes and building locations analyzed (map courtesy Google Earth).

Table 5-2. Building location per storm.

Location	Frances		Katrina		Ivan		Rita	
Number	Latitude	Longitude	Latitude	Longitude	Latitude	Longitude	Latitude	Longitude
1	26.5	80.1	30.4	89.8	30.4	87.5	29.5	94.5
2	26.5	80.5	30.4	89.4	30.4	87.9	29.7	94.1
3	27.1	80.3	31.4	90	31.4	90	29.7	93.9
4	27.1	80.7					29.8	93.7
5	27.5	80.3					29.8	93.3
6	27.5	80.7					29.6	92.7
7	27.9	80.5					29.7	94.3
8	27.9	80.9					29.9	94.5
9	28.3	80.7					29.9	94.1
10	28.3	80.9					29.9	93.5
11	28.7	80.7					29.9	92.9
12	28.7	80.9					29.8	92.7
13	28.9	80.9					30.1	94.5
14							30.1	94.1
15							30.1	93.7
16							30.1	93.1
17							30.1	92.7
18							30.3	93.5
19							30.5	94.1
20							30.5	93.7
21							30.5	93.1
22							30.9	94.1
23							30.9	93.7
24							30.9	93.3

5.1.3.2 Analysis Stratified by Hurricane

Building 1 (Table 5.1) was analyzed at these 43 locations among the four hurricanes. For each building and location results were gathered using the minimum, mean, and maximum K_d value among all areas on the building surface. The K_d is determined for each area and building orientation by identifying the P_{i_max} corresponding to the 5% probability of exceedance ($P_{max5\%}$) of these 500 maximum wind pressure samples for an area and fixed building orientation. This 5% represents a threshold that corresponds to a specific level of risk. This study analyzed the variations of the K_d with respect to different probability of exceedance (percentile) in order to draw conclusions regarding K_d for the component and system perspective. A level of risk corresponding to 1-15% probability of exceedance was chosen as a reasonable range to analyze the results obtained. The results can be interpreted as follows (Fig 5-14):

- A K_d equal to 1.0 represents that there is exactly 5% probability of the load exceeding the worst case pressure (Fig. 5-14 A).
- A K_d greater than 1.0 represents that there is more than 5% probability of the load exceeding the worst case pressure (Fig. 5-14 B).
- A K_d less than 1.0 represents less than 5% probability of the load exceeding the worst case pressure (Fig. 5-14 C).

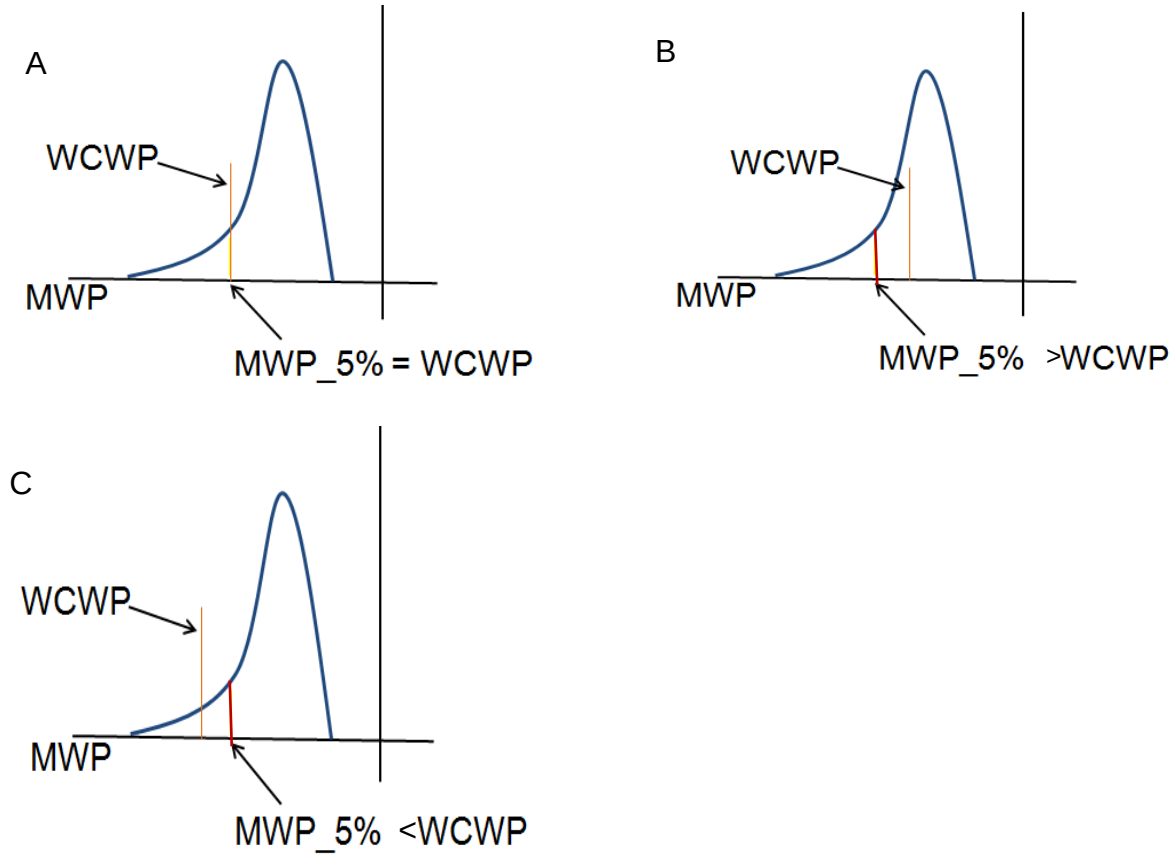

Figure 5-14. K_d definition corresponding to a 5% probability of exceedance (percentile).

The results provide the probability of exceedance associated with the current K_d=0.85 for components and claddings in the ASCE 7 to determine the level of risk. Also, the results can give a perspective of what would be the probability of exceedance by fixing a (e.g., K_d=0.90, 0.95 or 1.0). Appendix B provides the results corresponding to the scenario analysis for area averaged 3ft x 3ft, 5ftx5ft, and 7ft x 7ft, and single tap. A brief explanation of the information presented in Appendix B is discussed as follows.

Figures B-1 and B-2 compare the results obtained for single taps (left column) and area averaged 3 ft x 3ft (right column) for building 1 subjected to hurricanes Frances and Katrina in open exposure following the component perspective. The top, middle, and bottom row in each figure are the results for Frances [26.5N 80.1W, 27.5N 80.3W, and 28.7N 80.7] and Katrina [30.4N 89.4, 30.4 89.8, and 31.4N 88.3W].

The system perspective results for area averaged 3 ft x 3ft are presented in Figure B-3 for Frances (left) and Katrina (right). The right column in Figure B-1 vs. the left column in Figure B-3 contrasts the component and system perspectives (respectively) for Frances. Likewise, the right column in Figure B-3 vs. the right column in Figure B-2 contrasts the components and system perspectives (respectively) for Katrina. It is observed that the system perspective (weakest component in the system) produces considerably higher K_d values.

Before expanding the results for additional storms, locations and area sizes, a detailed discussion of Figures B-1 and B-2 is provided in order to assist in the proper interpretation of the results presentation. Recall that Equation 5-16 defines the directionally dependent K_d as the ratio of the 5% percentile of the 500 samples of maximum pressure (Equation 5-15) to the worst case pressure using the maximum hurricane scenario wind speed and worst case 22% percentile pressure coefficient (Equation 5-13). Results in Figure 5-16 shows the directionally weighted K_d (Equation 5-17) as a function of probability of non-exceedance (horizontal axis). The horizontal axis is the complement of the 5% percentile in the numerator in Equation 5-16. For example, a 5% percentile is represented in the plots as the 95% probability of non-exceedance. Thus from left to right in a given plot in Figure B-1 represents a decreasing probability of

exceeding the worst case pressure in the denominator in Equation 5-16. Consider Figures B-1 A and B. The mean result for the roof areas is presented as a gray line with square icons. If a 95% probability of non-exceedance is accepted as an appropriate risk (the proposed value in Equation 5-15), the corresponding appropriate K_d value is ~0.85 for the single taps and 3ft x 3ft (shown by the purple lines). In this same plot, the corresponding K_d value is ~1.07 for the maximum result for the roof areas for a probability non exceedance of 95% or a 5% probability of exceeding the denominator in Equation 5-16. Thus the presentation of results is intended to provide some guidance as to the risk associated with any given K_d value. Using the interpretation of the results provided in Figure B-1 it can be inferred for example that where the mean roof value is used there is less than a 5% chance of the load exceeding the worst case pressure. However, when the maximum roof value is used there is a change greater than 5% of the load exceeding the worst case pressure. These examples illustrated no significant variation between single taps (Fig. B-1 A) and 3ft x 3ft (Fig. B-1 B) since most of the subdivided 3 ft x 3ft areas were based on a single tap. Also, it important to highlight that the results for single taps using the new K_d approach aligned with the results obtained in Chapter 4. For instance, with the previous approach for two locations of Katrina (Figures 4-11 through 4-12) the K_d corresponding to 5% POE for the roof ranges between 0.90-0.98. In contrast, with the new approach (Fig B-2 A and C) the K_d corresponding to 5% POE for the maximum value for the roof is around 0.90-0.96 (light blue lines).

The results explanation of the scenario analysis is now extended to 5x5 ft areas and 7x7 ft areas in all hurricanes and locations (Figure 5-13) for the component perspective and system perspective. Table 5-3 provides a guide to the contents of the

results for areas 5x5 ft and 7x7 ft where the corresponding plots are located in Appendix B (Figures B-4 through B-59). Each Figure from Appendix B presents both component and system perspective results (left and right columns, respectively) at a specific location (row) in a given storm. The figures in Appendix B are arranged such that component perspective and system perspective results for a given storm and area size are adjacent for easy comparison. For example, Figures B-12 and B-13 present component and system perspective results for open and suburban exposure (respectively) for Hurricane Katrina using 5x5 ft areas. The analysis of the plots in Appendix B (section 5.2) is presented as follows. This includes two additional plots that consolidate the findings presented in Appendix B (Figures B-1 through B-59) and aid in illustrating the conclusions.

Table 5-3. Appendix B figures guideline for the component and system perspective

		Frances	Katrina	Ivan	Rita
Open Exposure	5x5 ft areas	B-4:B-7	B-12	B-14	B-16:B-23
	7x7 ft areas	B-32:B-35	B-40	B-42	B-44:B-51
Suburban Exposure	5x5 ft areas	B-8:B-11	B-13	B-15	B-24:B-31
	7x7 ft areas	B-36:B-39	B-41	B-43	B-52:B-59

5.2 Analysis of the Results

The previous sections presented the methodology and some results for the deterministic, probabilistic, and scenario analysis. Recall that deterministic and probabilistic approaches were used as a frame of reference to replicate the ASCE 7 assumption that the wind damage is based on a single gust coming from a single direction. These two approaches were also used to present the concept of the component and system perspectives. The scenario analysis considered the variations of

wind speed and direction during the passage of a hurricane. The wind directionality factor is presented with respect to probability of non-exceedance (level of risk).

A series of observations based on plots located in Appendix B (Figures B-1 through B-59) are first presented. This is followed by a presentation and discussion of Table 5-4 and Figure 5-15, which consolidate critical data from Appendix B (B-32 through B-35, B-40, B-42 and B-44 through B-51).

- Results in Figures B-1 and B-2 show the K_d (Eq. 5-17) as a function of probability of non-exceedance (horizontal axis). Recall, that the horizontal axis is the complement of the 5% percentile in the numerator in Eq. 5-16. These figures present a comparison between single taps and 3ftx3ft where no significant variations were observed. The highest K_d value was obtained for both locations on the weakest side of the storm for hurricane Katrina. For Frances the highest K_d values were on one of the weakest side (26.5N, 80.1W) follow up by the location on the strong side (27.5N, 80.3W).

- Figure B-1 B provides the guideline to identify the level of risk associated with a probability of non-exceedance for the component perspective corresponding to the location on the weak side of the storm for Frances (where higher K_d values were observed). For a level of risk up to 65% probability of exceedance (light green line) a $K_d > 0.85$ was obtained for the maximum roof value for area 3ftx3ft and single taps.

- Following the above, recall Fig. B-32A (green line) provides the same information as Fig. B-1, but for an area averaged size of 7ftx7ft. When larger areas are used the level of risk associate with exceeding the $K_d > 0.85$ tends to get reduced. However, there is still a high level of risk (up to 50%) in exceeding the current K_d.

- When comparing component vs. system for the maximum result for the roof areas (7ftx7ft) in open exposure (Fig. B-32 A and B-32 B) for a 5% risk level or 95% probability of non-exceedance (light blue line) the K_d is ~ 1.0 for the component perspective and ~1.18 for the system perspective. In both perspectives the current $K_d = 0.85$ was exceeded, however, higher values were observed in the system perspective.

- For all areas, hurricanes, locations and exposures a $K_d > 0.85$ for a 5% risk level or 95% probability of non-exceedance were observed using the mean and maximum roof values for the component perspective, but more likely to occurred in the system perspective and in the maximum values. Figure 5-15 will clarify this further.

- When comparing component in open exposure vs. component in suburban exposure minimal variation of the K_d value was found for a 5% risk level. For instance, figures B-42 A and B-43 A show results obtained for Ivan in open and suburban exposure,

respectively. Using the results of maximum roof for a 5% risk level or 95% probability of non-exceedance light blue lines) a K_d of ~0.89 and 0.90 were observed for open and suburban exposure, respectively.

- Following the above for the system perspective, minimal variation was observed in terms of exposure. Figures B-42 B and B-43 B illustrate that using maximum roof values for a 5% risk level or 95% probability of non-exceedance (light blue lines) a K_d of ~1.01 and 1.04 were observed in open and suburban.

- Comparing the results obtained for the maximum wall values among all combinations for a 5% risk level or 95% probability of non-exceedance, i.e.,4 storms, 39 locations, and 2 exposures (Figures B-4 through B-59), the current K_d = 0.85 was observed to be exceeded in most combinations for the component perspective, but were more likely to occurred in the system perspective.

- Table 5-4 provides the measures of variability that were calculated to identify the degree of deviation from the mean value and the dispersion of the K_d values obtained throughout all locations for a given storm. For instance, the results under Frances were obtained for a 5% risk level based on the minimum, average, and maximum K_d value obtained among all the areas averaged and the thirteen locations considered. In the table, the K_d range provides the lowest and largest K_d value throughout all locations considered for a given storm, however, the range is the maximum difference in K_d values. The standard deviation measures the variation from the mean throughout all locations for a given storm using the mean and maximum wall and roof values. The COV provides the dispersion throughout all locations for a given storm.

- In Table 5-4 the COV among multiple locations for a given storm was typically less than 10%, with the largest exception at 13.01%. This indicates that the K_d value as determined by the proposed methodology is only mildly sensitive to the specific building location. Thus the results presented to date suggest that regional dependence is not a substantial factor beyond the delineation between hurricane and non-hurricane prone regions. However, additional hurricane prone regions beyond Florida should be included in future expansions of this analysis to either validate or alter this conclusion regarding regional sensitivity.

Table 5-4. Measures of spread for 95% probability of non-exceedance (5% risk level)

Area				Frances	Katrina	Ivan	Rita
5ft x 5ft	Component Perspective	K_d range	Walls	0.37-0.99	0.45-0.86	0.46-0.82	0.37-1.05
			Roof	0.43-1.09	0.50-0.96	0.51-0.92	0.44-1.06
		Range	Walls	0.62	0.41	0.36	0.69
			Roof	0.66	0.46	0.41	0.63
		Standard Deviation	Walls	0.091(mean)	0.05(mean)	0.02(mean)	0.07(mean)
				0.11(max.)	0.06(max.)	0.02(max)	0.08(max.)
			Roof	0.085(mean)	0.04(min.)	0.02(mean)	0.07(mean)
				0.090(max.)	0.04(max.)	0.003(max)	0.06(max.)
		COV(%)	Walls	13.01	6.82	2.91	9.08
			Roof	9.52	3.90	0.34	6.48
	System Perspective	K_d range	Walls	0.56-1.16	0.69-1.00	0.70-0.96	0.56-1.13
			Roof	0.69-1.20	0.74-1.07	0.73-1.06	0.71-1.15
		Range	Walls	0.61	0.31	0.27	0.57
			Roof	0.51	0.32	0.33	0.43
		Standard Deviation	Walls	0.12(mean)	0.05	0.012(mean)	0.08(mean)
				0.09(max.)	0.03	0.013(max.)	0.05(max.)
			Roof	0.09(mean)	0.03	0.011(mean)	0.05(mean)
				0.06(max.)	0.02	0.013(max.)	0.04(max.)
		COV (%)	Walls	8.85	3.21	1.39	5.54
			Roof	5.63Katrina	1.78	1.25	3.65
7ft x 7ft	Component Perspective	K_d range	Walls	0.39-0.98	0.47-0.86	0.50-0.81	0.39-1.03
			Roof	0.46-1.06	0.53-0.92	0.54-0.92	0.45-1.03
		Range	Walls	0.59	0.39	0.31	0.64
			Roof	0.59	0.39	0.38	0.58
		Standard Deviation	Walls	0.089(mean)	0.05(mean)	0.019(mean)	0.07(mean)
				0.10(max.)	0.06(max.)	0.019(max.)	0.07(max.)
			Roof	0.084(mean)	0.04(mean)	0.02(mean)	0.07(mean)
				0.092 (max)	0.04(max.)	0.02(max.)	0.06(max)
		COV(%)	Walls	12.4(max)	7.25	2.41	8.79
			Roof	10.0(max)	3.97	2.47	7.00
	System Perspective	K_d range	Walls	0.58-1.14	0.72-1.00	0.73-0.96	0.59-1.13
			Roof	0.70-1.19	0.77-1.06	0.79-1.03	0.71-1.15
		Range	Walls	0.56	0.28	0.24	0.54
			Roof	0.50	0.29	0.24	0.44
		Standard Deviation	Walls	0.11(mean)	0.05	0.012(mean)	0.08(mean)
				0.083 (max.)	0.03	0.012(max.)	0.10(max.)
			Roof	0.082(mean)	0.03	0.010(mean)	0.06(mean)
				0.066(max.)	0.03	0.009(max.)	0.05(max.)
		COV (%)	Walls	8.29(max.)	3.37	1.31	6.00
			Roof	6.13(max.)	2.77	0.88	4.35

Mean: using mean values
Max: using maximum values
Range = max. value -min. value

The results of Appendix B [Figures B-32 through B-35, B-40, B-42 and B-44 through B-51 (row two of Table 5-3)]are consolidated in Figure 5-15, where the K_d values corresponding to 95% probability of non-exceedance are presented (vertical axis) vs 43 building locations (horizontal axis, all four storms) at open exposure and 7x7

ft areas. The maximum and mean roof K_d values and maximum and mean wall K_d values are included. The green dashed lines separate the results corresponding to Frances, Katrina, Ivan, and Rita. Figure 5-15 A presents the component perspective, and Figure 5-15 B presents the system perspective. For the component perspective, the K_d = 0.85 threshold is frequently exceeded for the maximum walls and roof results, but not so for the mean results. For the system perspective the K_d = 0.85 threshold is exceeded for all results other than the mean wall results.

Using the system perspective 95% probability of non-exceedance for the mean results as a baseline, it is concluded from Figure 5-15 B that an appropriate K_d factor is approximately 0.95 for the roof and 0.90 for the walls. A value of 1.0 for both roof and walls is defensible. These conclusions are contingent upon the use of 95% probability of non-exceedance. A lower value (higher risk) results in lower K_d values than those shown in Figure 5-15, while a higher value (less risk) results in higher K_d values.

Plots similar to Figure 5-15 were not produced for the figures delineated in rows 1, 3 and 5 in Table 5-3. Figure 5-15 used open exposure 7x7 ft areas. Using suburban exposure did not alter the aggregate results appreciably. Using 5x5 ft areas would produce slightly higher K_d values than shown in Figure 5-15.

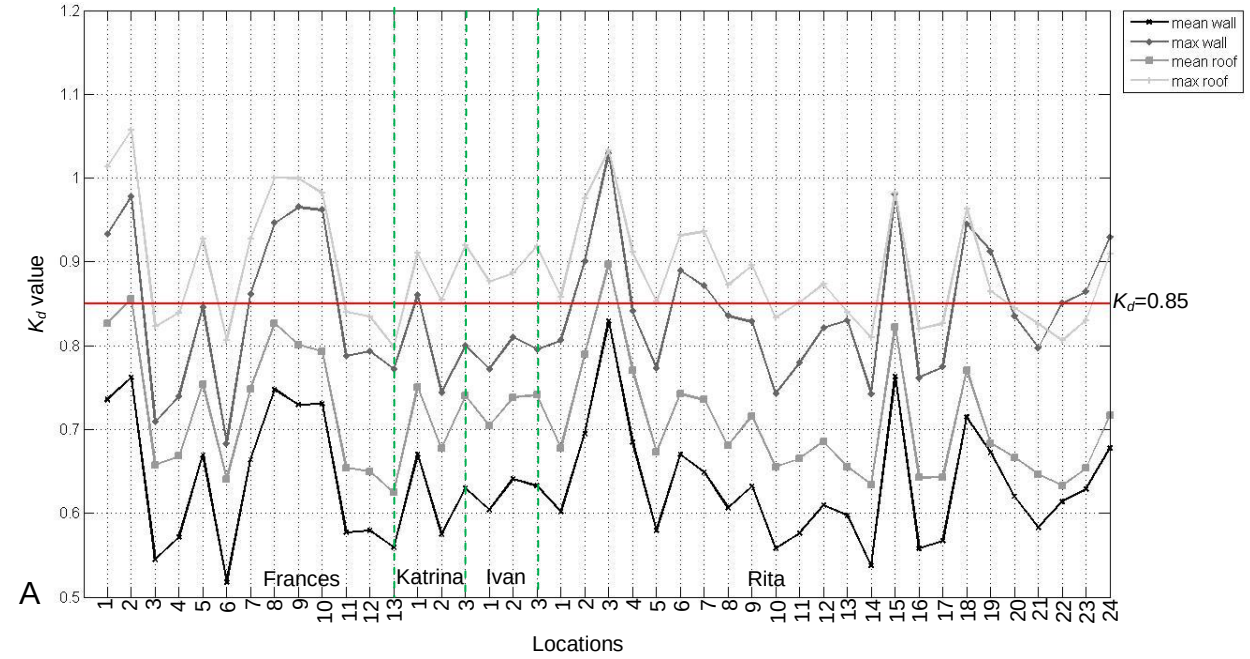

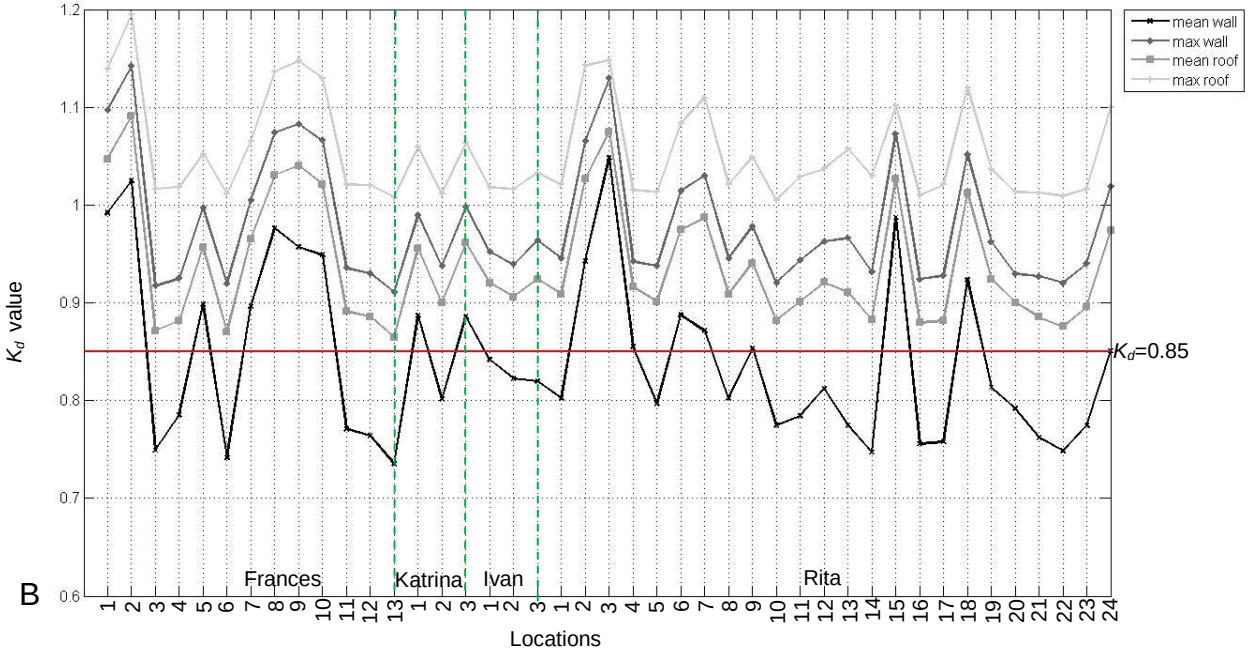

Figure 5-15. Aggregate open exposure, 7x7 ft area results for all four storms and locations. K_d values correspond to 95% probability of non-exceedance from Appendix B (Figures B-32 through B-51). A) Component perspective. B) System perspective.

The findings of the deterministic and probabilistic approaches are within the range of the results presented by Davenport (1977), Holmes (1981), Eric Ho (1992), and Vega (2008) as shown in Table 5.5. Isyumov et al. (2013) proposed a value of 0.90 for buildings in hurricane regions which is a value that lies within the observations based on the scenario analysis. Values larger than 1.0 (as shown in Table 5.5 for scenario analysis) represent the possibility that sampled values of the pressure coefficient may exceed the 22% probability of non-exceedence used to define the worst case Cp ($C_{p\_worstcase}$). The conclusions in this study are not based on the deterministic and probabilistic approach since these two do not consider the long durations and variations during the passage of the hurricane. To capture the variations in wind speed and direction that buildings in hurricane prone regions can experience it is recommended to apply the scenario analysis following the system perspective.

Table 5-5. Wind directionality factors for components and claddings

Reference	Wind Directionality Reduction Factor			
Davenport (1977)	0.56,0.72,1.0[1]			
Holmes (1981)	0.72-0.96[2]			
Eric Ho (1992)	0.75[3]			
Vegas (2008)	0.45 - 0.84[4]			
Isyumov et al. (2013)	0.90[5]			
Laboy (2013)	Approach		Walls	Roof
	Deterministic	Component	0.25-0.76	0.34-0.70
		System	0.41-0.79	0.59-0.89
	Probabilistic[7]	Component	0.29-0.76	0.34-0.67
		System	0.41-0.77	0.55-0.83
	Scenario[6]	Component	0.81-1.05	0.92-1.09
		System	0.96-1.16	1.03-1.20

Note:
[1] Three cases presented
[2,4]Min and max range for different mean recurrence interval
[3] Mean value obtained
[5] Hurricane prone regions
[6] Based on maximum values corresponding to a5% probabilities of exceedance among all areas 5ftx5ft and 7ftx7ft, storms, locations, and exposures
[7] 5-15% probability of exceedance

5.4 Chapter Summary

This chapter presented the analysis of a wind directionality factor in three distinct tiers (deterministic, probabilistic, and scenario) using both a component and system perspective. It is proposed that the scenario analysis using the system perspective is most representative of the hurricane hazard, and most appropriate for the determination of a rational K_d factor for hurricane prone structures. It is further proposed that an acceptable percentile in Equation 5-16 should be no larger than 5%, corresponding to a probability of non-exceedance no smaller than 95%. The results corresponding to a system perspective at 95% probability of non-exceedance using the maximum and mean values corresponding to areas among all building surfaces (roof and walls) produce the conclusion that 0.85 is not a conservative value (it is too low) for components and cladding on structures in hurricane prone regions. The results in this study support a conclusion of $K_d = 0.95$ for roofs and 0.90 for walls. These recommendations are contingent upon the acceptance of a system perspective and the 95% probability of non-exceedance.

CHAPTER 6
CONCLUSIONS

The previous chapters described the methodologies involved in the vulnerability study of residential infrastructure in hurricane prone regions. The studies investigated (1) the vulnerability of roof tile systems and metal hurricane shutters to roof tile debris and (2) the appropriateness of the current implementation of the load reducing directionality factor K_d in ASCE 7. The end results will help to better understand concerns that have been highlighted in FEMA 488 and the FEMA Region IV Capabilities Gap 2010-M-014. A discussion of the findings and limitations are presented as follows.

6.1 Roof Tile Frangibility and Puncture of Metal Window Shutters

This study addressed the frangibility of roof tile systems under impact by roof tiles, and the vulnerability of metal hurricane shutters under impact by roof tile fragments. The methodology developed consisted of two experimental phases (conducted by another graduate student) and the trajectory model (conducted by Laboy). Interpretation of results is based upon a combined view of puncture probability from Phase 2 experimental testing and speed of impact (from the modeling phase).

6.1.1 Conclusions

- Mechanically attached (single screw) roof systems produce more tile fragments than mortar set roof systems when impacted by a roof tile, all other variables equal (Table A-1).
- Each of the three forthcoming conclusions regarding likelihood of puncture is conditional upon a tile fragment being available and impacting a metal shutter. The determination of the probability of this conditional variable was not determined in this study. Thus each conclusion is prefaced by ‘given that a tile fragment impact occurs’.
- Given that a tile fragment impact occurs, the likelihood of shutter puncture in reference wind speeds between 100 mph and 120 mph isotachs (Category 1 and 2 wind events) is small but not insignificant. For exposure C and D conditions and

flight distances of > 148 ft, fragment impact speeds capable of puncture can be achieved.

- Given that a tile fragment impact occurs, the likelihood of shutter puncture in reference wind speeds between 130 mph and 140 mph isotachs (~ Category 3 wind events) is moderate. Minimal impact speed damage threshold can be achieved for short flights in exposures C and D. Impact speeds corresponding to a more significant probability of puncture are achieved for longer flight distances.

- Given that a tile fragment impact occurs, the likelihood of shutter puncture in reference wind speeds exceeding the 140 mph isotach (Category 4 or higher) is significant for all exposures and distances in this study. However, the conservative nature of the test protocol (point first perpendicular impact) and trajectory model (use of the highest five second wind trace) renders the achievement of puncture speed a possibility but not necessarily likely.

These conclusions are supported by anecdotal field observations. The authors observed several cases of shutter puncture from tile fragment impact in Punta Gorda, Florida (Charlotte County) caused by Category 4 winds in Hurricane Charley (Figure A-1) in exposure C conditions, although the vast majority of metal shutters they observed were not punctured. Shutter puncture was not observed by the authors in regions experiencing less than Category 3 winds from Hurricane Charley or any other sub Category 3 U.S. land falling hurricane since 1999. Lack of direct observation by the authors certainly does not rule out the occurrence of shutter puncture in sub Category 3 hurricanes, but to the authors' knowledge no such observation has been reported in damage investigation literature.

This study provides supporting evidence that common metal panel window shutters are capable and likely to provide significant protection against a prevalent form of WBD in tile roof neighborhoods. Puncture of these shutters from roof tile fragments is possible in more intense hurricanes, but not necessarily likely.

6.1.2 Study Limitations

This study contains uncertainties from several sources including testing limitations due to time and resource constraints as well as limits to the physical test set ups, and simplifying assumptions and limitations within the trajectory modeling. These limitations are listed by project phase.

6.1.2.1 Experimental testing phase 1: tile frangibility

- Only horizontal impact tile trajectories are used (physical limitation of test set up)
- Two tile fragments sizes are used (half and whole)
- Three impact speeds are used
- The experiments were not conducted within a wind field
- The probability of occurrence of tile impacting a roof system (the conditioning variable) is not quantified, only the resultant distribution of fragments generated

6.1.2.2 Experimental testing phase 2: shutter puncture vulnerability

- Only point first perpendicular to shutter plane impacts were conducted (conservative approach to limit the size of the test matrix)
- Two tile fragment sizes are used (the mean size from phase 1 and a larger fragment)
- The probability of puncture is conditioned upon the occurrence of impact at the tested condition. The probability of this conditional variable is in turn conditional upon the availability and quantity of tile fragments, which is not quantified in this study. Thus only the relative likelihood of puncture among different conditions (tile fragment size, mean wind speed, distance to target, shutter type) was determined, and not the nominal probability for each condition

6.1.2.3 Trajectory model

- The trajectory model is two dimensional, and is thus only an approximation to the real three dimensional behavior of windborne tile debris. An experimental study in the literature suggests that the 2D model overestimates trajectory height and distance
- The representation of the wind field is a simple longitudinal turbulence model. The influence of the local terrain (houses, roof of the source house, trees, etc.) is only represented via the use of three different terrain exposures, which determine the local mean hourly wind (with respect to the reference wind speed) and turbulence intensity
- Initial conditions of the tile fragment (horizontal, vertical, and angular velocity, horizontal position, horizontal, vertical, and angular accelerations) were set to zero. The vertical position was set to 28 ft. Thus the tiles are propelled by the wind field from a resting position at the ridge of the source roof. The influence of

a non-zero initial velocity imparted the fragmenting event (tile impacting tile roof system) was not quantified

6.2 Revisiting the Wind Directionality Factor in the ASCE 7

This study evaluated the efficacy of K_d on components and cladding for buildings located in hurricane prone regions by conducting a three part study. The first part of the study reviewed the wind directionality concept from researchers' methodologies, and building codes and standards around the world. The second part of the study introduced the original incarnation of the probabilistic scenario analysis. The approach was applied to individual taps rather than area averaged data, and K_d at each tap was then averaged over the ASCE7 C_p zones (Figures 4-14 and 4-15).

The third part of the study presented the revision of the methodology introduced in Chapter 4 to better represent the assumptions that the ASCE 7 follows. The revised methodology is composed of three main approaches: (1) deterministic, (2) probabilistic, and (3) scenario analysis. The first two approaches are suitable for non-hurricane regions since the climatological effects are ignored and adopt the ASCE 7 assumption that wind damage is due to a single gust coming from a single direction. The third approach follows the scenario analysis where the duration and variation of wind during the passage of a hurricane is considered. The applicability of this new methodology allows analyzing the wind directionality effect on a single component and a system (e.g. roof four corners). The sensitivity of the results was investigated by moving the same building from one location to another in the same hurricane (e.g. Fig. 5-13), changing the hurricane to other historical hurricane (i.e., Katrina, Rita, and Ivan), and using a series of different areas to acquire the area averaged pressure coefficient time histories.

6.2.1 Conclusions

The conclusions presented are based on a 5% level of risk or 95% probability of non-excedance.

- When comparing single taps using the approach presented in Chapter 4 vs. the new approach (Chapter 5) similar results were observed when comparing the maximum wall and roof K_d with the values presented in Fig.4-11 and Fig. 4-12.
- In terms of single taps (Chapter 5) vs. 3ftx3ft no significant variations were observed since most of the areas include a single tap which leads to the same result as using just single taps.
- In terms of area averaged, the results illustrated that when a larger area is used the range (spread) tends to get reduced, but leads to similar K_d values.
- Higher K_d values were observed in all cases for system vs. component perspective.
- K_d values that exceeded the current value used in the ASCE 7 were observed in the component perspective, but more likely to occur in the system perspective.
- No significant variations were observed between the results obtained for open and suburban exposures.

This study proposes the used of the scenario analysis following the system perspective for the determination of a rational K_d factor for hurricane prone structures since it captures the multi-directionality vulnerability of C&C. The system perspective is capable of analyzing all similar components in order to identify the weakest link that will define the performance of the entire system. The component perspective might be a feasible approach for walls leading to a lower K_d factor, however, the system perspective is recommended since during a hurricane the vulnerability should be measure based on whether “a” component can get damage rather than “this” component will get damage.

It is further proposed that an acceptable percentile in Equation 5-16 should be no larger than 5%, corresponding to no smaller a probability of non-exceedance value than

95% (horizontal axis in the results figures). The results corresponding to a system perspective at 95% probability of non-exceedance using the maximum values corresponding to areas among all building surfaces (roof and walls) produce a conclusion that 0.85 is not a conservative value (it is too low) for components and cladding on structures in hurricane prone regions. The maximum values from all building surfaces are considered as the appropriate range to draw conclusion since the approach followed by the ASCE 7 is based on the worst case.

The end results from the revised K_d analysis (Chapter 5) align with the conclusions from the single tap analysis (Chapter 4) where a K_d value no smaller than 0.95 and 0.90 can be justified for roof and walls, respectively. A value of 1.0 for both is defensible. It is proposed that the scenario analysis using the system perspective is most representative of the hurricane hazard, and most appropriate for the determination of a rational K_d factor for hurricane prone structures. It is important to highlight that any changes in the wind directionality factor need to be balance with the load factor to provide the appropriate reliability index. These findings to do not apply to main wind force resisting system (MWFRS) loads or to structures not located in hurricane prone regions.

6.2.2 Study Limitations

This study contains uncertainties from several sources, such as

- 43 locations among all four storms were considered.
- Four storms were used.
- The study was based on 1 gable roof building.
- Surroundings effects were not considered other than upwind terrain.

6.2.3 Future work

Based on the study it is proposed to study further changes in the variables that can alter the conclusions of this study. Therefore, it is recommended to apply the proposed methodology (Chapter 5) to address uncertainties involved with the following variables:

- Additional buildings with different characteristics, such as length, width, roof slope
- Additional locations
- Additional storms
- Buildings with complex roof lines and refine the system perspective based on the roof complexity to address the issues involved
- Access simulated hurricanes for regions were historical hurricane data is unavailable
- Additional area averaged that captures the wind directionality effect that a double garage door (longer walls) can experience
- Incorporate surrounding effects

Also, it is suggested to develop new reliability studies since the ASCE 7 follows research studies that were conducted over three decades ago. In addition, it is recommended to study and analyze in detail the load factor and how it is combined with the current wind directionality factor. The conclusions presented in this dissertation are preliminary and further studies are recommended.

APPENDIX A
ACCEPTED PAPER: ROOF TILE FRANGIBILITY AND PUNCTURE OF METAL WINDOW SHUTTERS

Sylvia T. Laboy-Rodriguez[1], Daniel Smith[1], Kurtis R. Gurley[*2a] and Forrest J. Masters[2b]

[1]*Ph.D Candidate, Department of Civil and Coastal Engineering, University of Florida*
[2]*Faculty of the Department of Civil and Coastal Engineering, University of Florida*

(To Appear in the August 2013 Issue Wind and Structures Journal – email from editor)

Abstract
The goal of this study was to investigate the vulnerability of roof tile systems and metal shutters to roof tile debris. Three phases addressed the performance of tile roof systems and metal shutters impacted by roof tile debris. The first phase experimentally evaluated the tile fragment size and quantity generated by a tile striking a tile roof system. The second phase experimentally quantified the puncture vulnerability of common metal panel shutter systems as a function of tile fragment impact speed. The third phase provided context for interpretation of the experimental results through the use of a tile trajectory model. The results provide supporting evidence that while metal panel window shutters provide significant protection against a prevalent form of windborne debris, these systems are vulnerable to tile fragment puncture in design level tropical cyclones. These findings correlate with field observations made after Hurricane Charley (2004).

***Keywords*:** Windborne Debris, Missile Impact, Roof Tiles, Window Shutters, Puncture

1. Introduction

Post storm investigations have demonstrated that windborne debris can cause significant damage to the building envelope (Meloy, et al. 2007) and that window protection can be an effective mitigation measure (Gurley and Masters 2011). This report discusses the third in a series of investigations regarding the vulnerability of windows and window protection systems to windborne debris. The two previous studies addressed the vulnerability of unprotected residential window glass to impact from roof shingles and small vegetation (Masters, et al. 2010), and the performance of metal shutters under impact by full roof tiles (Fernandez, et al. 2010).

The current study addresses the frangibility of roof tile systems under impact by roof tiles, and the vulnerability of metal shutters under impact by roof tile fragments. The distribution of

* a Corresponding author. Associate Professor,Ph.D. E-mail:kgurl@ce.ufl.edu

b Associate Professor,Ph.D.,P.E. E-mail:masters@ce.ufl.edu

tile fragment sizes (ratio of tile fragment weight to full tile weight) produced when a tile roof system is impacted by a roof tile, and the speed and momentum thresholds that lead to metal shutter puncture by tile fragments were quantified experimentally. Additionally, a numerical study of tile fragment trajectories was conducted to quantify the speed of tile fragment impact on fenestration. Variables included mean wind speed, tile fragment size (by weight), turbulence intensity, and the distance between fragment source and impacted fenestration. The results from these three phases were combined to provide an assessment of the risk of metal shutters to puncture from tile fragments as a function of tropical cyclone severity.

2. Background

Windborne debris is a large contributor to building envelope damage during windstorm events. This problem can be defined in terms of the windborne debris load (types and sources of debris, trajectory and speed) and the vulnerability of building components to the windborne debris impacts. The literature addresses the former problem in numerous studies of windborne debris trajectories via numerical modeling and experiments. The subject of component capacity has largely focused on glass damage and the development of impact standards for protective devices. The current study addresses both aspects of the problem within the context of roof tile fragments impacting metal shutters.

Several researchers have conducted studies to document vulnerability and quantify the risk of damage to fenestration (e.g., Beason 1974, Minor 1994, 2005, Masters, et al. 2010, Fernandez, et al. 2010, Lin and Vanmarcke 2008, 2010a and 2010b, Yau Siu, et al. 2011). Masters, et al. (2010) identified the momentum threshold required to damage unprotected residential glazing impacted by asphalt shingles and small vegetation representing tree branches. In a follow up study, the deformation of metal shutters under impact by a full 4.1 kg roof tile and 4.1 kg 2x4 lumber (as per ASTM) was quantified (Fernandez, et al. 2010). The deformations caused by the tile impact typically exceeded the installed distance from the glass (setback) required for the tested product. Shutter puncture was not observed in these experiments, but this is known to occur from post-tropical cyclone field studies. This prompted the current study of tile fragment impact on these same metal shutter products.

During the 2004 Atlantic hurricane season, field observations demonstrated that roof tile windborne debris caused severe damage to the building envelope. Fig. 1 shows two examples of such damage in Punta Gorda, Florida after Hurricane Charley. Tile debris was identified to be a significant source of windborne debris in this region (Meloy, et al. 2007).

Many researchers have conducted experiments and developed models to predict the trajectory of windborne debris. Tachikawa (1983, 1988) conducted experiments to measure the trajectory of debris in a wind tunnel and compared the results with the numerical solutions by applying the two dimensional equations of motion for square and rectangular flat plates in uniform flow. Wills, et al. (2002) modeled and validated a flight initiation condition. Wang (2003) conducted wind tunnel tests to investigate flight initiation speed and behavior for sheet debris. Holmes and Mullins (2001) presented an analysis that estimates the distance and travel time of debris. Holmes (2004) studied the trajectories of spheres in severe storm weather considering the effect of turbulence in the wind velocities. Lin, et al. (2006) conducted wind tunnel and full scale experiments to investigate the trajectory, and velocity of plate type debris. Holmes, et.al (2006) developed a numerical model of a square plate and presented a comparison

of the results with the experimental data obtained from Tachikawa. Baker (2007) presented equations of motion for sheet and compact objects, and presented a comparison of the numerical solutions with experimental results of Tachikawa (1983) and Wills, et al. (2002). Visscher and Kopp (2007) studied the flight mechanics for a plate initially mounted on a roof of a 1:20 scale model to determine the motion type and the trajectory. Following this study, Kordi, et al. (2010) conducted experiments to analyze the flight of sheathing panels subjected to different wind directions. Kordi and Kopp (2009a) performed an analysis of windborne plates based on the quasi-steady model and compared the numerical solution with the experimental results from Tachikawa (1983) and Lin, et al. (2006). Scarabino and Giacopinelli (2010) conducted a dynamic analysis on the 2D equations for sheet debris by comparing aerodynamic coefficients of two models. Richards, et al. (2008) presented a 3D model of the trajectory of windborne debris.

3. Methodology and Results

This section presents the methodology and results for the three study phases. Phase 1 experimentally quantified the statistical distribution of tile fragment sizes (ratio of tile fragment weight to full tile weight) produced when a tile roof system is impacted by a tile. Phase 2 experimentally quantified the probability of metal shutter puncture when impacted by a tile fragment. Phase 3 numerically evaluated the velocity of a tile fragment impacting the roof and windows of a house through the use of a trajectory model and coefficients adopted from the literature (Tachikawa 1983,1988, Holmes 2004, Holmes, et al. 2006, Baker 2007, Lin, et al. 2007, Kordi and Kopp 2009b]. The outcomes of the three phases were combined to provide an assessment of the risk of tile fragments puncturing shutters as a function of wind conditions.

3.1 Phase 1: Tile Frangibility

Phase 1 was designed to produce a statistical assessment of the size of tile fragments produced when a tile roof system is impacted by a tile or tile fragment from a neighboring house. The influence of tile installation (mechanical or mortar set), and speed and weight of the impacting tile were considered.

A series of roof structures were constructed. Tile roof cover was installed by a licensed roofing contractor (Fig. 2). These roof systems were then subjected to impact by tiles using an apparatus that allows precise control of impact location and speed. The test matrix consists of 24 combinations of the following variables:

- Two shapes of concrete tile
- Mortar set or mechanical fastening (single screw)
- Impacting tile: half size (by weight) and whole tile
- 3 impact speeds (15.2, 22.4, 29.5 m/s)

3.1.1 Tile launching apparatus

The tile launching apparatus is comprised of four components; the pneumatic ram that propels the tile along a track toward the target, the air reservoir and barrel that supply propulsion force to the ram, the electronic valve that releases the pressure from the tank to the barrel, and the integrated electronic system.

Fig. 3 presents an illustration of the launching apparatus. The air reservoir is coupled to a steel pipe connected to an electronic valve. The ram fits within the barrel and harnesses the

released pressure. The far end of the ram bears against the tile projectile. A launch deck extends from the exit of the barrel toward the target. The tile projectile sits upon this deck and is propelled toward the target via the ram. The electronic system includes feedback control for filling, purging and maintaining air reservoir pressure, control of the electronic valve for launch, and measurement of the projectile speed using photoelectric sensors. This system is controlled from a custom National Instruments LabVIEW application.

3.1.2 Tile projectile impact angle and speeds

Concrete roof field tiles were impacted with half and full size concrete tiles. The impact angle is horizontal in all cases. Tests were conducted at speeds of 15.2, 22.4 and 29.5 m/s. Speed was calibrated to the launch air pressure using a high speed camera and photoelectric sensors to monitor the speed of the projectile as it left the launcher.

3.1.3 Results of Phase 1: Tile frangibility tests

Each of the 24 test combinations was repeated three times and the results combined to produce Table 1. Concrete I are classic Spanish design high profile field tiles and weigh approximately 4500 grams. Concrete II are S-shaped high profile field tiles and weight approximately 4100 grams. Upon impact, the fragments from the impacted tiles and impacting tile were separated via color (the impacting tile was painted) and each fragment individually weighed and dimensioned. Many fragments were not much larger than small gravel, and were deemed too small to pose a threat of metal shutter puncture. Thus fragments with less than 2% of the full tile weight were discarded from the analysis and all discussion hereafter. Only fragments from the impacted tiles are included in Table 1. Each cell in the table contains three values: the mean size of the tile fragment (defined as the ratio of the fragment weight to full tile weight), the standard deviation of same (in parentheses), and the total number of fragments (larger than 2% of the full tile by weight) produced from the three tests [in brackets].

The value of this analysis lies in the relative statistics among the combinations (trends relative to test conditions). For example, tiles that were attached via mortar produced fewer fragments than the mechanically attached tiles. Fig. 4 (right) shows the tile fragments produced from the 15.2 m/s test of a full tile impacting a mechanically fastened roof tile system. The trends that emerge from the analysis are:

- The mean value of the fragment size is approximately $1/8^{th}$ of the full tile by weight. Lower mean values in Table 1 are associated with cases with very few fragments.
- Higher impact speeds produced more fragments, but the mean size of these fragments did not change significantly.
- Full tile debris produced more fragments than half tile debris, but the mean size of these fragments did not change significantly.
- Mechanically attached (single screw) roof systems produced more tile fragments than mortar set roof systems, all other variables being equal.
- The mean size and number of fragments did not change significantly between the two tile shapes (Concrete I or II).
- The probabilistic distribution of tile fragment sizes is closely modeled by an exponential distribution (not shown).

Phase 1 results justified the tile fragment shapes and sizes used for the phase 2 experimental testing to evaluate the vulnerability of metal shutters to tile fragment puncture. In phase 2, $1/8^{th}$

and 1/4th tile fragments (by weight) were used. The results from the phase 1 study did not include tile roof debris produced by wind uplift.

3.2 Phase 2: Shutter Puncture Vulnerability

Phase 2 investigated the vulnerability of metal shutters to puncture from roof tile debris. The probability of shutter puncture was quantified as a function of debris size, speed and momentum in the form of empirical vulnerability curves.

Tile fragments were launched toward properly installed (according to manufacturer specifications) metal shutters with a controlled speed, impact location and impact orientation. Twenty tests were conducted for any given set of control variables. The test matrix consists of the following variables:

- Tile fragment size (1/8th and 1/4th of a full tile by weight)
- Impact speed (ranging from 21 m/s to 37 m/s)
- Metal shutter material (aluminum or steel)
- Metal shutter thickness (aluminum – 1.27 mm and 1.56 mm, steel – 22 gage and 24 gage)

3.2.1 Tile launching apparatus

The tile launching apparatus is discussed in the previous section and shown in Fig. 3. Photoelectric sensors documented the launch speed of every test. The end of the launch deck, where the photoelectric sensor was located, was less than 10 feet from the shutter.

3.2.2 Tile fragment projectile

Impact testing was conducted using concrete tile fragments 1/4th and 1/8th of a full size concrete tile by weight. These fragments were cut from a full tile using identical dimensions for every fragment of a given size. Fig. 4 (left) shows the two fragment sizes used. Tile fragments from the phase 1 tile frangibility testing (Fig. 4 right) demonstrated that 'pointy' fragments were commonly produced. Impact orientation was always point first and perpendicular to the shutter plane. This is a conservative approach that will produce the low end of the range of puncture speeds under field conditions. A new fragment was used for every test.

3.2.3 Shutters tested

Steel shutters of two thicknesses (22 and 24 gage) and aluminum shutters of two thicknesses (1.27 and 1.56 mm, referred to as 050 and 060 respectively) were tested. All products are approved for use in Florida. Panels ranged between 330 and 378 mm wide and each was 1.68 m tall. Three overlapping panels were direct mount installed in a vertical orientation, bearing against the frame at the top and bottom with no bearing along the vertical edges. The wood frame has studs installed at 152 mm on center or 159 mm on center across the top and bottom horizontal framing boarders. The panels were fastened by a wing nut on each stud. A 1.70 m high and 1.52 m wide wood frame bolted to a strong floor supports the storm panels during testing. The dimensions of the frame opening are 1.60 m wide by 1.57 m high.

3.2.4 Puncture definition

The test conditions resulted in either deformation only, or deformation with tearing. The tile fragment shown in Fig. 5 (upper right) was used to define puncture. If this fragment passed through the tear, the result was defined as a puncture (Fig. 5 lower right). If this fragment could

not pass through the tear, the result was not a puncture (Fig. 5 lower left). Only punctures are considered a failed state.

3.2.5 Test protocol

The probability of failure for a given shutter type impacted by a given tile fragment was evaluated at a given speed by subjecting the shutter type to 20 identical impact tests. Each test targeted a corner of the panel system that had not been impacted (repeat impacts were not considered). The impact location was within 200 mm of the corner of a shutter panel (Fig. 5, upper left). The puncture probability is the number of punctures divided by 20. The series of 20 tests is conducted for at least three speeds for a given shutter type and fragment size.

The speed of every impact was recorded via photoelectric sensors located at the end of the guided track (Fig. 3). The highest coefficient of variation (COV) among the impact speeds for any set of 20 tests was less than 0.08 (worst case), and the average COV was less than 0.04. Results reference the mean impact speed among the 20 tests.

3.2.6 Results of Phase 2: Shutter puncture vulnerability tests

Fig. 6 presents the puncture probability results. Consider the diamond within a large circle in the bottom right plot in Fig. 6. This data point corresponds to the 22 gage steel product, and was produced from the result of 20 1/4th size concrete tile fragment impacts at the same impact speed of 34 m/s (coefficient of variation less than 0.05). In this case, 16 of the 20 tests resulted in puncture (0.8 vertical axis).

Each of the data points in Fig. 6 has an associated uncertainty based upon the use of 20 individual impacts to generate a given value. The 95% confidence interval for each data point is plus or minus 0.2 on the vertical axis. That is, if a given test sequence of 20 specimens was repeated many times, the confidence interval represents the range in which the probability of puncture results are expected to fall for 95% of these sequences. The confidence intervals were calculated assuming that the outcome from any 20 specimens is binomially distributed. This requires that any one test has two possible outcomes (puncture or non-puncture) and that each test is not influenced by any previous test. Both of these conditions are met by the test protocol. The 95% confidence interval was validated using a Monte Carlo simulation.

Results show that the speed associated with a given probability of puncture is higher for the 1/8th tile than the 1/4th tile, and that the thickest steel (22 gage) provides the highest resistance to puncture, as expected. For the 1/8th tile fragment, puncture becomes possible at impact speeds approaching 25 m/s, and exceed 50% likelihood at approximately 30 m/s. Beyond 35 m/s all products tested in this study are likely to experience puncture upon impact.

The impact speed of the tile fragment is related to the speed and turbulence characteristics of the wind carrying the tile fragment. The trajectory model study will provide relationships between the tile fragment impact speed and the speed of the wind carrying the fragment (referenced to 3 second open exposure isotachs from ASCE 7), the turbulence intensity, the size of the fragment, and the distance traveled from debris source to shutter. The discussion of likelihood of puncture will be recast in terms of tropical cyclone intensity upon presentation of the trajectory model.

3.3 Phase 3: Trajectory Model

Phase 2 determined the puncture vulnerability thresholds for shutter products impacted by roof tile fragments. The purpose of the trajectory model is to determine the velocity of tile fragment

impact on the roofs and shuttered windows on structures that are in close proximity to the source of the fragments (the target is a neighboring house across the street). The combined outputs of the experimental and modeling phases will project the tropical cyclone conditions in which metal shutter puncture becomes a possible scenario.

The trajectory model tracks the flight of a tile fragment that is released from rest on a sloped roof. The variables in this experiment include:

- Tile fragment size ($1/8^{th}$ and $1/4^{th}$ of full tile by weight)
- Distance from tile source to target house (from 30 m to 60 m)
- Reference wind speed carrying the fragment: Open exposure 3 second gust values of 44.72 m/s to 89.44 m/s in 4.47 m/s increments (referenced to the wind speed isotachs in ASCE 7 (ASCE 2010)
- Reference turbulence: Exposures D, C and B in ASCE 7 (ASCE 2010)

The trajectory of the fragment includes its position in space, orientation, and speed. Any given trajectory is calculated in time increments of 0.02 s throughout the duration of flight. This time stepping spatial position is used to determine speed upon impact. The tile fragment size, mass, distance to target, reference wind speed and reference turbulence are fixed for a given trajectory experiment.

A Monte Carlo simulation methodology was employed. 100,000 trajectory experiments were conducted for a given fragment size, distance to target, reference wind speed and reference turbulence. The horizontal wind speed acting on the tile fragment was based on the reference wind speed and turbulence, and is a random quantity. Any one trajectory experiment utilized a new randomized trace of instantaneous horizontal wind speed, providing a unique trajectory. These thousands of trajectories were used to project the probability of the fragment impacting the neighboring roof or fenestration across the street, and the fragment speed associated with that impact.

3.3.1 Calculation of wind speed traces

Wind speed traces were calculated for 11 ASCE 7 (ASCE 2010) isotachs from 44.72 m/s to 89.44 m/s in increments of 4.47 m/s. Each 3-second, exposure C, 10 m height isotach was converted to an hourly mean wind speed for exposures B, C, and D for a total of eleven mean wind speeds per exposure via:

$$\bar{U} = \hat{u}_{3\,\mathrm{sec}\,expC} * \frac{\sqrt{k_z}}{GF} \tag{A-1}$$

where $\hat{u}_{3\,\mathrm{sec}\,expC}$ is the 3-second gust wind speeds, kz is the velocity pressure exposure coefficient (table 27.3-1 ASCE 10), GF is the gust factor for exposures B, C, and D (values are 1.71,1.53,1.42, respectively).

The power spectrum of the fluctuating wind for each hourly mean velocity and exposure was assigned the form proposed by von Karman (1948) for homogeneous isotropic turbulence for strong winds in a neutral atmosphere:

$$\frac{nS_u(n)}{\sigma^2{}_u} = \frac{4\tilde{n}}{\left(1+70.8\widetilde{n^2}\right)^{5/6}} \tag{A-2}$$

where $\tilde{n} = \frac{nL_{ux}}{\bar{U}}$, n is the frequency, $\sigma^2{}_u$ is the variance of the wind velocity, and Lux is the horizontal integral length scale which is a function of the terrain roughness

$$L_{ux} = l\left(\frac{\bar{z}}{10}\right)^{\bar{\epsilon}} \tag{A-3}$$

where l is the integral length scale (ASCE 7-10 Table 26.9-1), $\bar{z}$ is the height of the structure, and $\bar{\epsilon}$ is the integral length scale power law exponent (ASCE 7-10 Table 26.9-1). This spectral model is a function of both mean wind speed and exposure. Thus 33 power spectra (11 isotachs for exposures B, C, D) were standardized and applied to generate 1 hr Gaussian signals using a random amplitude and random phase technique in the frequency domain (Shinozuka and Deodatis 1991).

This spectral model is for horizontal turbulence relative to a fixed point in the atmosphere. This simplified approach does not model the effect of vertical turbulence or a frame of reference that travels with the object. The inclusion of a moving perspective introduces a non-stationary aspect to the simulation which, following Holmes (2004), was deemed unnecessary for objects with short flight times and speeds that are a fraction of the wind speed carrying them. Initial experiments indicated that the tile fragment debris trajectories had flight times of one or two seconds, which conforms to previous study findings (e.g. Holmes 2004, Lin, et al. 2006, Holmes, et al. 2006). Holmes (2004) also noted a slight underestimation of horizontal velocity of the object when ignoring vertical turbulence. In the current study this is offset in part by an overestimate of horizontal velocity via use of a 2D model (discussed in section 3.3.4).

In order to be conservative in the trajectory analysis, the highest 5 s segment from each simulated hour was isolated using a moving average. Then Each five second signal was scaled and dilated to obtain an instantaneous horizontal wind speed trace (to be used as input to the trajectory model) as follows:

$$u = u' + \bar{U} \tag{A-4}$$

where u' is the component in the direction of the mean wind due to the turbulence (highest 5 s segment from the hour), and $\bar{U}$ is the hourly mean wind speed at 10 m (Table 2). The standard deviation (σ_u) was determined from the modified Harris and Deaves equation (1981):

$$\sigma_u = \frac{u_* 7.5\eta\left[0.538+0.09\ln\left(\frac{z}{z_0}\right)\right]^{\eta^{16}}}{1+0.156\ln\left(\frac{u_*}{fz_0}\right)} \tag{A-5}$$

The shear velocity u_* was calculated using the logarithmic law $u_* = \frac{\bar{U}*k}{ln\left(\frac{z}{z_0}\right)}$, where k is the von Karman constant (0.40), z0 is the roughness length (0.20, 0.02 and 0.005 for B, C and D from Table 27.3.1 ASCE 7-10, $\eta = 1 - \frac{6fz}{u_*}$, $f = 2 * w * \sin(\lambda)$ (coriolis force), w = earth rotation speed = 7.29*10-5 (rad/sec), and λ is latitude (25o is used for Florida). The application of Harris and Deaves and the hourly mean wind speeds in Table 2 produce turbulence intensities of 0.240, 0.185 and 0.168 for exposures B, C and D, respectively at 10 m.

Calculation of the debris trajectory

It was assumed that any loose fragments on the source roof will become airborne following the criteria of Wills, et al. (2002) and Holmes (2007). Once airborne, the motion of the fragment was calculated following a trajectory model and aerodynamic coefficients adopted from the literature (Tachikawa 1983,1988), Holmes (2004), Holmes, et al. (2006), Baker (2007), Lin, et al. (2007), Kordi and Kopp (2009b)]. The initial vertical position was assumed to be 8.54 m as the height at the ridge of a two story house.

3.3.3 Probability and speed of impact

For a given fragment to be counted as an impact on a house neighboring the source house, its trajectory must travel a specified horizontal distance and fall a certain vertical distance from its

original 8.54 m height. Typical across the street distances were measured in Punta Gorda, Florida using Google Earth. It was found that most houses have a distance from the ridge to the neighboring house across the street in a range of 30 and 60 m. This study considers horizontal distances of 30 m to 60 m in 5 m increments.

Given that a fragment does travel the specified horizontal distance prior to hitting the ground, potential impact on the neighbor is divided into three possibilities based on the vertical position of the fragment: Impact roof (fragment elevation = [6.09 8.54 m]), impact upper story window (fragment elevation = [3.66 5.49 m]), or impact lower story window (fragment elevation = [0.61 2.44 m]).

Fig. 7 illustrates 300 sample trajectories of the $1/8^{th}$ tile for 44.7 m/s isotach in exposure B. The vertical and horizontal axes represent the vertical and horizontal positions of the fragment after release. Each trajectory was created with a new randomized trace of instantaneous horizontal wind speed. A count of how many trajectories passed through the left face of the house (located 30 m away) at heights corresponding to 1^{st} or 2^{nd} story fenestration or the roof determined the probability of impact. The speed of each trajectory that resulted in impact was collected to determine the average speed of impact. For the Monte Carlo trajectory analysis that follows, 100,000 5 s wind speed traces were generated for each of the 11 isotach values at each of exposures B, C and D.

3.3.4 Trajectory model validation

No physical experiments were conducted in the current study to validate the outcomes of the trajectory model. However, the literature provides a means of validation.

The trajectories in Fig. 7 show that the tile fragments fall from their initial height early in the flight, then rise, level off and fall. This increase in height after the initial drop is due to the lift generated by the autorotation of the tile. As the rotational velocity (about the horizontal axis perpendicular to the wind direction) increases, the lift increases and produces the rise in flight. As the tile fragment accelerates in the horizontal plane, the speed differential between the tile and the surrounding wind decreases, which reduces lift and produces the downward trajectory. This behavior has been shown in previously published numerical trajectory studies (e.g., Baker 2007). This behavior was also observed experimentally in a scale model wind tunnel study of tile and shingle debris trajectories Kordi and Kopp (2011), but was not observed in a study of small plate flight (Lin, et al. 2006). The Kordi and Kopp (2011) study also observed that in wind tunnel experiments most debris rotates about all three axes (3D rotation) rather than just the axis horizontal and perpendicular to the wind direction. This rotation about all three axes reduces the lift from autorotation relative to 2D rotation, and reducing flight range. Thus, all other conditions equal, fragments autorotating about only the horizontal axis perpendicular to the wind direction (2D model) will travel higher and farther than the fragment rotating about three axes. This overestimate of trajectory range and height is a limitation of the 2D trajectory model which will be revisited during the discussion and interpretation of the results in the next section. The adoption of a 3D trajectory model (e.g. Richards, et al. 2008) may alleviate this overestimation of trajectory range and height.

The individual impact speeds were collected to determine the average speed of the tile fragment upon impact. The ratio of the average tile fragment impact speed to the expected 3 s gust at roof height was calculated for each isotach wind speed reference, exposure, fragment size, and distance from source to target. This provides a means of validating the trajectory model fragment speed via comparison to experimental findings reported in Kordi and Kopp (2011). In

that study it was observed that the in-flight tile velocities span a range of 30–60% of the estimated roof height gust speed. In the current study the range was found to be 40-80%, where the lower values correspond to shorter target distances. The Kordi and Kopp (2011) study utilized whole (intact) roof tiles as debris, whereas the current study modeled $1/8^{th}$ and $1/4^{th}$ tile fragments. Smaller, lighter tile fragments will accelerate more quickly than larger, heavier tiles. The ratios of tile fragment speed to gust wind speed in the current study and those found in the Kordi and Kopp (2011) experiments are therefore reasonably consistent. Based on these observations, the discussion of the results will emphasize the speed of impact more so than the probability of impact.

3.3.5 Results of Phase 3: trajectory model

Tile fragment trajectories were estimated for $1/8^{th}$ and $1/4^{th}$ tile fragments over a range of distances to target, reference wind speed, and reference turbulence. Results are presented in Fig. 8 for the 30 m (left column) and 60 m (right column) flight distances. Each figure contains the mean speed of fragment impact as a function of the 10 m open exposure 3-second reference wind speeds. The top, middle and bottom rows in each figure are results for exposures B, C and D, respectively. Within each plot, results are presented for 6 cases: $1/8^{th}$ tile fragment impacting the 1^{st} story fenestration, 2^{nd} story fenestration, and roof, and likewise for the $1/4^{th}$ tile fragment. The horizontal axis is marked with 'cat 2', 'cat 3', 'cat 4', and 'cat 5' separated by vertical boundaries. This is in reference to the Saffir-Simpson Hurricane Wind Intensity rating scale, referenced to sustained one minute winds at 10 m in marine exposure. A 1-min marine to 3-second open exposure conversion of 1.1 was applied to provide the boundaries as shown (Simiu, et al. 2007).

The probability of impact is conditional upon the availability of a single tile fragment at the source location (ridgeline of source house). The probability of this availability and the quantity of such fragments was not determined in this study. In addition, the previous section on validation presented a limitation of the 2D trajectory model regarding the overestimation of the height and distance of the debris flight track. Thus, the impact probabilities are not sufficiently validated to warrant inclusion within the results or conclusions, and the study focuses on the likelihood of puncture given that an impact has occurred.

In Fig. 8 there is no impact speed recorded at several wind speed reference values. This corresponds to no observed impacts at that wind speed. This should not be interpreted literally in light of the above discussion. There is some recourse to interpreting the sparse impact speed plots. Ultimately the speed of fragment impact is significant with respect to the metal shutter puncture vulnerability data in Fig. 6, which show that a 50% probability of puncture corresponds to an impact speed range of ~ 25 to 35 m/s. Among the exposure C and D impact speed plots in Fig. 8, the lowest impact speeds start at 22.35 m/s for the 44.7 m/s reference wind speed (isotach) and shortest target distance (Fig. 8, middle left). The missing impact speed data at higher isotachs and / or longer target distances will be greater than 22.35 m/s. Thus all of the missing impact speed data will fall within a range that approaches a significant probability of shutter puncture.

4. Results Interpretation:

Interpretation of results is based upon a combined view of puncture probability from phase 2 experimental testing (Fig. 6) and speed of impact (Fig. 8). Recall that the phase 2 experiments

were carried out with the fragments impacting point first and perpendicular to the shutter plane. The results in Fig. 6 are thus considered a lower bound for the speed for any given probability of puncture. Consider the circled diamond icon in Fig. 6. The 80% probability of puncture is likely higher than 34 m/s under real conditions. Recall also that each data point in Fig. 6 has a 95% confidence interval of plus or minus 0.2 on the vertical axis. Hence Fig. 6 presents a guideline and not a precise quantification of the impact speed necessary to produce puncture.

Observations:

- Fig. 6 indicates that a significant probability of puncture upon impact occurs for speeds in excess of 30 m/s for 1/8th tile fragments, and in excess of 25 m/s for 1/4th tile fragments. These thresholds are used as benchmarks to draw the forthcoming conclusions of puncture threat with respect to ASCE isotach as well as tropical cycloneintensity.
- In exposure B, 1/8th tile fragment impact speeds exceed 30 m/s at > 76 m/s isotach (Cat 5 winds) for the shortest target distance of 30 m, and > 50 m/s isotach (Cat 2) for the longest target distance of 60 m. This fragment speed threshold of 30 m/s is achieved at lower isotachs for exposure C and D conditions. For the lowest reference wind speed used in this study, 1/8th tile fragments in exposure D are capable of achieving an impact speed with a significant probability of metal shutter puncture.
- In exposure B, 1/4th tile fragment impact speeds exceed 25 m/s at > 60 m/s isotach (mid Cat 3) for the shortest distance of 30 m, and > 44.7 m/s isotach (high Cat 1) for the longest target distance of 60 m. For exposure D, this fragment speed threshold of 25 m/s is reached at the 44.7 m/s isotach for the smallest distance. That is, for the closest distance and lowest reference wind speed used in this study, 1/4th tile fragments in exposure D are capable of achieving an impact speed with a significant probability of metal shutter puncture.

5. Conclusions

The following conclusions are based on the combined results of all three phases of this study:

- Phase 1 (tile frangibility) indicated that the 1/8th tile fragment is the mean size produced from both full and half-size (by weight) tile impact on a tile roof system (Table 1).
- Mechanically attached (single screw) roof systems produce more tile fragments than mortar set roof systems when impacted by a roof tile, all other variables equal (Table 1).
- Given that a tile fragment impact occurs, the likelihood of shutter puncture in winds between 44.7 m/s and 53.6 m/s isotachs (Category 1 and 2 wind events) is small but not insignificant. For exposure C and D conditions and flight distances of > 45 m, fragment impact speeds capable of puncture can be achieved.
- Given that a tile fragment impact occurs, the likelihood of shutter puncture in winds between 58 m/s and 62.5 m/s isotachs (~ Category 3 wind events) is moderate. Minimal impact speed damage threshold can be achieved for short flights in exposures C and D. Impact speeds corresponding to a more significant probability of puncture are achieved for longer flight distances.
- Given that a tile fragment impact occurs, the likelihood of shutter puncture in winds exceeding the 62.5 m/s isotach (Category 4 or higher) is significant for all exposures and distances in this study. However, the conservative nature of the test protocol (point first

perpendicular impact) and trajectory model (use of the highest five second wind trace) renders the achievement of puncture speed a possibility but not necessarily likely.

These conclusions are supported by anecdotal field observations. The authors observed several cases of shutter puncture from tile fragment impact in Punta Gorda, Florida (Charlotte County) caused by Category 4 winds in Hurricane Charley (Fig. 1) in exposure C and D conditions, although the vast majority of metal shutters they observed were not punctured. Shutter puncture was not observed by the authors in regions experiencing less than Category 3 winds from Hurricane Charley or any other sub Category 3 U.S. land falling hurricane since 1999. Lack of direct observation by the authors certainly does not rule out the occurrence of shutter puncture in sub Category 3 tropical cyclones, but to the authors' knowledge no such observation has been reported in damage investigation literature.

The limitations in this study (e.g. 2D trajectory model, debris flight origination from the highest point on a two story roof) and the conservative assumptions employed (e.g. point first impact perpendicular to the shutter, fastest five second segment from each one hour wind simulation) must be considered when interpreting the results. They should be viewed as a conservative guideline rather than an explicit definition of the debris hazard. With this in mind, this study provides supporting evidence that common metal panel window shutters are capable of providing significant protection against a prevalent form of windborne debris in tile roof neighborhoods. However, puncture of metal shutters from roof tile fragments is possible in design level tropical cyclones, and should not be considered a rare or outlier type event.

6. Acknowledgements

The authors thank the Florida Building Commission for sponsoring this research. The contributions of Mr. Jim Austin and Mr. Scott Bolton are gratefully acknowledged.

7. References

ASCE 7-10 (2010), Minimum Design Loads for Buildings and Other Structures, American Society of Civil Engineers, Reston, Virginia.

Baker, C.J. (2007), "The debris flight equations", J. Wind Eng. Ind. Aerodyn., **95**, 329-353.

Beason, W.L. (1974), Breakage Characteristics of Window Glass Subjected to Small Missile Impacts, Thesis, Civil Engineering Department, Texas Tech University.

Fernandez, G., Masters, F.J. and Gurley, K.R. (2010), "Performance of hurricane shutters under impact by roof tiles", Eng. Struct.,**32**(10), 3384-3393.

Gurley, K. and Masters, F. (2011), "Post 2004 hurricane field survey of residential building performance", Nat. Haz. Rev., ASCE, **12**(4), 177-183.

Harris, R.I. and Deaves, D.M. (1981), "The structure of strong winds", Ciria Conference on Wind Engineering in the Eighties, Ciria, London.

Holmes, J.D. and Mullins, P.J. (2001), "The mechanics of flying debris and test criteria", In: Fifth Asia– Pacific Conference on Wind Engineering.

Holmes, J.D. (2004), "Trajectories of spheres in strong winds with application to windborne debris", J. Wind Eng. Ind. Aerodyn., **92**, 9-22.

Holmes, J.D., Letchford, C.W. and Lin, N. (2006), "Investigations of plate-type windborne debris – Part II: computed trajectories", J. Wind Eng. Ind. Aerodyn., **94**, 21-39.

Holmes, J.D. (2007), Wind Loading of Structures, 2nd Ed., Taylor & Francis, New York, NY.

Kordi, B. and Kopp, G.A. (2009a), "Evaluation of quasi-steady theory applied to windborne flat plates in uniform flow", J. Eng. Mech. ASCE, **135**, 657-668.

Kordi, B. and Kopp, G.A. (2009b), "The debris flight equations by CJ Baker", J. Wind Eng. Ind. Aerodyn., **97**, 151-154.

Kordi, B., Traczuk, G. and Kopp, G.A. (2010), "Effects of wind direction on the flight trajectories of roof sheathing panels under high winds", Wind and Structures, **13**, 145-167.

Kordi, B. and Kopp, G.A. (2011), "Effects of initial conditions on the flight of windborne plate debris", J. Wind Eng. Ind. Aerodyn.,**99**, 601-614.

Lin, N., Letchford, C.W. and Holmes, J.D. (2006), "Investigations of plate-type windborne debris. Part I. Experiments in wind tunnel and full scale", J. Wind Eng. Ind. Aerodyn., **94**(2), 51–76.

Lin, N. and Vanmarcke, E. (2008), "Windborne debris risk assessment", Prob. Eng. Mech., **23** (4), 523-530.

Lin, N. and Vanmarcke, E. (2010a), "Windborne debris risk analysis – Part I. Introduction and methodology", Wind and Structures, **13**, 191-206.

Lin, N. and Vanmarcke, E. (2010b), "Windborne debris risk analysis – Part II. Application to structural vulnerability modelling", Wind and Structures, **13**, 207-220.

Masters, F.J., Gurley, K.R., Shah, N. and Fernandez, G. (2010), "The vulnerability of residential window glass to lightweight windborne debris", Eng. Struct., **32**(4), 911-921.

Meloy, N., Sen, R., Pai, N., and Mullins, G. (2007), "Roof damage in new homes caused by Hurricane Charley", J. Perform. Constr. Facil. ASCE, **21**(2), 97-107.

Minor, J. (1994), " Windborne debris and building envelope", J. Wind Eng. Ind. Aerodyn., **53**(1-2), 207-227.

Minor, J. (2005), "Lessons learned from failures of the building envelope in windstorms", J. Archit. Eng. ASCE, **11**(1), 10-13.

Peng, X., Yang, L., Gurley, K., Prevatt, D., and Gavanski, E. (2013). Prediction of peak wind loads on a low-rise building. Proceedings of the 12th Americans Conference on Wind Engineering, Seattle, WA.

Richards, P.J., Williams, N., Laing, B., McCarty, M. and Pond, M. (2008), "Numerical calculation of the three-dimensional motion of wind-borne debris", J. Wind Eng. Ind. Aerodyn.,**96**,2188-2202.

Scarabino, A. and Giacopinelli, P. (2010), "Analysis of the two dimensional sheet debris flight

equations: initial and final state", Wind and Structures, **13**, 109-125.

Shinozuka, M. and Deodatis, G. (1991), "Simulation of stochastic processes by spectral representation", Appl. Mech. Rev., **44**(4), 191-204.

Simiu, E., Vickery, P. and Kareem, A. (2007), "Relation between Saffir-Simpson hurricane scale wind speeds and peak 3-s gust speeds over open terrain", J. Struct. Eng.,**133**(7), 1043 – 1045.

Tachikawa, M. (1983), "Trajectories of flat plates in uniform flow with application to wind-generated missiles", J. Wind Eng. Ind. Aerodyn., **14**, 443-453.

Tachikawa, M. (1988), "A method for estimating the distribution range of trajectories of wind-borne missiles", J. Wind Eng. Ind. Aerodyn., **29**(1–3), 175–84.

Visscher, B.T. and Kopp, G.A. (2007), "Trajectories of roof sheathing panels under high winds", J. Wind Eng. Ind. Aerodyn.,**95**, 697-713.

Von Karman, T. (1948), "Progress in the statistical theory of turbulence", Proc. Nat. Acad. Sci.,**34**, 530-539.

Wang, K. (2003). Flying Debris Behavior, Thesis, Civil Engineering Department, Texas Tech University.

Wills, J.A.B., Lee, B.E. and Wyatt, T.A. (2002), "A model of windborne debris damage", J. Wind Eng. Ind. Aerodyn., **90**(4–5), 555–565.

Yau Siu, C., Lin, N. and Vanmarcke,E. (2011), " Hurricane damage and loss estimation using an integrated vulnerability model", Nat. Haz. Rev.,ASCE,**12**(4),184-189.

Table A-1. Summary results of Phase 1 Tile Frangibility Testing

Tile Material	Size	Attachment	Cell Content: Mean (standard deviation) [# of fragments] Decimal values are a fraction of full tile by mass 15.2 m/s	22.4 m/s	29.5 m/s
Concrete I	Full	Mortar	0.034 (0.008) [3]	0.086 (0.090) [15]	0.087 (0.098) [23]
	Full	Mechanical	0.109 (0.148) [66]	0.146 (0.165) [48]	0.119 (0.189) [110]
	Half	Mortar	0.075 (0.078) [3]	0.042 (0.011) [3]	0.137 (0.155) [13]
	Half	Mechanical	0.097 (0.123) [24]	0.092 (0.132) [37]	0.105 (0.158) [42]
Concrete II	Full	Mortar	0.108 (0.194) [9]	0.094 (0.074) [31]	0.129 (0.167) [71]
	Full	Mechanical	0.130 (0.192) [70]	0.125 (0.149) [61]	0.121 (0.163) [110]
	Half	Mortar	0.123 (0.058) [3]	0.082 (0.103) [15]	0.108 (0.122) [28]
	Half	Mechanical	0.085 (0.062) [4]	0.122 (0.131) [24]	0.145 (0.171) [48]

Table A-2. 3 second gust exposure C isotach Reference and Hourly Mean Wind Speeds

3 sec gust isotach (m/s)	Hourly Mean Wind Speeds (m/s)		
Exposure C	Exposure B	Exposure C	Exposure D
44.72	22.14	29.20	34.17
49.20	24.38	32.16	37.57
53.67	26.57	35.06	41.01
58.14	28.80	37.97	44.41
62.62	30.99	40.92	47.85
67.08	33.23	43.83	51.25
71.56	35.47	46.74	54.65
76.03	37.66	49.69	58.09
80.50	39.89	52.60	61.49
84.97	42.08	55.50	64.94
89.45	44.32	58.45	68.34

List of Figures

A 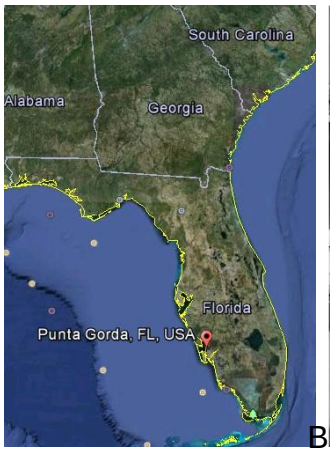

B 
C 

Figure A-1. Tile Debris Damage after Hurricane Charley, Punta Gorda, FL 2004. A) Map of Punta Gorda, FL (Courtesy of Google Maps). B) and C) Tile Debris Damage in Punta Gorda, FL.

A  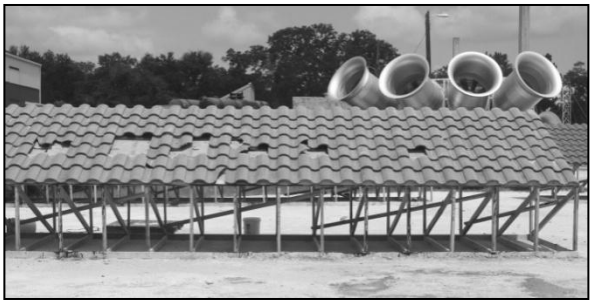 B

Figure A-2. Images of phase 1 frangibility testing. A) Set up for tile frangibility impact test prior to tile launch (phase 1 testing). B) Roof system post-impact testing.

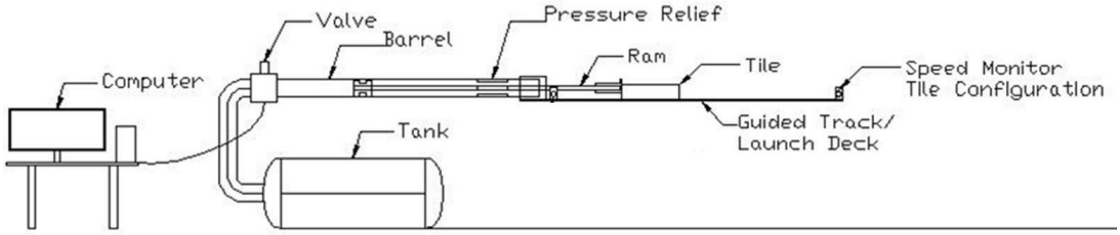

Figure A-3. Tile launch apparatus (Photo courtesy of Fernandez et al. 2010).

A 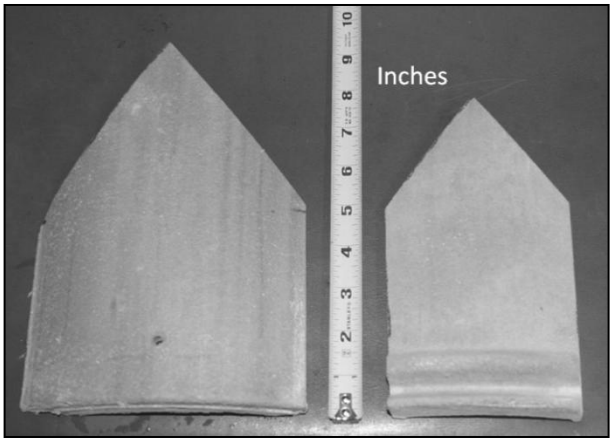

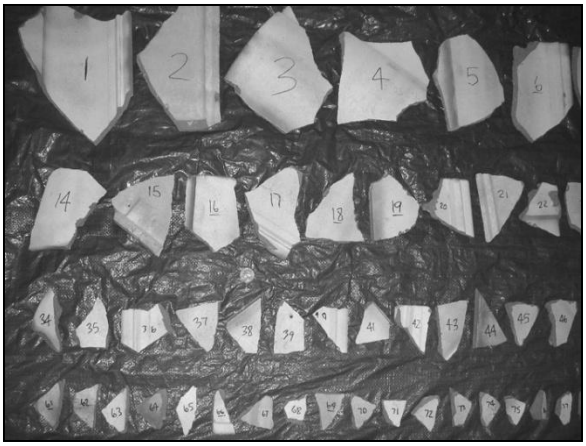
B

Figure A-4. Images from phase 2 and phase 1 testing. A) 1/4th and 1/8th size (by weight of a full tile) tile fragments used as the impact debris for phase 2. B) A sample of roof system tile fragments produced from phase 1 testing.

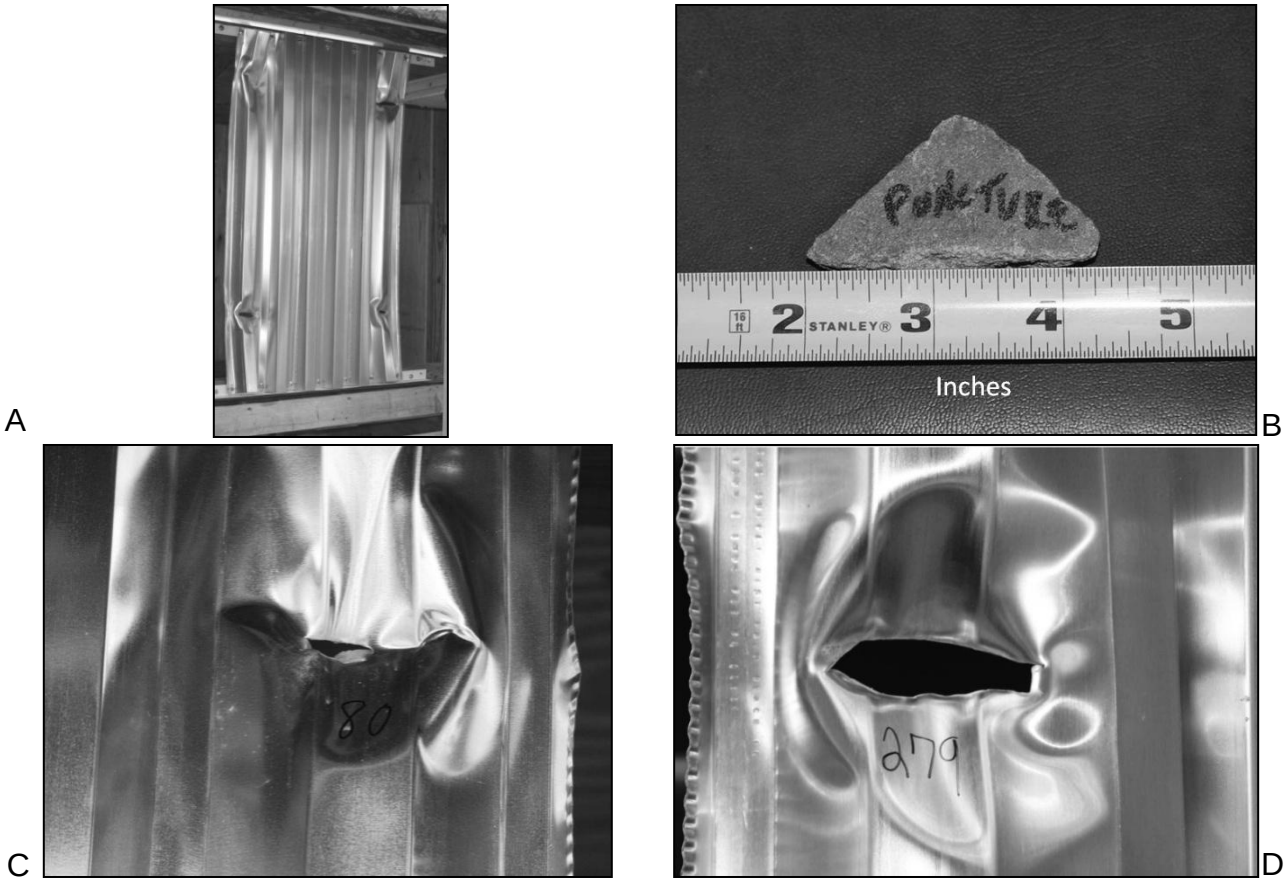

Figure A-5. Images from phase 2 shutter puncture testing. A) Installed three panel shutter system after four impact tests. B) Tile fragment used to define puncture. C) An example of a tear but not puncture. D) An example of a puncture.

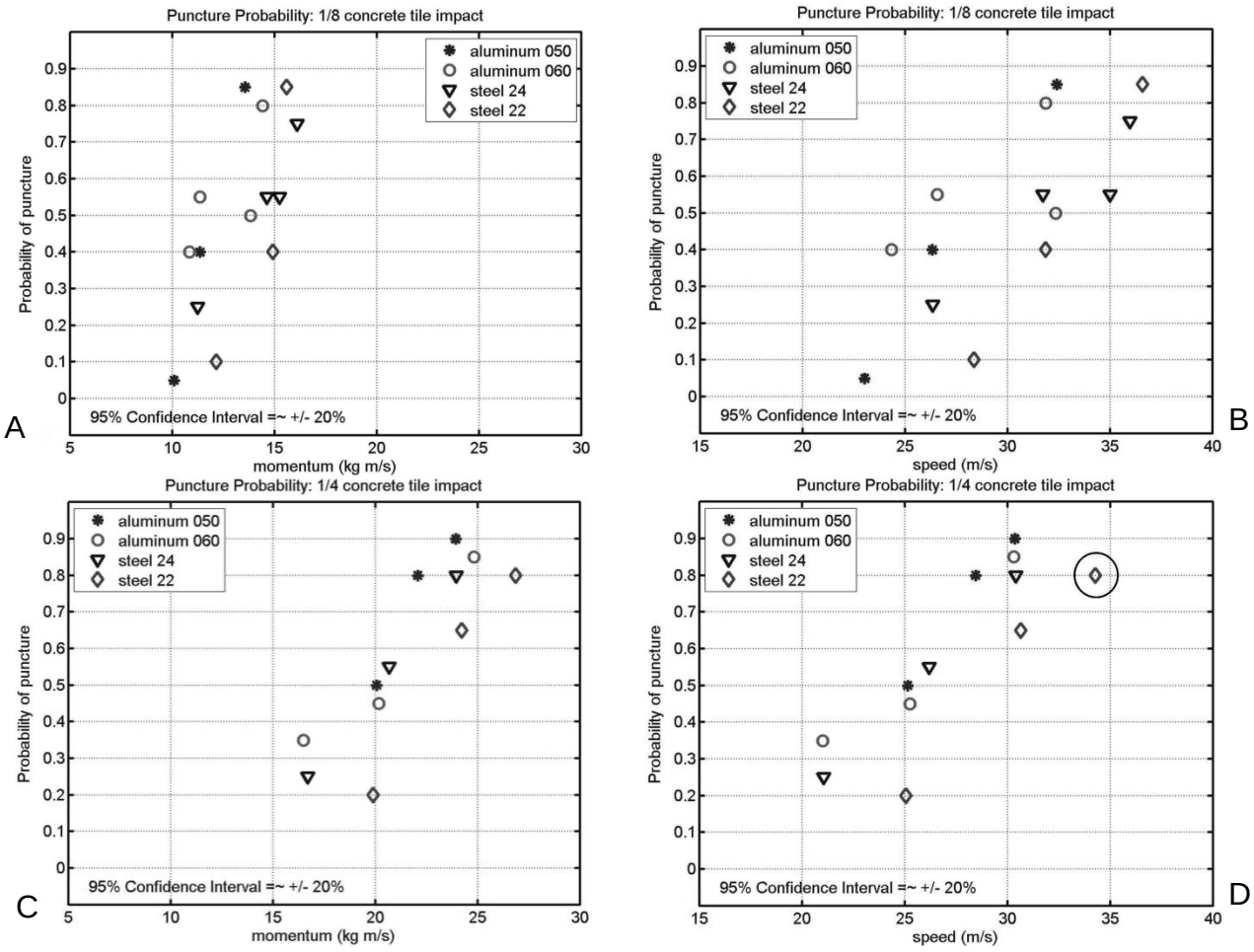

Figure A-6. Puncture vulnerability curves for 1/8th and 1/4th tile fragment impacts as a function of impact momentum (1/8th – A, 1/4th – C) and impact speed (1/8th – B, 1/4th – D). The 95% confidence interval refers to the vertical axis. The circled diamond is referred to within the text.

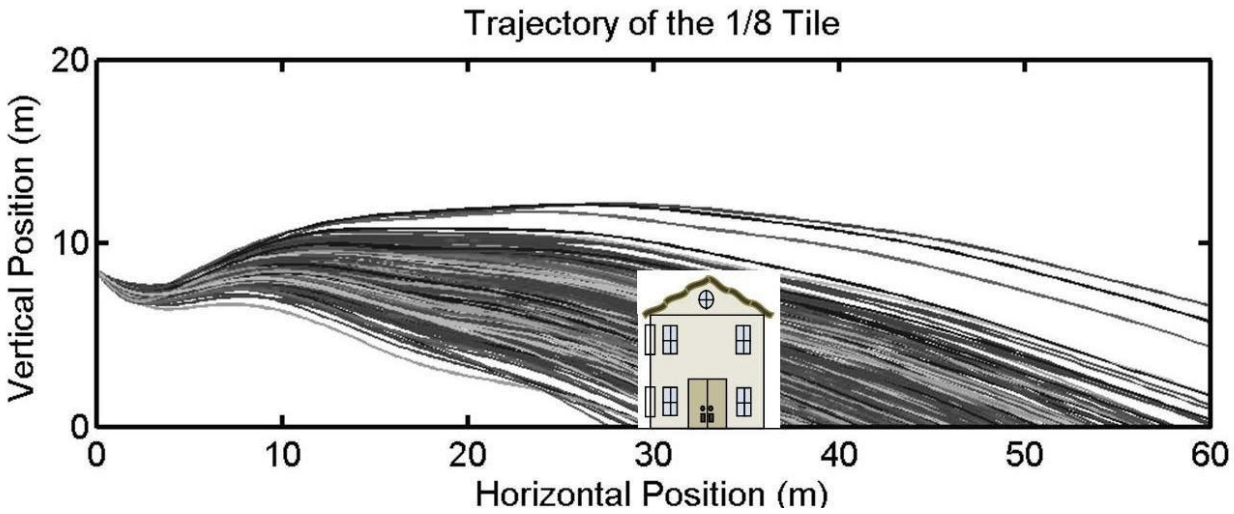

Figure A-7. 300 Trajectories of the 1/8th tile for the 100 mph isotach, exposure B.

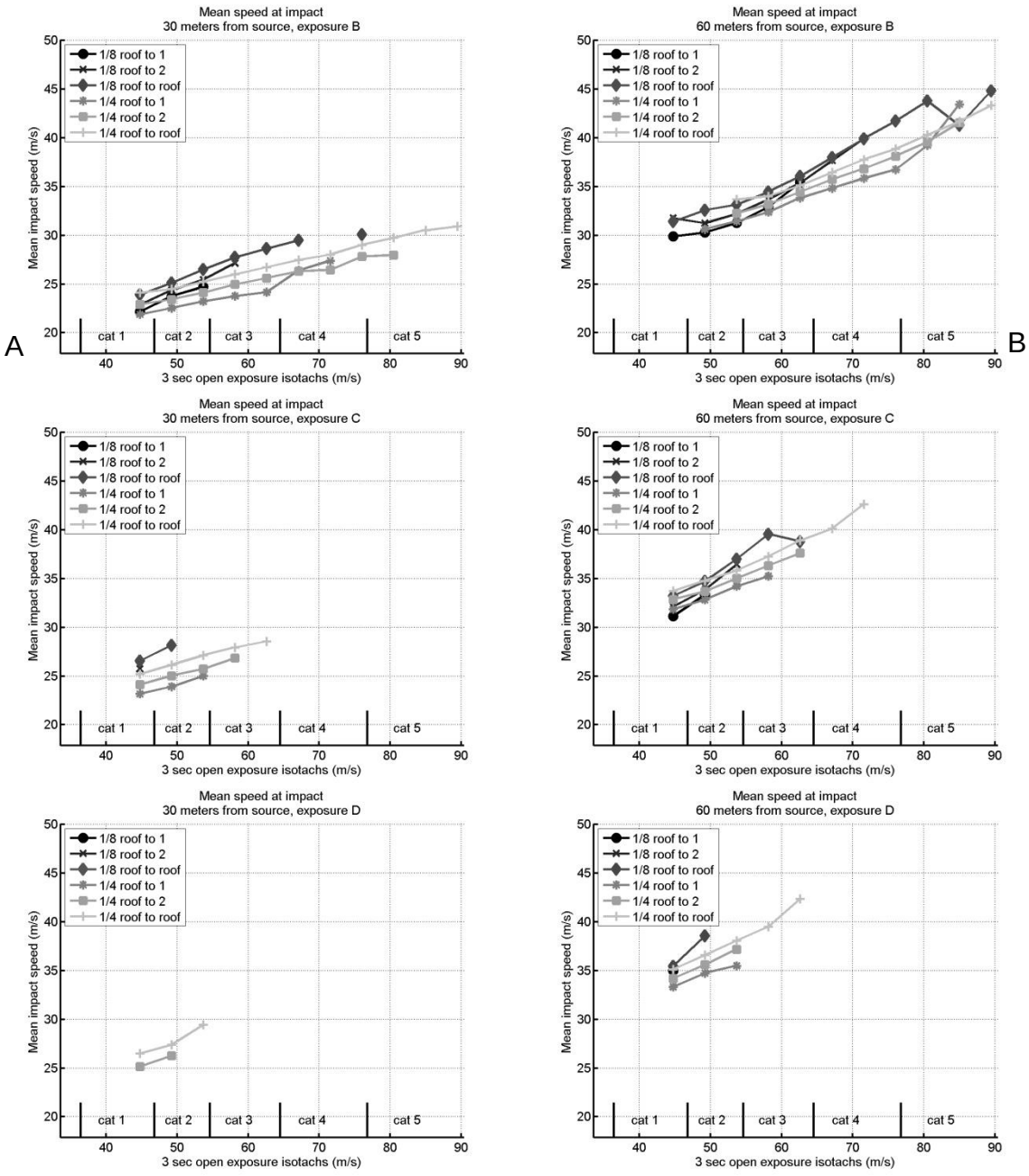

Figure A-8: Mean speed of tile fragment impact for B, C, D exposures. A) Distance from source to target = 30 m. B) Distance from source to target = 60 m.

APPENDIX B
COMPONENT AND SYSTEM PLOTS AREAS AVERAGED

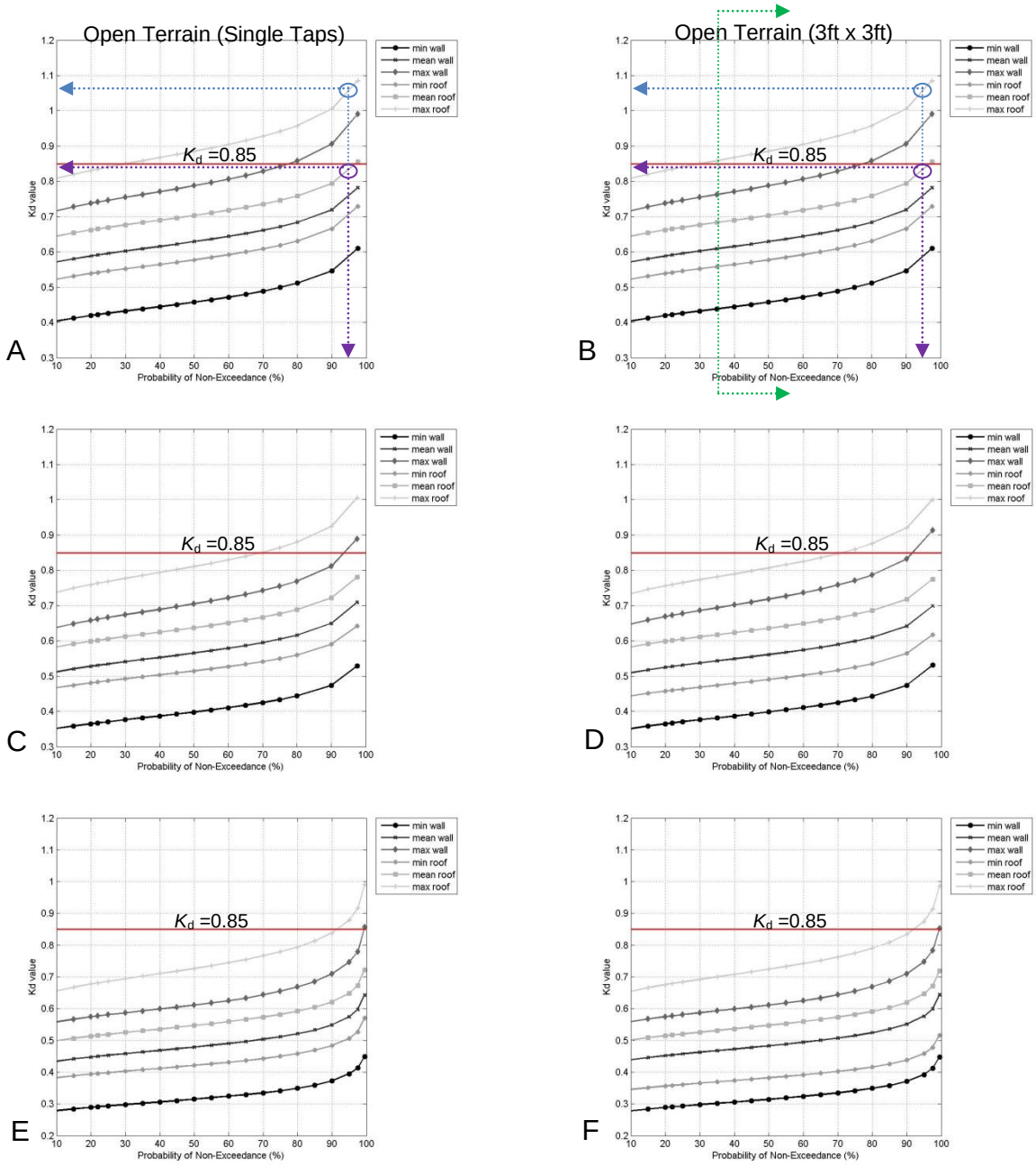

Figure B-1. Minimum, mean, and maximum K_d factor for wall and roof following scenario analysis component perspective for different probability of non-exceedance for Frances. A) Single taps Frances 26.5N, 80.1W.B) 3ft x 3ft Frances 26.5N, 80.1. C) Single taps Frances 27.5N, 80.3W. D) 3ft x3ft Frances 27.5N, 80.3W. E) Single taps Frances 28.7 N, 80.7W. F) 3ft x3ft Frances 28.7 N, 80.7W

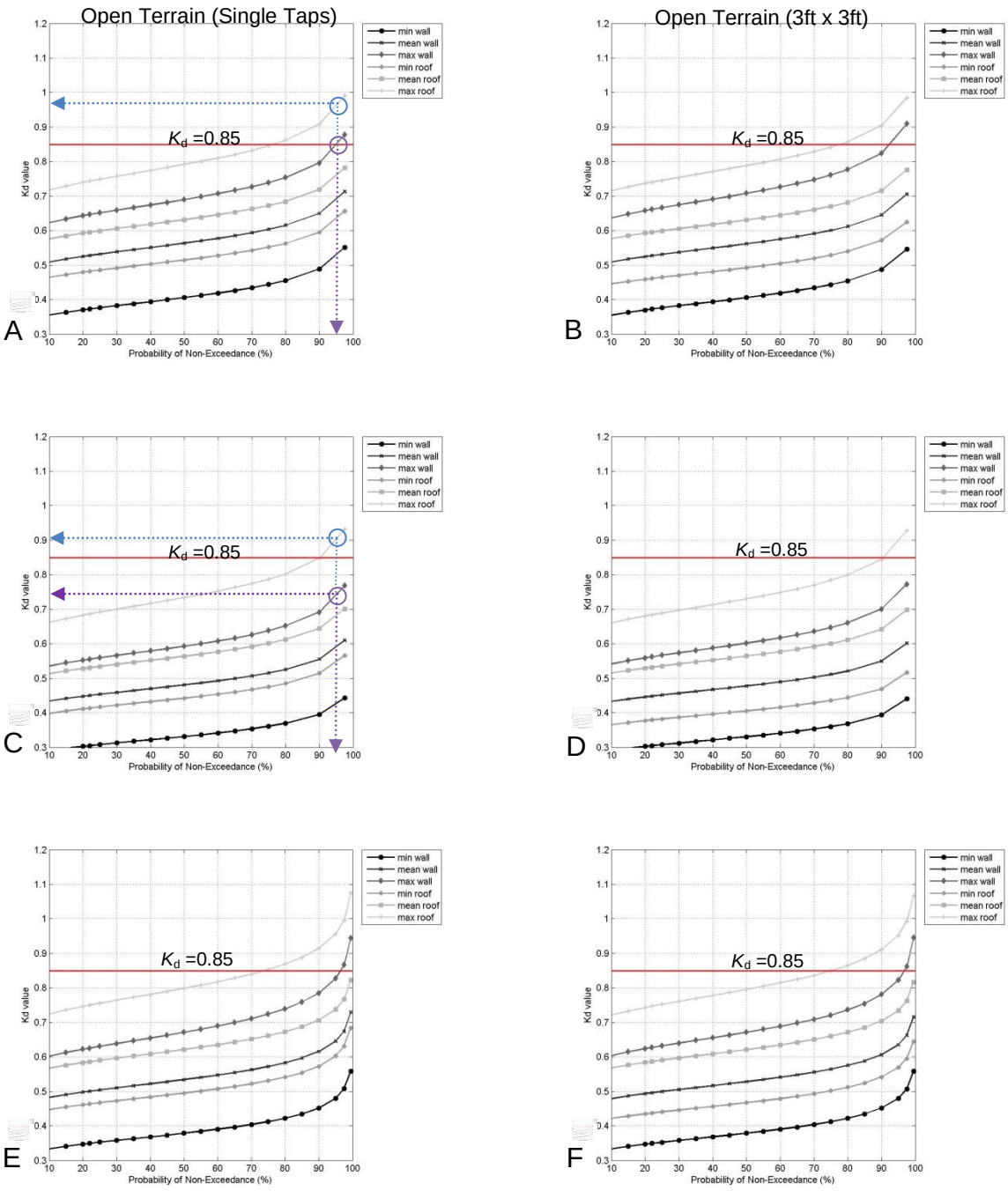

Figure B-2. Minimum, mean, and maximum K_d factor for wall and roof following scenario analysis component perspective for different probability of non-exceedance. A) Single taps Katrina 30.4N, 89.8W. B) 3ft x 3ft Katrina 30.4N, 89.8W. C) Single taps Katrina 30.4N,89.4W. D) 3ftx3ft Katrina 30.4N,89.4W E) Single taps Katrina 31.4N, 90.0W. F) 3ft x3ft Katrina 31.4N, 90.0W.

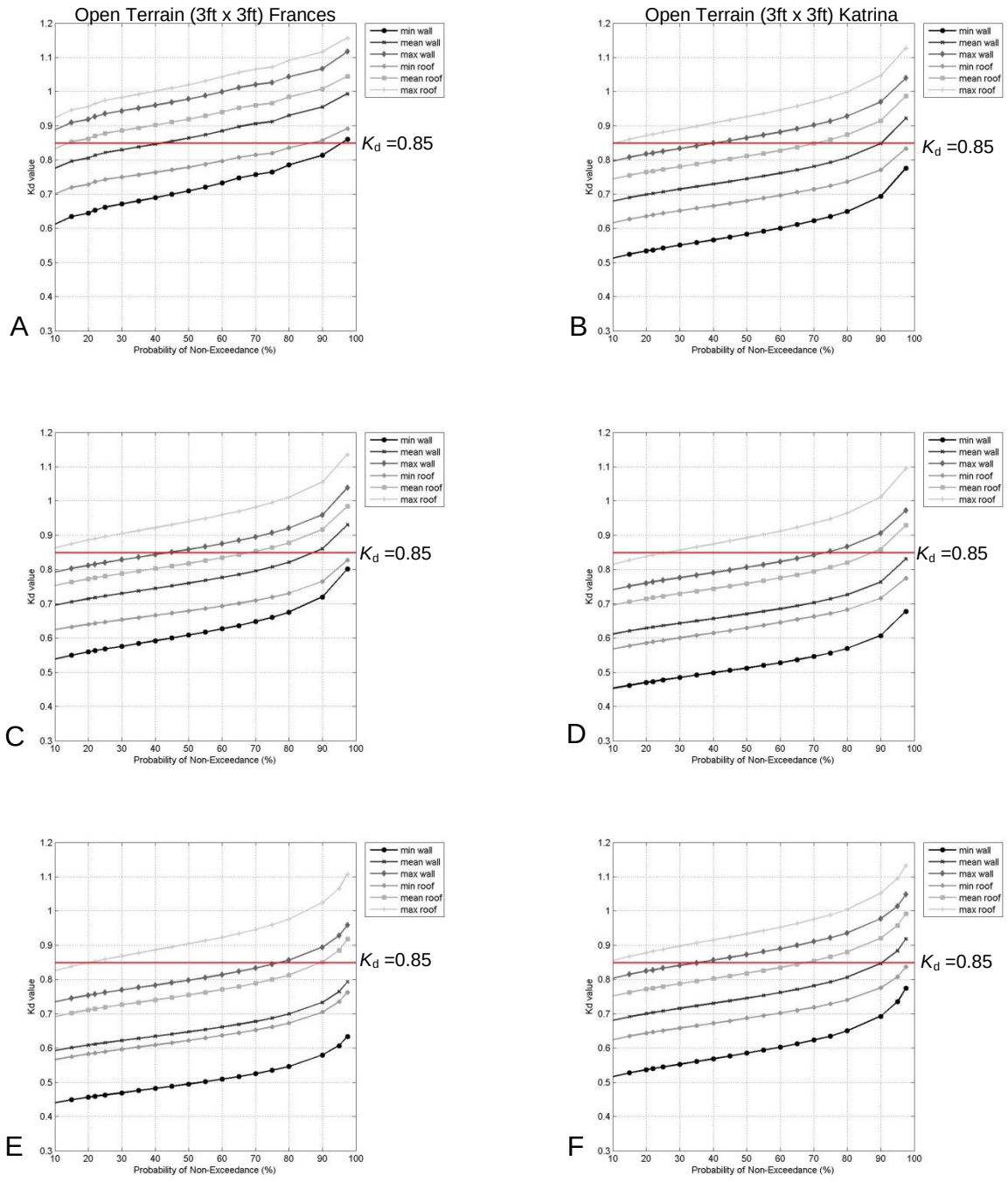

Figure B-3. Minimum, mean, and maximum K_d factor for squared area 3ft x 3ft following scenario analysis system perspective for different probability of non-exceedance. A) Frances 26.5,-80.1. B) Katrina 30.4,-89.8. C) Frances 27.5,-80.3. D) Katrina location 30.4,-89.4. E) Frances 28.7 N, 80.7W. F) Katrina 31.4N, 90.0W.

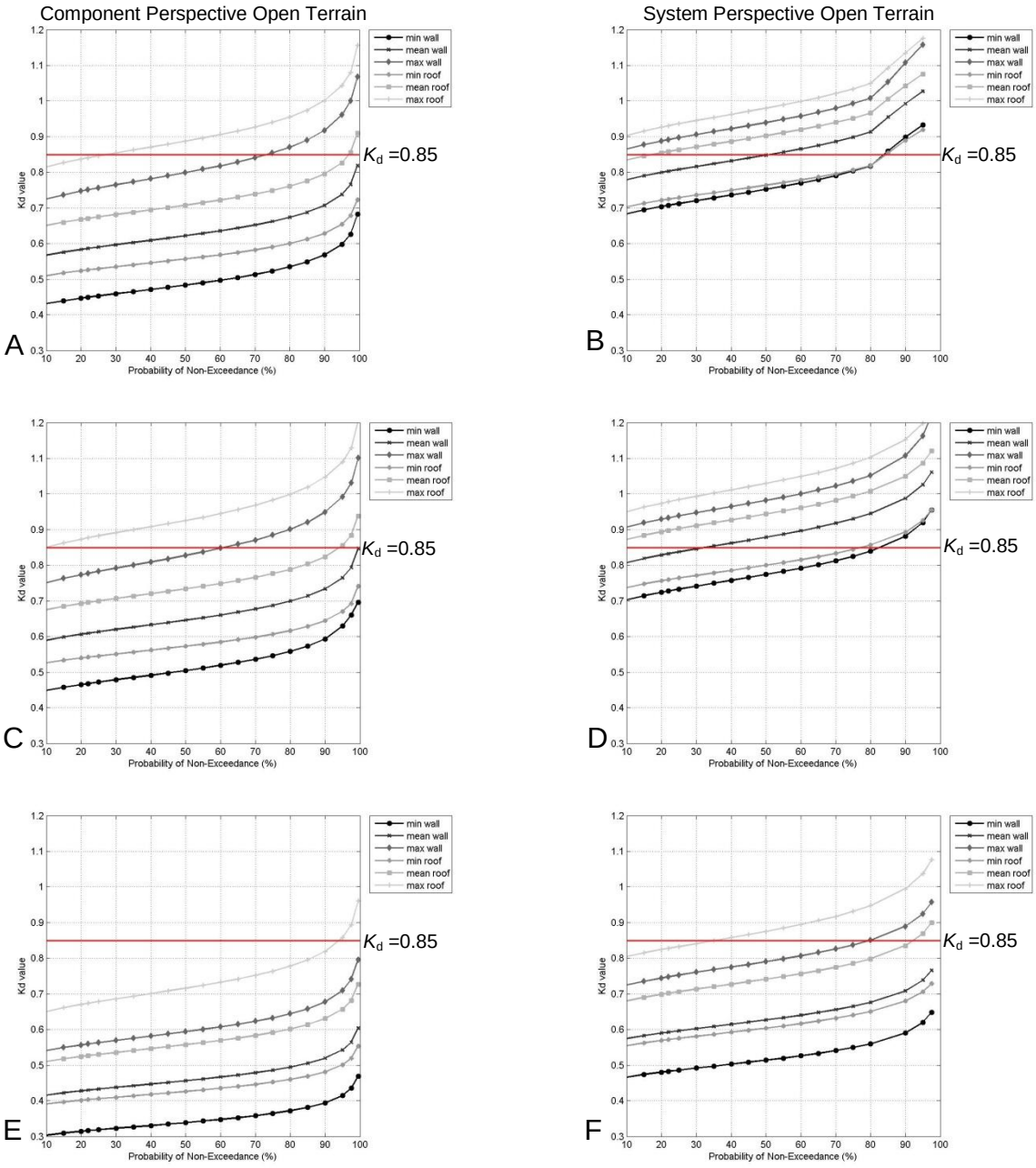

Figure B-4. K_d factor ranges for squared area 5ft x 5ft following scenario analysis open exposure for Frances grid (Fig.5-13). A) Component: 26.5,-80.1. B) System: 26.5,-80.1. C) Component: 26.5, -80.5. D) System: 26.5, -80.5. E) Component: 27.1,-80.3. F) System: 27.1,-80.3.

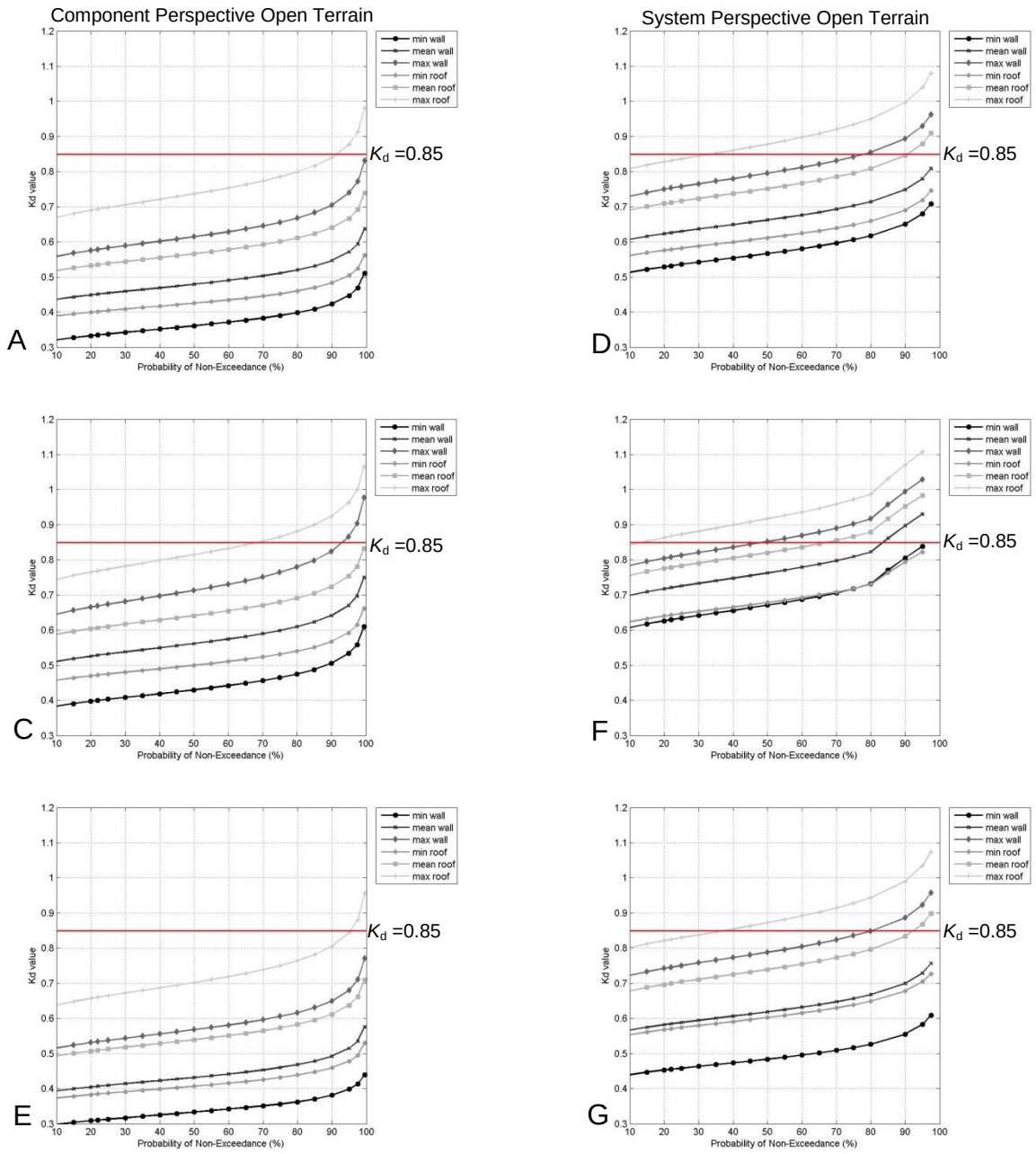

Figure B-5. K_d factor ranges for squared area 5ft x 5ft following scenario analysis open exposure for Frances grid (Fig.5-13). A) Component: 27.1,-80.7. B) System: 27.1,-80.7. C) Component: 27.5, -80.3. D) System: 27.5, -80.3. E) Component: 27.5,-80.7. F) System: 27.5,-80.7.

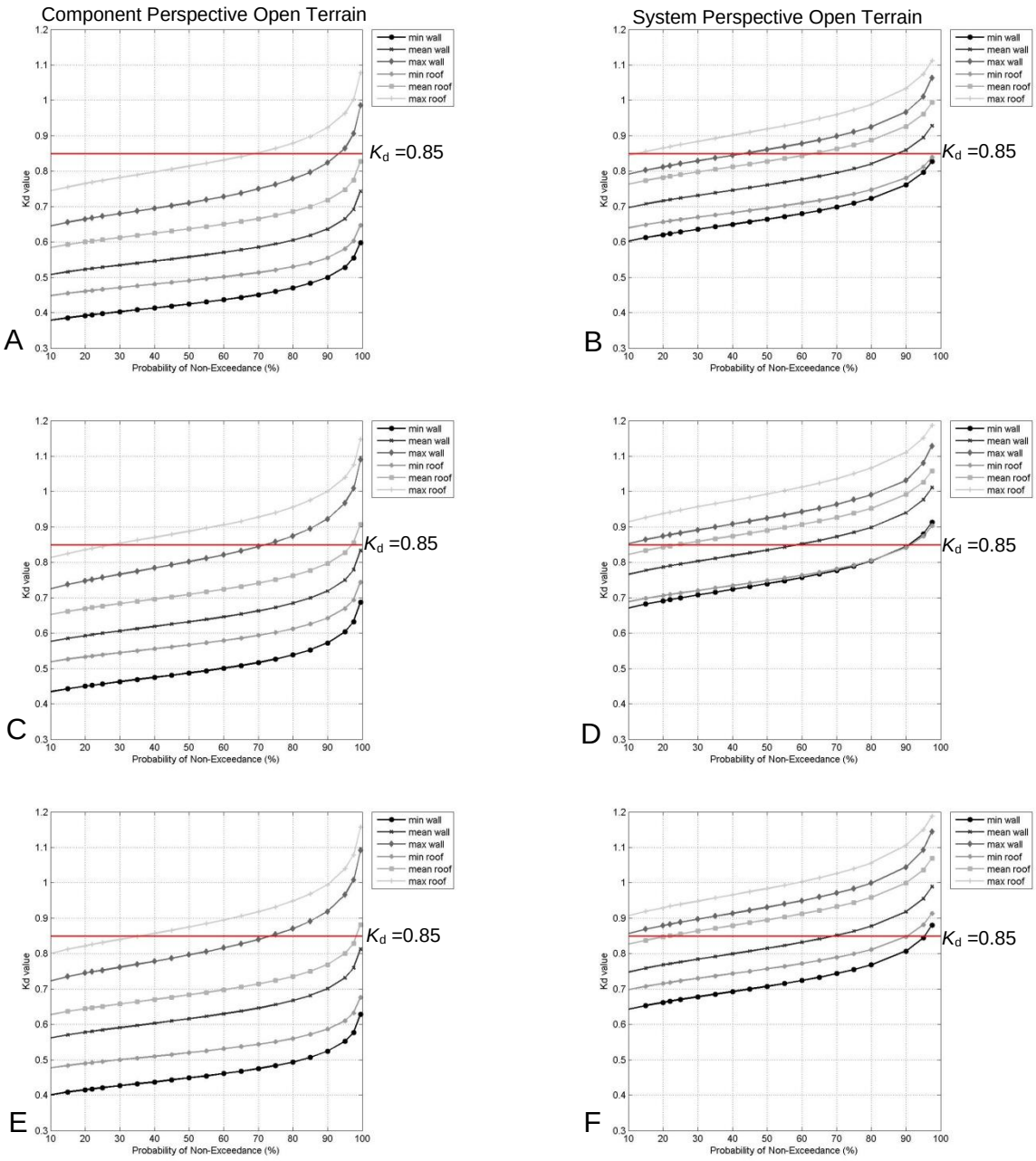

Figure B-6. K_d factor ranges for squared area 5ft x 5ft following scenario analysis open terrain for Frances grid (Fig.5-13). A) Component: 27.9,-80.5. B) System: 27.9,-80.5. C) Component: 27.9, -80.9. D) System: 27.9, -80.9. E) Component: 28.3,-80.7. F) System: 28.3,-80.7.

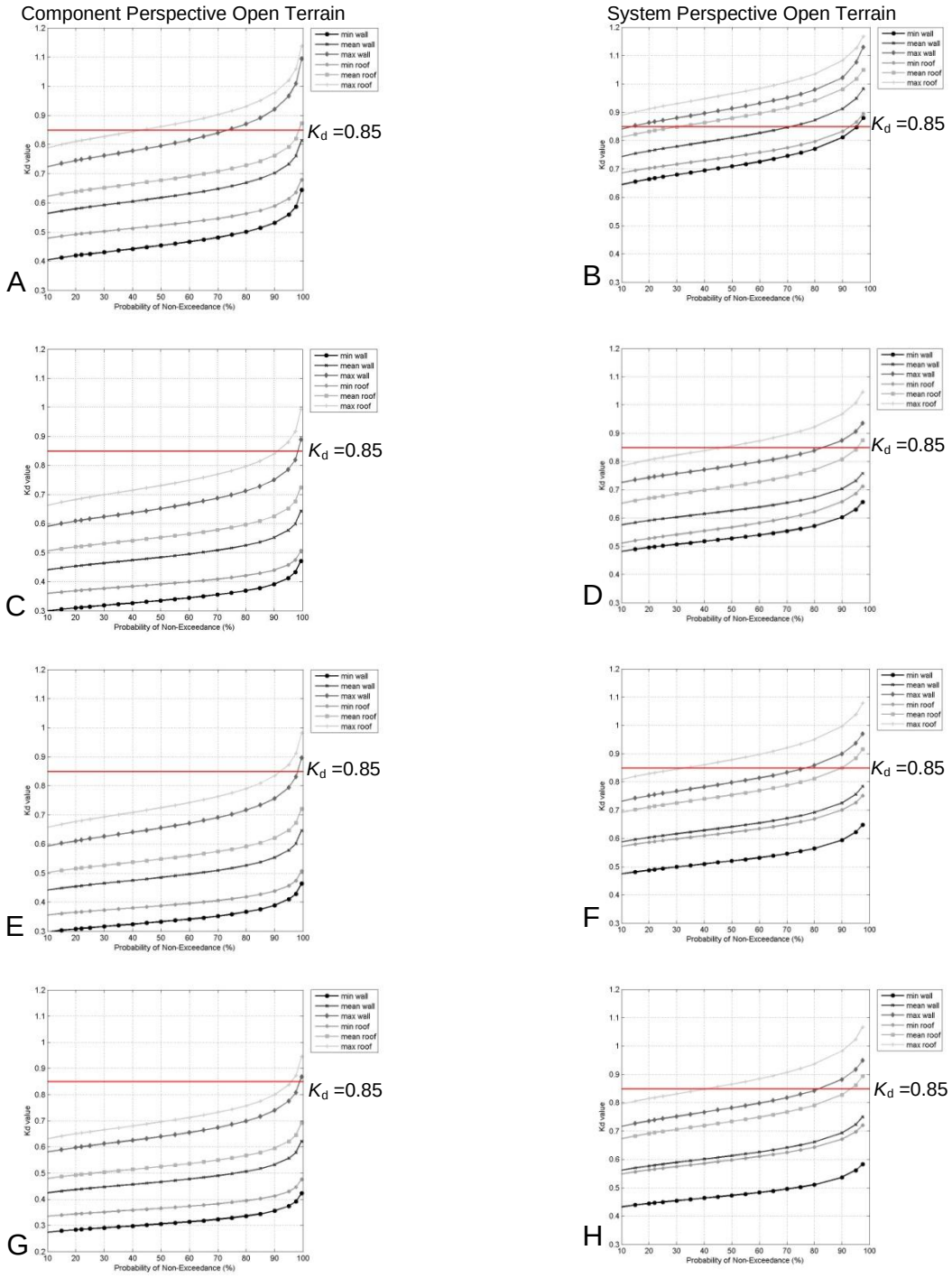

Figure B-7. K_d factor ranges for squared area 5ft x 5ft following scenario analysis open exposure for Frances grid (Fig.5-13). A) Component: 28.3 N, -80.9W. B) Perspective: 28.3 N, -80.9W. C) Component: 28.7N, -80.7W. D) Perspective: 28.7N, -80.7W. E) Component: 28.7N, -80.9W. F) Perspective: 28.7N, -80.9W. G) Component: 28.9N, -80.9W. H) Perspective: 28.9N, -80.9W.

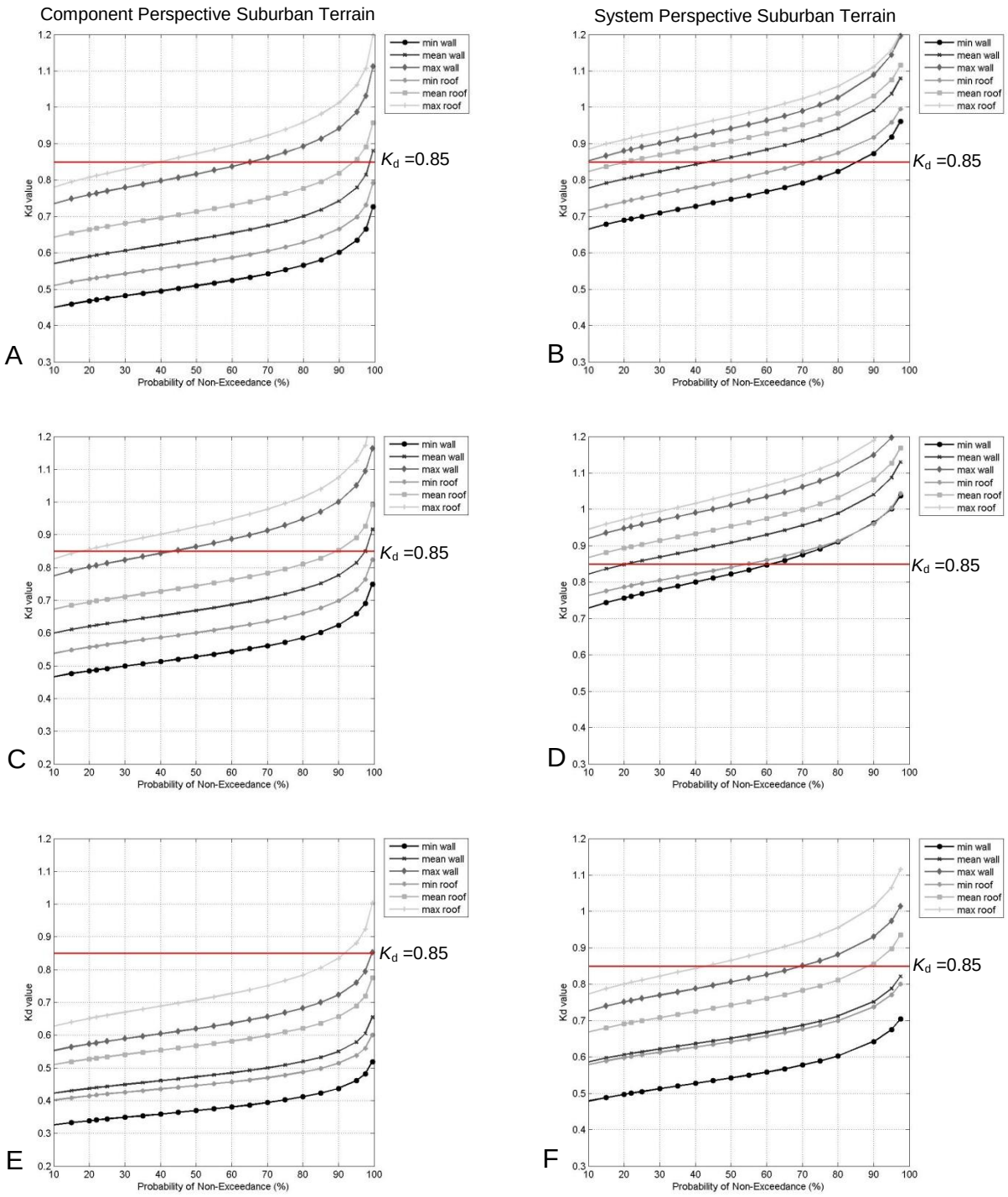

Figure B-8. K_d factor for squared area 5ft x 5ft following scenario analysis in suburban exposure for Frances grid (Fig.5-13). A) Component: 26.5,-80.1. B) Perspective: 26.5,-80.1. C) Component: 26.5,-80.5. D) Perspective: 26.5,-80.5. E) Component: 27.1,-80.3. F) Perspective: 27.1,-80.3.

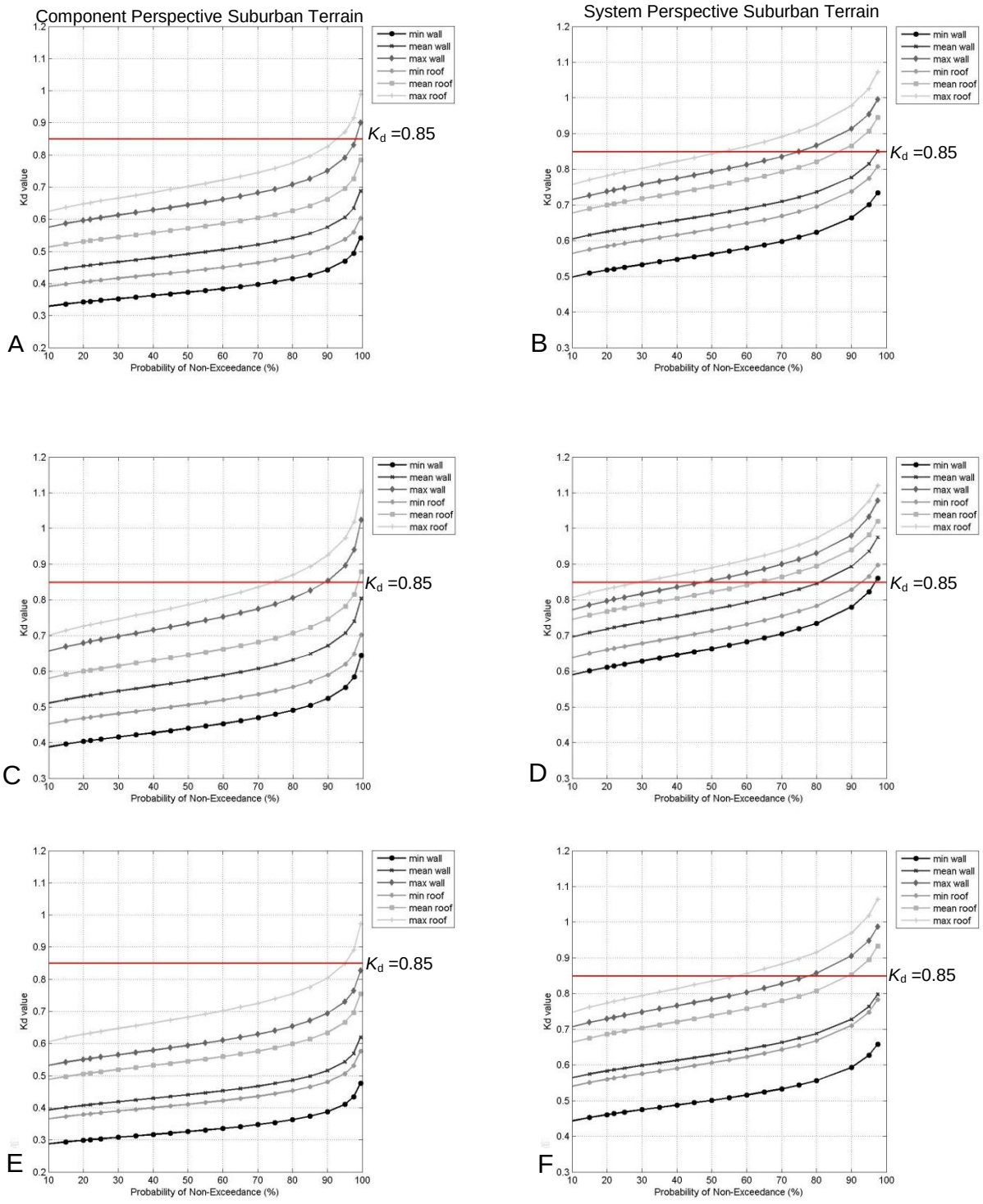

Figure B-9. K_d factor for squared area 5ft x 5ft following scenario analysis in suburban exposure for Frances grid (Fig.5-13). A) Component: 27.1 N, -80.7W. B) System: 27.1 N, -80.7W. C) Component: 27.5N, -80.3W. D) System: 27.5N, -80.3W. E) Component: 27.5N, -80.7W. F) System: 27.5N, -80.7W.

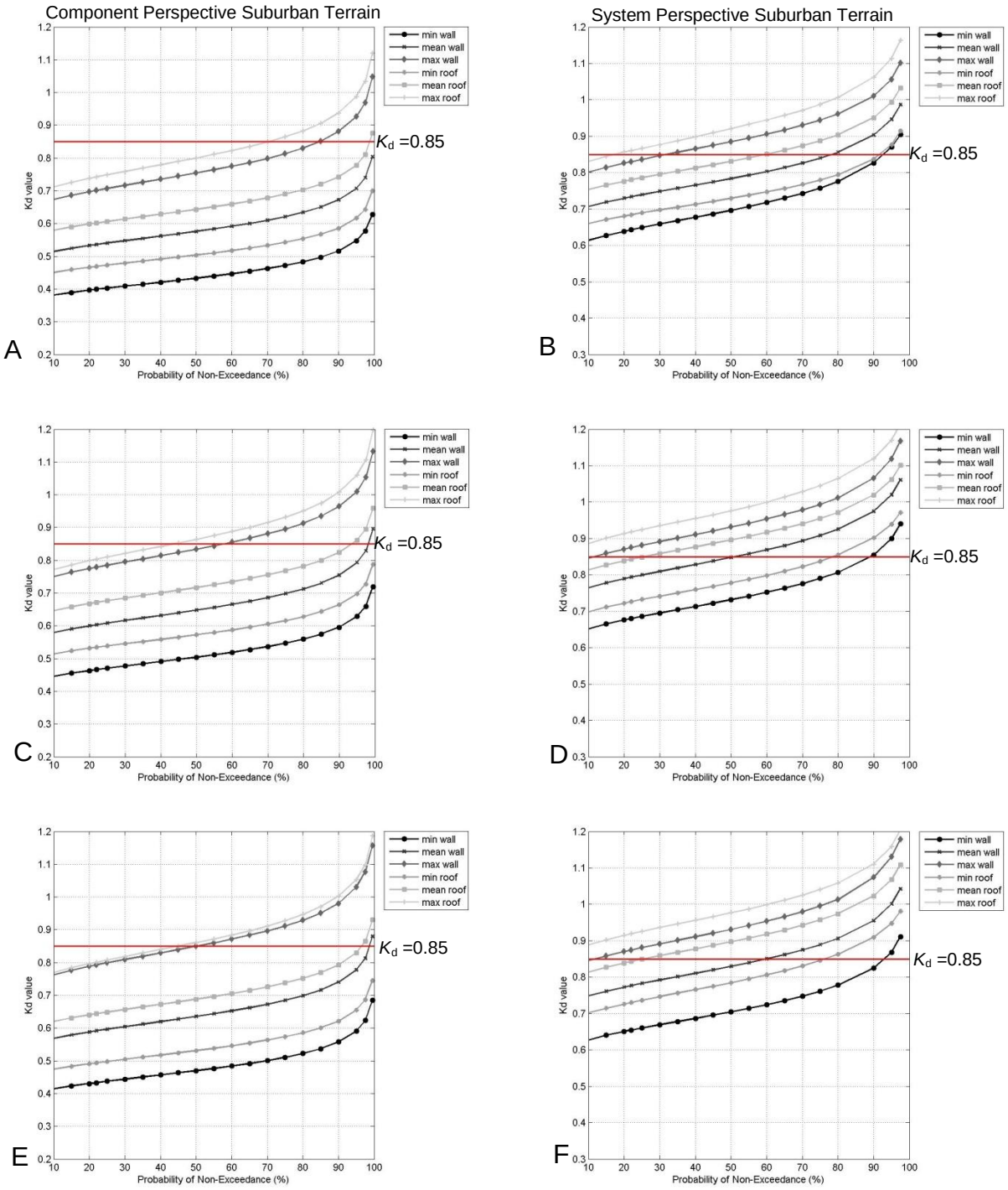

Figure B-10. K_d factor for squared area 5ft x 5ft following scenario analysis in suburban exposure for Frances grid (Fig.5-13). A) Component: 27.9 N, -80.5W. B) System: 27.9 N, -80.5W. C) Component: 27.9N, -80.9W. D) System: 27.9N, -80.9W. E) Component: 28.3N, -80.7W. F) System: 28.3N, -80.7W.

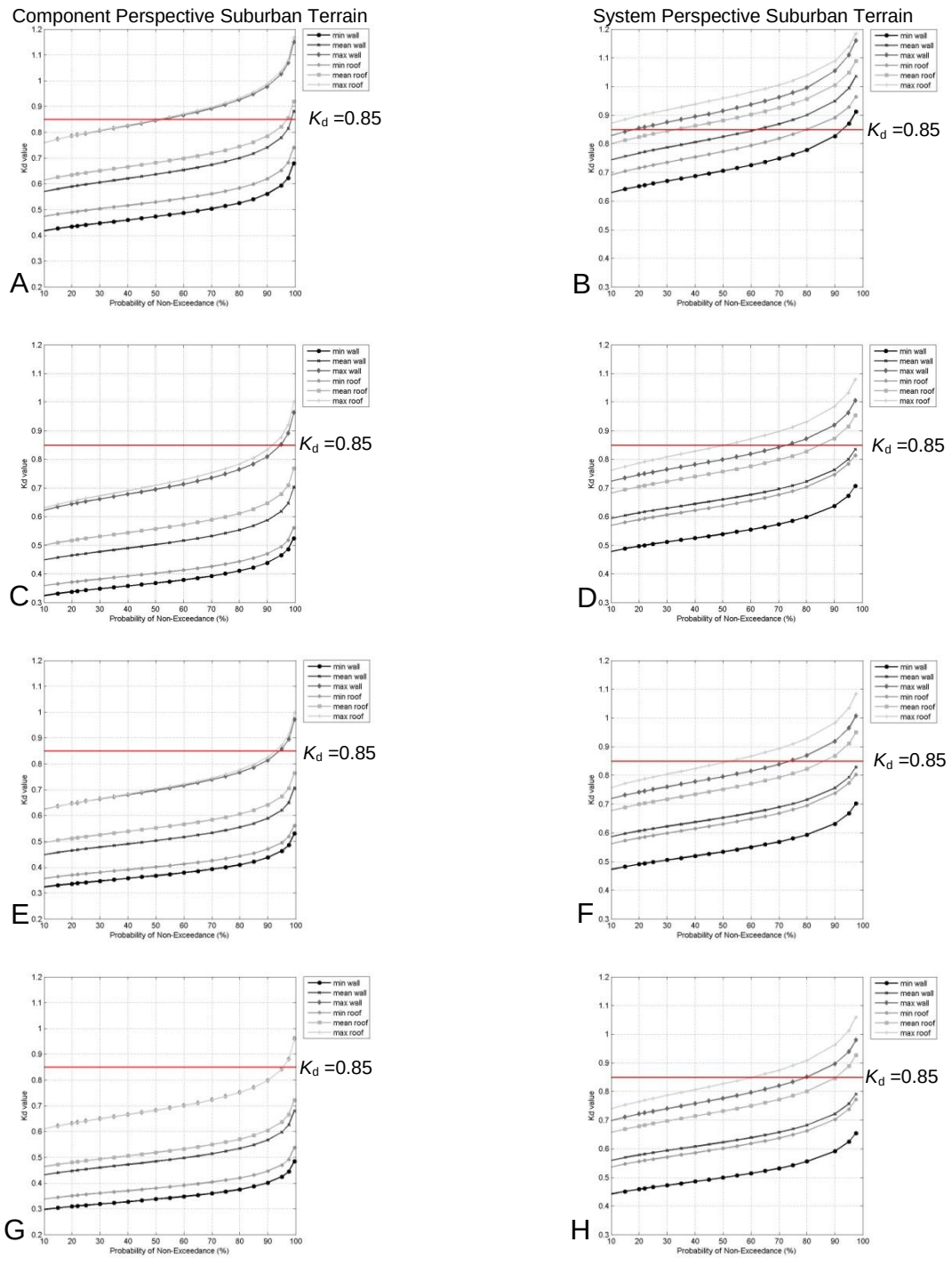

Figure B-11. K_d factor for squared area 5ft x 5ft following scenario analysis in suburban exposure for Frances grid (Fig.5-13). A) Component: 28.3 N,-80.9W. B) System: 28.3 N, -80.9W. C) Component: 28.7N,-80.7W. D) System: 28.7N, -80.7W. E) Component: 28.7N, -80.9W. F) System: 28.7N,-80.9W. G) Component: 28.9N,-80.9W. H) System: 28.9N,-80.9W.

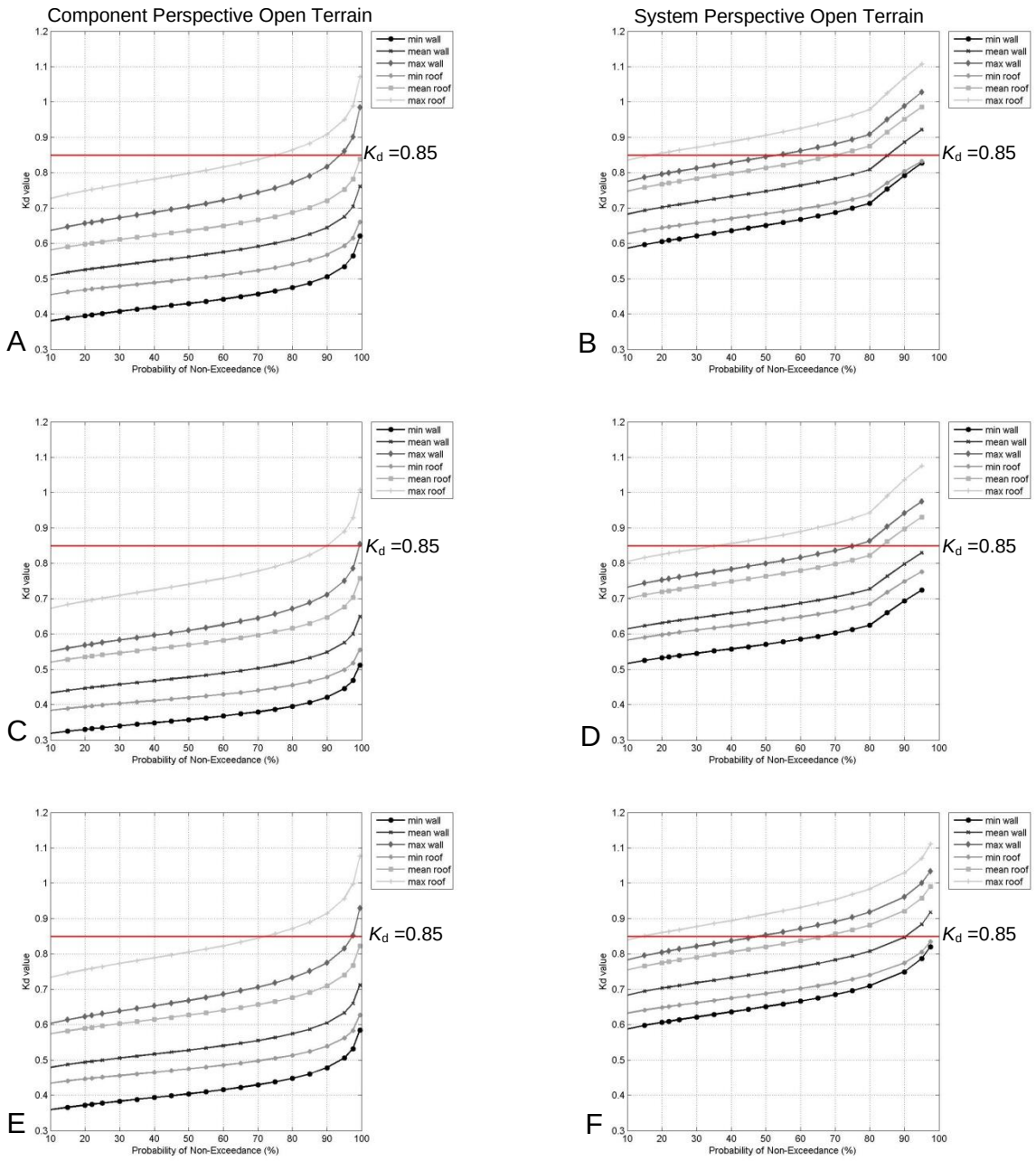

Figure B-12. K_d factor ranges for squared area 5ft x 5ft following scenario analysis open exposure for Katrina grid (Fig.5-13). A) Component: 30.4,-89.8. B) System: 30.4,-89.8. C) Component: 30.4,-89.4. D) System: 30.4,-89.4. E) Component: 31.4,-90.0. F) System: 31.4,-90.0.

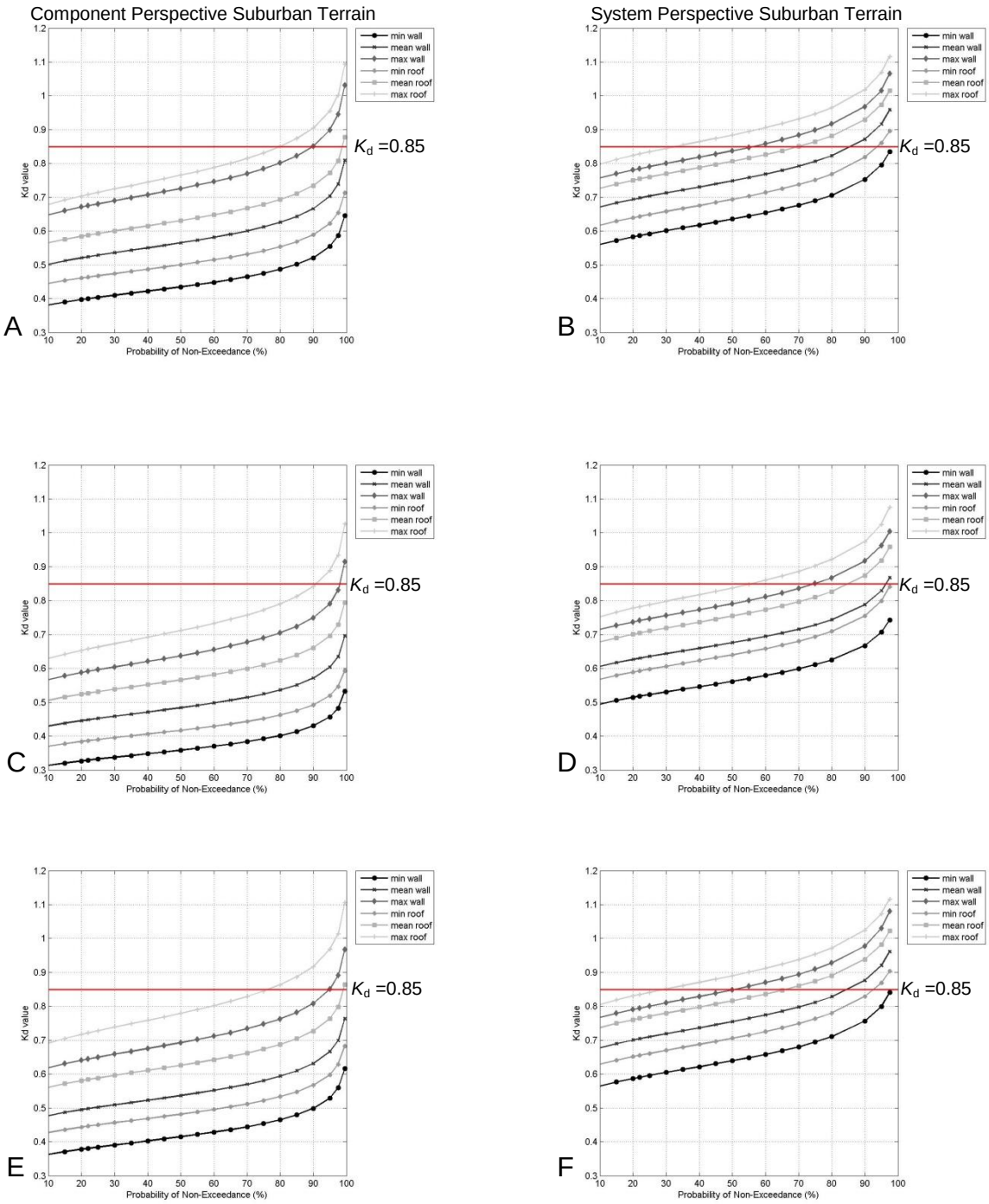

Figure B-13. K_d factor ranges for squared area 5ft x 5ft following scenario analysis in suburban exposure for Katrina grid (Fig.5-13). A) Component: 30.4,-89.8. B) Perspective: 30.4,-89.8. C) Component: 30.4,-89.4. D) Perspective: 30.4,-89.4. E) Component: 31.4,-90.0. F) Perspective: 31.4,-90.0.

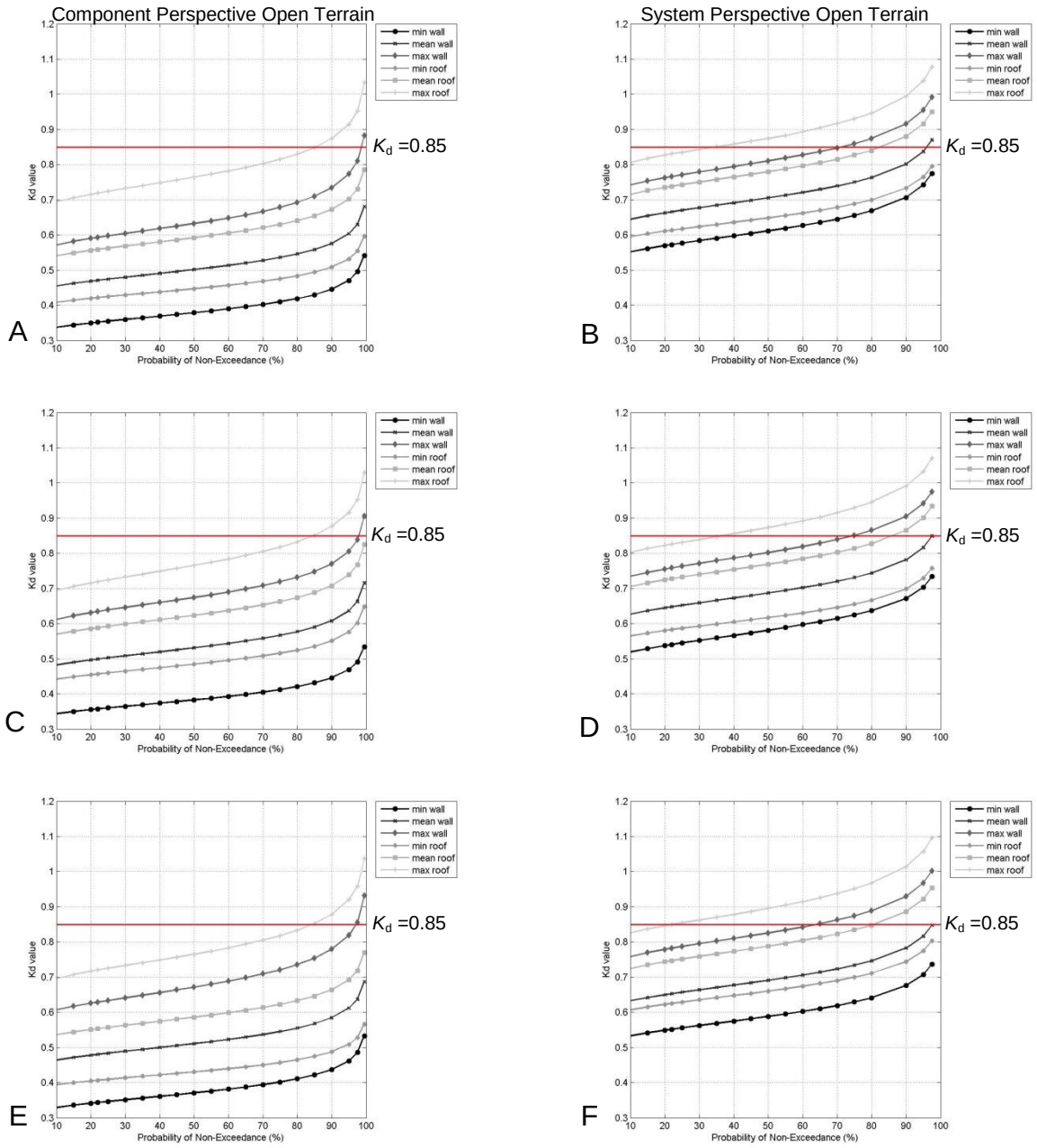

Figure B-14. K_d factor ranges for squared area 5ft x 5ft following scenario analysis in open exposure for Ivan grid (Fig.5-13). A) Component: 30.4,-87.5. B) System: 30.4,-87.5. C) Component: 30.4,-87.9. D) System: 30.4,-87.9. E) Component: 31.4,-88.3. F) System: 31.4,-88.3.

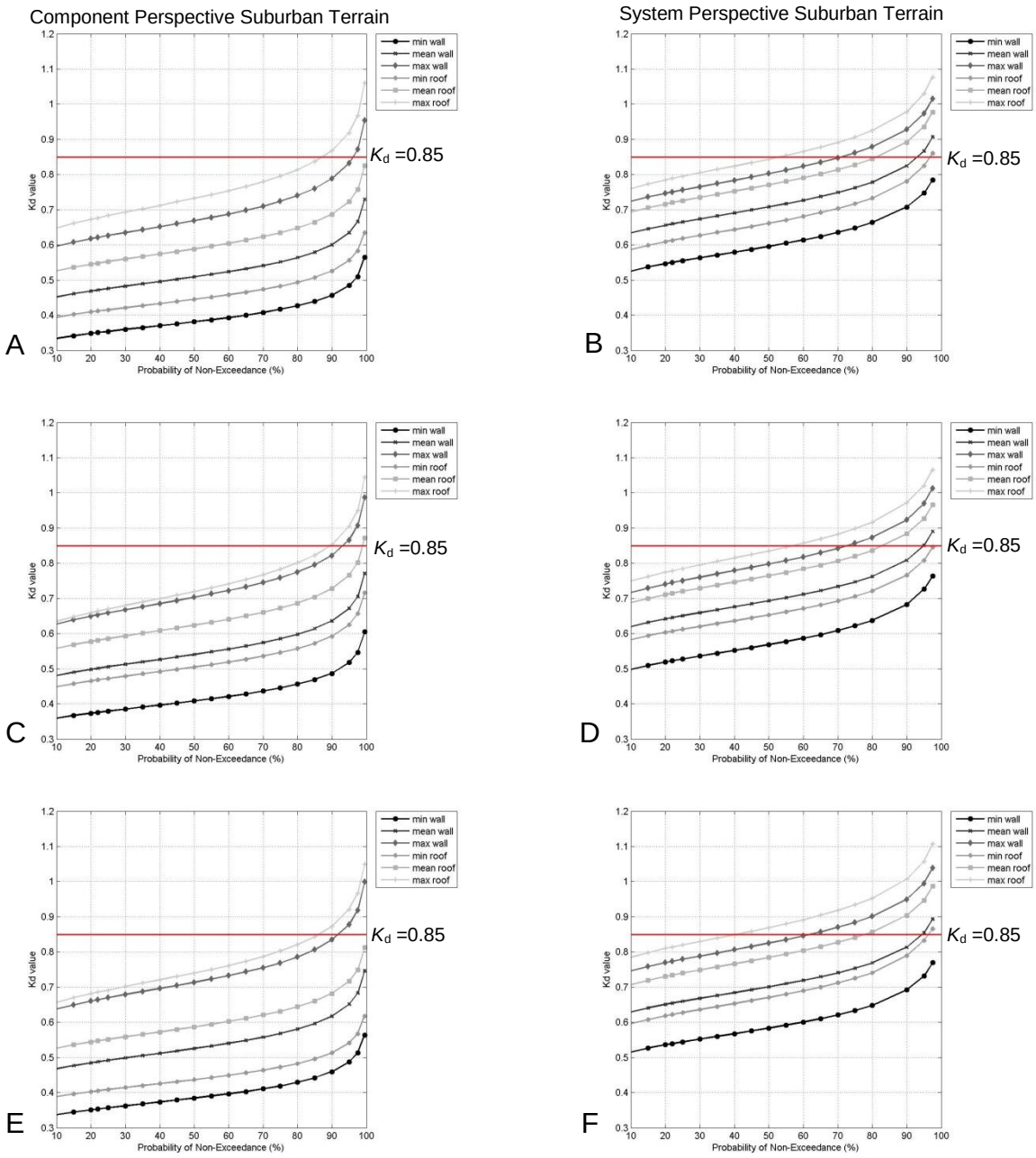

Figure B-15. K_d factor ranges for squared area 5ft x 5ft following scenario analysis in suburban exposure for Ivan grid (Fig.5-13). A) Component: 30.4,-87.5. B) System: 30.4,-87.5. C) Component: 30.4,-87.9. D) System: 30.4,-87.9. E) Component: 31.4,-88.3. F) System: 31.4,-88.3.

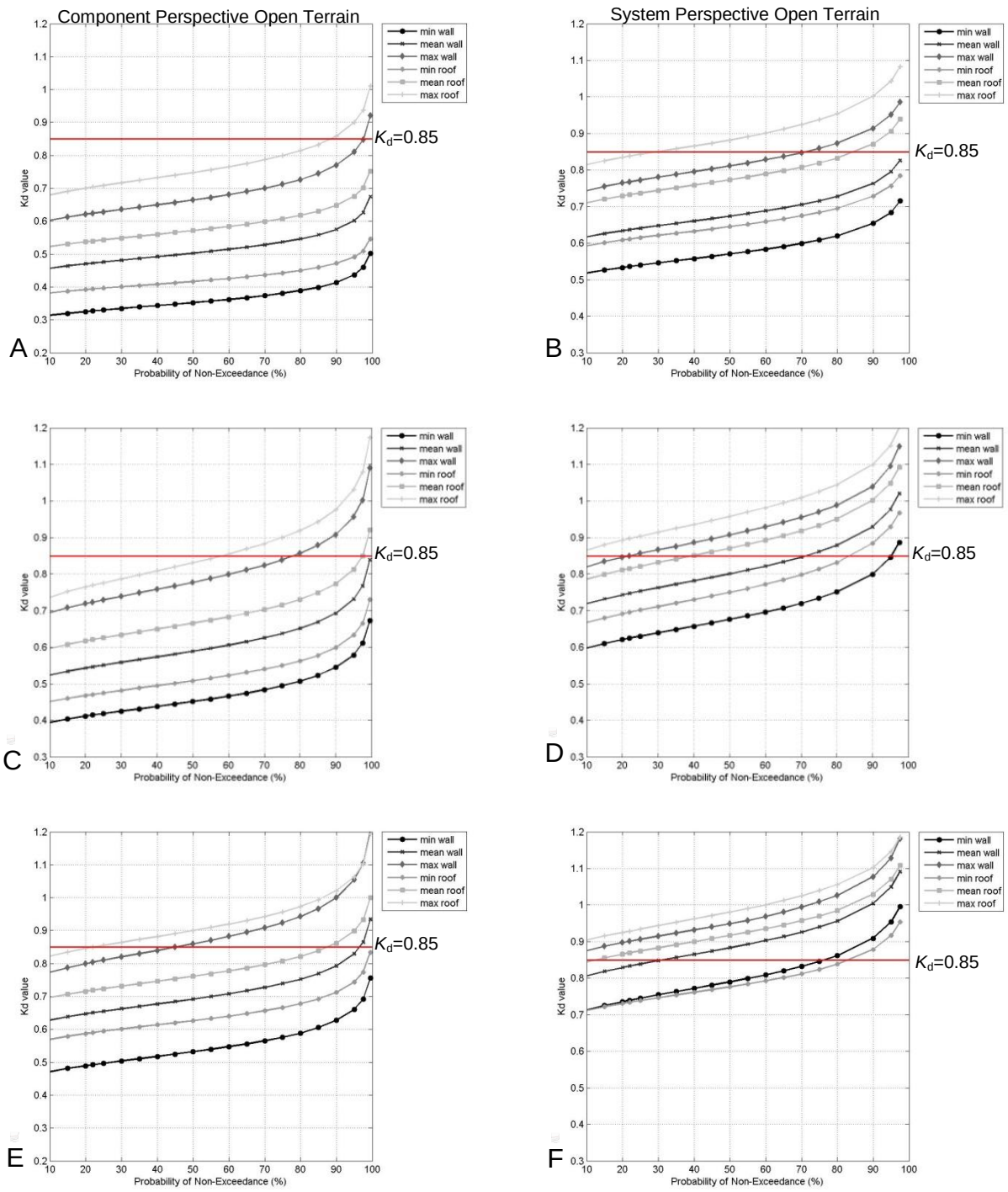

Figure B-16. K_d factor for squared area 5ft x 5ft following scenario analysis in open exposure for Rita grid (Fig.5-13). A) Component: 29.5,-94.5. B) System: 29.5,-94.5. C) Component: 29.7,-94.1. D) System: 29.7,-94.1. E) Component: 29.7, -93.9. F) System: 29.7,-93.9.

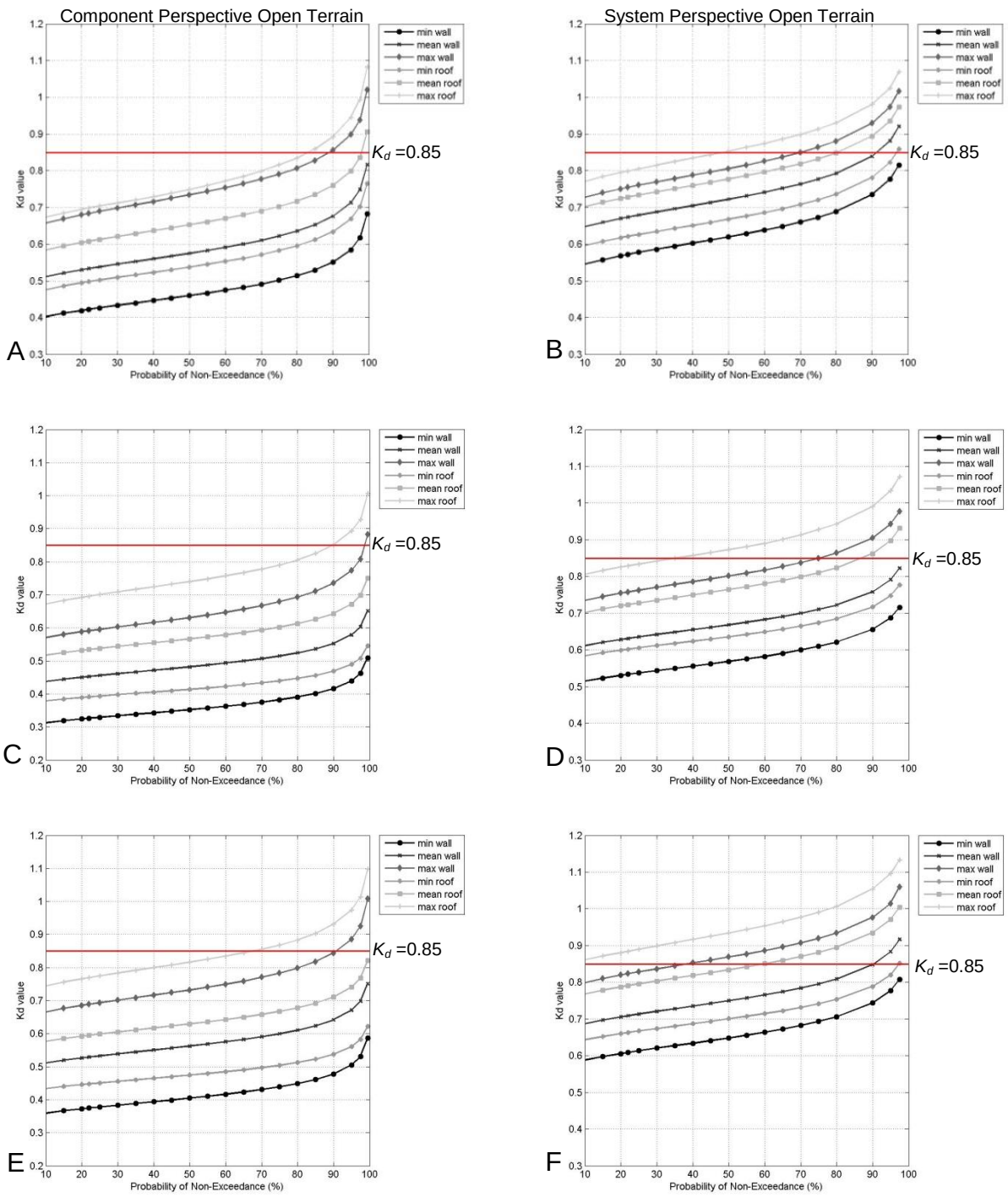

Figure B-17. K_d factor for squared area 5ft x 5ft following scenario analysis in open exposure for Rita grid (Fig.5-13). A) Component: 29.8,-93.7. B) System: 29.8,-93.7. C) Component: 29.8,-93.3. D) System: 29.8,-93.3. E) Component: 29.6, -92.7. F) System: 29.6, -92.7.

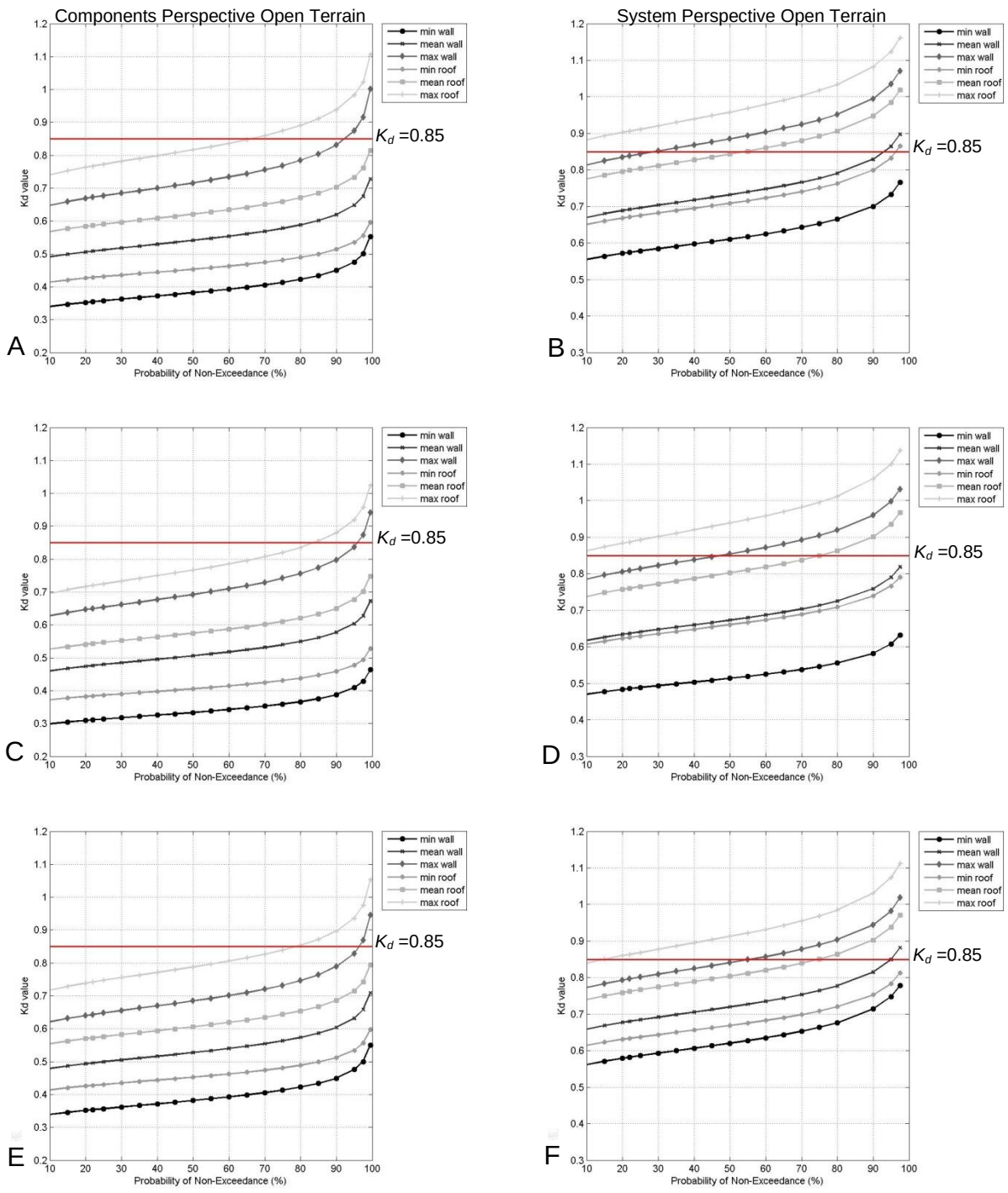

Figure B-18. K_d factor for squared area 5ft x 5ft following scenario analysis in open exposure for Rita grid (Fig.5-13). A) Component: 29.7,-94.3. B) System: 29.7,-94.3. C) Component: 29.9,-94.5. D) System: 29.9,-94.5. E) Component: 29.9, -94.1. F) System: 29.1, -94.1.

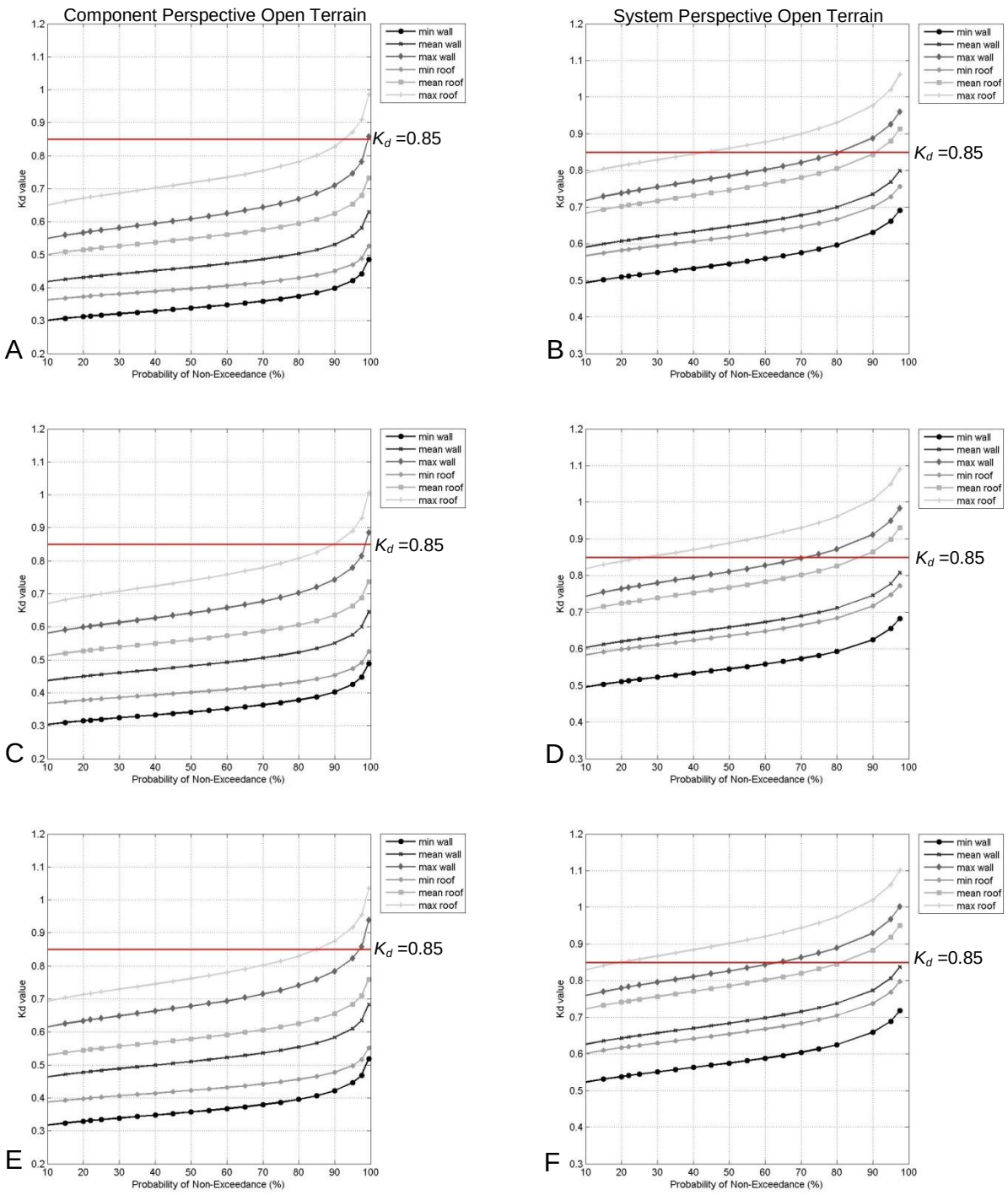

Figure B-19. K_d factor for squared area 5ft x 5ft following scenario analysis in open exposure for Rita grid (Fig.5-13). A) Component: 29.9,-93.5. B) System: 29.9,-93.5. C) Component: 29.9,-92.9. D) System: 29.9,-92.9. E) Component: 29.8, -92.7. F) System: 29.8, -92.7.

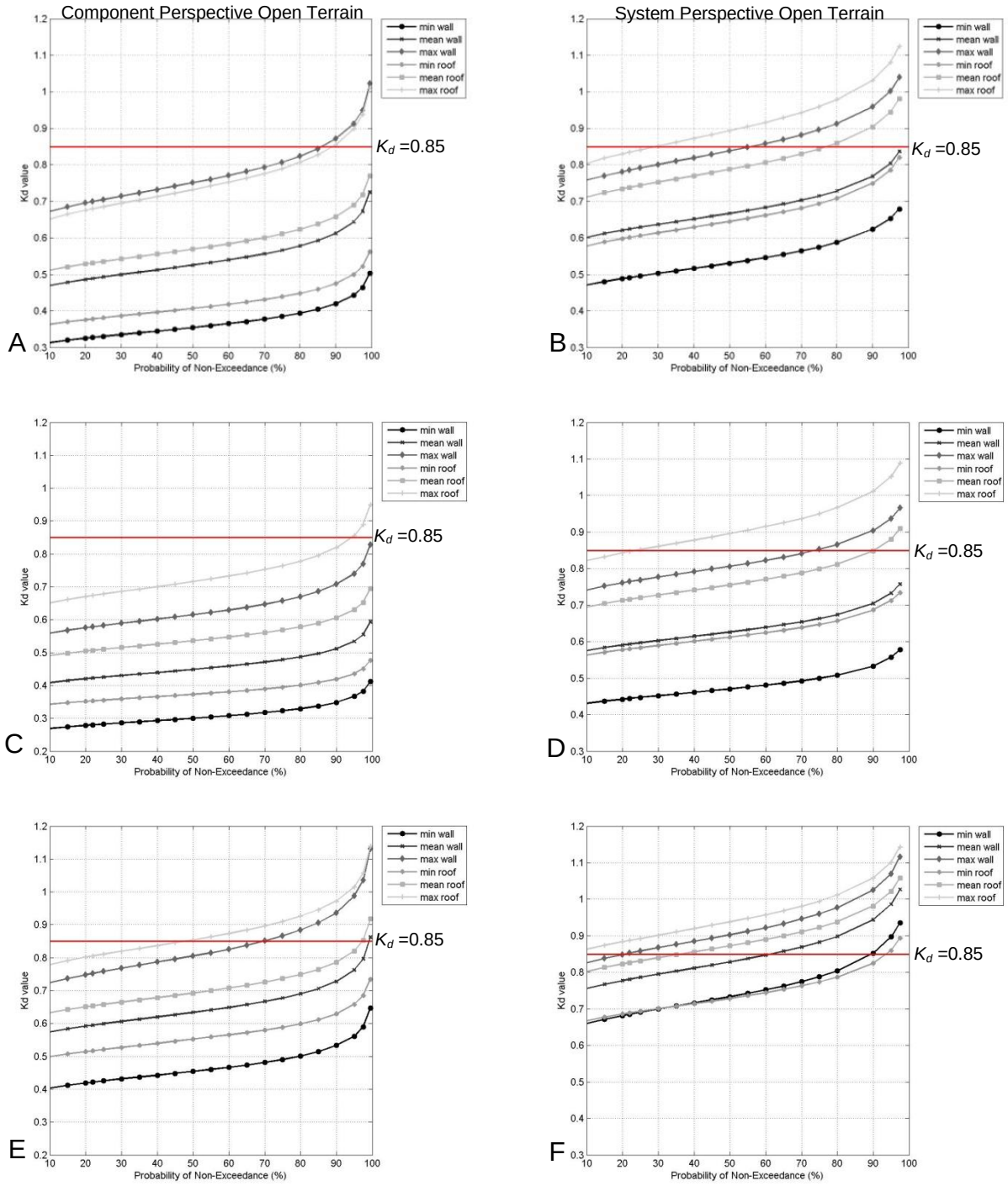

Figure B-20. K_d factor for squared area 5ft x 5ft following scenario analysis in open exposure for Rita grid (Fig.5-13). A) Component: 30.1,-94.5. B) System: 30.1,-94.5. C) Component: 30.1,-94.1. D) System: 30.1,-94.1. E) Component: 30.1, -93.7. F) System: 30.1, -93.7.

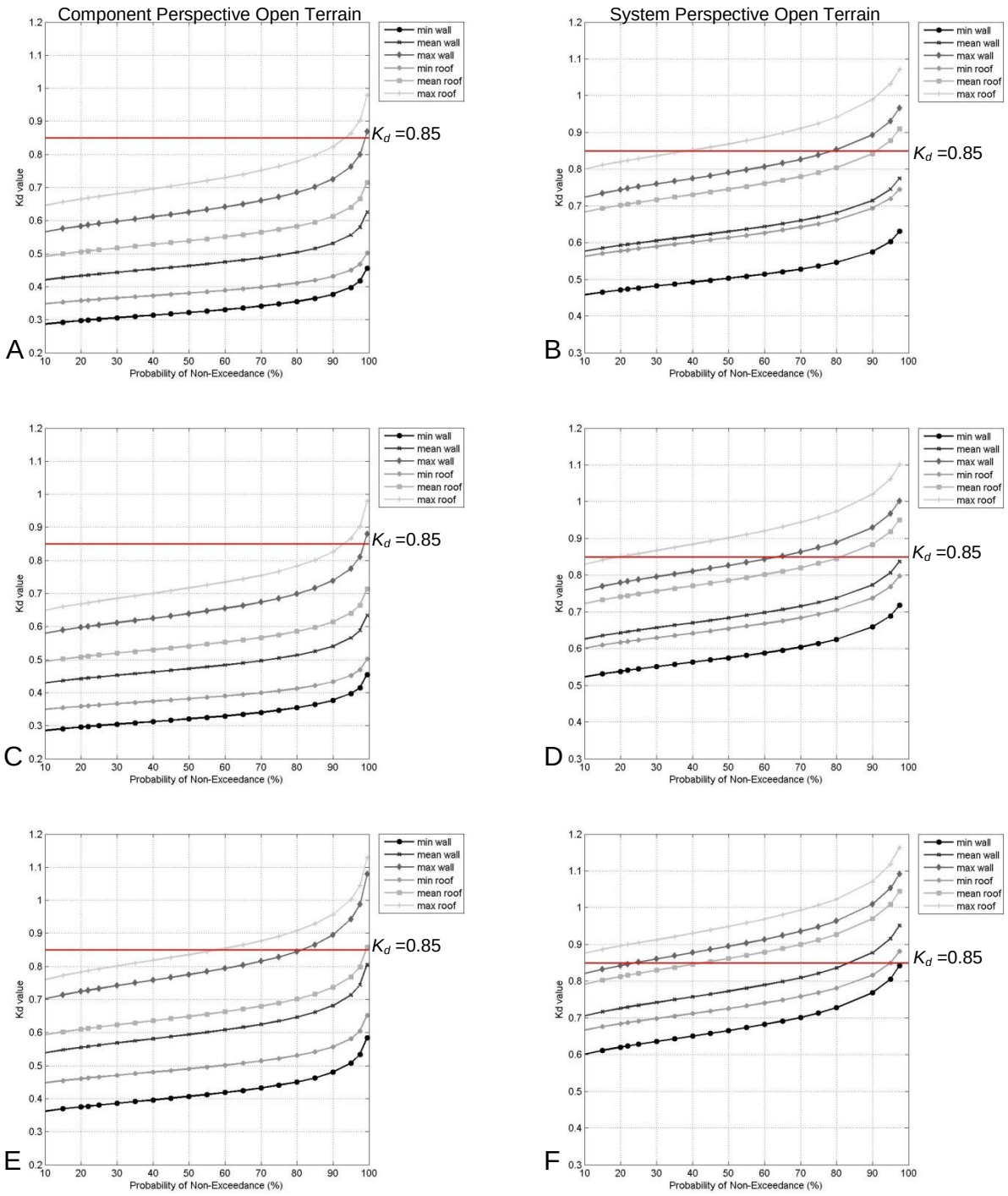

Figure B-21. K_d factor for squared area 5ft x 5ft following scenario analysis in open exposure for Rita grid (Fig.5-13). A) Component: 30.1,-93.1. B) System: 30.1,-93.1. C) Component: 30.1,-92.7. D) System: 30.1,-92.7. E) Component: 30.3, -93.5. F) System: 30.3, -93.5.

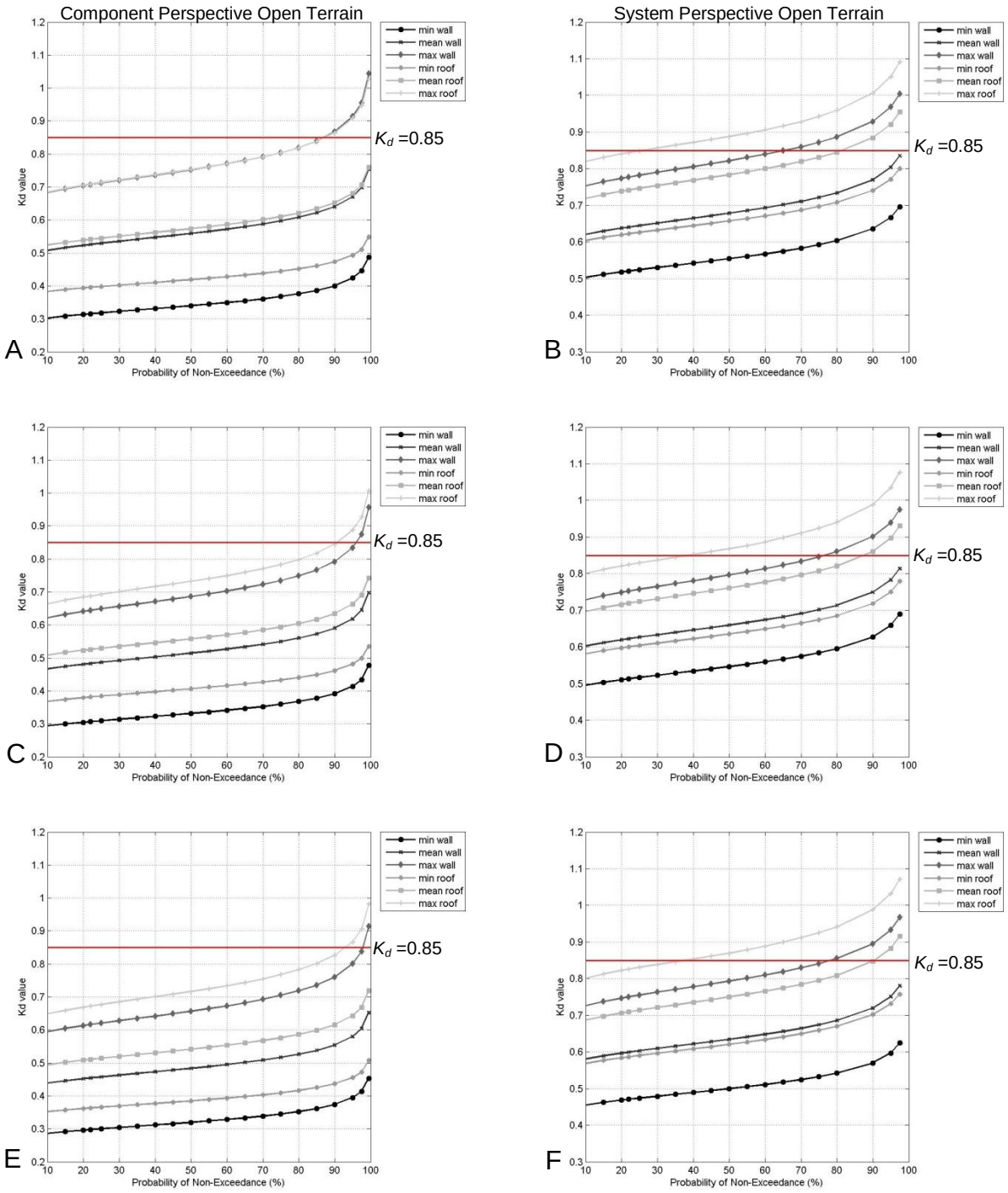

Figure B-22. K_d factor for squared area 5ft x 5ft following scenario analysis in open exposure for Rita grid (Fig.5-13). A) Component: 30.5,-94.1. B) System: 30.5,-94.1. C) Component: 30.5,-93.7. D) System: 30.5,-93.7. E) Component: 30.5, -93.1. F) System: 30.5, -93.1.

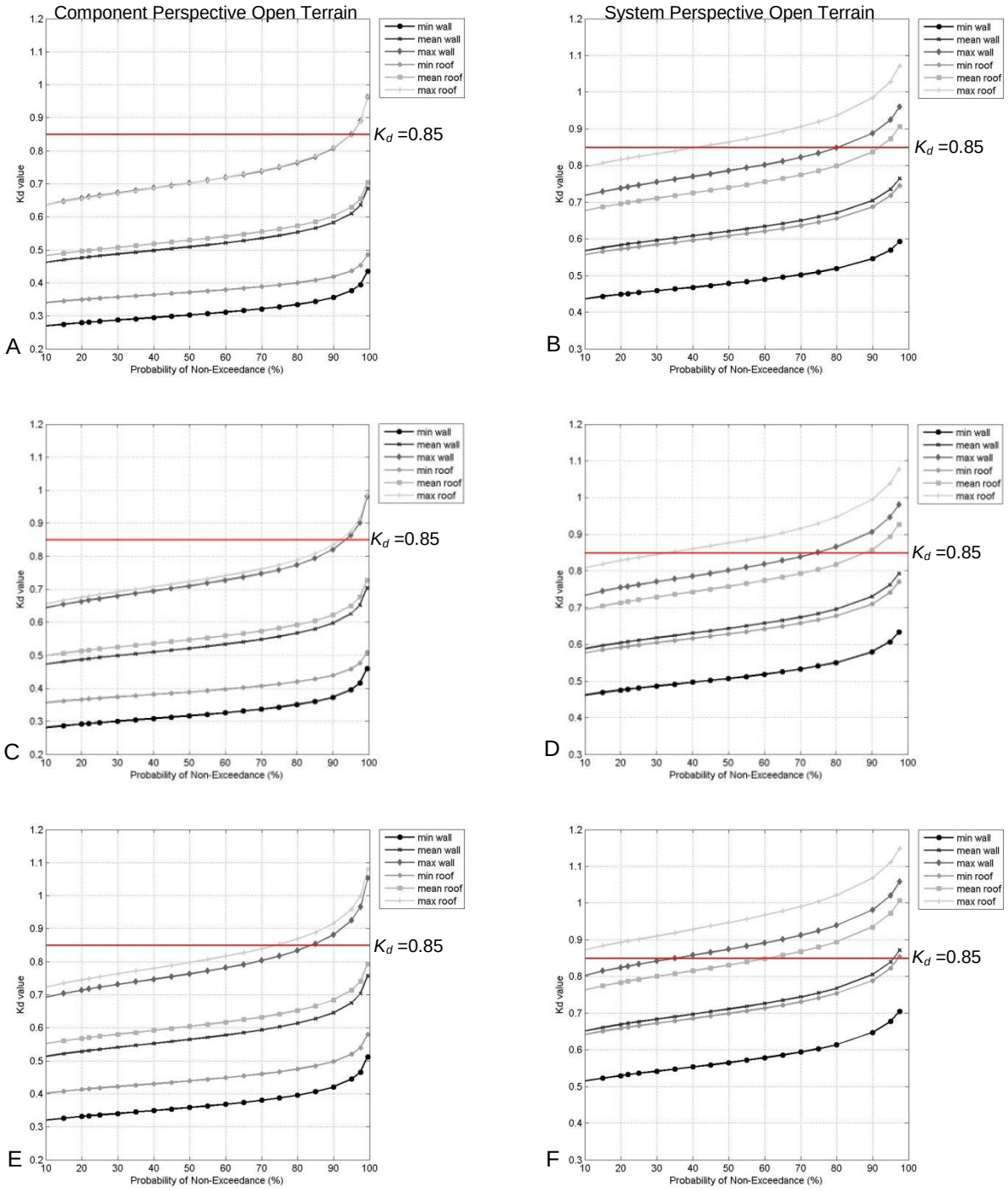

Figure B-23. K_d factor for squared area 5ft x 5ft following scenario analysis in open exposure for Rita grid (Fig.5-13). A) Component: 30.9,-94.1. B) System: 30.9,-94.1. C) Component: 30.9,-93.7. D) System: 30.9,-93.7. E) Component: 30.9, -93.3. F) System: 30.9, -93.3.

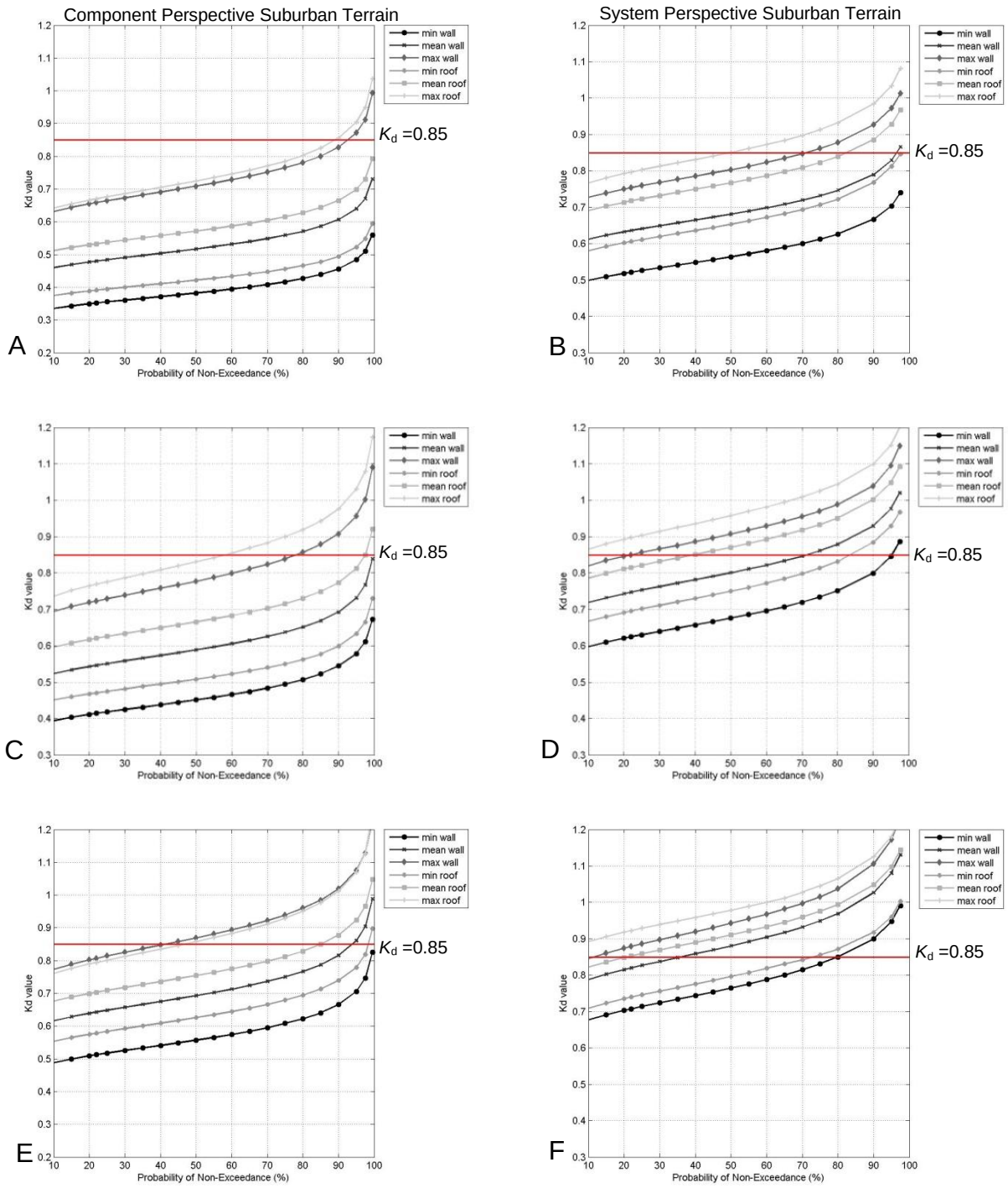

Figure B-24. K_d factor for squared area 5ft x 5ft following scenario analysis in suburban exposure for Rita grid (Fig.5-12). A) Component: 29.5,-94.5. B) System: 29.5,-94.5. C) Component: 29.7,-94.1. D) System: 29.7,-94.1. E) Component: 29.7, -93.9. F) System: 29.7,-93.9.

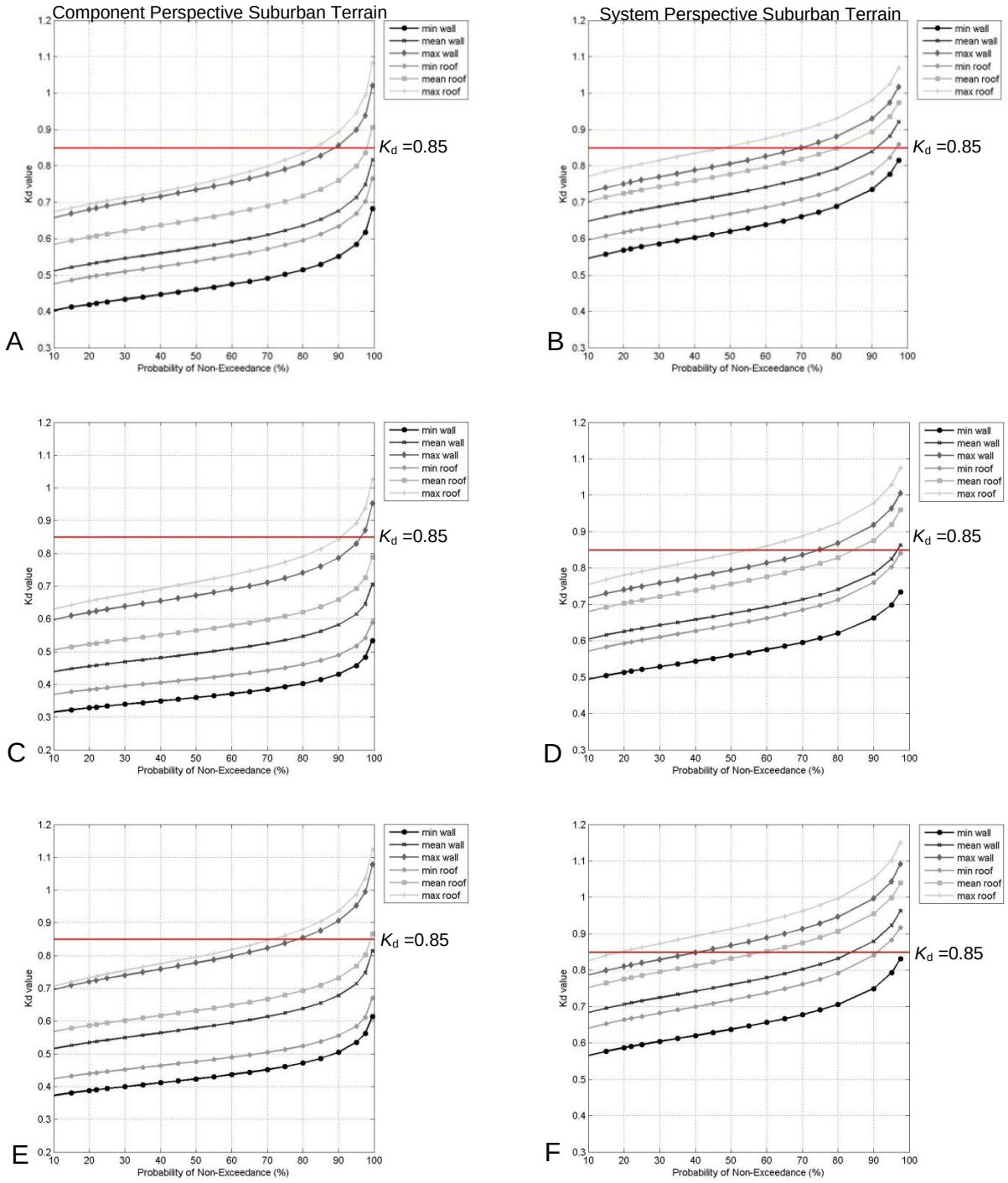

Figure B-25. K_d factor for squared area 5ft x 5ft following scenario analysis in suburban exposure for Rita grid (Fig.5-12). A) Component: 29.8,-93.7. B) System: 29.8,-93.7. C) Component: 29.8,-93.3. D) System: 29.8,-93.3. E) Component: 29.6, -92.7. F) System: 29.6, -92.7.

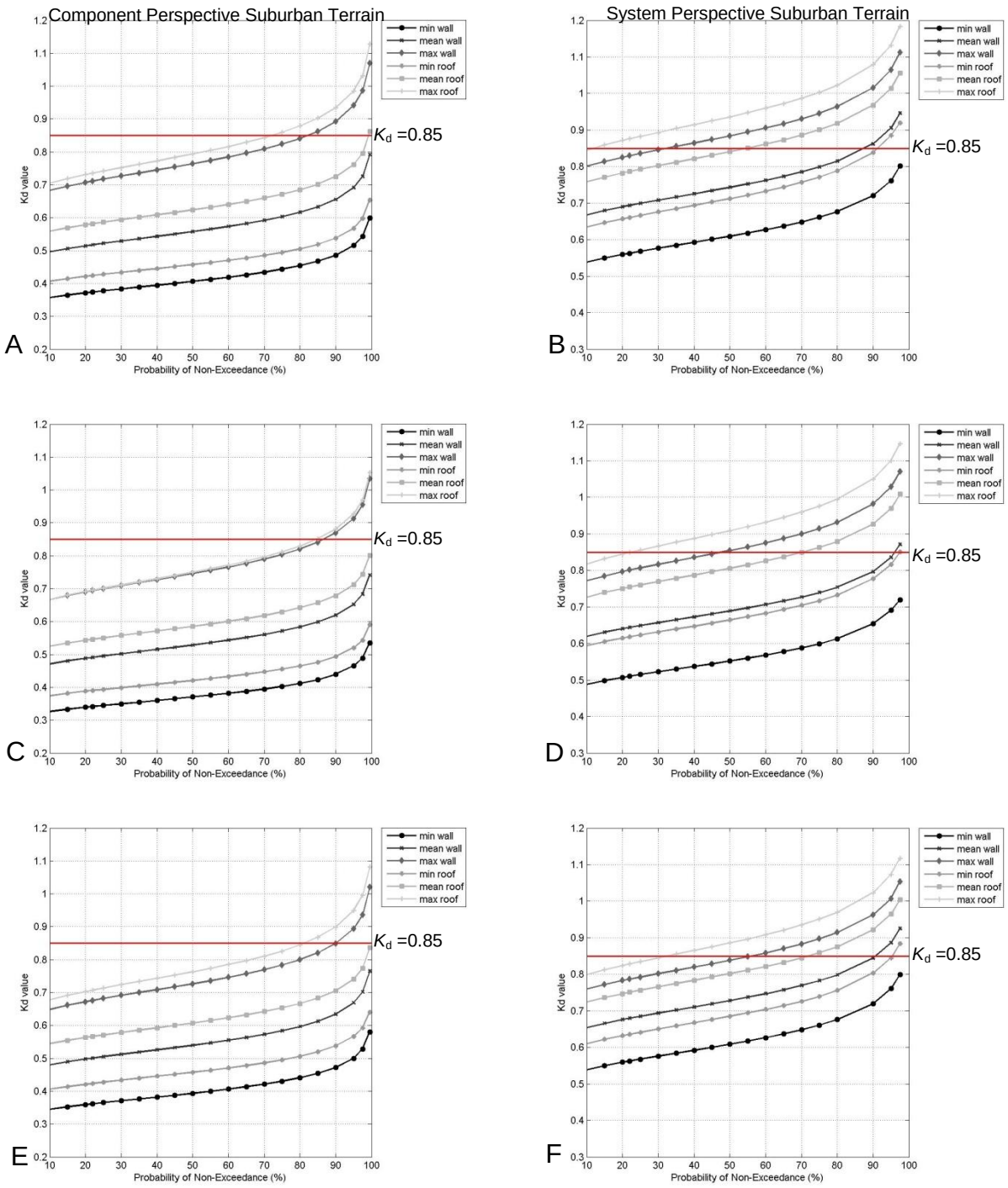

Figure B-26. K_d factor for squared area 5ft x 5ft following scenario analysis in suburban exposure for Rita grid (Fig.5-12). A) Component: 29.7,-94.3. B) System: 29.7,-94.3. C) Component: 29.9,-94.5. D) System: 29.9,-94.5. E) Component: 29.9,-94.1. F) System: 29.9,-94.1.

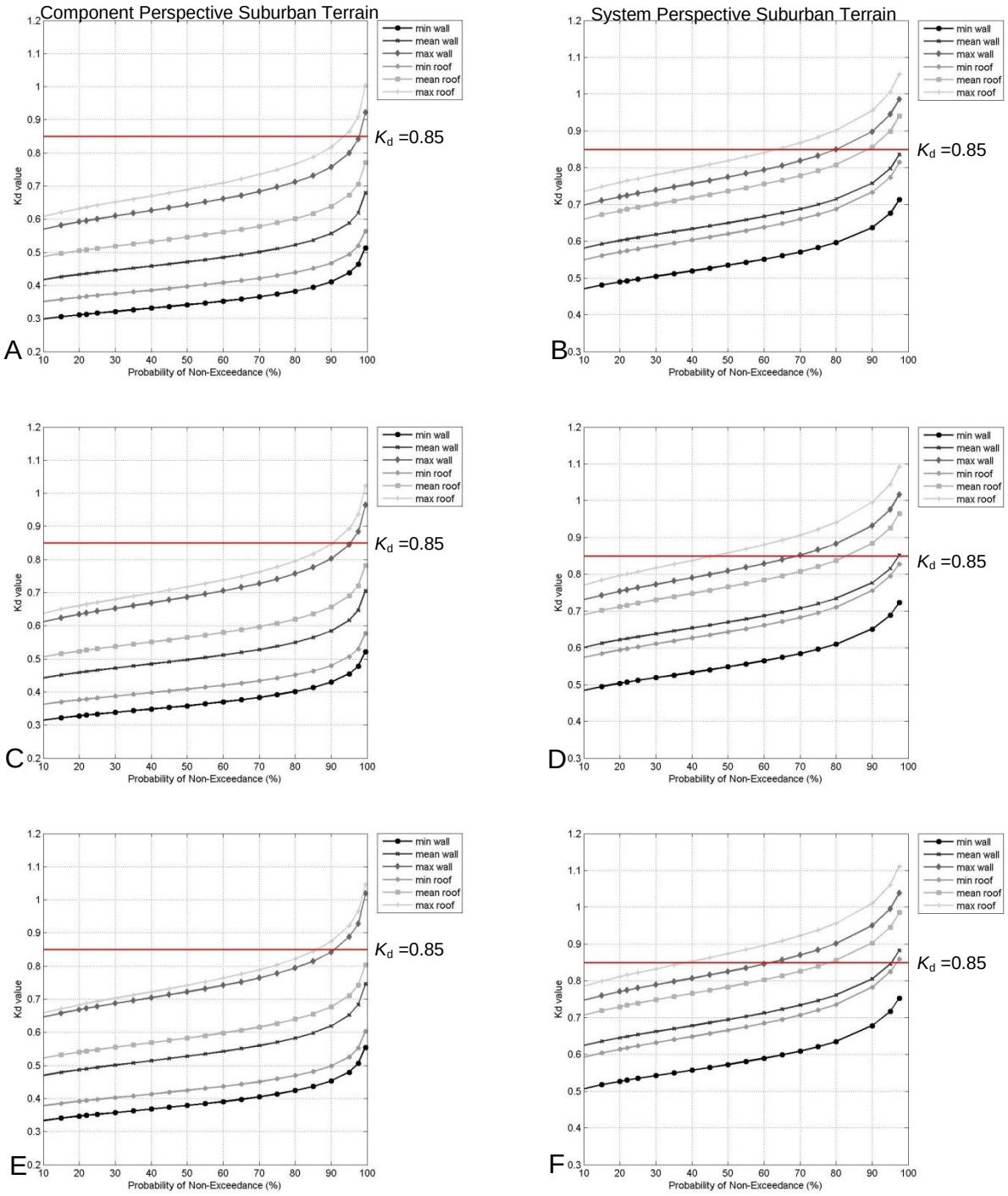

Figure B-27. K_d factor for squared area 5ft x 5ft following scenario analysis in suburban exposure for Rita grid (Fig.5-12). A) Component: 29.9,-93.5. B) System: 29.9,-93.5. C) Component:29.9,-92.9. D) System:29.9,-92.9. E) Component: 29.8,-92.7. F) System: 29.8,-92.7.

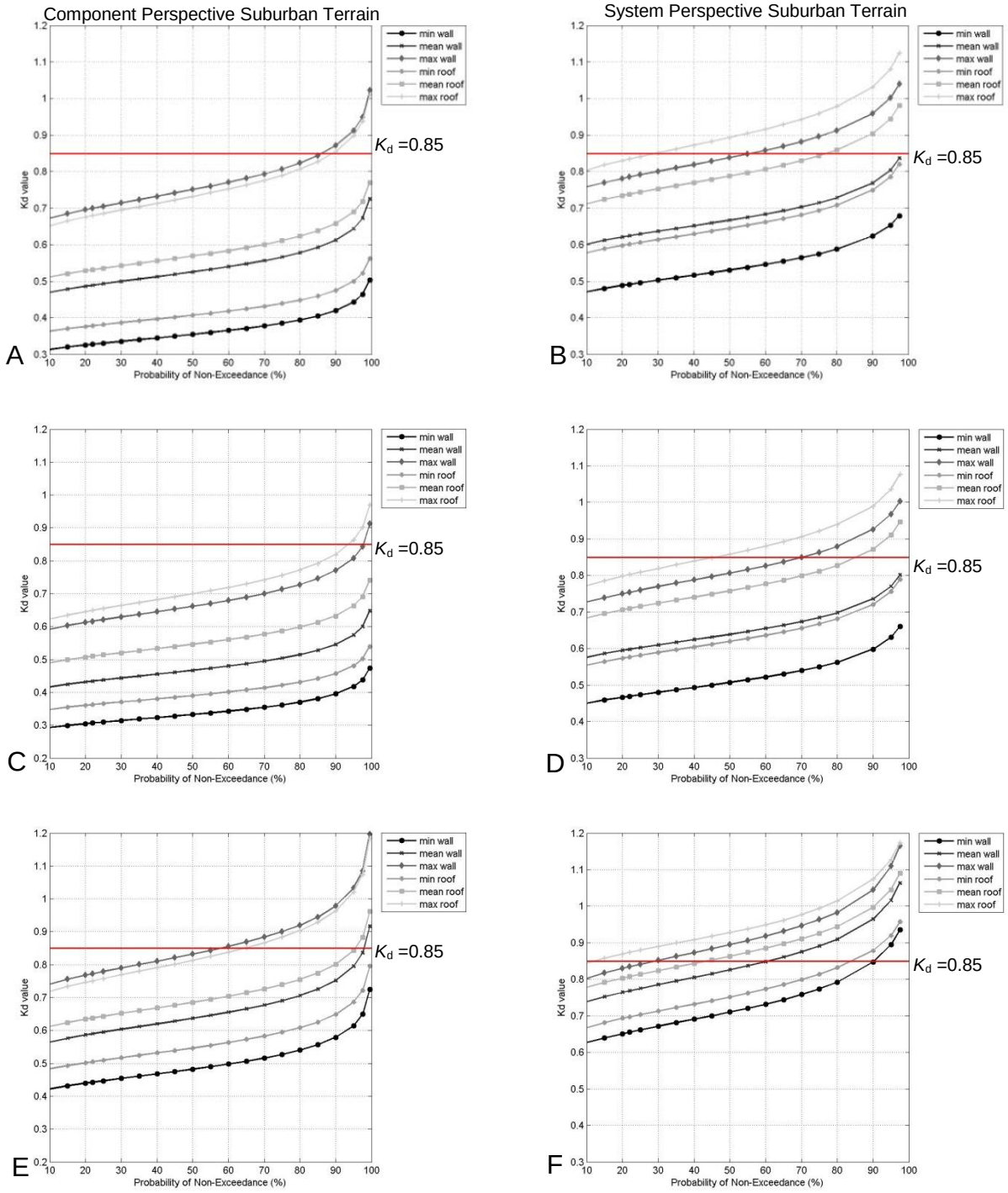

Figure B-28. K_d factor for squared area 5ft x 5ft following scenario analysis in suburban exposure for Rita grid (Fig.5-12). A) Component: 30.1,-94.5. B) System: 30.1,-94.5. C) Component: 30.1,-94.1. D) System: 30.1,-94.1. E) Component: 30.1,-93.7. F) System: 30.1, -93.7.

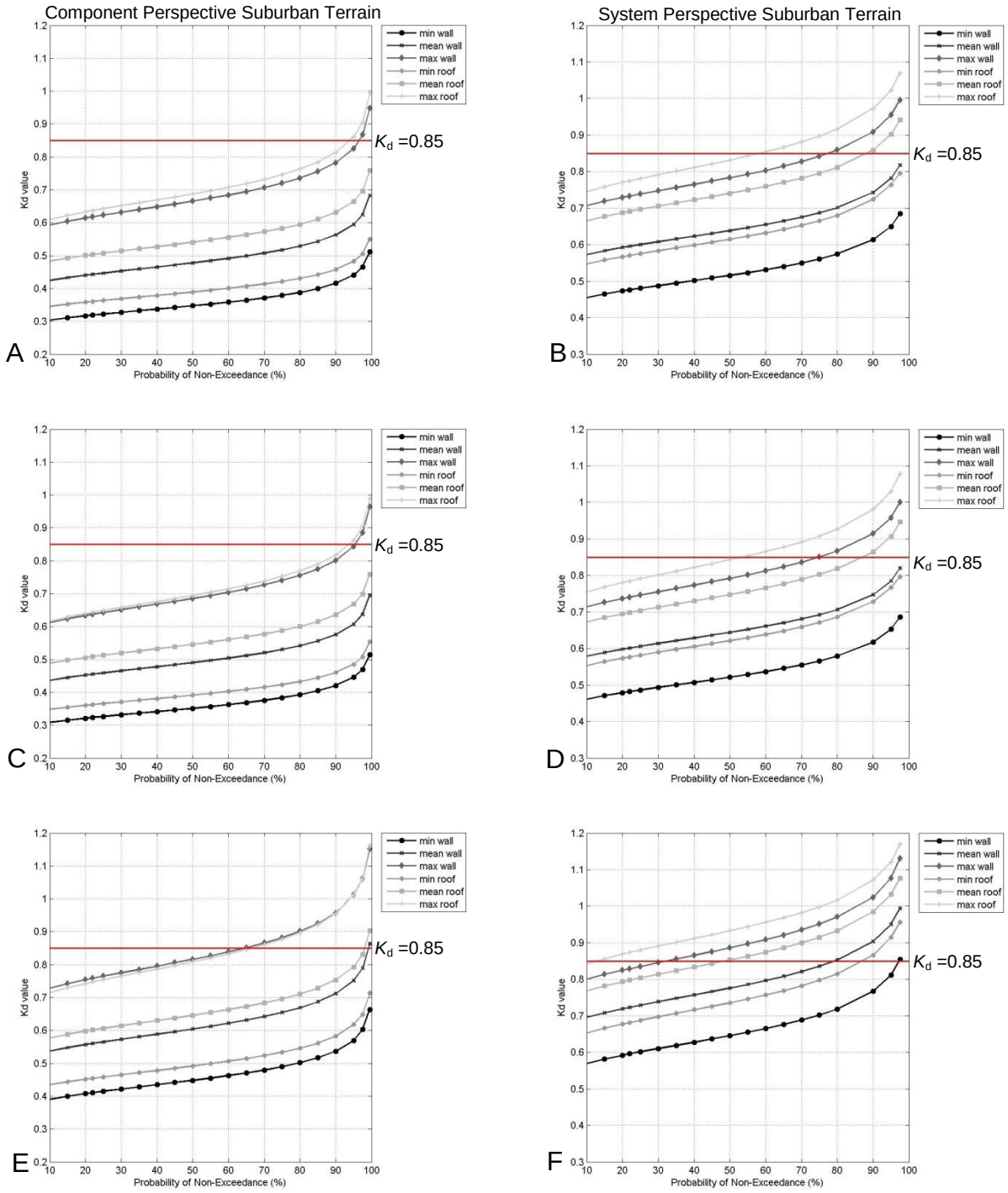

Figure B-29. K_d factor for squared area 5ft x 5ft following scenario analysis in suburban exposure for Rita grid (Fig.5-12). A) Component: 30.1,-93.1. B) System: 30.1,-93.1. C) Component: 30.1,-92.7. D) System: 30.1,-92.7. E) Component: 30.3, -93.5. F) System: 30.3,-93.5.

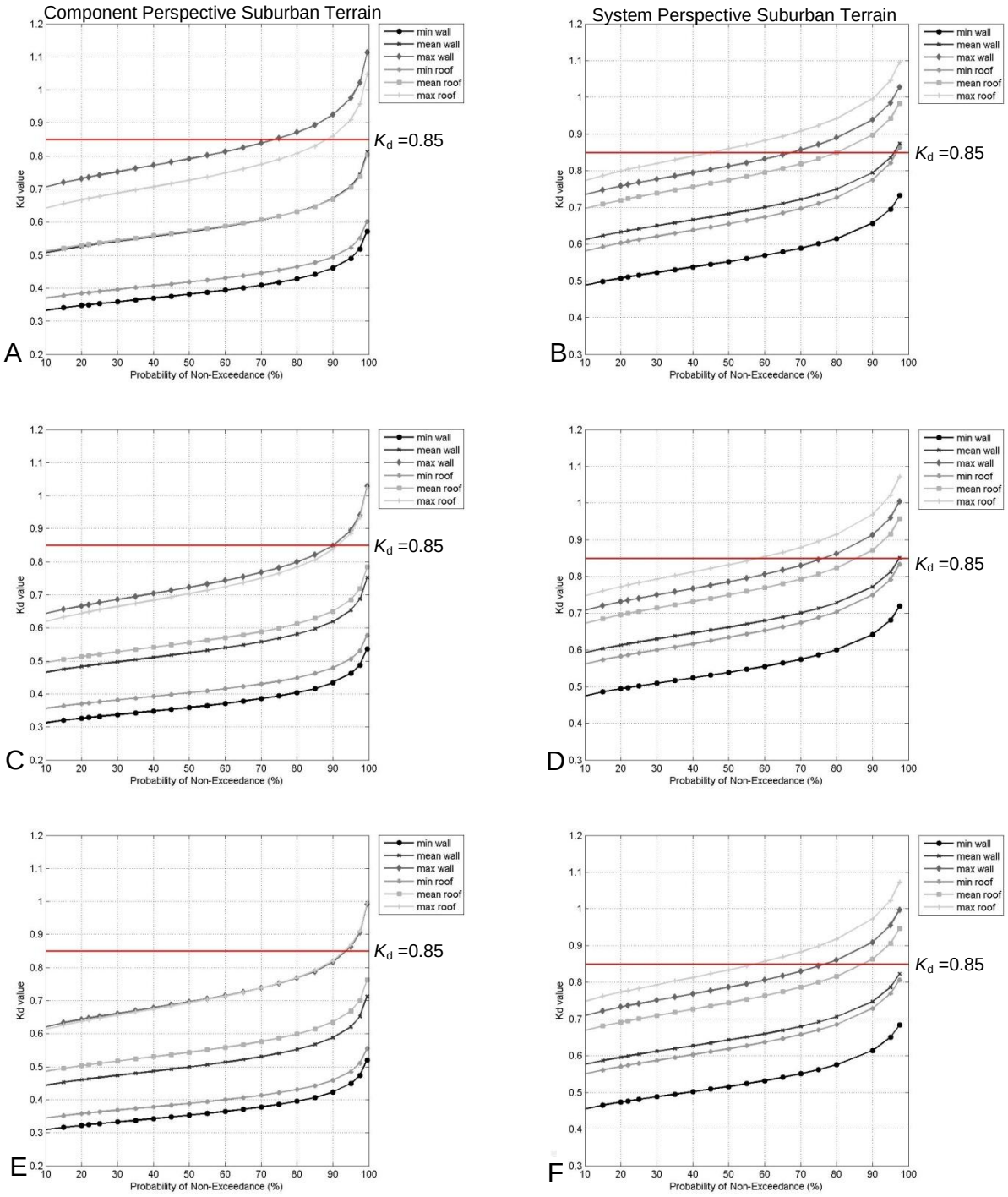

Figure B-30. K_d factor for squared area 5ft x 5ft following scenario analysis in suburban exposure for Rita grid (Fig.5-12). A) Component: 30.5,-94.1. B) System: 30.5,-94.1. C) Component: 30.5,-93.7. D) System: 30.5,-93.7. E) Component: 30.5, -93.1. F) System: 30.5,-93.1.

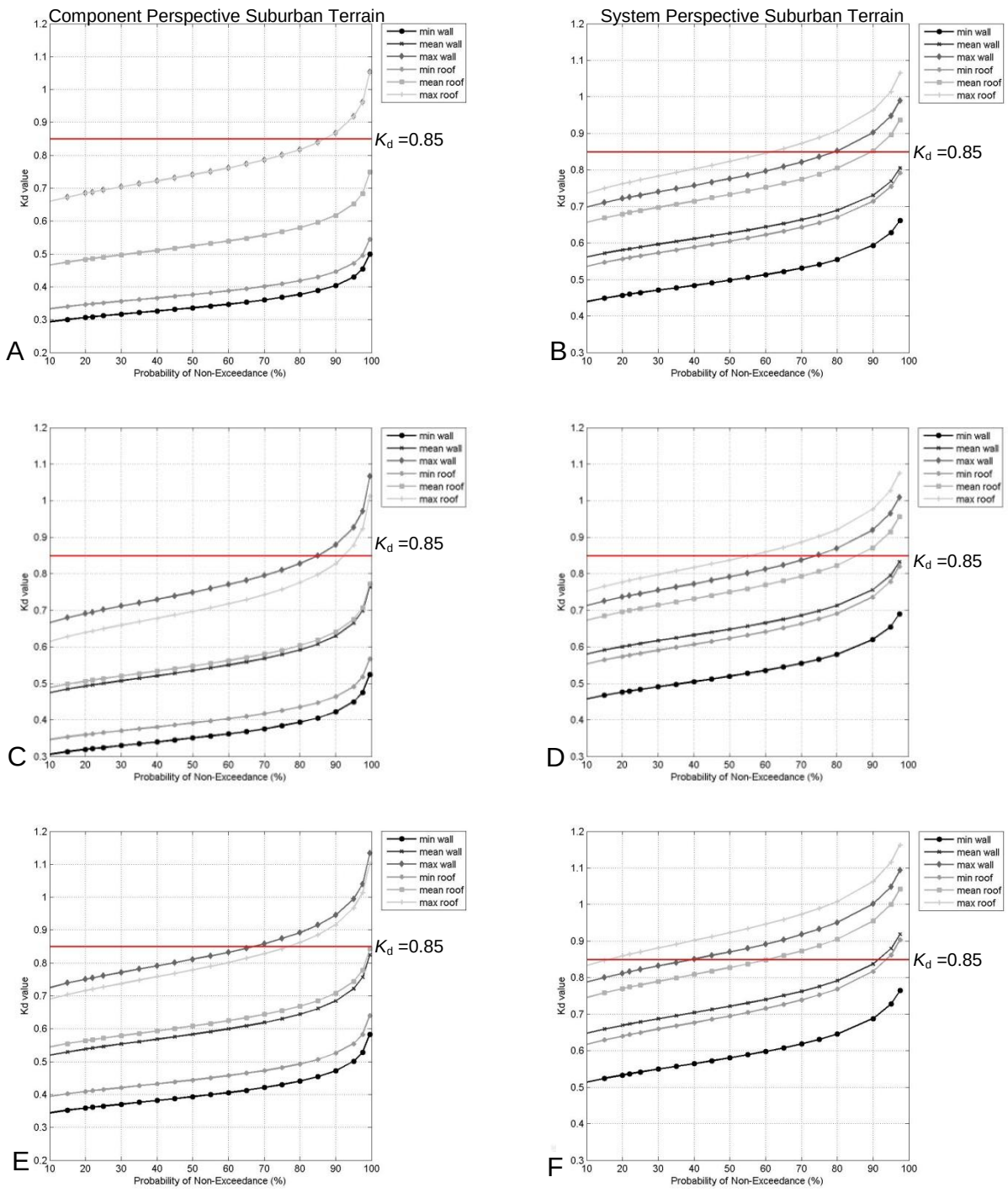

Figure B-31. K_d factor for squared area 5ft x 5ft following scenario analysis in suburban exposure for Rita grid (Fig.5-12). A) Component: 30.9,-94.1. B) System: 30.9,-94.1. C) Component: 30.9,-93.7. D) System: 30.9,-93.7. E) Component: 30.9, -93.3. F) System: 30.9, -93.3.

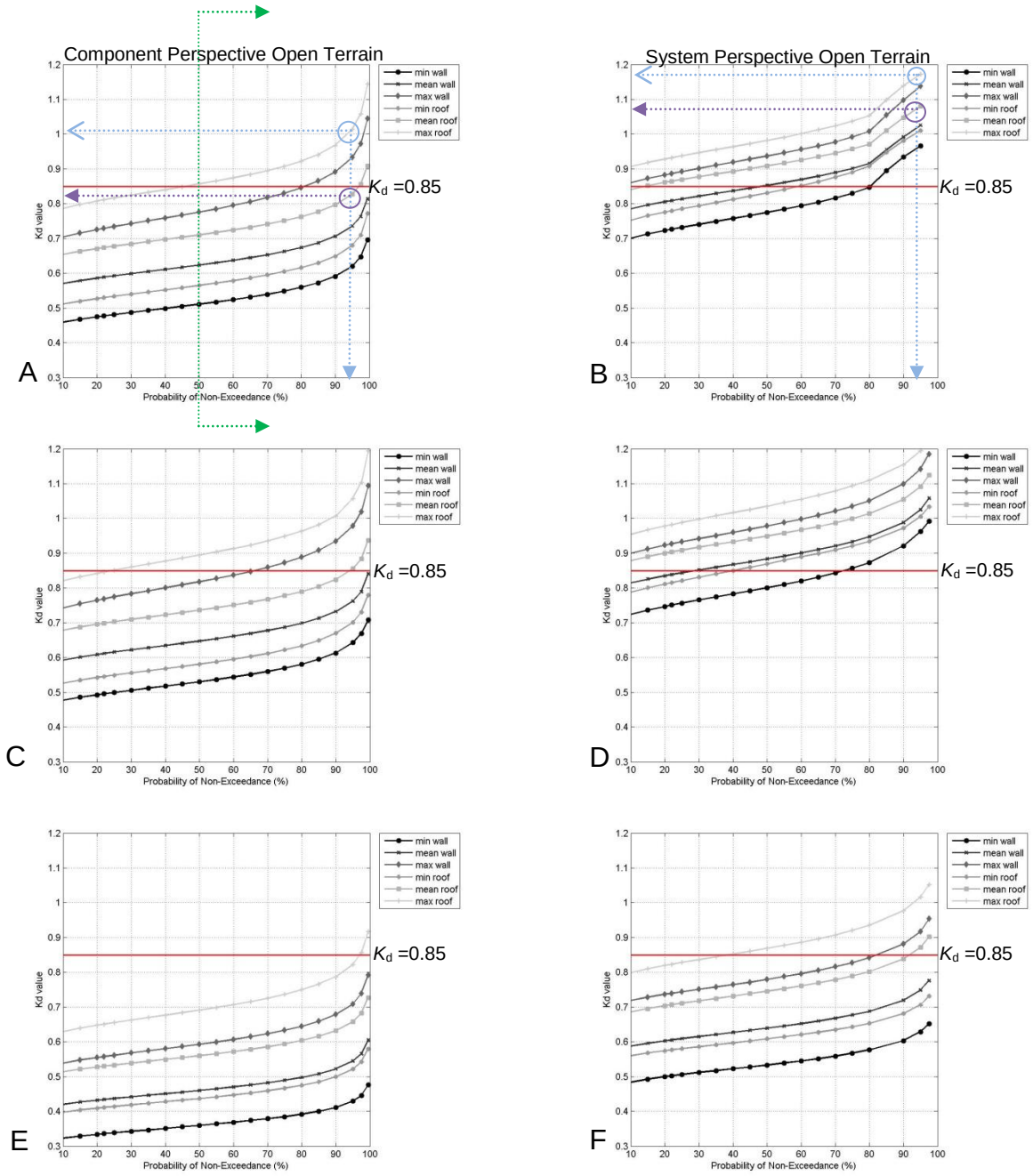

Figure B-32. K_d factor for squared area 7ft x 7ft following scenario analysis in open exposure for Frances grid (Fig.5-13). A) Component: 26.5,-80.1. B) Perspective: 26.5,-80.1. C) Component: 27.5,-80.3. D) Perspective: 27.5,-80.3. E) Component: 28.7,-80.7. F) Perspective: 28.7,-80.7.

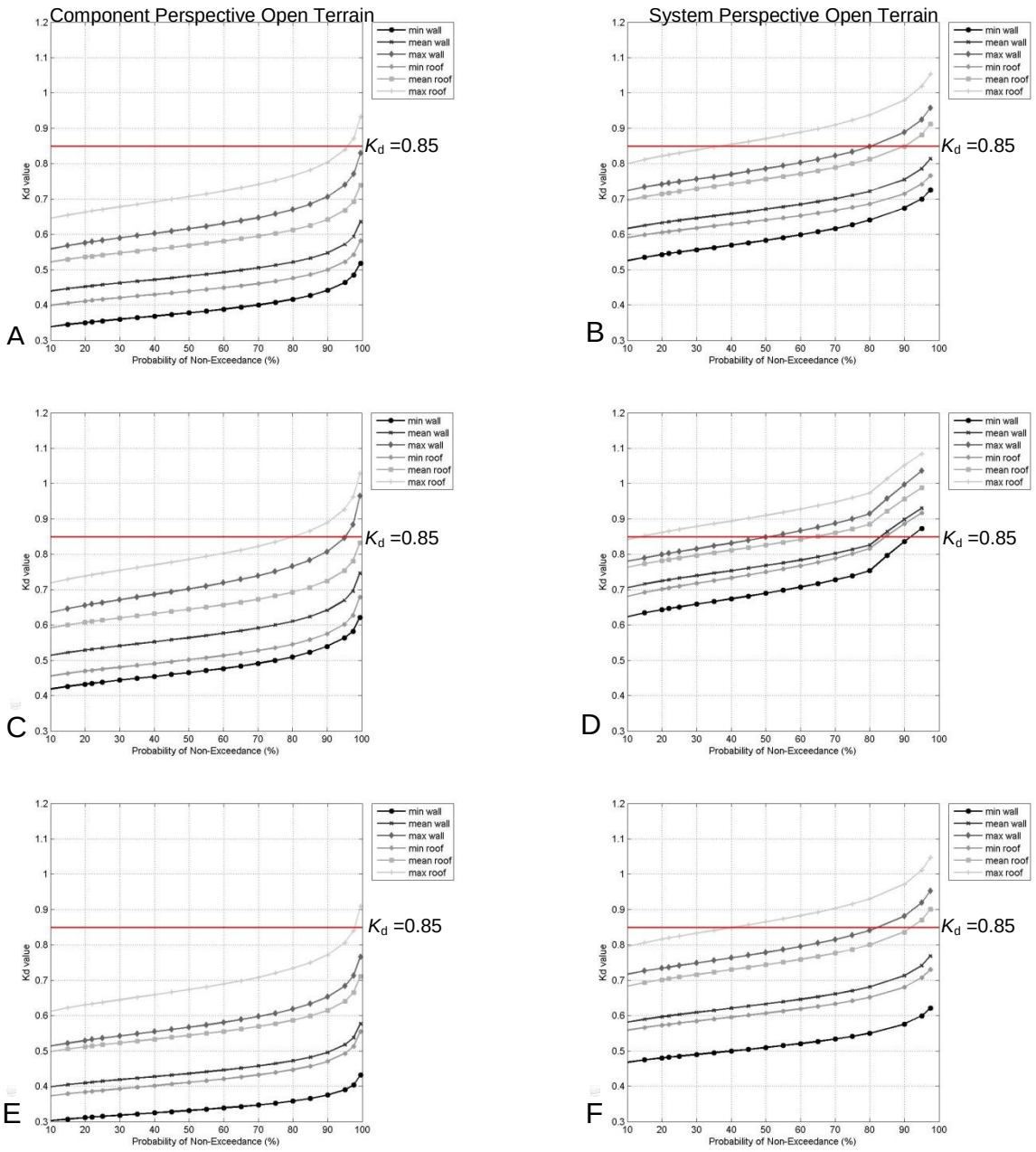

Figure B-33. K_d factor for squared area 7ft x 7ft following scenario analysis in open exposure for Frances grid (Fig.5-13). A) Component: 27.1 N, -80.7W. B) System: 27.1 N, -80.7W. C) Component: 27.5N, -80.3W. D) System: 27.5N, -80.3W. E) Component: 27.5N, -80.7W. F) System: 27.5N, -80.7W.

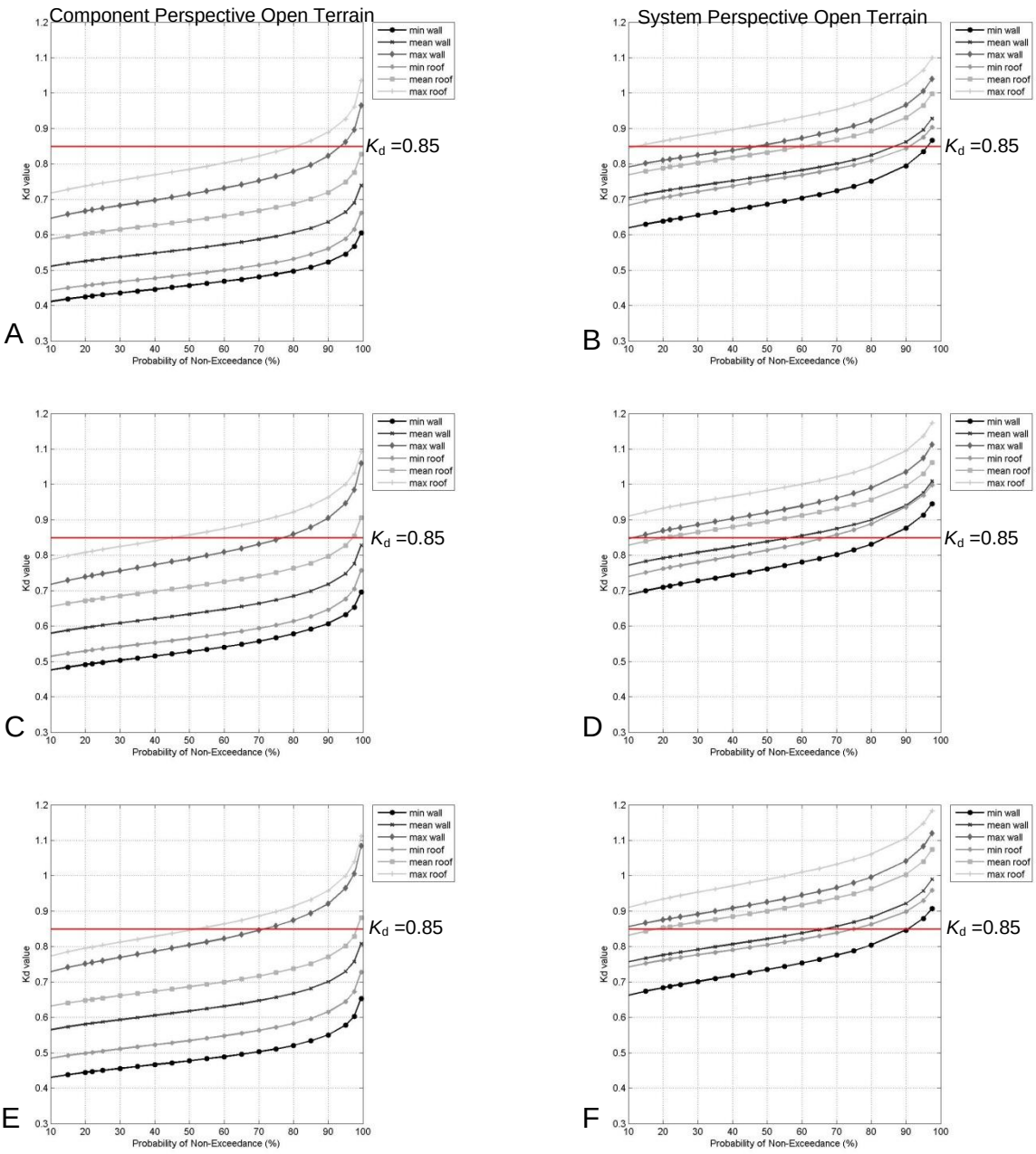

Figure B-34. K_d factor for squared area 7ft x 7ft following scenario analysis in open exposure for Frances grid (Fig.5-13). A) Component: 27.9 N, -80.5W. B) System: 27.9 N, -80.5W. C) Component: 27.9N, -80.9W. D) System: 27.9N, -80.9W. E) Component: 28.3N, -80.7W. F) System: 28.3N, -80.7W.

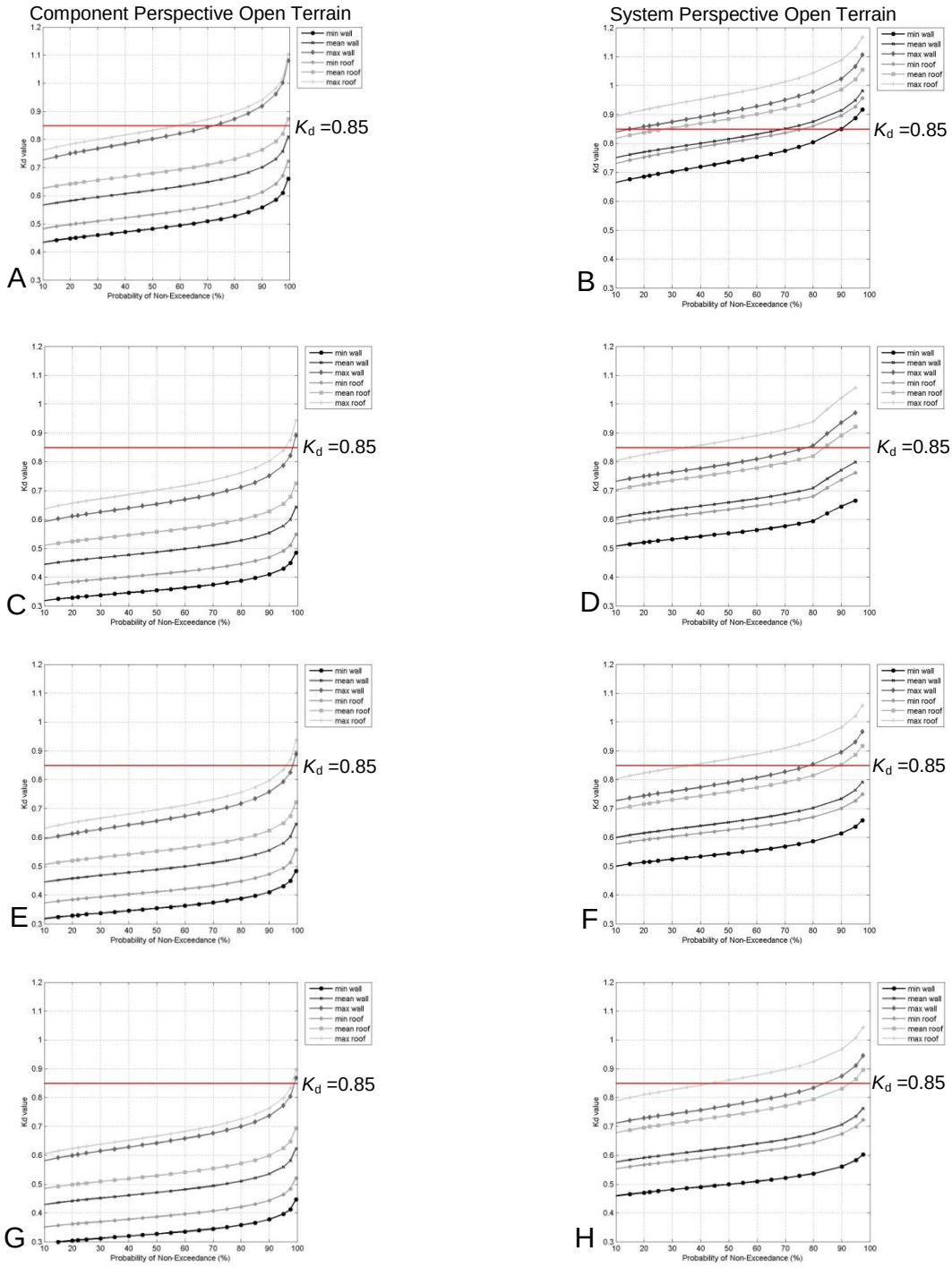

Figure B-35. K_d factor for squared area 7ft x 7ft following scenario analysis in open exposure for Frances grid (Fig.5-13). A) Component: 28.3 N,-80.9W. B) System: 28.3 N, -80.9W. C) Component: 28.7N,-80.7W. D) System: 28.7N, -80.7W. E) Component: 28.7N, -80.9W. F) System: 28.7N,-80.9W. G) Component: 28.9N,-80.9W. H) System: 28.9N,-80.9W.

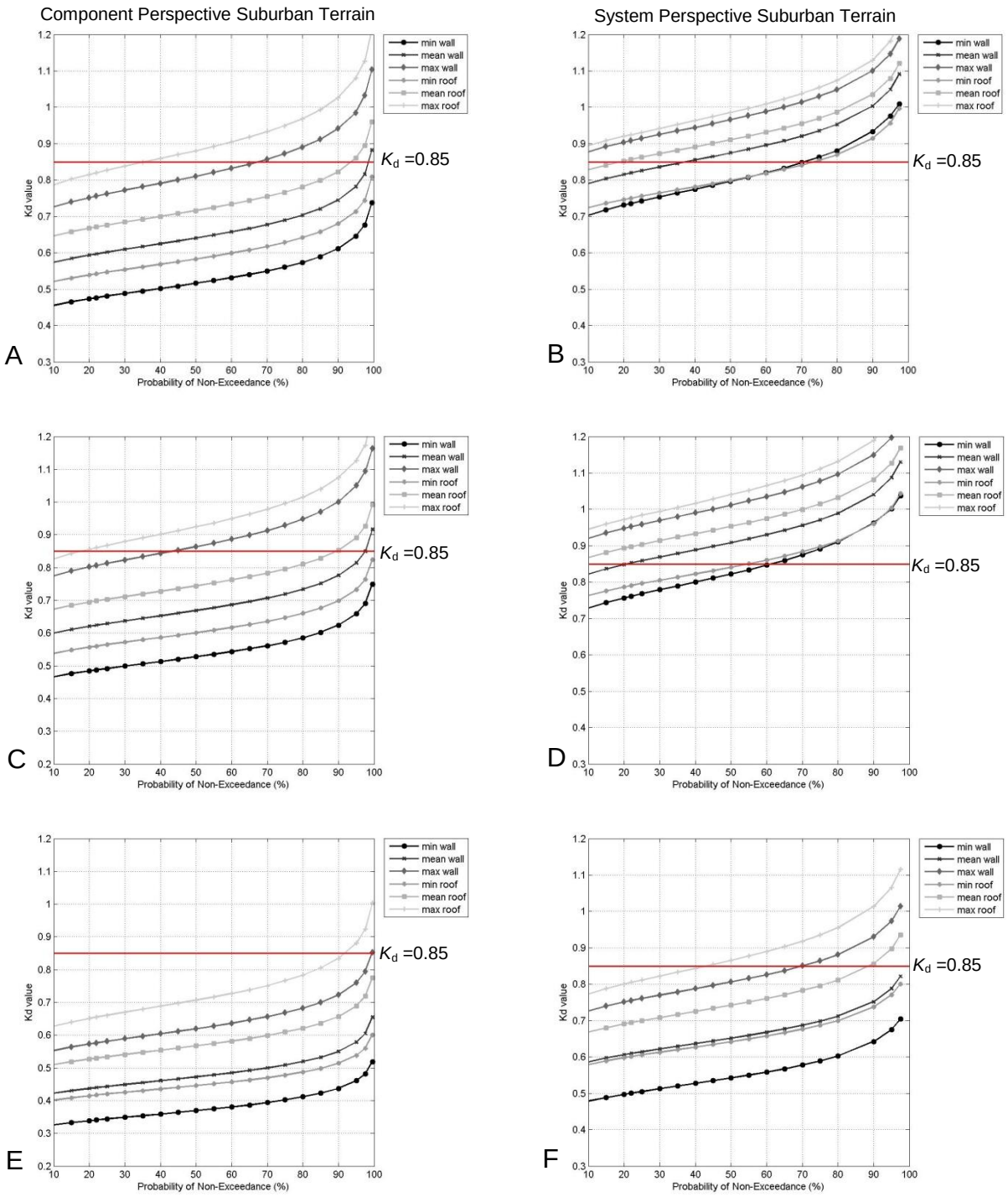

Figure B-36. K_d factor for squared area 7ft x 7ft following scenario analysis in suburban exposure for Frances grid (Fig.5-13). A) Component: 26.5,-80.1. B) Perspective: 26.5,-80.1. C) Component: 26.5,-80.5. D) Perspective: 26.5,-80.5. E) Component: 27.1,-80.3. F) Perspective: 27.1,-80.3.

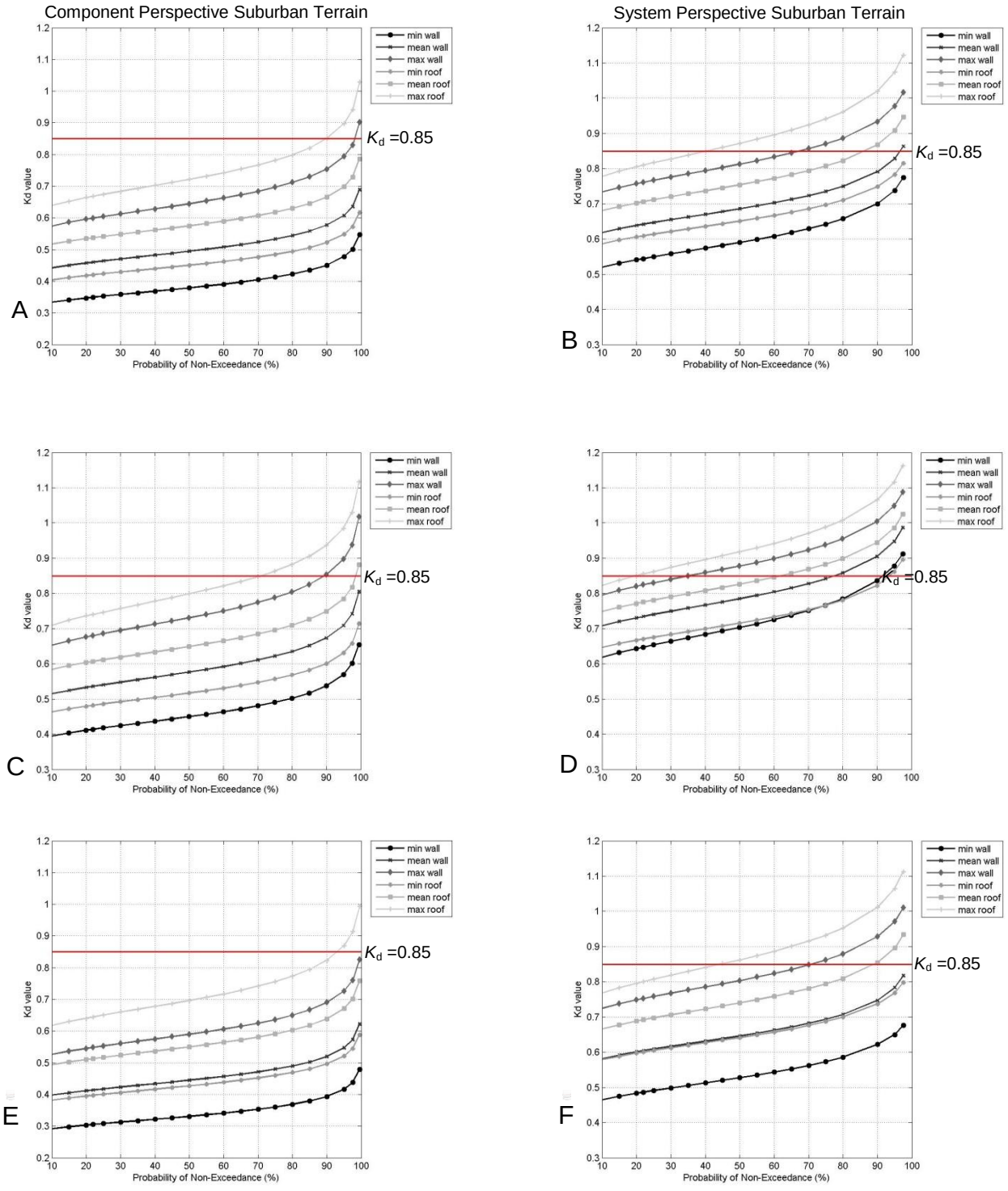

Figure B-37. K_d factor for squared area 7ft x 7ft following scenario analysis in suburban exposure for Frances grid (Fig.5-13). A) Component: 27.1 N, -80.7W. B) System: 27.1 N, -80.7W. C) Component: 27.5N, -80.3W. D) System: 27.5N, -80.3W. E) Component: 27.5N, -80.7W. F) System: 27.5N, -80.7W.

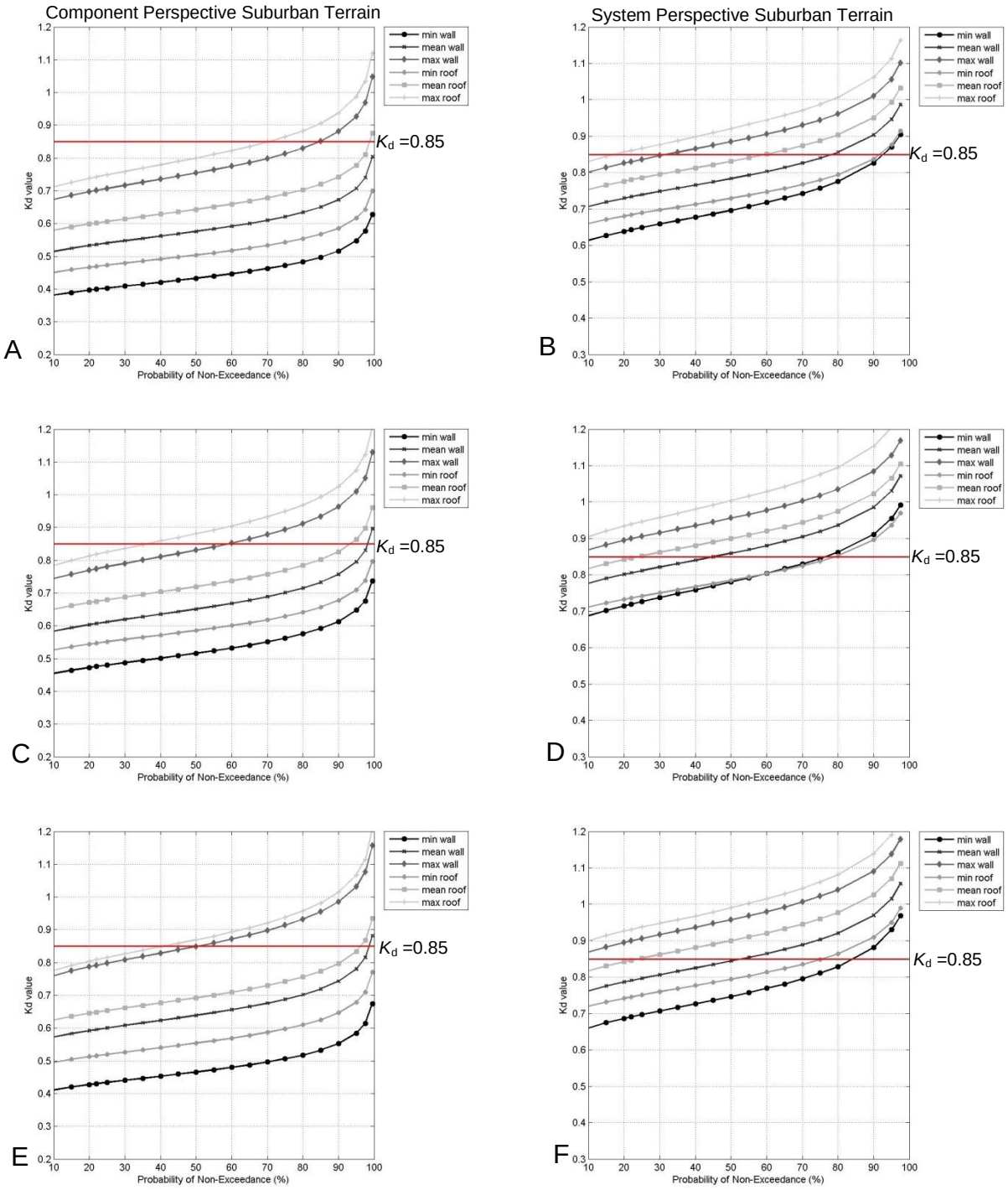

Figure B-38. K_d factor for squared area 7ft x 7ft following scenario analysis in suburban exposure for Frances grid (Fig.5-13). A) Component: 27.9 N, -80.5W. B) System: 27.9 N, -80.5W. C) Component: 27.9N, -80.9W. D) System: 27.9N, -80.9W. E) Component: 28.3N, -80.7W. F) System: 28.3N, -80.7W.

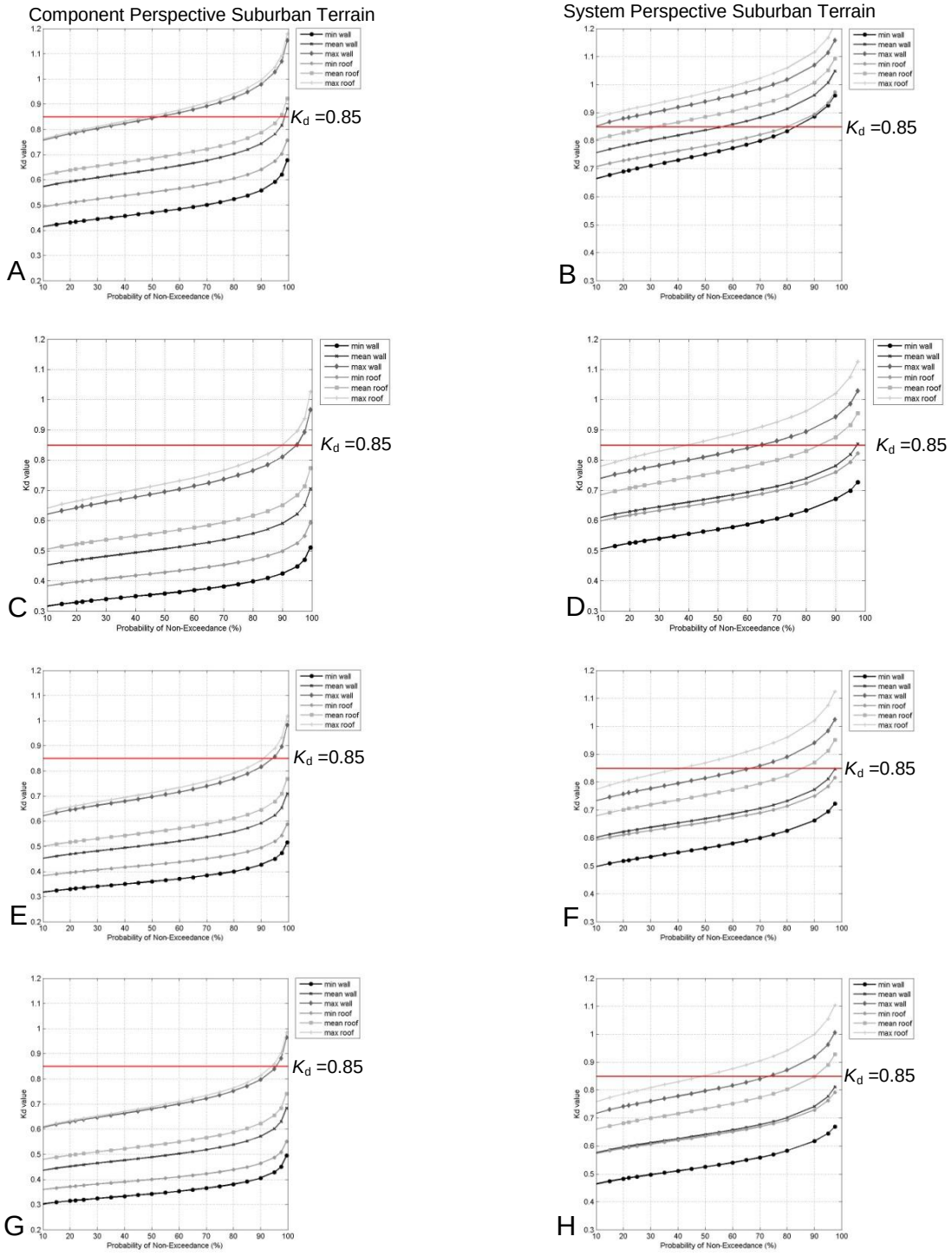

Figure B-39. K_d factor for squared area 7ft x 7ft following scenario analysis in suburban exposure for Frances grid (Fig.5-13). A) Component: 28.3 N,-80.9W. B) System: 28.3 N, -80.9W. C) Component: 28.7N,-80.7W. D) System: 28.7N, -80.7W. E) Component: 28.7N, -80.9W. F) System: 28.7N,-80.9W. G) Component: 28.9N,-80.9W. H) System: 28.9N,-80.9W.

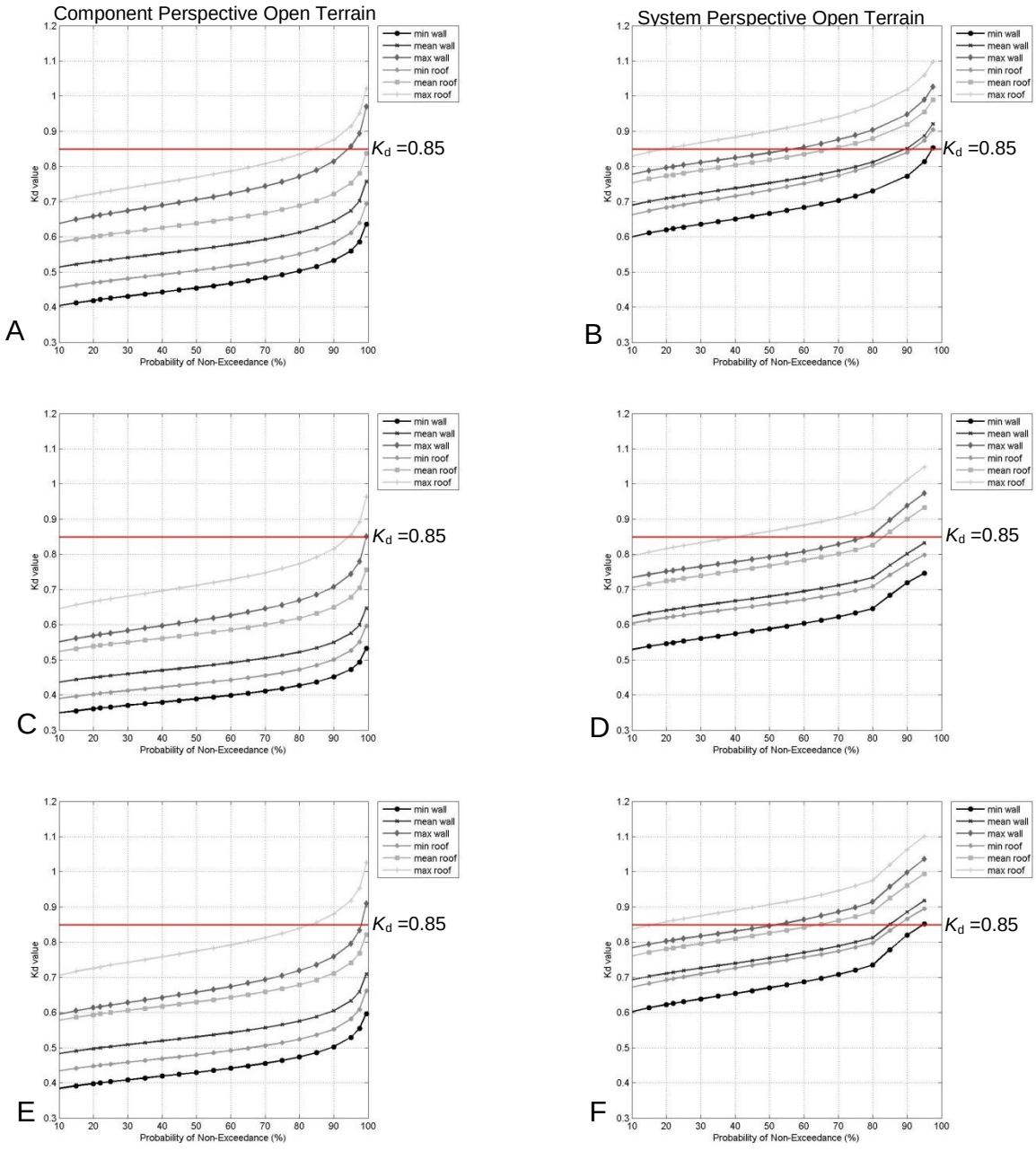

Figure B-40. K_d factor for squared area 7ft x 7ft following scenario analysis in open exposure for Katrina grid (Fig.5-13). A) Component: 30.4,-89.8. B) System: 30.4,-89.8. C) Component: 30.4,-89.4. D) System: 30.4,-89.4. E) Component: 31.4,-90.0. F) System: 31.4,-90.0.

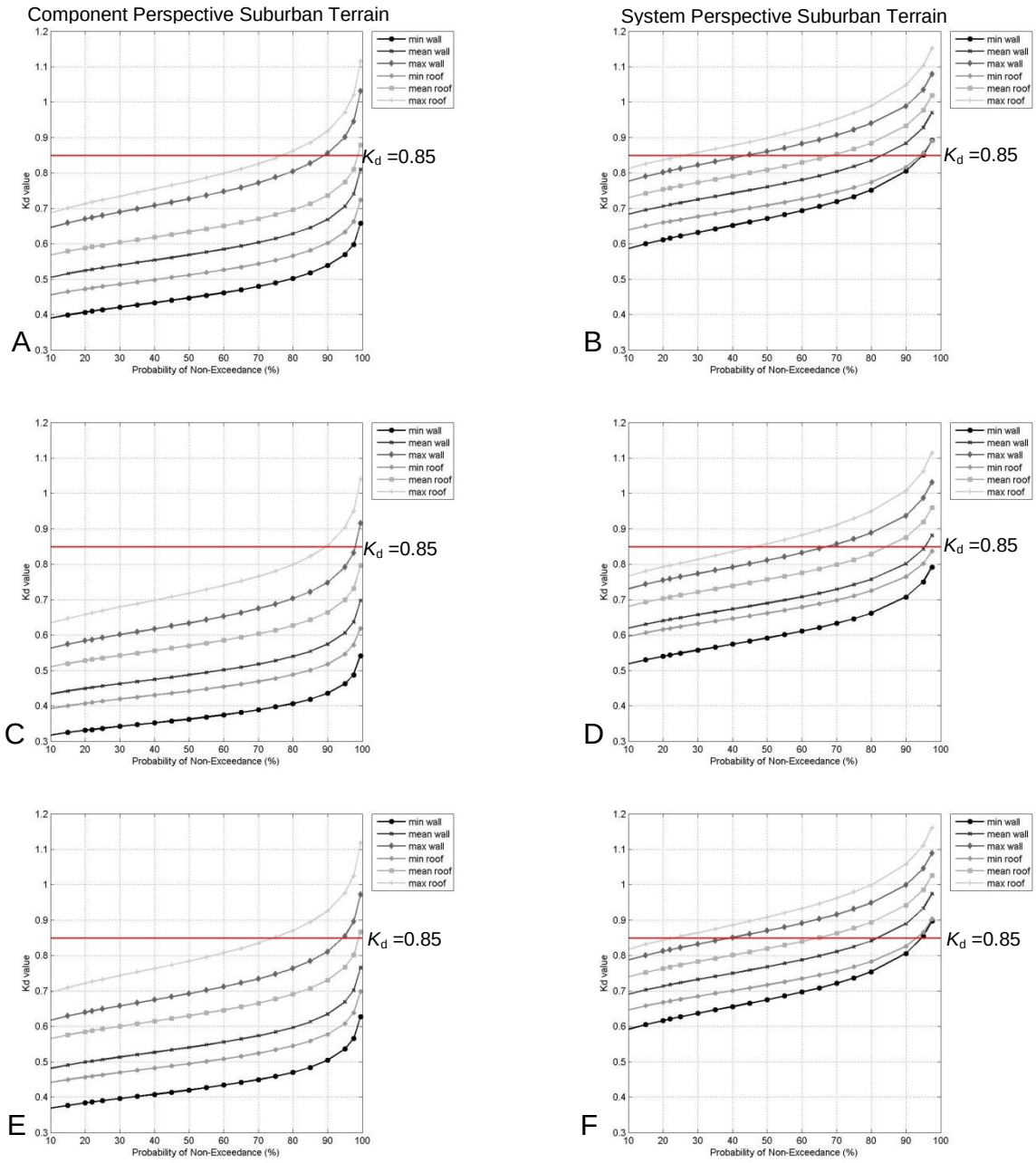

Figure B-41. K_d factor for squared area 7ft x 7ft following scenario analysis in suburban exposure for Katrina grid (Fig.5-13). A) Component: 30.4,-89.8. B) System: 30.4,-89.8. C) Component: 30.4,-89.4. D) System: 30.4,-89.4. E) Component: 31.4,-90.0. F) System: 31.4,-90.0.

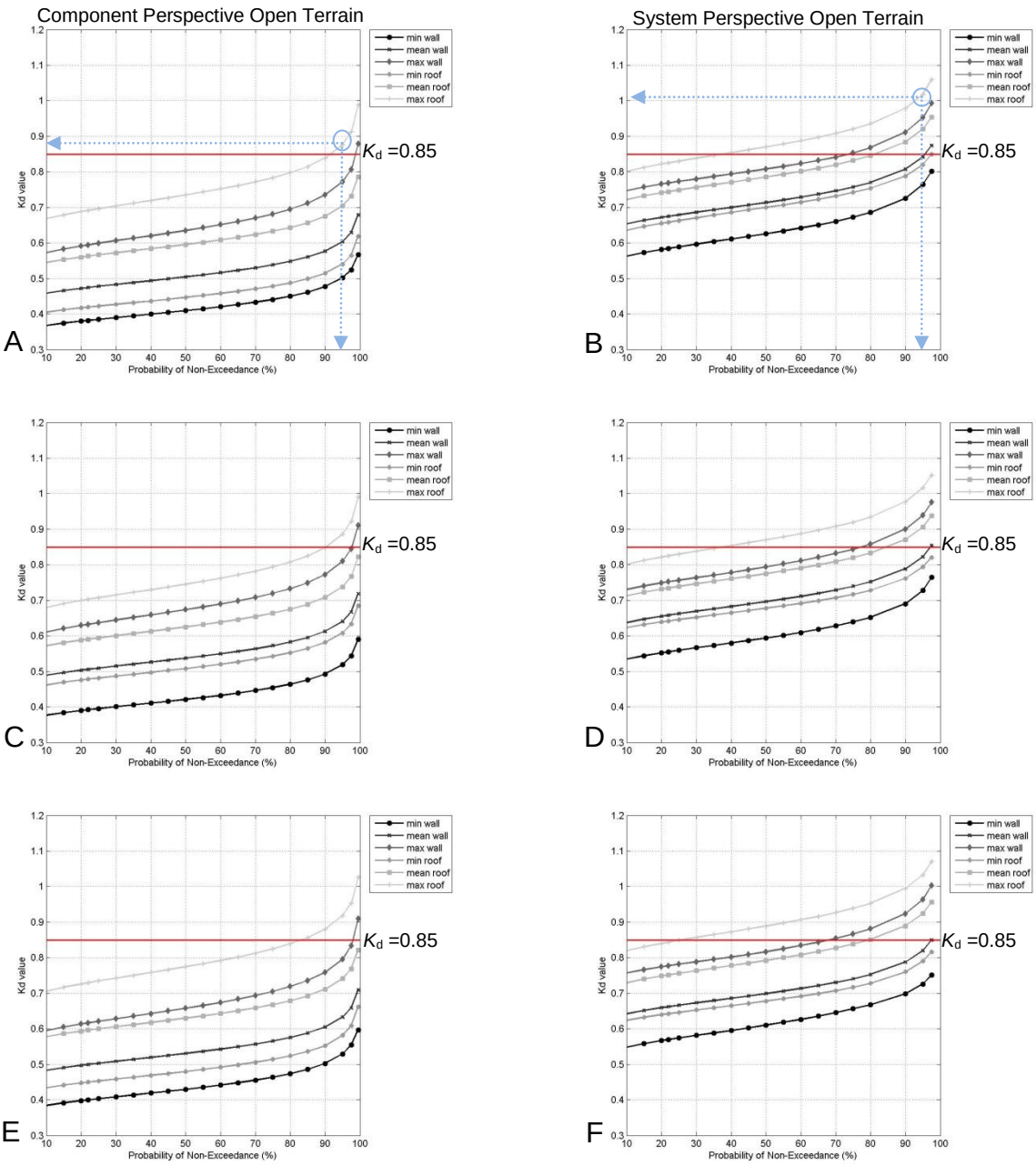

Figure B-42. K_d factor for squared area 7ft x 7ft following scenario analysis in open exposure for Ivan grid (Fig.5-13). A) Component: 30.4,-87.5. B) System: 30.4,-87.5. C) Component: 30.4,-87.9. D) System: 30.4,-87.9. E) Component: 31.4,-88.3. F) System: 31.4,-88.3.

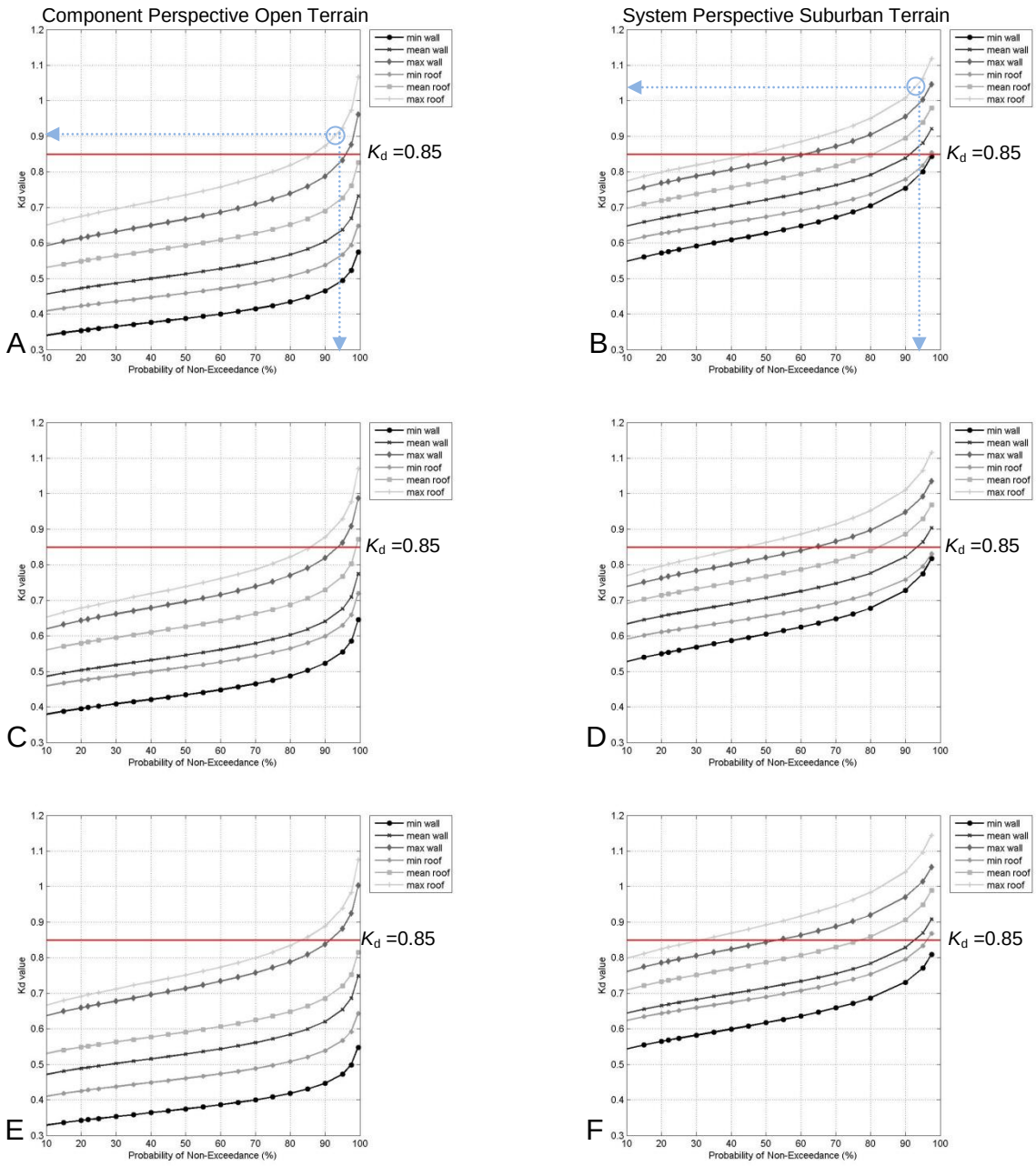

Figure B-43. K_d factor for squared area 7ft x 7ft following scenario analysis in suburban exposure for Ivan grid (Fig.5-13). A) Component: 30.4,-87.5. B) System: 30.4,-87.5. C) Component: 30.4,-87.9. D) System: 30.4,-87.9. E) Component: 31.4,-88.3. F) System: 31.4,-88.3.

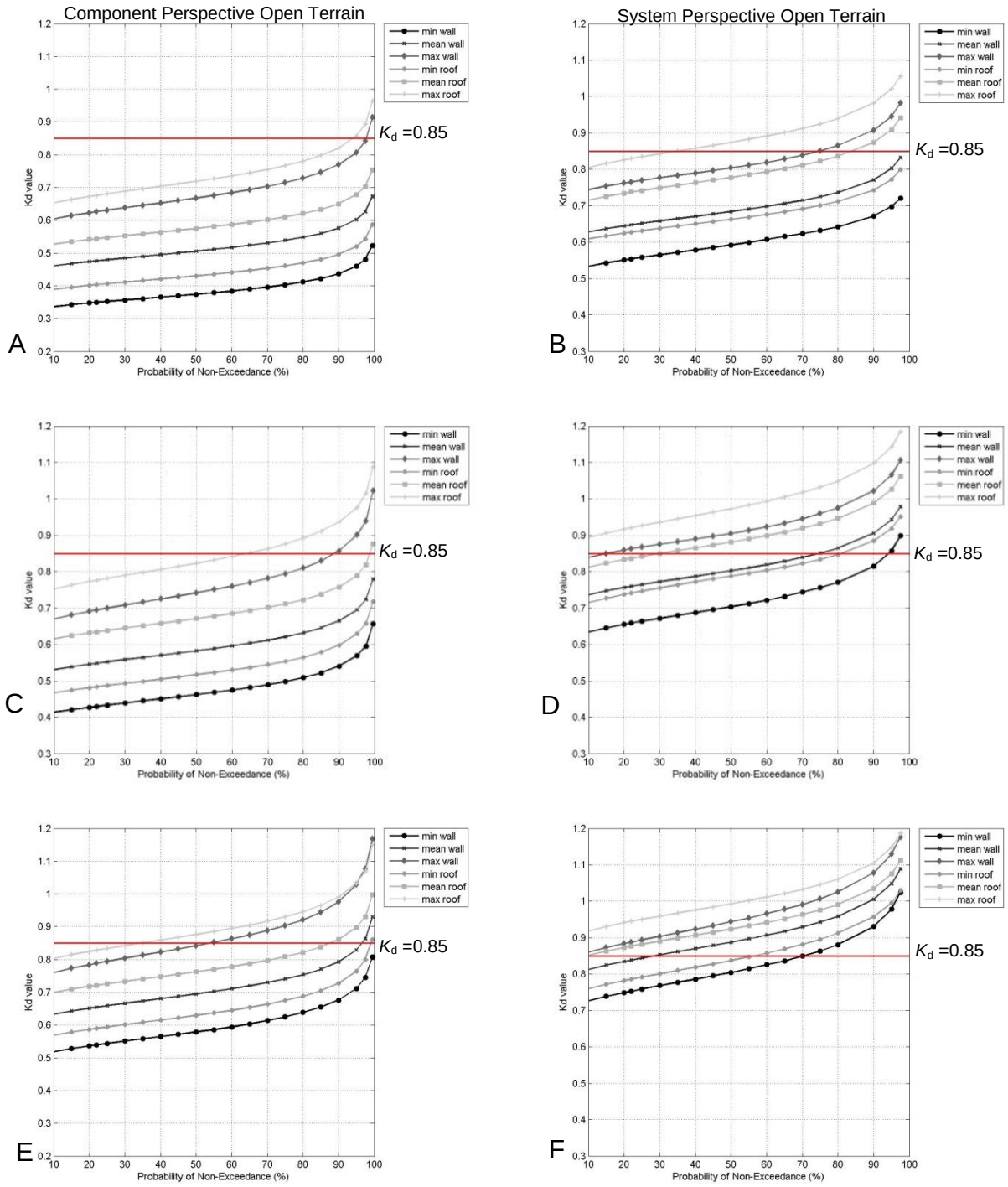

Figure B-44. K_d factor for squared area 7ft x 7ft following scenario analysis in open exposure for Rita grid (Fig.5-13). A) Component: 29.5,-94.5. B) System: 29.5,-94.5. C) Component: 29.7,-94.1. D) System: 29.7,-94.1. E) Component: 29.7, -93.9. F) System: 29.7,-93.9.

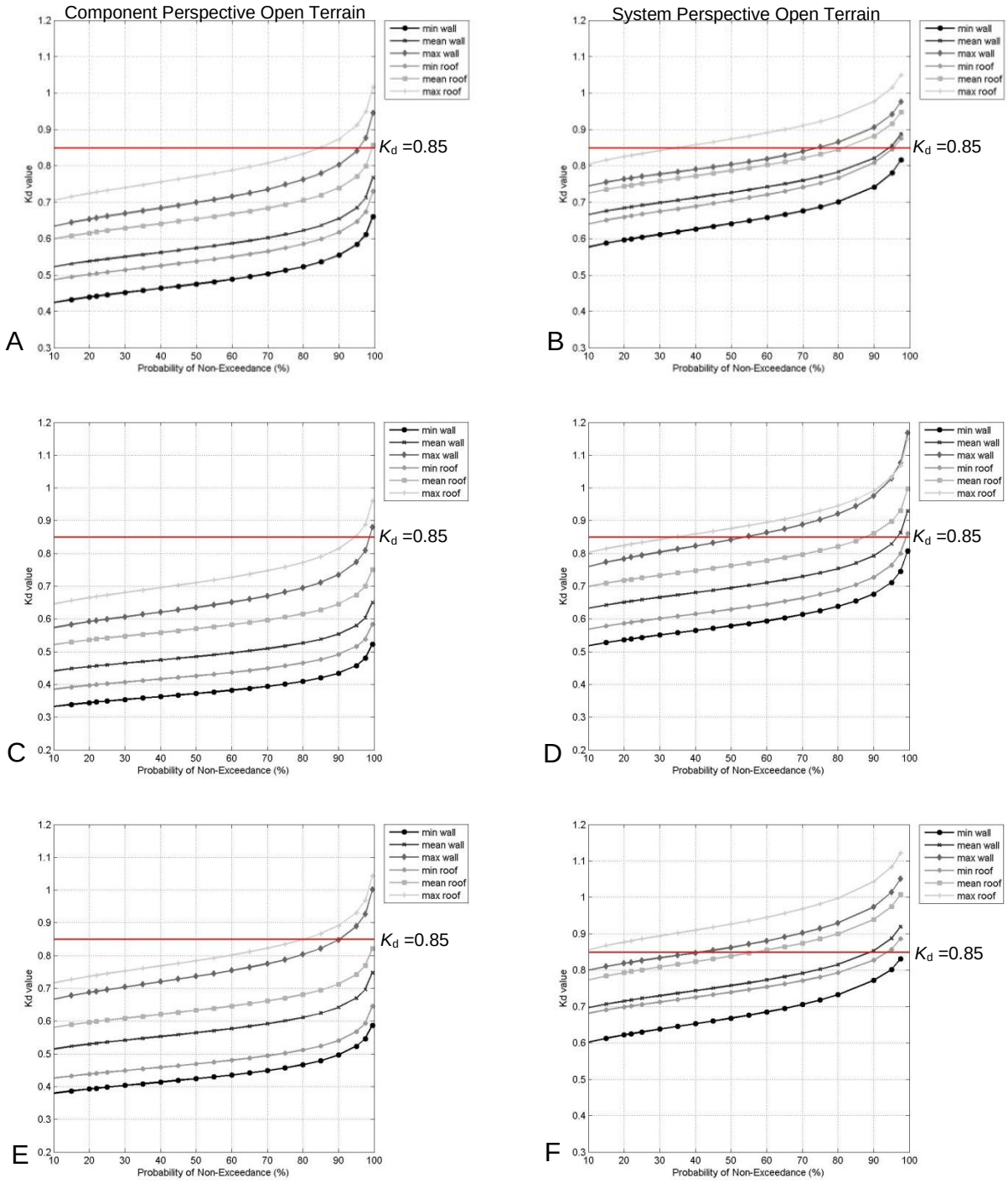

Figure B-45. K_d factor for squared area 7ft x 7ft following scenario analysis in open exposure for Rita grid (Fig.5-13). A) Component: 29.8,-93.7. B) System: 29.8,-93.7. C) Component: 29.8,-93.3. D) System: 29.8,-93.3. E) Component: 29.6, -92.7. F) System: 29.6, -92.7.

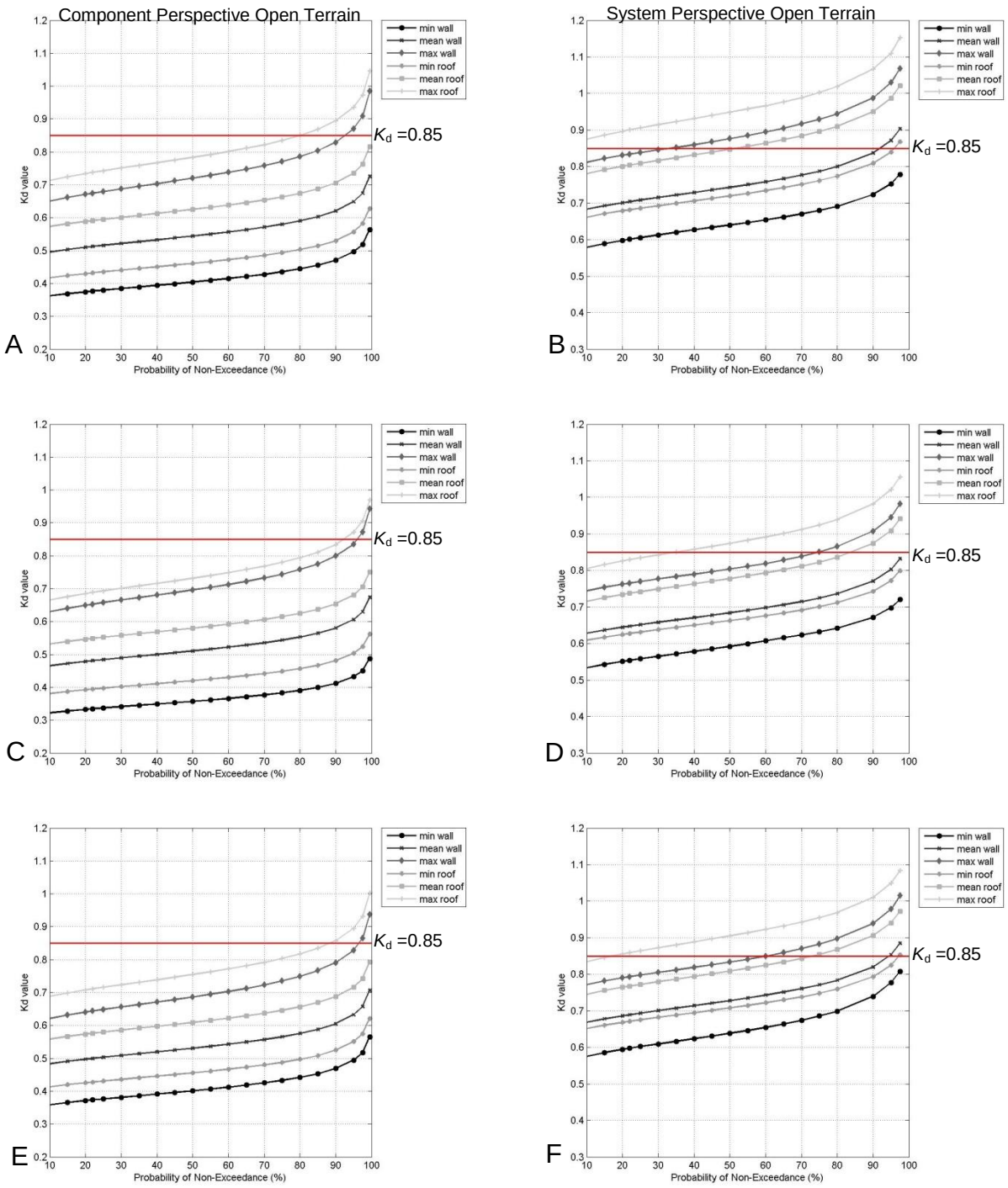

Figure B-46. K_d factor for squared area 7ft x 7ft following scenario analysis in open exposure for Rita grid (Fig.5-13). A) Component: 29.7,-94.3. B) System: 29.7,-94.3. C) Component: 29.9,-94.5. D) System: 29.9,-94.5. E) Component: 29.9,-94.1. F) System: 29.1,-94.1.

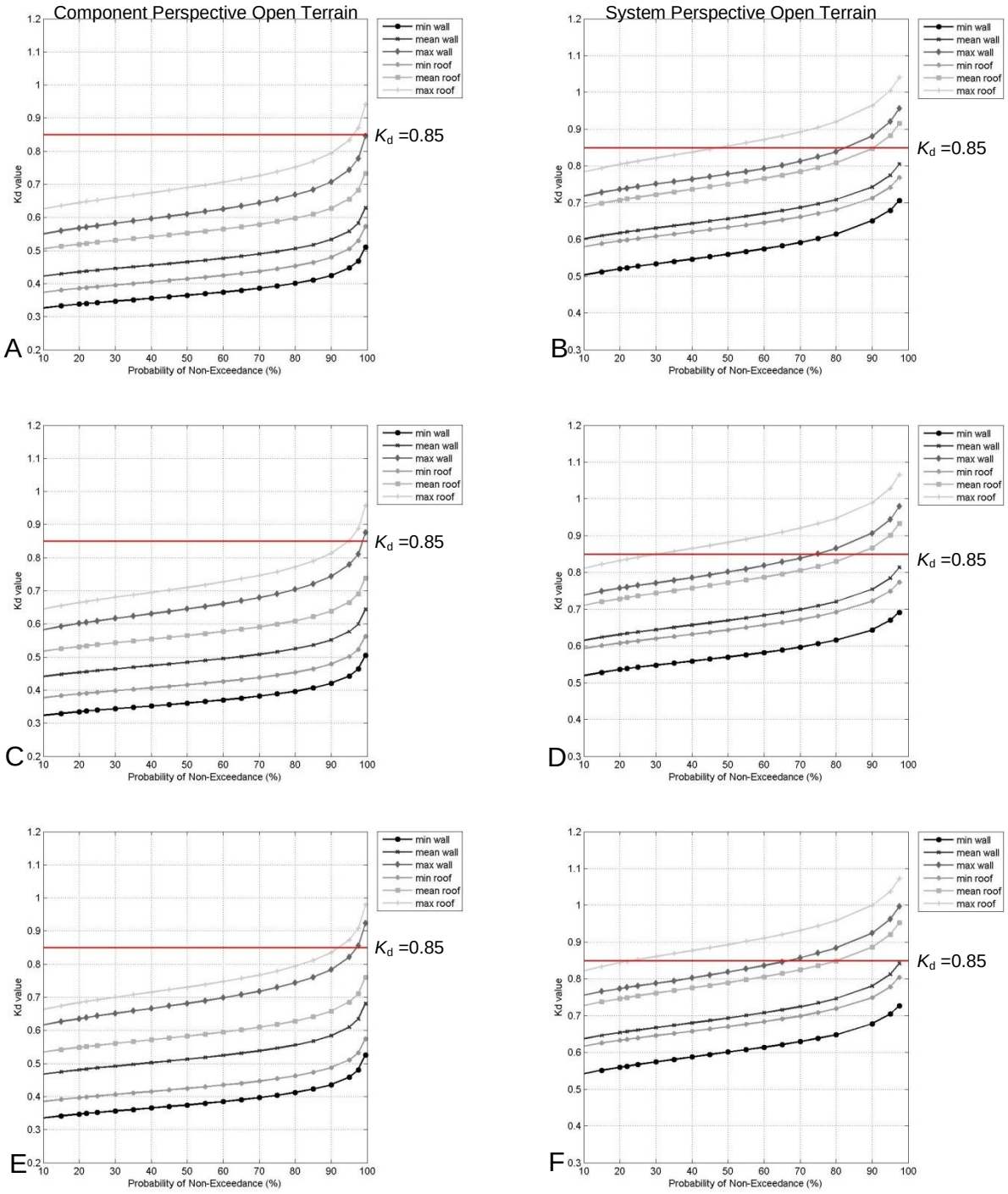

Figure B-47. K_d factor for squared area 7ft x 7ft following scenario analysis in open exposure for Rita grid (Fig.5-13). A) Component: 29.9,-93.5. B) System: 29.9,-93.5. C) Component:29.9,-92.9. D) System:29.9,-92.9. E) Component: 29.8,-92.7. F) System: 29.8,-92.7.

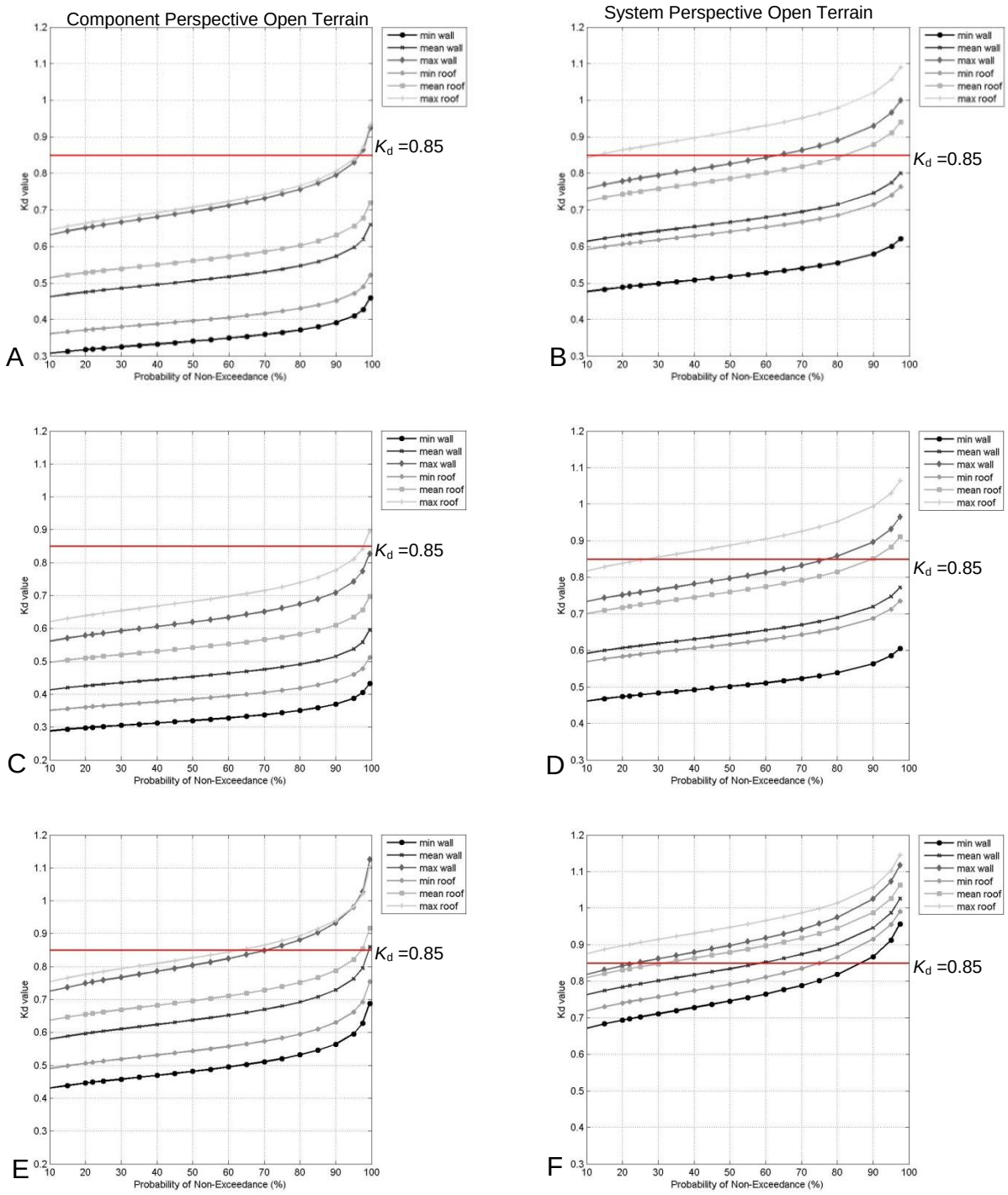

Figure B-48. K_d factor for squared area 7ft x 7ft following scenario analysis in open exposure for Rita grid (Fig.5-13). A) Component: 30.1,-94.5. B) System: 30.1,-94.5. C) Component: 30.1,-94.1. D) System: 30.1,-94.1. E) Component: 30.1,-93.7. F) System: 30.1, -93.7.

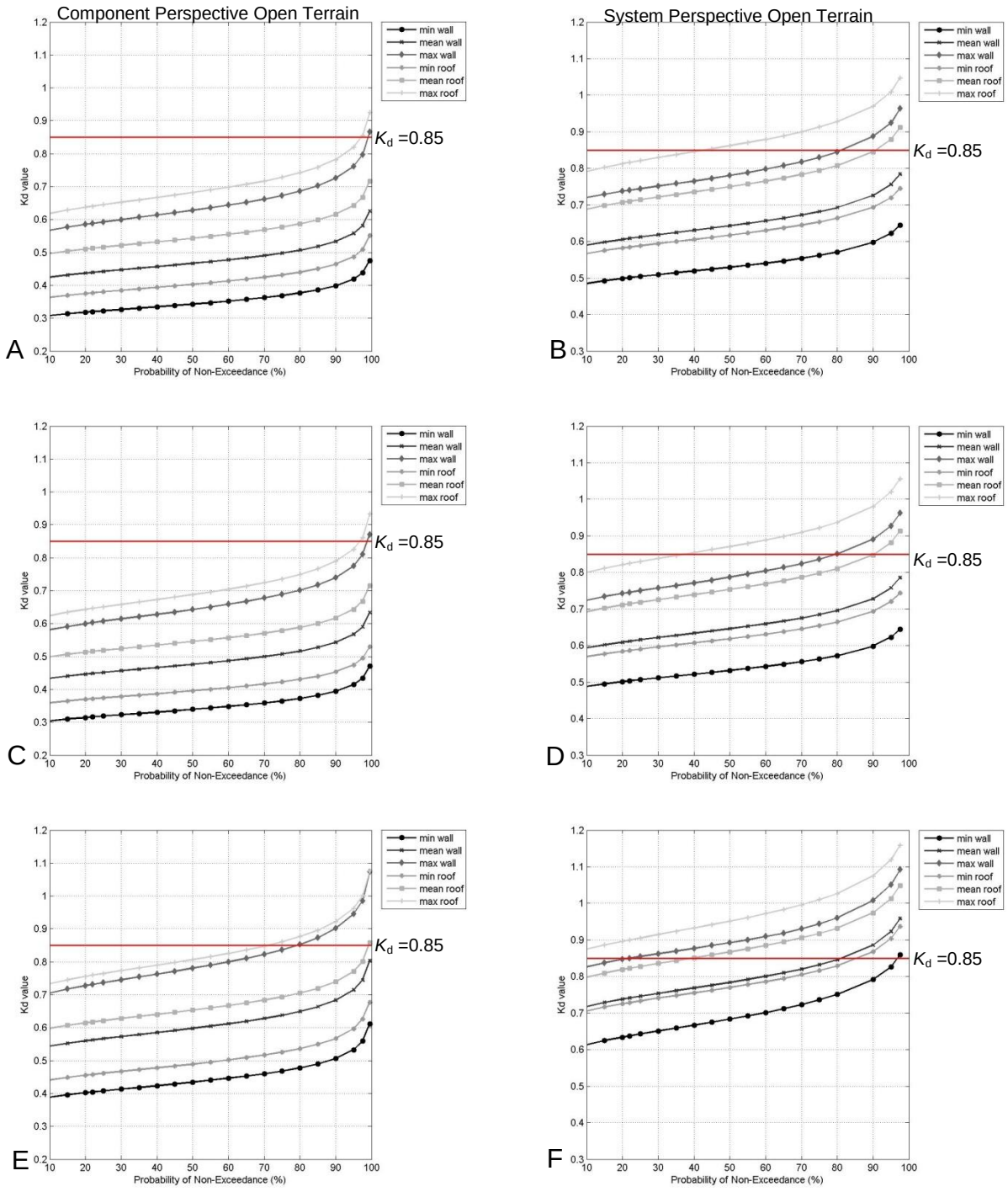

Figure B-49. K_d factor for squared area 7ft x 7ft following scenario analysis in open exposure for Rita grid (Fig.5-13). A) Component: 30.1,-93.1. B) System: 30.1,-93.1. C) Component: 30.1,-92.7. D) System: 30.1,-92.7. E) Component: 30.3, -93.5. F) System: 30.3,-93.5.

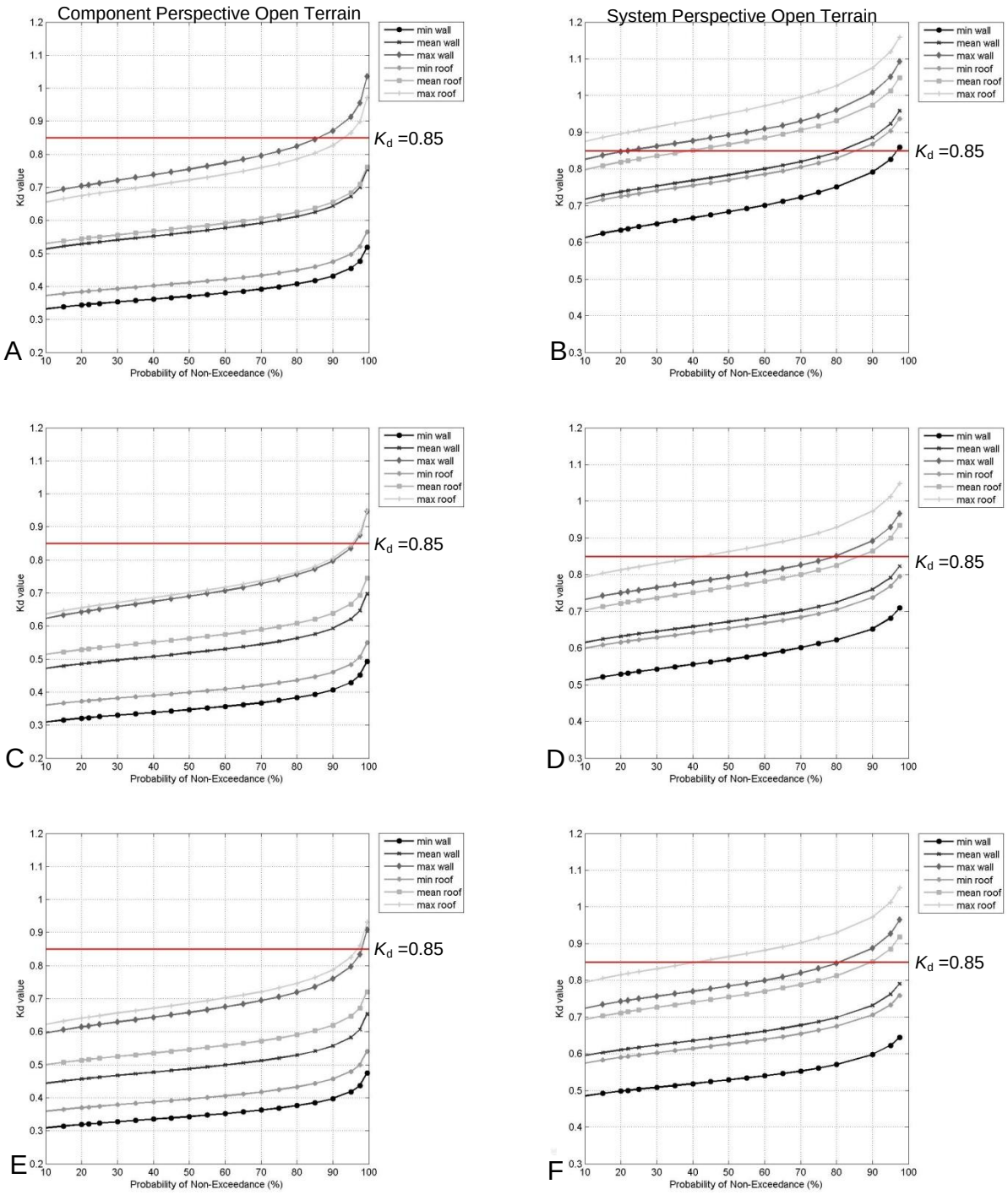

Figure B-50. K_d factor for squared area 7ft x 7ft following scenario analysis in open exposure for Rita grid (Fig.5-13). A) Component: 30.5,-94.1. B) System: 30.5,-94.1. C) Component: 30.5,-93.7. D) System: 30.5,-93.7. E) Component: 30.5, -93.1. F) System: 30.5,-93.1.

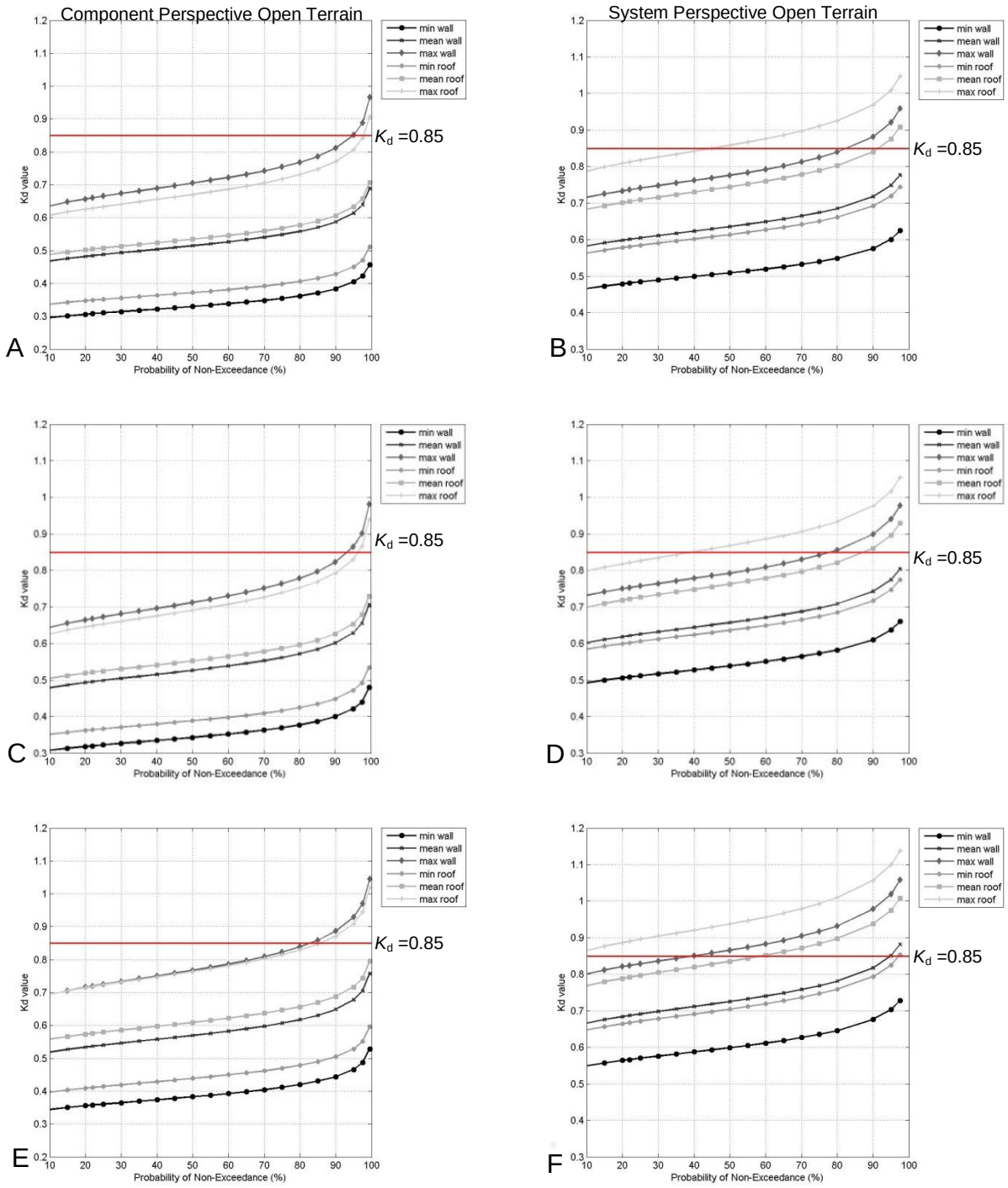

Figure B-51. K_d factor for squared area 7ft x 7ft following scenario analysis in open exposure for Rita grid (Fig.5-13). A) Component: 30.9,-94.1. B) System: 30.9,-94.1. C) Component: 30.9,-93.7. D) System: 30.9,-93.7. E) Component: 30.9, -93.3. F) System: 30.9, -93.3.

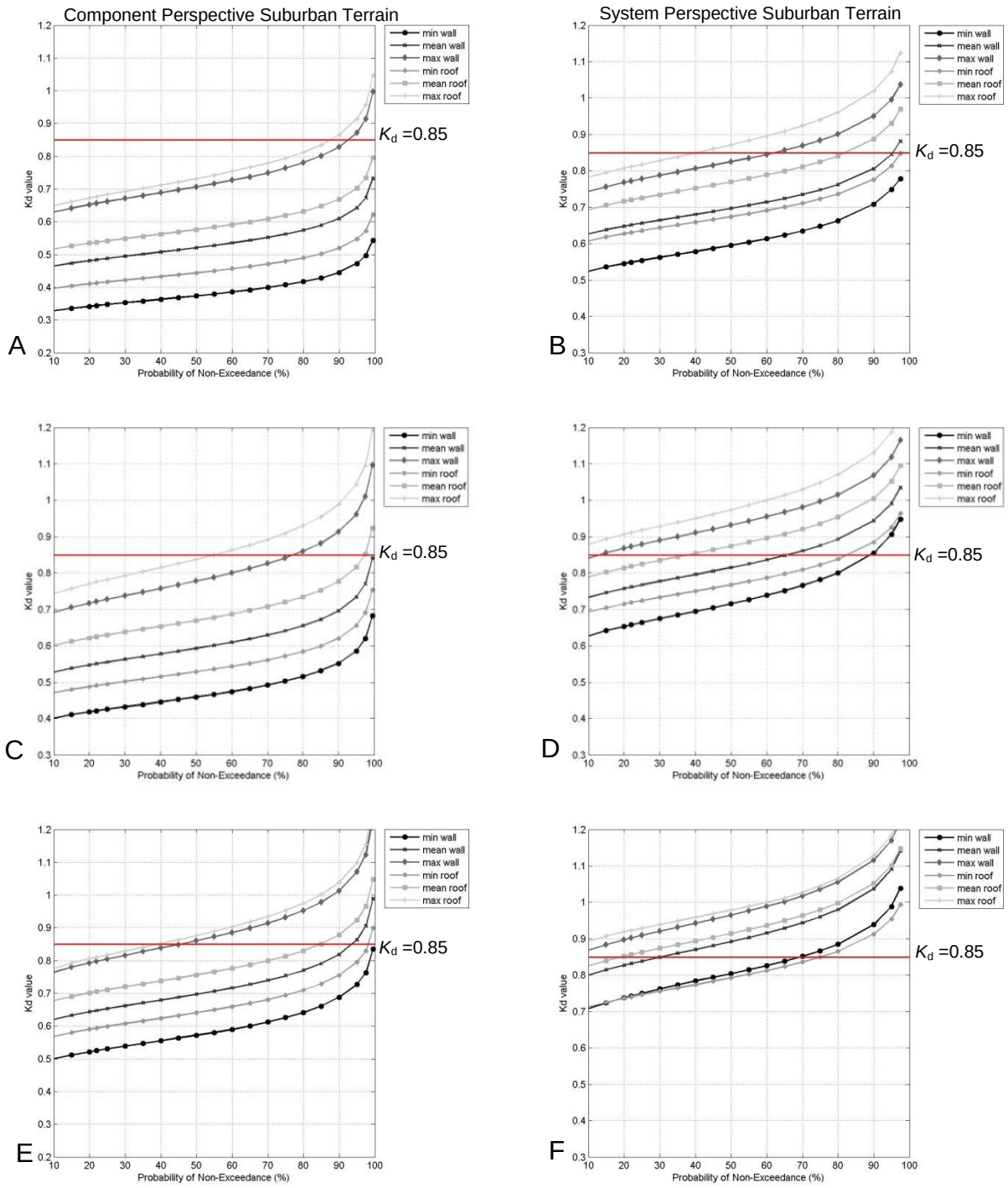

Figure B-52. K_d factor for squared area 7ft x 7ft following scenario analysis in suburban exposure for Rita grid (Fig.5-13). A) Component: 29.5,-94.5. B) System: 29.5,-94.5. C) Component: 29.7,-94.1. D) System: 29.7,-94.1. E) Component: 29.7, -93.9. F) System: 29.7,-93.9.

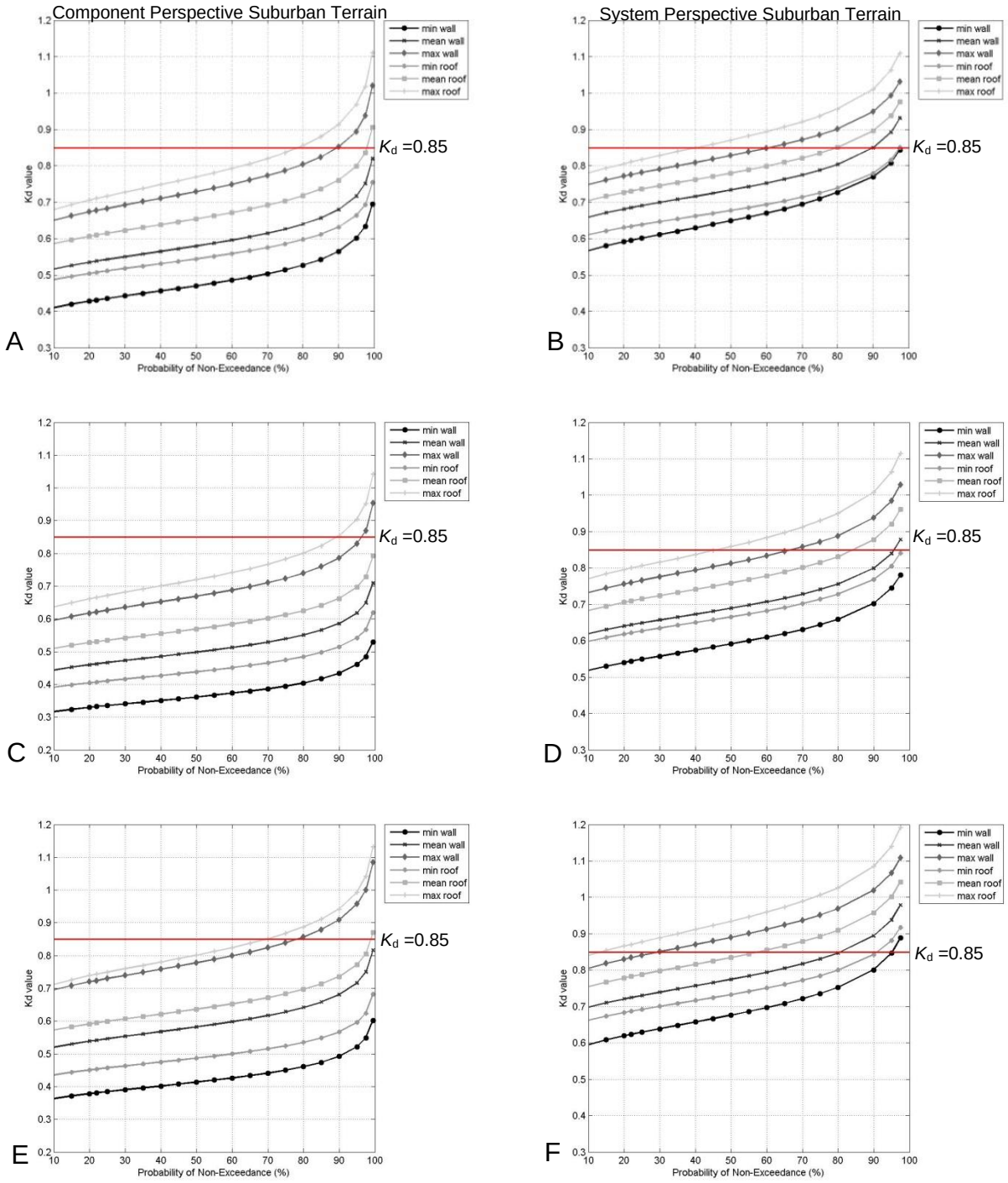

Figure B-53. K_d factor for squared area 7ft x 7ft following scenario analysis in suburban exposure for Rita grid (Fig.5-13). A) Component: 29.8,-93.7. B) System: 29.8,-93.7. C) Component: 29.8,-93.3. D) System: 29.8,-93.3. E) Component: 29.6, -92.7. F) System: 29.6, -92.7.

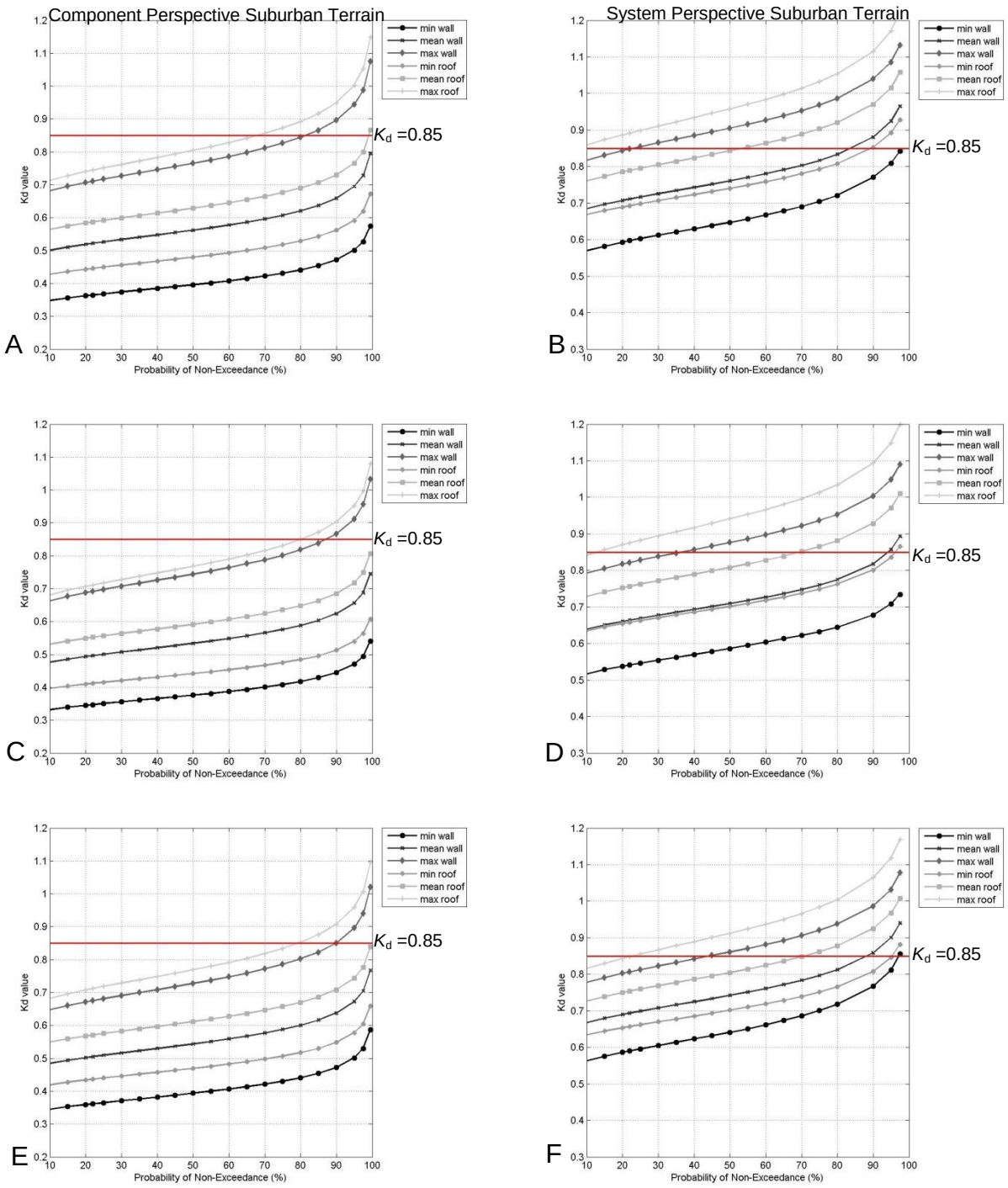

Figure B-54. K_d factor for squared area 7ft x 7ft following scenario analysis in suburban exposure for Rita grid (Fig.5-13). A) Component: 29.7,-94.3. B) System: 29.7,-94.3. C) Component: 29.9,-94.5. D) System: 29.9,-94.5. E) Component: 29.9,-94.1. F) System: 29.9,-94.1.

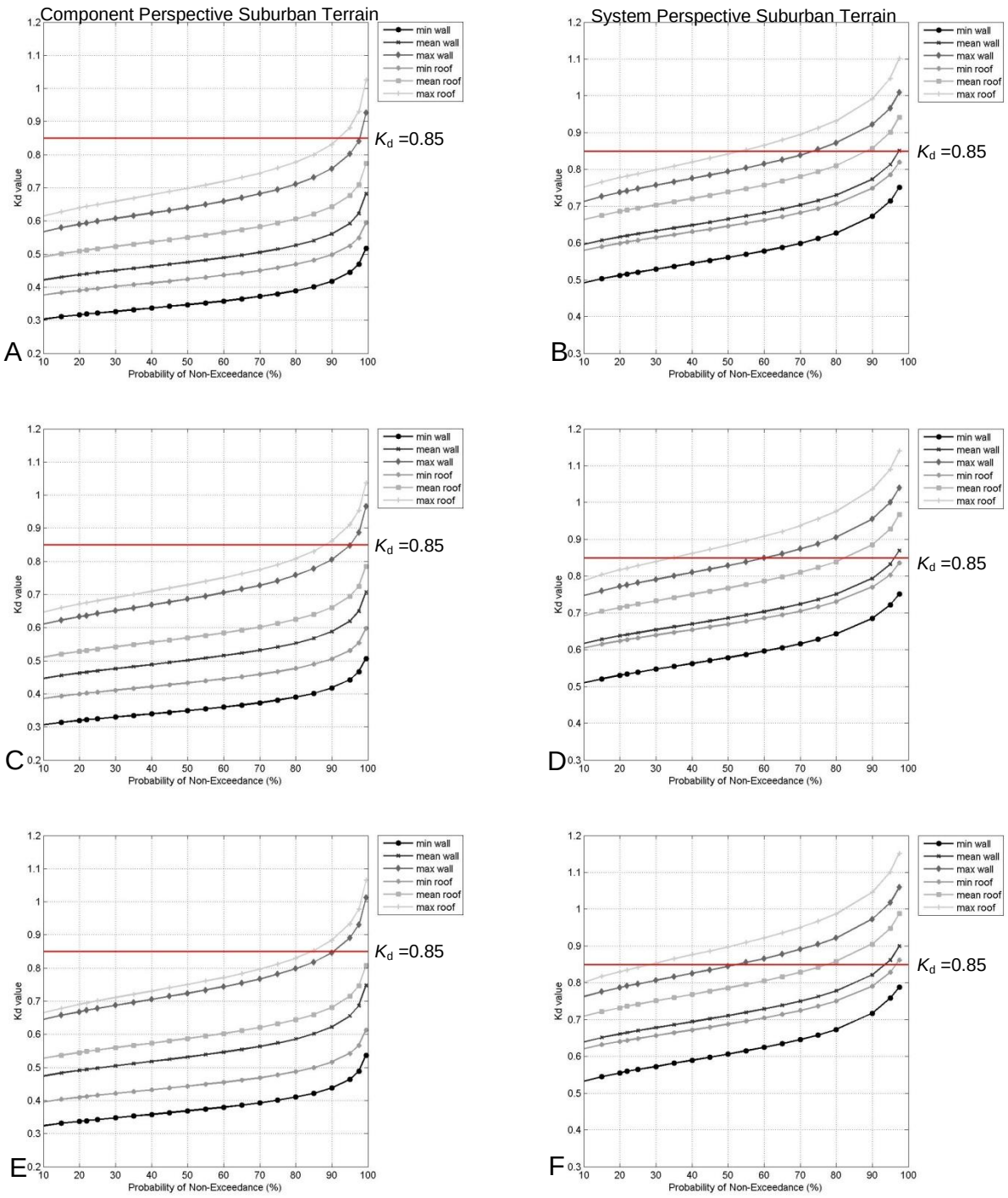

Figure B-55. K_d factor for squared area 7ft x 7ft following scenario analysis in suburban exposure for Rita grid (Fig.5-13). A) Component: 29.9,-93.5. B) System: 29.9,-93.5. C) Component:29.9,-92.9. D) System:29.9,-92.9. E) Component: 29.8,-92.7. F) System: 29.8,-92.7.

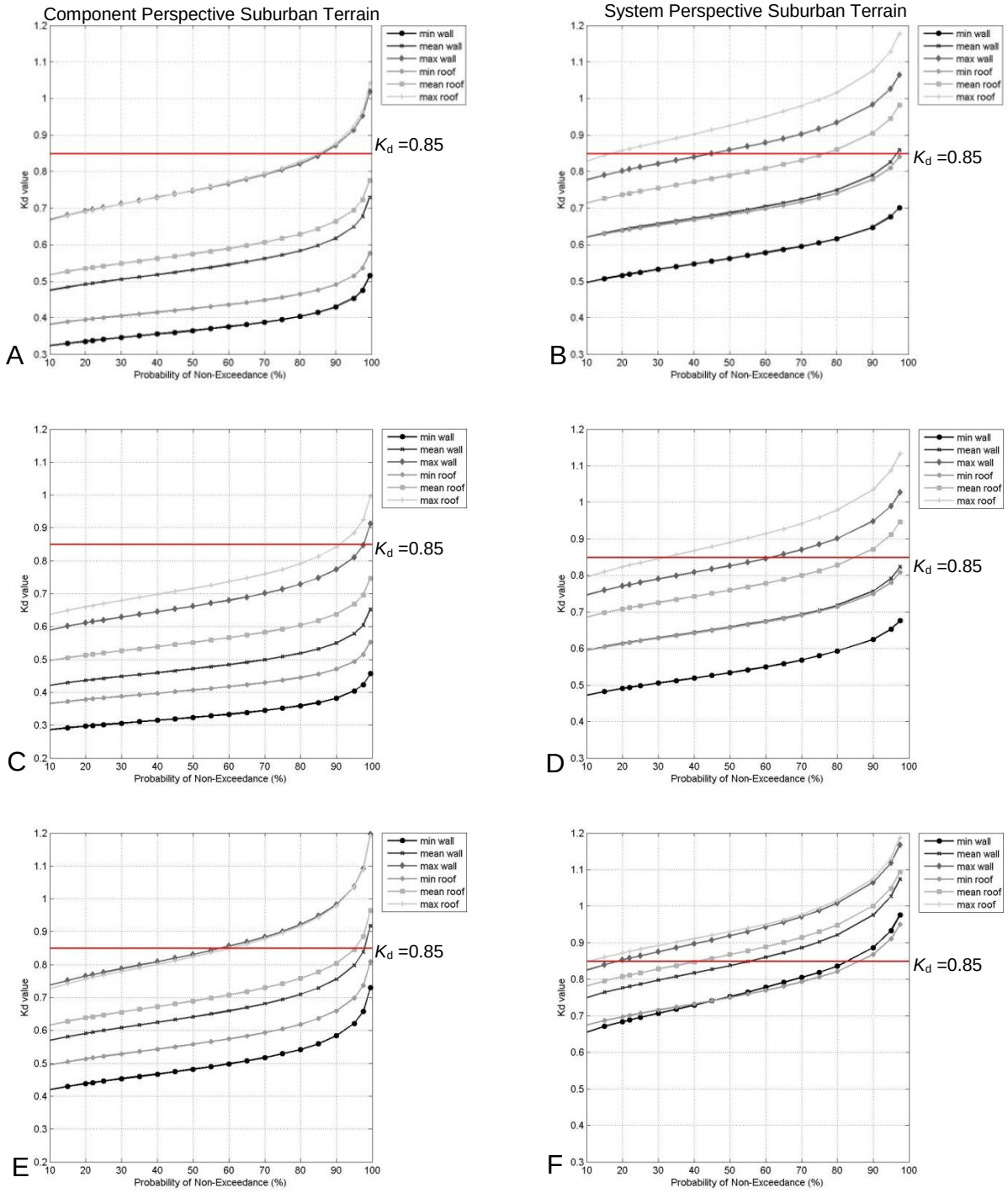

Figure B-56. K_d factor for squared area 7ft x 7ft following scenario analysis in suburban exposure for Rita grid (Fig.5-13). A) Component: 30.1,-94.5. B) System: 30.1,-94.5. C) Component: 30.1,-94.1. D) System: 30.1,-94.1. E) Component: 30.1,-93.7. F) System: 30.1, -93.7.

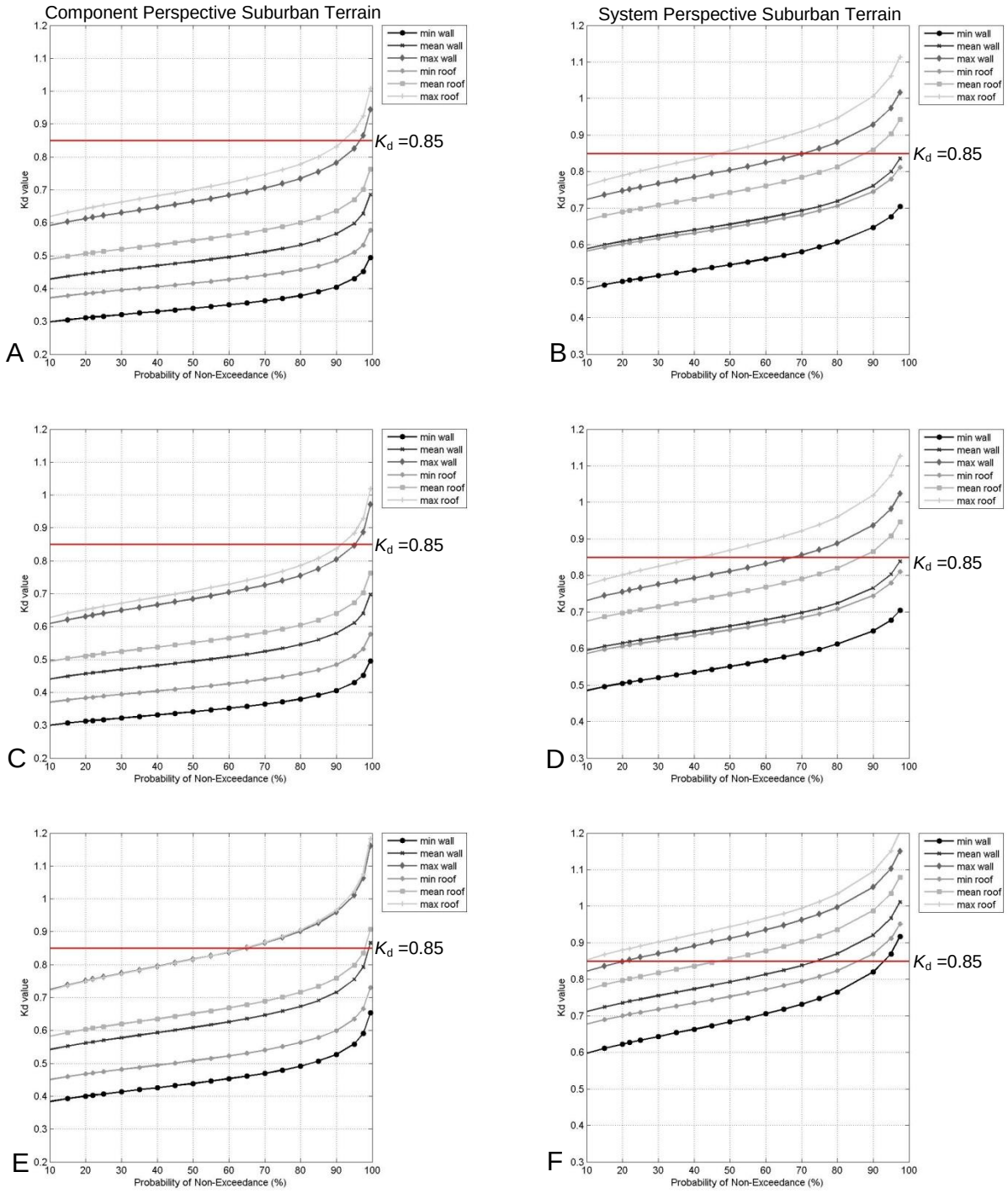

Figure B-57. K_d factor for squared area 7ft x 7ft following scenario analysis in suburban exposure for Rita grid (Fig.5-13). A) Component: 30.1,-93.1. B) System: 30.1,-93.1. C) Component: 30.1,-92.7. D) System: 30.1,-92.7. E) Component: 30.3, -93.5. F) System: 30.3,-93.5.

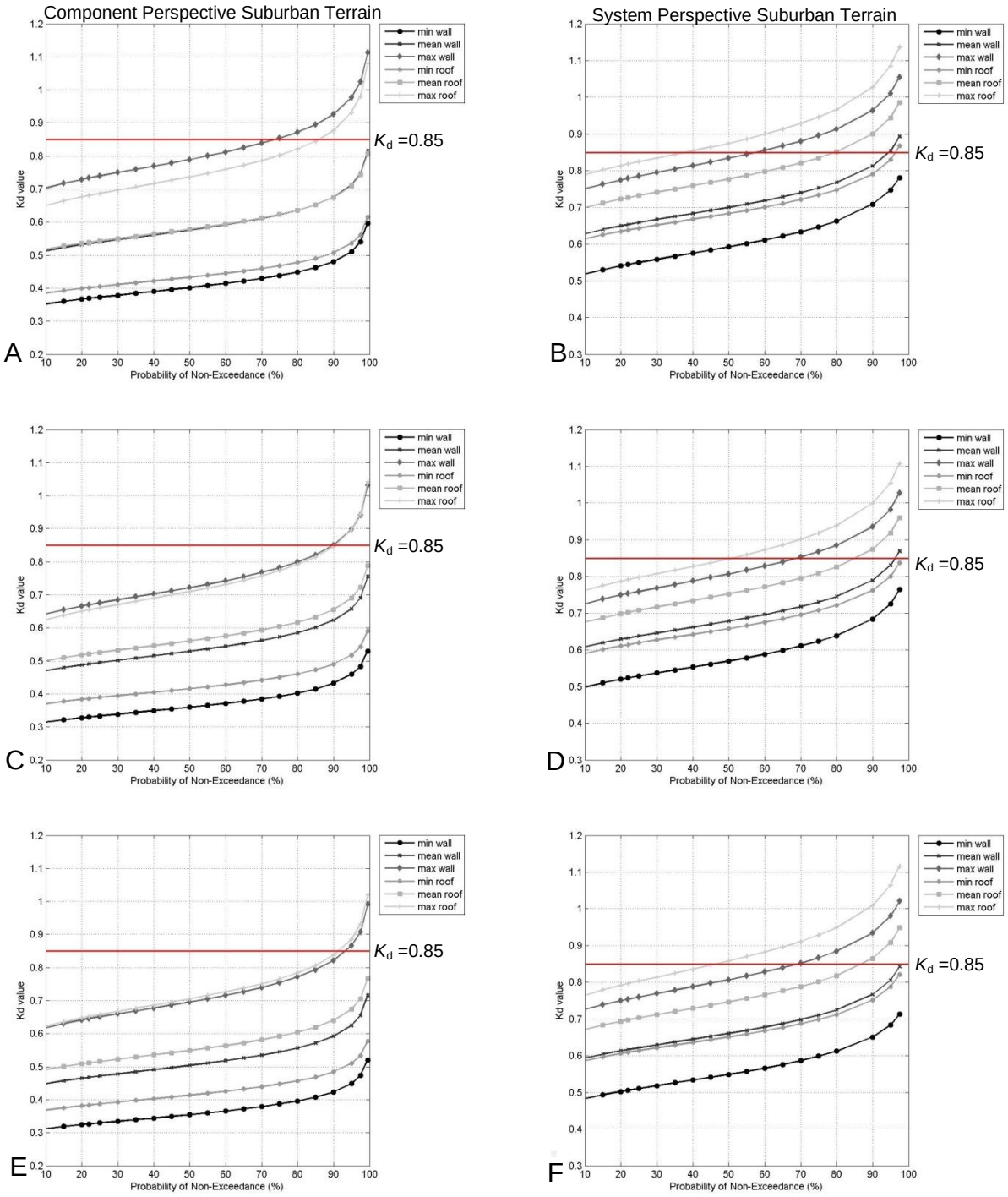

Figure B-58. K_d factor for squared area 7ft x 7ft following scenario analysis in suburban exposure for Rita grid (Fig.5-13). A) Component: 30.5,-94.1. B) System: 30.5,-94.1. C) Component: 30.5,-93.7. D) System: 30.5,-93.7. E) Component: 30.5, -93.1. F) System: 30.5,-93.1.

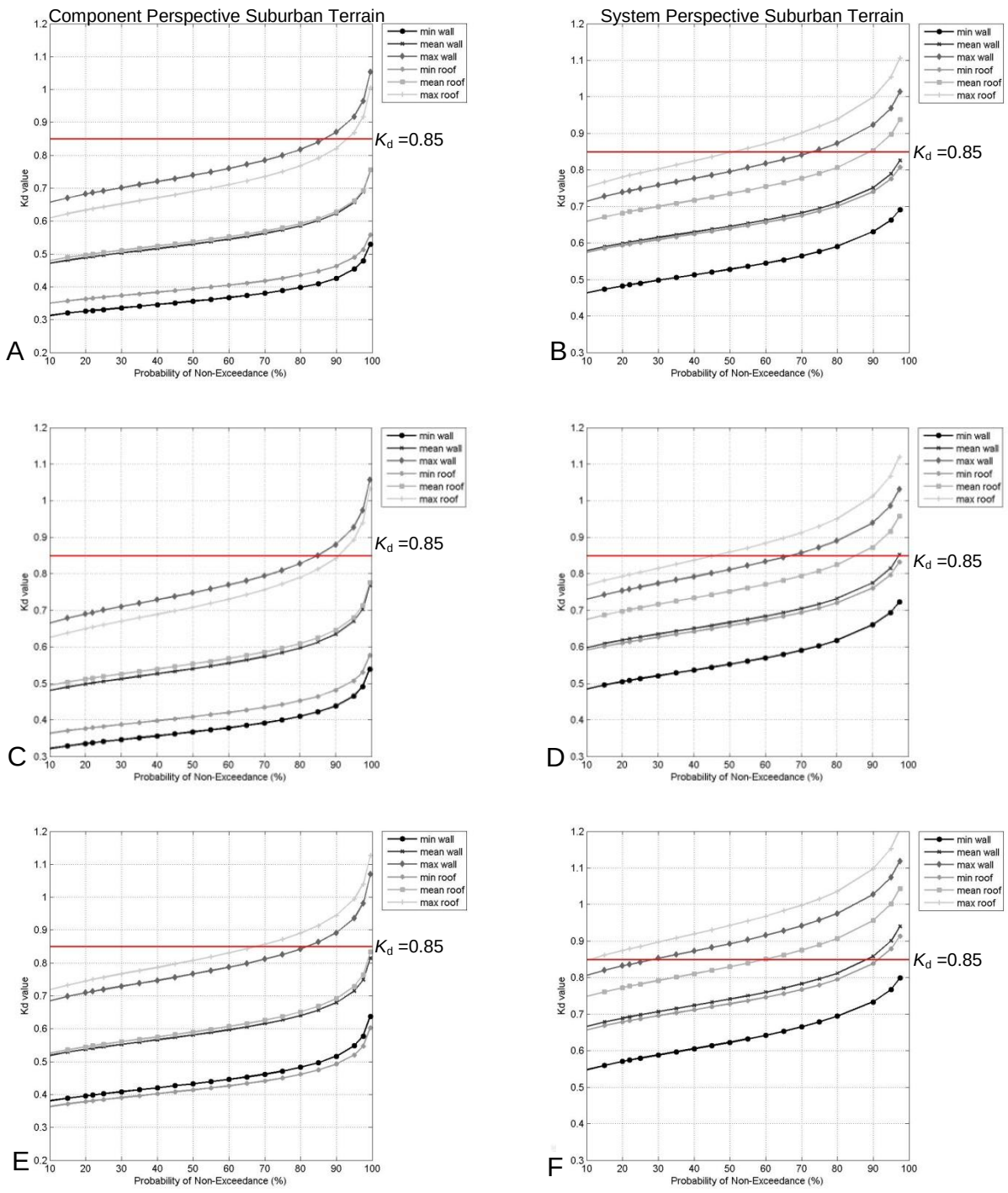

Figure B-59. K_d factor for squared area 7ft x 7ft following scenario analysis in suburban exposure for Rita grid (Fig.5-13). A) Component: 30.9,-94.1. B) System: 30.9,-94.1. C) Component: 30.9,-93.7. D) System: 30.9,-93.7. E) Component: 30.9, -93.3. F) System: 30.9, -93.3.

LIST OF REFERENCES

ANSI A58.1 (1972), Building code requirements for minimum design loads in Buildings, American National Standards Institute, New York.

ANSI A58.1 (1982), Building code requirements for minimum design loads in Buildings, American National Standards Institute, New York.

Architectural Institute of Japan (2006), Recommendations for Loads on Buildings, Japan.

ASCE 7-88 (1988), Minimum design loads for buildings and other structures, American Society of Civil Engineers, Reston, Virginia.

ASCE 7-93 (1993),Minimum design loads for buildings and other structures, American Society of Civil Engineers, Reston, Virginia

ASCE 7-95 (1995), Minimum design loads for buildings and other structures, American Society of Civil Engineers, Reston, Virginia.

ASCE 7-98 (1998), Minimum design loads for buildings and other structures, American Society of Civil Engineers, Reston, Virginia.

ASCE 7-05 (2005), Minimum design loads for buildings and other structures, American Society of Civil Engineers, Reston, Virginia.

ASCE 7-10 (2010), Minimum Design Loads for Buildings and Other Structures, American Society of Civil Engineers, Reston, Virginia.

Association of Structural Engineers of the Philippines (2010), National Structural Code of the Philippines: Volume I Buildings, Towers, and Other Vertical Structures, 6th Ed., Phillipines.

Baker, C.J. (2007), “The debris flight equations”, *J. Wind Eng. Ind. Aerod*., **95**,329-353.

Beason, W.L. (1974), “Breakage characteristics of window glass subjected to small missile impacts”, Thesis, Civil Engineering Department, Texas Tech University.

Blake, E.S., Landsea, C.W., and Gibney, E.J. (2011), NOAA Technical Memorandum: The Deadliest, Costliest, and Most Intense United States Tropical Cyclones from 1851 to 2010, Miami and North Carolina.

British Standard Institute: Loading for Buildings (2002), Part 2: Code of Practice for Wind Loads, BS 6399-2, United Kingdom.

Buildings Department, Hong Kong Special Administrative Region (2004), Code of Practice on Wind Effects, Hong Kong.

Bureau of Indian Standards (2002), Wind Loads on Buildings and Structures IS: 875 (Part 3), India.

China Architecture and Building Press (2001), Load Code for the Design of Building Structures, GB 50009-2001,China.

Chock, G., Peterka, J. and Yu, G. (2005), "Topographic wind Speed-up and directionality factors for use in the city and county of honolulu building code",*In Proceedings of 10th Americas Conference in Wind Engineering*, Baton Rouge, La.

Chock, G., and Yu, G. (2013), "Analysis of directionality factor for hurricanes incorporating topographic wind effects",*The 12th Americas Conference in Wind Engineering*, Seattle, Washington.

Cook, N.J. (1983), "Note on directional and seasonal assessment of extreme winds for design", *J. Wind Eng. Ind. Aerod*., **12**, 365-372.

Cook, N.J., and Miller, C.A. (1999), "Further note on directional assessment of extreme winds for design", J. Wind Eng. Ind. Aerodyn., **79**, 201-208.

Cuba Wind Load Evaluation (2003), "Wind pressure loads calculating method", NC 285.

Davenport, A. G. (1961), "The spectrum of horizontal gustiness near the ground in high winds", J*. Royal Meteorological Society*, **87**, 194-211.

Davenport, A.G. (1969), "Structural safety and reliability under wind action", *Proc. Int. Conf. on Structural Safety and Reliability Proceedings*, April, 131-145.

Davenport, A.G. (1977), "The prediction of risk under wind loading", *In: Second International Conference on Structural Safety and Reliability Proceedings*, Sep., 511-538.

Department of Standards Malaysia (2002),Code of Practice on Wind Loading for Building Structure, MS 1553:2002.

Ellingwood, B. (1979), "On reliability of structures against winds", *In: Third Division Specialty Conference*, September 17-19, 259-263.

Ellingwood, B.,Galambos,T.V., MacGragor,J.G., and Cornell, C.A. (1980), Report No. 577:Development of a Probability Based Load Criterion for American National Standard A58 Building Code Requirements for Minimum Design Loads in Buildings and Other Structures, United States Government Printing Office, Washington: United States Department of Commerce/National Bureau of Standards.

Ellingwood, B. (1981), "Wind and snow load statistics for probabilistic design*", J.*

Struct. Div., July; **107**(7), 1345-1350.

European Committee for Standardization (2005), Eurocode 1: Actions on Structures Part 1-4: General Actions – Wind Actions, EN 1991-1-4-2005,Brussels.

Federal District Mexico (2004), Technical notes for wind design, Mexico City.

Federal Emergency Management Agency (FEMA) (2005), Mitigation Assessment Team Report: FEMA 488 Hurricane Charley in Florida, Washington D.C.

Federal Emergency Management Agency (FEMA) (2006), Mitigation Assessment Team Report: FEMA 549 Hurricane Katrina in the Gulf Coast, Washington D.C.

Fernandez, G., Masters, F.J. and Gurley, K.R. (2010), "Performance of hurricane shutters under impact by roof tiles", *Eng. Struct*.,**32**(10), 3384-3393.

Gurley, K. and Masters, F. (2011), "Post 2004 hurricane field survey of residential building performance", *Nat. Haz. Rev*., *ASCE*, **12**(4), 177-183.

Harris, R.I. and Deaves, D.M. (1981), "The structure of strong winds", *Ciria Conference on Wind Engineering in the Eighties*, Ciria, London.

Ho, E. (1992), "Variability of low building wind loads", PhD. Dissertation in Civil in Engineering, University of Western Ontario.

Holmes, J.D. (1981),"Reduction factors for wind direction for use in codes and standards", *In: Symposium on Designing with the Wind*, June.

Holmes, J.D. (1986), "The application of probability theory to the directional effects of wind", *In: 10th Australian Conference of the Mechanics of Structures and Materials*, Australia.

Holmes, J.D. (1990), "Reduction factors for wind direction for use in codes and standards", *In: Symposium on Designing with the Wind*, June.

Holmes, J.D. and Mullins, P.J. (2001), "The mechanics of flying debris and test criteria", *In: Fifth Asia– Pacific Conference on Wind Engineering*.

Holmes, J.D. (2004), "Trajectories of spheres in strong winds with application to windborne debris", *J. Wind Eng. Ind. Aerod*., **92**, 9-22.

Holmes, J.D., Letchford, C.W. and Lin, N. (2006), "Investigations of plate-type windborne debris – Part II: computed trajectories", *J. Wind Eng. Ind. Aerod*., **94**, 21-39.

Holmes, J.D. (2007), Wind Loading of Structures, (2nd Ed.), Taylor & Francis, New York, NY.

Huang, Z., and Rosowsky, D.V. (2000), “Analysis of hurricane directionality effects using event based simulation”, *Wind Struct.*, **3**(3), 177-191.

Isyumov, N., Ho, E., and Case, P. (2013), “Influence of wind directionality on wind loads and responses”, *The 12th Americas Conference in Wind Engineering*, Seattle, Washington.

Kordi, B. and Kopp, G.A. (2009a), “Evaluation of quasi-steady theory applied to windborne flat plates in uniform flow”, *J. Eng. Mech. ASCE*, **135**, 657-668.

Kordi, B. and Kopp, G.A. (2009b), “The debris flight equations by CJ Baker”, *J. Wind Eng. Ind. Aerod*., **97**, 151-154.

Kordi, B., Traczuk, G. and Kopp, G.A. (2010), “Effects of wind direction on the flight trajectories of roof sheathing panels under high winds”, *Wind and Structures,* **13**, 145-167.

Kordi, B. and Kopp, G.A. (2011), “Effects of initial conditions on the flight of windborne plate debris”, J*. Wind Eng. Ind. Aerod*.,**99**, 601-614.

Laboy-Rodriguez, S.T., Smith, D., Gurley, K., and Masters, F.J. (2012), “Roof tile frangibility and puncture of metal window shutters”, *Wind and Structures* (Accepted October 2012).

Lin, N., Letchford, C.W. and Holmes, J.D. (2006), “Investigations of plate-type windborne debris. Part I. Experiments in wind tunnel and full scale”, *J. Wind Eng. Ind. Aerod*., **94**(2), 51–76.

Lin, N. and Vanmarcke, E. (2008), “Windborne debris risk assessment”, *Prob. Eng. Mech*., **23** (4), 523-530.

Lin, N. and Vanmarcke, E. (2010a), “Windborne debris risk analysis – Part I. Introduction and methodology”, *Wind and Structures*, **13**, 191-206.

Lin, N. and Vanmarcke, E. (2010b), “Windborne debris risk analysis – Part II. Application to structural vulnerability modelling”, *Wind and Structures*, **13**, 207-220.

Masters, F.J., Gurley, K.R., Shah, N. and Fernandez, G. (2010), “The vulnerability of residential window glass to lightweight windborne debris”, *Eng. Struct*., **32**(4), 911-921.

Meloy, N., Sen, R., Pai, N., and Mullins, G. (2007), “Roof damage in new homes caused by Hurricane Charley”, J*. Perform. Constr. Facil. ASCE*, **21**(2), 97-107.

Minor, J. (1994), “ Windborne debris and building envelope”, J*. Wind Eng. Ind. Aerod.*, **53**(1-2), 207-227.

Minor, J. (2005), “Lessons learned from failures of the building envelope in windstorms”, *J. Archit. Eng. ASCE*, **11**(1), 10-13.

National Annex to Eurocode 1(2007), Actions on Structures – Part 1-4: General Actions – Wind Actions. NF EN 1991-1-4 NA, France.

National Annex to Eurocode 1 (2007), Actions on Structures – Part 1-4: General Actions – Wind Actions. SR EN 1991-1-4 NA, Romania.

National Annex to Eurocode 1 (2008), Actions on Structures – Part 1-4: General Actions – Wind Actions. DIN EN 1991-1-4 NA, Germany.

National Annex to Eurocode 1 (2010), Actions on Structures – Part 1-4: General Actions – Wind Actions. CSN EN 1991-1-4-2005/AC: 2010-01, Czech Republic.

National Annex to Eurocode (2010), Actions on Structures – Part 1-4: General Actions – Wind Actions. DS/EN 1991-1-4 DK NA: 2010-03, Denmark.

National Annex to Eurocode 1(2010), Actions on Structures – Part 1-4: General Actions – Wind Actions. SFS – EN 1991-1-4 NA, Finland.

NIST Aerodynamic Database: URL: http://fris2.nist.gov/winddata/

National Research Council of Canada (2010), National Building Code of Canada, NRCC ,Ottawa.

NOAA HRD AOML Surface Wind Anslysis (H*Wind): URL: www.aoml.noaa.gov/hrd/data_sub/wind.html.

Peng, X., Yang, L., Gurley, K., Prevatt, D., and Gavanski, E. (2013), “Prediction of peak wind loads on a low-rise building”, *The 12th Americas Conference in Wind Engineering*, Seattle, Washington.

Ravindra, M.K., Cornell, C,A., and Galambos, T.V. (1978), “Wind and snow load factors for use in LRFD”, *J .Struct. Div*., Sept; **104**(9),1443-1457.

Revised Ordinances of Honolulu (2011), Honolulu Building Code, Hawai.

Richards, P.J., Williams, N., Laing, B., McCarty, M. and Pond, M. (2008), “Numerical calculation of the three-dimensional motion of wind-borne debris”, J*. Wind Eng. Ind. Aerod*., **96, 2188**-2202.

Sadek, F., & Simiu, E. (2002), “Peak non-Gaussian wind effects for database-assisted low-rise building design” *J. Eng. Mech*., **128**,530-539.

Scarabino, A. and Giacopinelli, P. (2010), “Analysis of the two dimensional sheet debris flight equations: initial and final state”, *Wind and Structures*, **13**, 109-125.

Shinozuka, M. and Deodatis, G. (1991), “Simulation of stochastic processes by spectral representation”, *Appl. Mech. Rev*., **44**(4), 191-204.

Simiu, E., and Filliben, J.J. (1981), “Wind direction effects on cladding and structural loads”, *Eng. Struct.*, **3**, 181-186.

Simiu, E., Vickery, P. and Kareem, A. (2007), “Relation between Saffir-Simpson hurricane scale wind speeds and peak 3-s gust speeds over open terrain”, *J. Struct. Eng*.,**133**(7), 1043 – 1045.

Standards Australia/Standards New Zealand (2011), Structural design actions. Part2 Wind actions: AS/NZS1170.2, Australia.

Tachikawa, M. (1983), “Trajectories of flat plates in uniform flow with application to wind-generated missiles”, *J. Wind Eng. Ind. Aerod*., **14**, 443-453.

Tachikawa, M. (1988), “A method for estimating the distribution range of trajectories of wind-borne missiles”, *J. Wind Eng. Ind. Aerod*., **29**(1–3), 175–84.

Tamura, Y., Kawai, H., Uematsu, Y., Okada, H., and Ohkuma, T. (2004), Report: Documents for Wind Resistant of Buildings in Japan.

Vega, R. (2008), “Wind directionality: a reliability-based approach”, PhD. Dissertation in: wind and science engineering, Texas Tech University.

Vickery, B.J. (1974), “Some characteristics of wind speed and structural response and their recognition in a limit-state design”, *Conference on Application of Probability Theory to Structural Design*, 45-54.

Vietnam Standard. (1995), Loads and Effects Design Standard, TCVN 2737-1995.

Visscher, B.T. and Kopp, G.A. (2007), “Trajectories of roof sheathing panels under high winds”, *J. Wind Eng. Ind. Aerod*.,**95**, 697-713.

Von Karman, T. (1948), “Progress in the statistical theory of turbulence”, *Proc. Nat. Acad. Sci.*,**34**, 530-539.

Wang, K. (2003), Flying debris behavior, Thesis, Civil Engineering Department, Texas Tech University.

Wen, Y. (1983), “Wind direction and structural reliability”, *J. Struct. Eng*., **109**(4), 1028-1041.

Wills, J.A.B., Lee, B.E. and Wyatt, T.A. (2002), “A model of windborne debris damage”, *J. Wind Eng. Ind. Aerod*., **90**(4–5), 555–565.

Yau Siu, C., Lin, N. and Vanmarcke,E. (2011), “Hurricane damage and loss estimation using an integrated vulnerability model”, *Nat. Haz. Rev.,ASCE*,**12**(4), 184-189.

BIOGRAPHICAL SKETCH

Sylvia Teresa Laboy-Rodriguez was born in San Juan, P.R. in 1980. During her educational career at the University of Puerto Rico she participated in a research project during the 2002-2003 academic year. The project was to analyze data collected for the development of a Liquefaction Map for the Puerto Rico Insurance Commission in order to identify areas more susceptible to the liquefaction effect due to seismic movements.

As an undergraduate she was selected several years to be part of the dean's list and civil engineer department honor student. She graduated magna Cum laude earning a Bachelor in Science in civil engineering from the University of Puerto Rico at Mayaguez in 2003.

During 2003-2005 she was awarded the Olson Fellowship which helped her to focus on graduate studies in the area of construction management at Purdue University. A subset of this program introduced her to the specialization of hazard mitigation, a subject of great significance in Puerto Rico. She earned a Master of Science in civil engineering on May 2005, with a thesis title A Cost Effectiveness Model to Evaluate Anti-Terrorist Countermeasures for Bridges.

After earning her master's degree in 2005, she decided to put the training to practice by developing a construction company in Puerto Rico in conjunction with her sister (also a civil engineer). As a contractor she had the opportunity to work in different areas related to civil engineering which enriched her field experience. However, early 2008 she had the opportunity to join the engineering faculty at Caribbean University as an instructor and investigator in hazard mitigation developing fragility curves for concrete frame buildings with passive controllers.

This experience heightened her desire to pursue her PhD. She started working towards her Doctor in Philosophy with a specialization in structural and wind Hazard engineering in the spring of 2010 at the University of Florida in the Department of Civil and Coastal Engineering working under the guidance of Dr. Gurley. During her PhD studies she worked as a research and teacher assistance and was awarded the Bill & Bryon Bushnell Graduate Fellowship and Rubinos-Mesia Scholarship from the Structural Engineers Foundation IL. Her dissertation topic is Vulnerability of Residential Infrastructure in Hurricane Prone Regions which is composed of two phases (small research projects). The first phase was to investigate the vulnerability of roof tile systems and metal hurricane shutters to roof tile debris (RTD) which was completed in the fall 2011 (funded by Florida Building Commission). The second phase evaluated the current value of the directionality factor (K_d) used in the ASCE 7 (funded by SERRI). Her primary research interests are in vulnerability/risk assessments and hazard mitigation.